Porous Carbons – Hyperbranched Polymers – Polymer Solvation

266
Advances in Polymer Science

Aims and Scope

The series Advances in Polymer Science presents critical reviews of the present and future trends in polymer and biopolymer science. It covers all areas of research in polymer and biopolymer science including chemistry, physical chemistry, physics, material science.

The thematic volumes are addressed to scientists, whether at universities or in industry, who wish to keep abreast of the important advances in the covered topics.

Advances in Polymer Science enjoys a longstanding tradition and good reputation in its community. Each volume is dedicated to a current topic, and each review critically surveys one aspect of that topic, to place it within the context of the volume. The volumes typically summarize the significant developments of the last 5 to 10 years and discuss them critically, presenting selected examples, explaining and illustrating the important principles, and bringing together many important references of primary literature. On that basis, future research directions in the area can be discussed. Advances in Polymer Science volumes thus are important references for every polymer scientist, as well as for other scientists interested in polymer science - as an introduction to a neighboring field, or as a compilation of detailed information for the specialist.

Review articles for the individual volumes are invited by the volume editors. Single contributions can be specially commissioned.

Readership: Polymer scientists, or scientists in related fields interested in polymer and biopolymer science, at universities or in industry, graduate students.

Special offer:

For all clients with a standing order we offer the electronic form of Advances in Polymer Science free of charge.

More information about this series at
http://www.springer.com/series/12

Timothy E. Long • Brigitte Voit • Oguz Okay
Editors

Porous Carbons – Hyperbranched Polymers – Polymer Solvation

With contributions by

S. Banerjee · A. Bazargan · A. Ghosh · C. W. Hui · G. McKay ·
F. A. Plamper · B. Voit

Editors
Timothy E. Long
Virginia Polytechnic Institute and State
   University (Virginia Tech)
Dept. Chemistry
Blacksburg, Virginia
USA

Oguz Okay
Istanbul Technical University
Istanbul
Turkey

Brigitte Voit
Leibniz-Institut für Polymerforschung
   Dresden e. V. (IPF)
Dresden
Germany

Publisher's Note

The present volume of *Advances in Polymer Science* is a collection of substantial review articles on interesting and valuable subjects from different areas of Polymer Science. The volume was not originally planned as a topical volume. The articles were invited and reviewed by the Series Editors of *Advances in Polymer Science* on an independent basis. The collected articles were put together for publication by the publisher.

Publishing Editor, Springer   Tobias N. Wassermann

Contents

Porous Carbons from Plastic Waste

Alireza Bazargan, Chi Wai Hui, and Gordon McKay

Abstract Thermoplastic polymers (such as polypropylene, polyethylene, polyvinyl chloride, polystyrene, etc.) are major constituents of municipal solid waste. Millions of tons of plastic waste are discarded each year, most of which is either incinerated or dumped in landfills. As an alternative, methods using these wastes as feeds for the production of value-added products such as fuels, carbon nanotubes, and porous carbons have been proposed by various researchers. In recent years there has been considerable research in the area of activated carbon production from plastic wastes and products with high surface areas and pore volumes have been produced. However, no literature survey has yet summarized the findings. Thus, herein, the studies pertaining to the production of porous carbon (such as activated carbon) from plastic wastes are reviewed for the first time. This review is organized on the basis of the type of plastic polymer used as the precursor. The first part covers various thermoplastics, whereas the second focuses more deeply on poly(ethylene terephthalate) (PET). This is because the majority of research in this area has used PET. The low carbon yield may make the production of porous carbons from plastic waste impractical. Hence, the authors suggest an alternative integrated approach for future studies so that porous carbons can be produced as a byproduct during the conversion of plastics to gaseous and liquid products.

Keywords Activation methods · Plastic wastes · Polymer pyrolysis · Porous carbon

A. Bazargan (✉), C.W. Hui and G. McKay (✉)
Department of Chemical and Biomolecular Engineering, Hong Kong University of Science and Technology, Clearwater Bay, Hong Kong
e-mail: bazargan@ust.hk; kehui@ust.hk; kemckayg@ust.hk

Contents

Abbreviations

AC	Activated carbon
HDPE	High density polyethylene
LDPE	Low density polyethylene
PE	Polyethylene
PET	Poly(ethylene terephthalate)
PP	Polypropylene
PS	Polystyrene
PVC	Polyvinyl chloride

1   Introduction

Plastic polymers form a considerable portion of the volume of waste produced across the world. Although around 5–15% by weight of municipal solid waste is composed of plastics, this waste stream corresponds to 20–30% of the volume [1]. Around 1.45 million people work in Europe's plastic industry, which generates an estimated 300 billion euros in the EU-27 countries each year. Nonetheless, more than 25 million tons of plastic waste is annually generated in this region [2]. For years, researchers have been looking for various ways to overcome the problems of such large quantities of waste polymers. Currently, the use of landfills and incineration are the two most widespread solutions [3]. However, the increase in cost, environmental concerns, and the decreasing space for landfills make alternative treatment options desirable [4]. Various alternative routes have been proposed in order to process the plastic wastes [5–7].

One area of intense research is plastic pyrolysis, with the goal of obtaining oily products that could be later modified and treated to produce fuels [8]. The issue of plastic waste feedstock recycling has been so popular that from 1999 until now, the "International Symposium on Feedstock Recycling of Polymeric Materials (ISFR)" has been held in Japan (1999), Belgium (2002), Germany (2005), Korea (2007), China (2009), Spain (2011), and India (2013). The issues considered include mechanical and

chemical recycling, life cycle assessment, dehalogenation of plastics containing chlorine and bromine, various reactor designs such as rotary kilns and fluidized beds, and various heating methods such as microwave heating, molten baths and so on. Unfortunately, there is no golden rule that can be employed for optimizing the pyrolysis of all plastic species in a mixture because the optimal temperature for the degradation of one plastic polymer might be too low for another [9].

Catalysts (mostly zeolites) have been employed in order to improve the conditions of the pyrolysis to yield more useful products and lower the operation temperatures. Nevertheless, the produced oils require further processing in order to meet standard fuel qualities [10]. Various problems such as blockages caused by the production of unwanted products such as coke, waxes, and organic acids have been encountered. Another problematic issue is the thermal conductivity of plastics, which is low. Values as low as 0.17 and $0.33\ \mathrm{Wm^{-1}\,K^{-1}}$ have been reported for the thermal conductivity of polypropylene (PP) and polyethylene (PE), respectively [11, 12]. Although most of these problems have been overcome one way or another and some industrial-scale units are operational in the world today, in general, the scale of production is too small to make these processes economically viable. Political and environmental pressure obliges the continuation of such endeavors [13].

The ultimate/elemental analysis of mixed plastics has shown a carbon content of about 80% mass [14, 15]. Hence, another option for plastic waste treatment could be to target the production of solid and gaseous products instead of liquids. In recent years, there have been many studies that have aimed to do this. The authors have discussed the various methods of obtaining carbon nanotubes from plastic waste polymers in a detailed review elsewhere [16].

The present article will aim to give a literature survey of the studies pertaining to the production of porous carbons (in particular activated carbon) from plastic polymers. As far as the authors are aware, this is the first such review article. Activated carbons (ACs) are porous solids with desirable properties that include high thermal stability, high surface area, and high chemical resistance. The high surface area is produced by the numerous pore networks inside the material. It should be noted that the current IUPAC classification of pores is as follows [17]:

1. Micropore: pore width smaller than 2 nm
2. Mesopore: pore width between 2 and 50 nm
3. Macropore: pore width greater than 50 nm

The pore sizes and volumes are a function of various parameters including the precursor material, the pretreatment of the precursor prior to carbonization, the carbonization process itself, and the activation process carried out after or simultaneously with the carbonization. To date, a variety of materials have been used for AC production, including coals [18], bio and agricultural products [19–23], polymeric materials [24], tires [25], etc. [26]. At the moment, the use of coals and agricultural byproducts seem to be the most widespread industrial production paths [27]. Often, porous carbons investigated in research function better than the commercially available carbons [28, 29]. The economic analyses of AC plants are very sensitive to production yield and the activation route. In addition to plant capacity, another

important parameter in the cost of AC production is the availability and cost of its precursor [30].

This review will be organized on the basis of the plastic polymer used as the precursor for porous carbon production. Section 2 will include studies using various thermoplastics as precursors, whereas Sect. 3 will focus more deeply on poly (ethylene terephthalate) (PET) due to its popularity.

2 Porous Carbons from Various Plastic Precursors

2.1 Steam Activation

Activation with steam, also known as physical activation, has been employed for activated carbon production. Qiao et al. have used hot steam for the activation of PVC, which was prepared in the form of spinnable pitch [31]. The virgin plastics were first held at 260°C for 2 h and at 410°C for 1–2 h. The temperature of the second stage is not increased further because higher temperatures resulted in pitches with poor spinnability. A three-stage heat treatment (260, 360, and 410°C) was also tested but no particular difference was found. In the two-stage process, a weight loss of 58% is seen in the first significant step (200–320°C), which is attributed to the removal of HCl. It is interesting to note that this amount of recovered HCl is almost the same as the theoretical maximum amount of recoverable HCl from PVC (58.4%). The carbon content of PVC is approximately 43%, and the weight loss of the second step is approximately 23.2%, leaving only about 18.4% of the PVC as carbon to be used for AC synthesis. The pitch is spun and in turn stabilized in air without preoxidation treatment. The sample is carbonized at 900°C in the presence of air and finally activated with steam at 900°C for 30–90 min. The obtained activated carbons were predominantly microporous and had surface areas of 1,000–2,000 m^2/g. In relation to the various activation times, the final yields varied from 4 to 8% of the initial PVC mass. This value corresponds to a yield of 9–18% with respect to the actual carbon content of PVC. Finally, it should be noted that the PVC used in the study was virgin resin material rather than waste. The additives and inorganic substances present in PVC waste might make pitch spinning difficult.

2.2 Chemical Activation

To obtain high BET specific surface areas (S_{BET}, i.e., surface area divided by mass, as measured using the Brunauer–Emmett Teller method) for activated carbons from plastic polymers, chemicals such KOH and NaOH have been used either alongside [32] or after the carbonization step.

In a recent example, the syntheses of activated carbons from different synthetic waste polymers were tested [33]. PVC pellets of 1–3 mm were bought from a

Chinese supplier and PET was obtained from cutting water bottles into small pieces. A 50% solid yield of carbonized residue was claimed after the raw material was carbonized at 600°C in nitrogen. Then, the residue was activated by ground KOH (1:2 plastic to KOH mass ratio) in a nitrogen stream at 850°C. After 90 min of activation, a further burn-off of about 50% occurred. Then the products were washed and dried. These conversions would amount to a final yield of approximately 25%. If these numbers are accurate, they are exceptionally high. Unfortunately, the explanation of the AC preparation procedures published in the study is quite short. Most of the study was centered on the characterization and application of the products with maximum BET surface areas of 2,831 and 2,666 m^2/g for PET and PVC, respectively. It was speculated that this extremely high surface area is due to the uniform structure of the polymers as well as their small ash content. The adsorption capacities of the products for the remediation of wastewater were tested and it was concluded that in some cases they were more than twice that of the commercial F400 activated carbon. Table 1 contains information regarding the various samples in this study. Figure 1 shows the adsorption isotherms of methylene blue for these polymer-based activated carbons compared to commercial F400. Activated PET and activated PVC showed maximum removals higher than 2 mmol of pollutant per gram of adsorbent. Unfortunately regeneration studies have not been performed yet. The uptake of other liquid pollutants has been tested by the same group elsewhere [34].

PVC is a widely used plastic with a net calorific value of 22 MJ/kg and is used in long-life products such as window frames, flooring, fittings, door frames, and piping, which might not enter the waste stream for decades. PVC composed a little less than 7% of the municipal plastic waste collected in Western Europe in the year 2000 [1]. As an advantage in waste separation, the pieces of PVC are typically big, so their sorting is simple. Polystyrene (PS) and PVC both have an advantage when it comes to separation due to the difference in their densities compared to other plastics [35].

Various studies show that a two-stage heat treatment of PVC can be utilized in order to recover the chlorine content in the form of HCl. The remaining residue can then be used for other purposes such as porous carbon production and/or further volatilization [36]. As an example, the production of activated carbon from carbon residues has been investigated in conjunction with the removal of Cl from PVC containing plasticizer and inorganic filler [37]. After a heat treatment to remove the chlorine, the carbon residues were pre-oxidized at 300°C for 3 h under a flow of air. This was followed by a carbonization of 2 h at various temperatures under a flow of nitrogen. About 40–55% of the solid remained as carbonized residue (the difference in yield depends on the amount of plasticizer and inorganic filler used in the experiments). The material was then impregnated with KOH at various ratios, dried, and activated at 750°C in the presence of nitrogen for 1 h. The final yields after the activation were unfortunately not reported. When comparing the different samples, although the presence of the plasticizer and inorganic filler prolonged and hindered the evolution of HCl, they also improved the final AC product surface area.

Table 1 Properties of the waste polymers and produced activated carbons (elemental composition on a dry mass basis)

		Sample name					
		Tire rubber	Activated tire rubber	PVC	Activated PVC	PET	Activated PET
Elemental composition % (results from elemental analysis)	C	62.1	82.9	40	86.7	62	80
	H	6.7	2.01	5.36	1.31	5.2	1.76
	N	0.47	0.43	n/d	0.5	n/d	0.52
	O	5.4	2.66	17	6.12	32.8	16.6
	S	1.53	1.5	n/d	n/d	n/d	n/d
	Cl	n/d	n/d	21.4	n/d	n/d	n/d
Surface atomic composition % (results from XPS analysis)	C	–	87.5	–	95.4	–	77.6
	O	–	10.3	–	3.7	–	21.7
	Si	–	2.15	–	0.44	–	0.55
	Cl	–	0.07	–	0.05	–	0.12
	Sb	–	n/d	–	0.37	–	n/d
	Pb	–	n/d	–	0.06	–	n/d
Ash content (%)		–	23.8	10.5	16.2	5.37	0.12	1.17
Pore structure of the materials	S_{BET} (m²/g)	–	398.5	–	2,666	–	2831
	D_P (nm)	–	3.81	–	2.16	–	2.37
	V_{tot} (cm³/g)	–	0.38	–	1.44	–	1.68
	V_{micro} (cm³/g)	–	0.11	–	0.25	–	0.25
	V_{mes} (cm³/g)	–	0.27	–	1.19	–	1.43
	V_{mes}/V_{tot} (%)	–	71.1	–	82.6	–	85.1

Reconstructed from Lian et al. [33] Elsevier 2011

S_{BET} BET surface area, D_P pore size distribution, V_{tot} total pore volume, V_{micro} micropore volume, V_{mes} mesopore volume, n/d not detected

The presence of $CaCO_3$ as inorganic filler was particularly effective because it resulted in activated carbons with maximum surface areas above 1,700 m²/g [37].

Polyurethane foam has also been used as a precursor for AC production by chemical activation with K_2CO_3, and a maximum BET surface area of about 2,800 m²/g has been obtained. It is speculated that K_2CO_3 plays a large role in creating the high obtained surface area [38]. The use of K_2CO_3 seems particularly attractive because it does not pose a hazard. The role of K_2CO_3 in chemical activation using KOH has been recently studied elsewhere [39].

Refuse paper and plastic fuel (which is a mixture of old paper and plastic with a ratio in the range of 3:7 to 7:3) has also been used to produce porous materials consisting of activated carbon and amorphous $CaO–Al_2O_3–SiO_2$ [40]. Both physical activation with wet N_2 (20 mol% steam) and chemical activation with K_2CO_3 were tested. Chemical activation resulted in higher BET surface areas (as high as

1,330 m^2/g) and lower ash content ($\leq$28 mass%). Physical activation resulted in BET
surface areas of approximately 500 m^2/g with a higher ash content ($\leq$45 mass%).
Although the samples created by both activation methods showed potential
multisorption properties for heavy metals, the chemically activated samples showed
higher sorption capacity for organic dye, while the physically activated samples
were favorable for removal of heavy metals and oxyanions. The pore sizes of both
samples were relatively small as compared to the size of the methylene blue
(MB) molecule [41].

3 Porous Carbons from PET

Poly(ethylene terephthalate) (PET) is used for bottles, carpets, and food packaging
and is a very common waste polymer. It comprises 11.7% of the municipal waste
plastic in Western Europe. Due to the fact that over 90% of all PET is used in
packaging (in particular drink bottles because of its gas barrier characteristics) the
majority of PET becomes waste within less than a year of production [1]. This
plastic is commonly seen in studies attempting to derive porous carbons from
plastic wastes due to the relatively higher residue that remains after its pyrolysis.
A complete section in the review is allocated to PET due to its relative popularity
for AC production.

The production of porous carbons is certainly not the only way of treating PET
waste. Other recycling methods such as alcoholysis, hydrolysis, and glycolysis have
been considered. Glycolysis is the oldest and simplest chemical recycling method
for PET. With this technique, glycols are inserted into PET chains in order to obtain
bis(hydroxyethyl) terephthalate (BHET), which is itself a substrate for the synthesis
of various oligomers including PET. The main drawback of this method is the
formation of various products along with BHET of higher oligomers, which are
difficult to purify. Alcoholysis (which usually employs methanol) has the

noticeable disadvantage of methanol volatilization; and hydrolysis (which is done under acidic or alkali conditions) results in corrosion and pollution problems [41].

There are a wide range of studies that investigate the production and utilization of activated carbons derived from PET [42–47]. The production of activated carbons from blends such as coal/pitch and PET [48, 49], as well as the preparation of porous polyester fiber by using supercritical carbon dioxide, have also been studied [50].

In contrast to the studies mentioned previously, there has also been an investigation of the use of PET in conjunction with fly ash [51]. Although fly ash has the potential of being used in wastewater treatment its adsorption capacities are limited. Furthermore, the heavy metals within the ash might leach out and cause additional problems. By melting and blending waste PET bottles with fly ash, followed by subsequent thermal treatment, various adsorbents were produced that favorably restricted metal leaching. These were tested for removal of methylene blue and heavy metals from solution. It was speculated that after acid treatment, these adsorbents could ultimately be used for treatment of wastewater from dye processes, steel mills, mine factories, and electroplating plants. The BET surface area of these low-cost adsorbents was no more than 485 m^2/g [51].

Due to the use of heavy metals as catalysts during the synthesis of PET bottles, there are concerns regarding human expose (in particular by the leaching of antimony into drinking water) [52]. Nonetheless, if plastic bottle manufacturers consider the contamination during the manufacturing process and wash the bottles before their first use, the degree of exposure to these contaminants will be reduced [53]. The presence of small amounts of antimony oxides has been detected in PET pyrolysis studies. The presence of antimony can also slightly decrease the decomposition temperature [54].

3.1 Steam Activation

In the 1990s, several studies attempting to produce ACs from PET emerged. ACs produced from PET and cellulose sheets with BET surface areas of 1,190 and 780 m^2/g, respectively, were compared and contrasted [55]. First, the materials were carbonized at 700°C in the presence of nitrogen. Although unfortunately the carbon yield was not reported, judging from other similar studies by the same authors it can be predicted to be about 20% [56]. The carbonized chars were subsequently activated with steam diluted with nitrogen (1:1 ratio) at 900°C until a burn-off of 50% related to the mass of the char was obtained. Based on other studies, the final yield compared to the initial amount of PET was 9–12%. The details of the yields can be seen in Table 2. The researchers went on to investigate the adsorption of a binary benzene–methanol liquid mixture and concluded that morphological differences exist in the ACs that correspond to the different links between their crystallites [55].

László and coworkers conducted more studies regarding the production of porous adsorbents from PET in the following years [57]. The samples were first

Table 2 Yields after treatment, relative to initial carbonaceous precursors

Precursor	Carbonization (wt%)	Activation (wt%)
Polyacrylonitrile	48–52	26–31
PET	17–21	9–12
Cellulose	17–22	11–14

Reproduced with permission from László et al. [56] Elsevier

carbonized under nitrogen flow at 750°C for 30 min, and then activated at 900°C under steam and nitrogen flow (1:1 molar ratio) for 90 min [58]. Microporous carbons were produced with BET surface areas of 1,170 m^2/g, a total pore volume of 0.625 cm^3/g, an amphoteric surface (due to oxygen functionalities), and with a majority of basic functional groups. The adsorption of phenol and 2,3, 4-trichlorophenol were studied at various pH values. It was found that both the pH and pK of the phenols affect the adsorption mechanism. The final yield was 9–12%. The researchers proposed that these carbons could be used for wastewater treatment because, although the majority of their pores were micropores, a sufficient amount of mesopores were also available, which play a vital role for the diffusion of the pollutants into the sample [59]. The same preparation and activation method for PET was used by the researchers in a later study [60]. The researchers concluded that the surface properties and morphologies of the carbonaceous products are dependent on the heat treatment method as well as the temperature applied for their preparation. Surprisingly, the porosity and surface areas were found to decrease as the temperature and heat treatment increased. This is because the pore structure showed a gate effect and the open pores closed during heat treatment. As temperatures rises, however, the carbon skeleton becomes much more ordered.

In a later study, additional treatment was carried out on the porous products from PET [61]. The samples were treated with nitric acid to obtain various degrees of surface functionalization. Additional heat treatment was also sometimes incorporated for modification and distribution of some surface functional groups. Overall, various porous carbons with BET surface areas of 1,200–1,500 m^2/g were obtained. Buffered aqueous phenol and aniline solutions were used to assess the waste removal capacity of the products. It was seen that the concentration of the pollutant molecule was always more than that of the functional groups, meaning that "the major contribution to the adsorption came from the dispersion effect" and that "the enhancement of the interactions was obtained only through attractive electrostatic forces" [61]. Various differences were seen between phenol and aniline. For example, phenol adsorption showed a maximum peak, whereas aniline adsorption strongly increased monotonically with pH. The maximum uptake of phenol was higher than that of aniline. In addition, the lower solubility of aniline in water did not lead to increased adsorption capacity. Complementary techniques and analysis of the porous carbons was carried out elsewhere [62]. Surface oxygen content was not greatly increased due to acid treatment at room temperature and the adsorption properties and structural parameters remained unchanged. Nevertheless, treatment with boiling acid resulted in significant differences in morphology, leading to approximately 75% loss of BET surface area.

Further examination of phenol adsorption by such porous carbons was carried out [63]. Both adsorption and desorption of phenol were seen to be influenced by not only the pH of the solution, but also by the method of pH setting. The thermal regeneration of the carbon adsorbents was studied and it was found that with unbuffered solutions, only a part of the surface area could be regenerated. If NaOH is used for regeneration, the surface area of the carbons will significantly increase; and when physisorption is dominant no substantial variation in the surface area is observable. It is noteworthy that surface oxidation lessens the adsorption capacity for phenol and favors physisorption. Carbon deposition and subsequent pore blocking during thermal regeneration are also reduced when high concentrations of surface acidic groups are present.

3.2 Chemical Activation

The combination of chemical activation (heat treatment by sulfuric acid) and physical activation (by steam) has been investigated [64]. The impregnation coefficient of 28% was found to be particularly important. An increase in the activation temperature enhanced the surface area and pore volume in addition to increasing burn-off. With a yield of 15%, a maximum BET surface area of approximately 1,000 m^2/g was obtained. The adsorption of methylene blue and iodine were also examined. The effects of soaking the PET precursors with chemicals (in particular sulfuric acid) have also been investigated elsewhere [65, 66].

In studies by other researchers, compounds such as $Ca(OH)_2$ and $Ca(NO_3)_2$ together with HNO_3 treatment have been used to produce better quality ACs [67]. Nakagawa et al. used a mixture of several metal salts (5 wt%) and acid pretreatment (HCl for 24 h) prior to steam activation and discussed the effects of the various mixtures on the pore properties [68]. The samples showed a larger mesoporosity than carbons with no such pretreatment. Although the mesopores were dependent on the kind of metal salt used, the microporous structure was not influenced by this factor. Compared with commercial carbon, these samples show better adsorption capacity for C_4H_{10}. The details of the various prepared samples can be seen in Table 3. It should be noted that the values reported for "burn-off" are relative to the chars produced from prior pyrolysis of the PET at 773 K for 1 h under nitrogen flow. So, in fact, the final yields compared to the initial waste material are much less [68]. In addition to PET, the researchers applied their method to waste tires, refuse-derived fuel, and waste generated during lactic acid fermentation from garbage [69]. The surface of PET-derived adsorbents had a fairly strong hydrophobic nature. Phenol and Black5 adsorption were tested and it was concluded that the adsorption capacities of the samples are comparable to commercially available activated carbon and that these porous carbons are suitable for the adsorption of bulky molecules in aqueous solutions.

Increasing the hydroxide content in the treatment often increases the micropore volume and the formation of mesopores, while an increase in nitrogen flow enhances ultramicropore volume and homogenous porosity, yielding molecular

Table 3 Properties of prepared porous carbons from the mixing of PET pellets with 5% metal compounds, followed by acid treatment and subsequent steam activation

Chemical	Activation time (min)	Burn-off (wt%)	S_{BET} (cm^2/g)	V_{mic} (cm^3/g)	V_{mes} (cm^3/g)
None	0	12.5	394	0.21	0.04
	5	12.7	456	0.24	0.06
	120	68.7	1,450	0.72	0.13
	240	77.8	1,740	0.93	0.15
Ca(NO$_3$)$_2$·4H$_2$O	0	13.2	396	0.20	0.04
	5	18.0	521	0.25	0.08
	150	63.7	1,460	0.66	0.27
	180	85.7	2,190	0.81	0.90
Ca(OH)$_2$	0	25.0	419	0.21	0.07
	5	29.4	495	0.23	0.08
	150	60.6	1,200	0.55	0.19
	180	81.0	1,960	0.86	0.50
CaCO$_3$	0	14.4	421	0.22	0.09
	5	20.7	446	0.23	0.05
	150	57.1	1,170	0.59	0.14
	240	87.5	2,180	0.93	0.78
ZnO	0	13.9	416	0.20	0.09
	5	20.5	459	0.25	0.05
	1,150	61.6	1,240	0.66	0.16
	240	85.9	2,240	1.10	0.87
AlNH$_4$(SO$_4$)$_2$·12H$_2$O	0	15.6	370	0.17	0.03
	5	23.3	493	0.27	0.04
	150	63.5	1,220	0.66	0.11
	240	85.1	2,080	0.82	0.61

Reproduced with permission from Nakagawa et al. [68] Elsevier

S_{BET} BET surface area, V_{mic} micropore volume, V_{mes} mesopore volume

sieves. An increase in the pyrolysis temperature while other parameters remain constant increases the micropore volume [70]. Plasma pretreatment of PET with a microwave apparatus prior to carbonization showed positive results, which could help reduce the need for a subsequent activation step [71]. The use of these carbons as electrode material in supercapacitors has also been investigated by the group of researchers [72].

Parra and coworkers also focused on the production of porous carbons from PET [73, 74]. Sometimes, the surfaces of the produced activated carbons do not have enough strength for particular adsorbate–adsorbent interactions. When facing such a problem, it is possible to modify the chemistry by incorporating heteroatoms such as nitrogen on the AC. As an example, PET from soft-drink bottles was compounded with different functionalities, namely acridine, carbazole, and urea. PET and the N-compound were mixed and stirred (1:1 ratio) in a solution of water containing KOH. Then, the slurry mixture was vacuum-dried overnight followed by heating up to a 30-min carbonization at 500°C. Secondary interactions and

reactions occur during the carbonization, which incorporates nitrogen into the carbonized material. This alteration significantly influences pore structure and pore size. The researchers went on to examine how the adsorption of CO_2 is affected by this nitrogen enrichment. Results showed moderate effectiveness, and indicated that in addition to the surface area and the nitrogen content, the nature of the N-functionalities is important [75]. Modification of activated carbon from PET by urea impregnation and pyrolysis has shown an increase in the mean pore size, total pore volume, and the point zero charge. By contrast, sodium hydroxide treatment reduced the total pore volume and mean pore size of PET-based activated carbons. This was not the case for cork-based or other activated carbons [76].

3.3 Carbon Dioxide Activation

Almazán-Almazán et al. attempted to change the textural properties of activated carbons from PET by controlling various variables and showed that these carbons can be tailored to range from molecular sieves to samples with variant pore sizes and high adsorption volume [70]. Chars were obtained after pyrolysis at 800 and 950°C with 19% yield. Subsequent activation under CO_2 flow took place for 4 or 8 h. The activation resulted in further burn-offs of 81–87%. In the carbonization process at 800°C under carbon dioxide, the amorphous carbon is eliminated but the micropore system is not affected. These porous samples show molecular sieve behavior for cyclohexane/benzene as well as 2,2-DMB/benzene pairs. At 950°C, however, micropore textural characteristics are changed and the samples do not exhibit molecular sieve behavior due to constrictions at the entrance of the micropores [77].

Porous materials with high capacities have been proposed for the storage of gases such as hydrogen, methane, and carbon dioxide. In gas storage, the gaseous molecules accumulate in the pores of the sorbent material. Various adsorbents have been developed and tested. Studies show high dependence on the surface area, porosity, and pore-size distribution. Regardless of which type of adsorbent is used, the following characteristics are favorable [78]:

1. The adsorbent should be composed of light elements
2. The adsorbent should have high stability under working conditions
3. The adsorbent should be chemical inert – especially towards the adsorbed gas
4. The density of the material should be high as to avoid undesirable large volumes

High hydrogen uptake, equal to that of other high-technology carbon materials, is possible with the ACs produced from PET. In a particular study, PET waste was first pyrolyzed in a quartz tube reactor to yield around 20% char. Further activation was carried out under a CO_2 flow of 10 mL/min at 925°C [79]. Samples with different activation degrees were obtained and denoted as PC#, where # is a number showing the percentage of burn-off resulting from activation (PC12, PC35, PC58, and PC76). Although the samples were not highly ordered structures, XRD analysis showed that elongation of the activation process (and thus additional burn off) increased the

Table 4 BET surface areas of various samples as well as adsorption capacities obtained from phenol and naphthalene breakthrough curves

Sample[a]	BET surface area (m²/g)	Adsorption capacity (mg/g)	
		Phenol[b]	Naphthalene[c]
PC12	668	125	24
PC35	1,405	200	26
PC58	1,920	239	27
PC76	2,468	291	28
Q	1,149	289	30
CM	849	263	24
F400	1,164	346	33

Reproduced with permission from Parra et al. [79] Elsevier
[a]PC12, PC35, PC38, and PC58 are PET-derived porous carbons of increasing degree of activation (see text). Q, CM, and F400 are three commercially activated carbons
[b]Solution of phenol (2,000 ppm)
[c]Saturated solution of naphthalene (30 ppm)

crystallographic parameters of the crystallites to some extent. This could be due to two reasons: first, the disordered fraction of the carbon is more liable to destruction during activation because it is more reactive; and second, the longer activation time may cause some ordering to take place. The hydrogen adsorption capacities of the samples were studied in the 0–1 bar pressure range and showed reversible physisorption in all samples. The maximum hydrogen uptake (2.3%) was by the PC76 sample at $-196°C$. The adsorption seems non-dissociative since no hysteresis is seen in the uptake–release process. It is thought that higher hydrogen adsorption is observed in samples with more activation due to their increased volume of micropores [80]. The BET surface areas of various samples, as well as adsorption capacities obtained from phenol and naphthalene breakthrough curves, can be seen in Table 4 (Q, CM, and F400 are three commercially activated carbons). Figure 2 shows the correlation of H_2 adsorption capacity with surface area and the volume of the micropores. Figure 3 is a depiction of the pore size distribution of the samples with an increase in heat treatment/burn-off [79].

Parra and coworkers also investigated the removal of the widely used drug ibuprofen using such activated carbons [81]. For adsorption of ibuprofen, the existence of mesopores is vital for accessibility to the inner porosity. In addition, the microporosity must be large enough for the compound molecule. The PET porous carbons outperformed the adsorption capacity of commercial activated carbons for the targeted drug. However, the adsorption kinetics were much slower due to the lack of enough mesopores to establish an internal transport network in the adsorbent (less than 10%). Nonetheless, high ibuprofen uptake was achieved over a longer pH range by the PET-derived carbons than by commercial adsorbents. This is linked to the basicity of the PET-derived carbons, due to the delocalized π electron density of their graphene layers, which may act as Lewis base sites for adsorbing protons [82].

Fig. 2 Correlation of H_2 adsorption capacity with surface area and the volume of the micropores (W_0). Reproduced with permission from Parra et al. [79] Elsevier
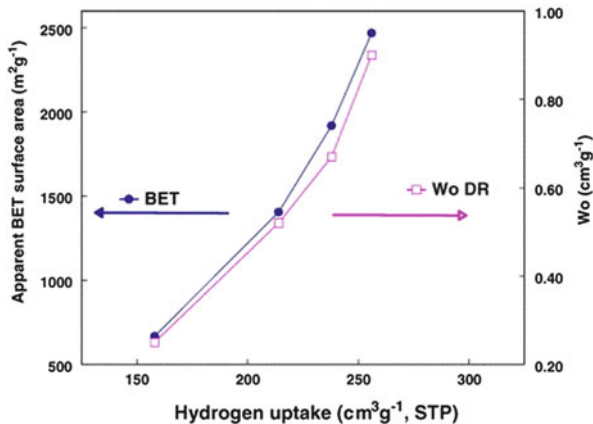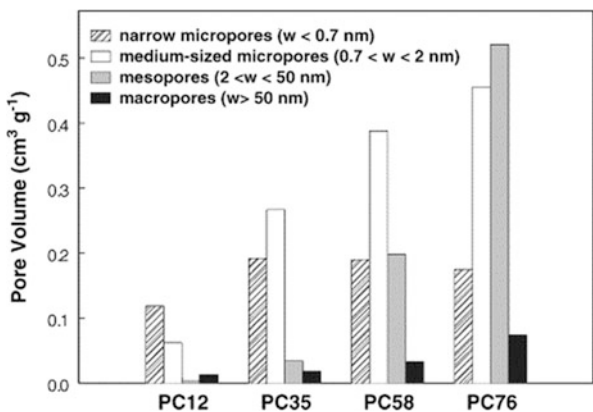

Fig. 3 Pore size distribution of PET-derived porous carbon samples with the increase of heat treatment/burn-off. Sample number indicates the percentage of burn-off resulting from activation: *PC12*, *PC35*, *PC58*, and *PC76* signifying 12, 35, 58 and 76% respectively; *w* pore width. Reproduced with permission from Parra et al. [79] Elsevier

The Iranian team of Esfandiari and coworkers has also investigated activated carbon production from PET [83]. Carbon dioxide activation was used and the effects of variables such as temperature, heating rate, flow rate, and duration of heat treatments were investigated. It was observed that the most influential parameters are the activation time, activation temperature, and carbonization time. At the expense of further burn-off, the iodine number of the sample was seen to increase with elongation of the activation time. The experimental values for the iodine number were in good agreement with those obtained by the Taguchi optimization model [84].
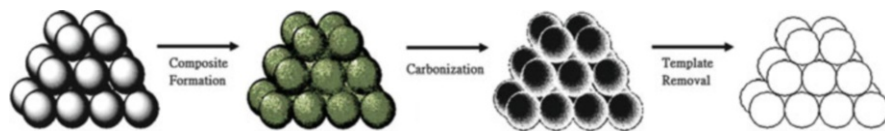
Fig. 4 Illustration of hard template method for porous carbon production. Modified and adapted with permission from [86] Copyright 2011 American Chemical Society

4 Hard Template Method

Producing porous carbons from templates has a general three-step procedure. First, a composite is produced from the carbon precursor and the template. Then, the mixture is carbonized. Finally, the template is removed [85]. A schematic of the hard template method is provided in Fig. 4.

A good review has already been published on the production of porous carbons by mixing carbonaceous precursors with MgO precursors, subsequent carbonization, and the dissolution of the MgO substrate by a diluted acid [87]. The carbon precursors included (but were not limited to) thermoplastics such as poly(vinyl alcohol) and PET. Even though there is no classic "activation" method used in this process, BET surface areas as high as $2{,}000\,\mathrm{m}^2/\mathrm{g}$ and large pore volumes as high as 3 mL/g are obtainable. Interestingly, as can be seen from Fig. 5, the ratio of MgO to precursor does not affect the yield when poly(vinyl alcohol) or hydroxyl propyl cellulose is used as the carbon source. Porous carbon yield from PET is dependent on the mixing ratio.

In addition to the fact that the resulting materials are obtained in powder form, the following four advantages have been distinctly mentioned for this method:

1. The MgO template is easily removable with a non-corrosive acid
2. The MgO is recyclable
3. Although the arrangement of mesopores in carbon is random, the size and volume of the mesopores in the porous carbon can be tuned by adjusting the MgO precursor
4. Various carbon precursors can be selected for tuning the size and volume of resulting micropores

These porous carbons, referred to as MgO-templated carbons, have been applied in various areas such as electrodes for electric double-layer capacitors [88], as absorbents for gasoline, and as anodes for lithium ion batteries. The application of these MgO-templated porous carbons has been reviewed elsewhere in Japanese [89].

The use of polystyrene-based materials has also been investigated for porous carbon formation with the hard template method using amorphous silica gel, mesoporous alumina, and microporous zeolites as inorganic templates [90].
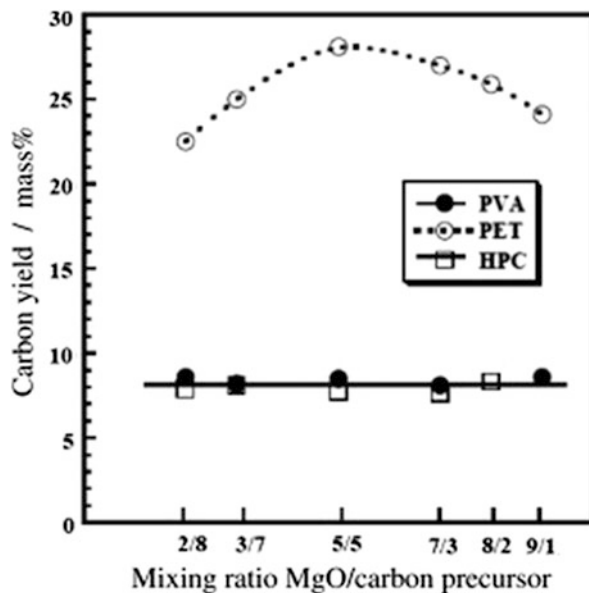
5 Outlook and Future Prospects

Low production yields seem to be the main hindrance to the feasibility of producing porous carbons from plastics. Lower pyrolysis temperatures do give higher yields of solid amorphous products; however, these carbons require further high-temperature processing for activation, which would in turn cause additional burn-off [3] [31]. In addition, the residues from plastic waste pyrolysis often leave behind inorganic impurities and additives. Hence, using them to produce solid products such as activated carbons might incur further problems. With calorific values of about 20 MJ/kg, it has been suggested that these solid residues be used as fuels on a par with brown coal [91]. If the low yields of the process are not to cause concern, the justification would lie in looking at porous carbon products as "byproducts" alongside the simultaneous production of other gaseous and/or liquid products with heat. Only is such a condition would low solid porous carbon yields be economically attractive.

Another option would be to employ an alternative method for plastic carbonization that would overcome the problem of low yields posed by classic carbonization and activation methods. A possible route would be the employment of pressurized pyrolysis. For purposes other than activated carbon production, hydrocarbon precursors have been heated under pressure to produce solid carbon products with high yields and high purity [92–94]. As an example, exceptionally hard carbon microspheres have been produced from PET waste via the closed autoclave method. This autogenic method has been patented for the production of carbon spheres for use in batteries [95]. Pol et al. further explained their method in a more extensive article [96]. In order

to overcome the problems associated with the separation of various plastic types, Pol et al. evaluated the process for mixed polymers, namely low density polyethylene (LDPE), high density polyethylene (HDPE), poly(ethylene terephthalate) (PET), and polystyrene (PS). Most of the break down is presumed to occur between 600 and 700°C. The conversion of the plastics to solids in this study resulted in yields ranging from 30 to 55%, with 40% being characteristic. The plastic polymers in this particular study (which were processed together) account for more than three quarters of all plastics found in municipal solid waste. The high-pressure processing of combined plastics is particularly favorable because in plastic recycling it is difficult to obtain homogeneous streams from household waste due to their variety. One of the main obstacles is the existence of food contamination on lightweight plastics. Due to energy requirements, it is often not justifiable both economically and environmentally to clean and recycle such plastics. That is why almost all selective collection schemes in the EU for household waste plastics focus on bottles that are mostly composed of PET and HDPE [1]. Also, the obtained solid yields of high-pressure pyrolysis are particularly important because plastics such as LDPE and HDPE normally produce very minute amounts of solids under atmospheric carbonization. Furthermore, high pressure pumps/compressors are not required in the proposed high-pressure system. This is because the utilization of an autoclave can lead to high pressures just by containing the gases evolving during the break down of the polymers. The economic importance of this phenomenon should not be overlooked. Nonetheless, the main obstacle of such high pressure systems is the capital cost of high pressure equipment, including the alloy that the reactor must be constructed from.

As early as the 1970s, Inagaki et al. considered the pressure pyrolysis of plastic products[97]. Generally, when pressures are applied to the evolved gases during the reaction of a precursor, the carbonization behavior changes and the carbon products are different from those obtained without pressure. The differences can be seen in the structure, properties, and even the morphology of the residue carbon particles. It is important to note that although the solid yield is increased for all carbonaceous precursors, the magnitude of the increase is dependent on the precursor material. Again, it was shown that although the atmospheric pyrolysis of PE does not leave behind significant residues under atmospheric heat treatment, considerable solid yields are obtained under pressure. When powder mixtures of PE with the addition of a smaller mass percentage of PVC (5–30%) were carbonized in a gold tube under a pressure of 10–30 MPa, solid yields as high as 45% were obtained [98–100]. The process is also applicable when polypropylene (PP) is used to replace PE. When a specially designed autoclave is used instead of a gold tube, the yield falls to about 30% [101]. The effects of some impurities on the residue product in a pressurized method have also been studied [102].

If the temperatures and pressures of the pressurized carbonization are not high enough, less solids will emerge and a high amount of liquid will be obtained [103]. With higher pressure, the carbon number distribution of products shifts to lower molecular weights. At lower temperatures, the co-pyrolysis of plastics has been shown to produce different products compared to when individual polymers

Table 5 Solid carbon yields after treatment for various durations and temperatures

	Treatment conditions							
	500°C, 3 h	600°C, 3 h	650°C, 0 h	650°C, 0.5 h	650°C, 1 h	650°C, 2 h	650°C, 3 h	650°C, 9 h
Carbon yield (wt%)	23.8	27.0	13.0	22.7	33.5	42.1	45.4	47.5

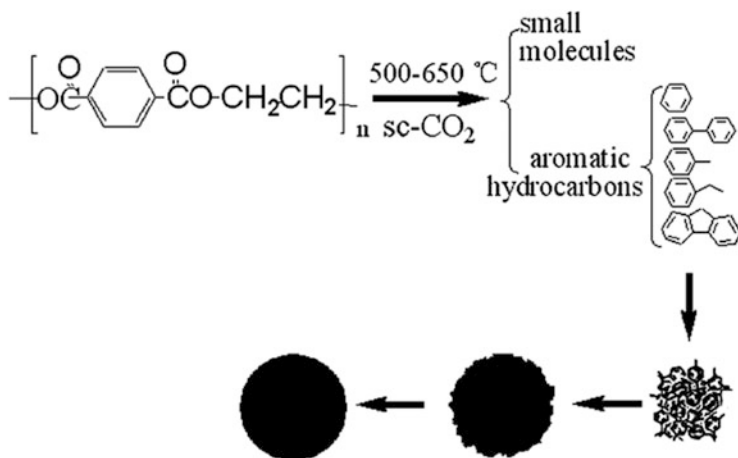Reprinted with permission from Wei et al. [105]. Copyright 2011 American Chemical Society

Fig. 6 Solid carbon yields after treatment for various durations and temperatures. Reconstructed from Wei et al. [105]. Copyright 2011 American Chemical Society

are used. Aromatic compounds are speculated to have a role in increased char formation due to the condensation of the aromatic ring structure [104].

Adding CO_2 into an autoclave system to create supercritical conditions has also been considered. Soft-drink PET bottles were used as precursors and 1.5 g of the PET cut foil was placed inside a 25-mL stainless steel autoclave alongside 12 g of solid CO_2. The mixture was kept at 350–650°C for 3 h under autogenic pressures, prior to being naturally cooled to room temperature, washed, filtered, and dried. As can be seen in Table 5, the yield increased with reaction time and temperature. At a temperature of 650°C, the carbon yield increased from 22.7 to 45.4 as reaction times increased from 30 min to 3 h. At a temperature of 500°C, the yield stood at 23.8 after 3 h. Elemental analysis showed that the PET sample (61.73% carbon prior to reaction) contains 93.15% carbon after 3 h reaction at 650°C. Figure 6 shows the formation mechanism. When no dry ice was used (1 g PET/16.67 cm^3), a coke cake rather than carbon spheres was obtained. Increasing the amount of PET (g PET/cm^3) resulted in formation of carbon spheres. The researchers indicated that when the PET precursor is smashed into a powder (and not used as a foil), then multiple conglomerates of irregular carbon spherules appear with larger BET

surface areas (values not reported). Unfortunately, obtaining a larger BET surface area is only passingly mentioned by the researchers but not fully explored [105].

The hopes of generating pores in solid carbon spheres formed under pressure seems to be a valid supposition because other non-porous carbon spheres have been successfully activated previously, showing large increases in specific surface areas [106, 107]. As an example, Yuan et al. [108] were able to activate hard carbon spheres with initially low surface areas in molten KOH at 600°C for 1–2.5 h. Measurements showed that depending on the KOH/carbon ratio, the specific surface areas could increase to more than 1,100 m^2/g. Elsewhere, solid carbon spheres derived from glucose have been activated with KOH, resulting in a 100-fold increase of their surface area from 13.9 to 1,283 m^2/g [109]. Meanwhile, although some other researchers have failed to increase the BET surface area from low surface area carbon spheres, they were nevertheless able to achieve satisfactory adsorption of compounds during experimentation [110].

The use of various pretreatments of the plastic wastes such as chemical soaking, heat treatments, microwave, and plasma treatments, etc. in conjunction with the pressurized method might be attractive areas for future research. Co-pyrolysis with other wastes such as food wastes is also plausible. Much work has been carried out on other pressurized carbonization methods such as biomass hydrothermal carbonization [111, 112]. If an industrial process is to emerge from the research, the combined use of various carbon sources would be attractive for economy-of-scale purposes. Producing porous carbons for further applications from plastic wastes would not only yield useful products from cheap precursors, but it would also help reduce the problems associated with the ever-growing plastic waste stream.

Overall, not many studies utilizing the pressurized method for treating plastic wastes have exclusively focused on the production of porous carbons with high surface areas [113, 114]. Recently, one research group has reported the production of porous carbons and porous carbon composites using a high temperature, high pressure system [115]. The only other study that has addressed the issue of porous carbon production via a high pressure system is in the Chinese language [116]. In the study, SBA-15 was used alongside a surfactant that acted both as a soft template and carbon source. A carbon/silica composite was produced under high pressure, followed by the removal of the silica using H_2O, ethanol, and NaOH. The final product was highly mesoporous with a narrow pore size distribution.

6 Conclusion

Activated porous carbon can be created from plastic wastes by using various activation routes. The ACs can have high BET surface areas, pore volumes, and good adsorption capacities. However, the carbon yields are rather low (usually around 10%). Large volatilization and burn-off under vacuum, atmospheric, and moderate pressure pyrolysis conditions makes the production of AC from plastics less attractive. Nonetheless, coupling AC production from plastic wastes with other processes such as the production of liquid fuels and high calorific value gases could

be helpful in achieving better economic feasibility. Such research is greatly in line with the goals of waste reduction and sustainability.

On the other hand, if only solid carbon products are sought, high pressure pyrolysis could potentially be used. Although hard non-porous spheres have been repeatedly produced by this method, further research is needed to assess the possibility of obtaining porous carbons. The lack of diverse literature regarding the use of plastic wastes as precursors of autogenic methods leaves the door open for further investigations.

References

1. ACCR (2004) Good practices guide on waste plastics recycling: a guide by and for local and regional authorities. Association of Cities and Regions for Recycling, Brussels
2. PlasticsEurope (2012) Plastics – the facts 2012. PlasticsEurope, Association of Plastics Manufacturers, Brussels
3. Williams PT (2006) Yield and composition of gases and oils/waxes from the feedstock recycling of waste plastic. In: Scheirs J, Kaminsky W (eds) Feedstock recycling and pyrolysis of waste plastics: converting waste plastics into diesel and other fuels. Wiley, Chichester, pp 285–314
4. Zia KM, Bhatti HN, Bhatti IA (2007) Methods for polyurethane and polyurethane composites, recycling and recovery: a review. React Funct Polym 67(8):675–692
5. Howard GT (2002) Biodegradation of polyurethane: a review. Int Biodeterior Biodegradation 49(4):245–252
6. Al-Salem SM, Lettieri P, Baeyens J (2009) Recycling and recovery routes of plastic solid waste (PSW): a review. Waste Manage 29(10):2625–2643
7. Nnamchi CI, Obeta JAN, Ezeogu LI (2006) Isolation and characterization of some polycyclic aromatic hydrocarbon degrading bacteria from Nsukka soils in Nigeria. Int J Environ Sci Technol 3(2):181–190
8. Kumar S, Panda AK, Singh RK (2011) A review on tertiary recycling of high-density polyethylene to fuel. Resour Conserv Recycl 55(11):893–910
9. Buekens AG, Schoeters JG (1998) Technical methods in plastics pyrolysis. Macromol Symp 135(1):63–81
10. Blaszo M (2005) Pyrolysis oils of plastic wastes. In: Müller-Hagedorn M, Bockhorn H (eds) Feedstock recycling of plastics. Selected papers presented at the third international symposium on feedstock recycling of plastics, Karlsruhe, Sept, 2005. Universitätsverlag Karlsruhe, Karlsruhe, pp 11–17
11. Grause G, Buekens A, Sakata Y, Okuwaki A, Yoshioka T (2011) Feedstock recycling of waste polymeric material. J Mater Cycles Waste Manag 13(4):265–282
12. Ranzi EM, Dente M, Faravelli T, Bozzano G, Fabini S, Nava R, Cozzani V, Tognotti L (1997) Kinetic modeling of polyethylene and polypropylene thermal degradation. J Anal Appl Pyrolysis 40–41:305–319
13. Buekens A (2006) Introduction to feedstock recycling of plastics. In: Feedstock recycling and pyrolysis of waste plastics: converting waste plastics into diesel and other fuels. Wiley, Chichester, pp 3–41
14. Ding W, Liang J, Anderson LL (1997) Hydrocracking of waste plastics to clean liquid fuels. ACS Division Fuel Chem Preprints 42(4):1008–1010
15. Cho M-H, Jung S-H, Kim J-S (2010) Pyrolysis of mixed plastic wastes for the recovery of benzene, toluene, and xylene (BTX) aromatics in a fluidized bed and chlorine removal by applying various additives. Energy Fuels 24(2):1389–1395

16. Bazargan A, McKay G (2012) A review – synthesis of carbon nanotubes from waste plastics. Chem Eng J 195–196:377–391

17. Mays TJ (2007) A new classification of pore sizes. In: Llewellyn P, RodríguezReinoso F, Rouqerol J, Seaton N (eds) Studies in surface science and catalysis, vol 160. Elsevier, Amsterdam, pp 57–62

18. Rafsanjani HH, Jamshidi E (2008) Kinetic study and mathematical modeling of coal char activation. Chem Eng J 140(1–3):1–5

19. Keypour J, Haghighi Asl A, Rashidi A (2012) Synthesis of hybrid nano-adsorbent for separation of hydrogen from methane. Chem Eng J 183:510–514

20. Valix M, Cheung WH, Zhang K (2008) Role of chemical pre-treatment in the development of super-high surface areas and heteroatom fixation in activated carbons prepared from bagasse. Micropor Mesopor Mater 116(1–3):513–523

21. Cerino-Córdova FJ, Díaz-Flores PE, García-Reyes RB, Soto-Regalado E, Gómez-González R, Garza-González MT, Bustamante-Alcántara E (2013) Biosorption of Cu(II) and Pb(II) from aqueous solutions by chemically modified spent coffee grains. Int J Envir Sci Technol 10(3):611–622

22. Saka C, Şahin O, Küçük MM (2012) Applications on agricultural and forest waste adsorbents for the removal of lead (II) from contaminated waters. Int J Environ Sci Technol 9(2):379–394

23. Zhu Y, Zhang H, Zeng H, Liang M, Lu R (2012) Adsorption of chromium (VI) from aqueous solution by the iron (III)-impregnated sorbent prepared from sugarcane bagasse. Int J Environ Sci Technol 9(3):463–472

24. Fallah RN, Azizian S (2012) Rapid and facile desulphurization of liquid fuel by carbon nanoparticles dispersed in aqueous phase. Fuel 95(1):93–96

25. Mui E, Ko D, McKay G (2004) Production of active carbons from waste tyres – a review. Carbon 42(14):2789–2805

26. Stavropoulos GV (2005) Precursor materials suitability for super activated carbons production. Fuel Process Technol 85:1165–1173

27. Alcañiz-Monge J, Illán-Gómez MJ (2008) Modification of activated carbon porosity by pyrolysis under pressure of organic compounds. Adsorption 14(1):93–100

28. Mahvi AH (2008) Application of agricultural fibers in pollution removal from aqueous solution. Int J Environ Sci Technol 5(2):275–285

29. Hussein M, Amer AA, Sawsan II (2008) Oil spill sorption using carbonized pith bagasse: trial for practical application. Int J Environ Sci Technol 5(2):233–242

30. Stavropoulos GG, Zabaniotou AA (2009) Minimizing activated carbons production cost. Fuel Process Technol 90(7–8):952–957

31. Qiao W, Yoon SH, Korai Y, Mochida I, Inoue SI, Sakurai T, Shimohara T (2004) Preparation of activated carbon fibers from polyvinyl chloride. Carbon 42(7):1327–1331

32. Almazán-Almazán MC, Pérez-Mendoza MJ, López-Domingo FJ, Fernández-Morales I, Domingo-García M, López-Garzón FJ (2007) A new method to obtain microporous carbons from PET: characterisation by adsorption and molecular simulation. Micropor Mesopor Mater 106(1–3):219–228

33. Lian F, Xing B, Zhu L (2011) Comparative study on composition, structure, and adsorption behavior of activated carbons derived from different synthetic waste polymers. J Colloid Interface Sci 360(2):725–730

34. Lian F, Chang C, Du Y, Zhu L, Xing B, Liu C (2012) Adsorptive removal of hydrophobic organic compounds by carbonaceous adsorbents: a comparative study of waste-polymer-based, coal-based activated carbon, and carbon nanotubes. J Environ Sci 24(9):1549–1558

35. Abbasi M, Salarirad MM, Ghasemi I (2010) Selective separation of PVC from PET/PVC mixture using floatation by tannic acid depressant. Iran Polym J (Engl Ed) 19(7):483–489

36. Liu H (2000) Carbon materials based on poly(phenylene oxide): preparation, characterization and application in electrochemical devices. State University of New York, New York

37. Kakuta N, Shimizu A, Ohkita H, Mizushima T (2009) Dehydrochlorination behavior of polyvinyl chloride and utilization of carbon residue: effect of plasticizer and inorganic filler. J Mater Cycles Waste Manag 11:23–26
38. Hayashi J, Yamamoto N, Horikawa T, Muroyama K, Gomes VG (2005) Preparation and characterization of high-specific-surface-area activated carbons from K_2CO_3-treated waste polyurethane. J Colloid Interface Sci 281(2):437–443
39. Lu C, Xu S, Liu C (2010) The role of K_2CO_3 during the chemical activation of petroleum coke with KOH. J Anal Appl Pyrolysis 87(2):282–287
40. Kadirova Z, Kameshima Y, Nakajima A, Okada K (2006) Preparation and sorption properties of porous materials from refuse paper and plastic fuel (RPF). J Hazard Mater 137(1):352–358
41. Wang H, Liu Y, Li Z, Zhang X, Zhang S, Zhang Y (2009) Glycolysis of poly(ethylene terephthalate) catalyzed by ionic liquids. Eur Polymer J 45(5):1535–1544
42. Marzec M, Tryba B, Kaleńczuk RJ, Morawski AW (1999) Poly(ethylene terephthalate) as a source for activated carbon. Polym Adv Technol 10(10):588–595
43. Mourao PAM, Cansado IPP, Carrott PJM, Carrott MMLR (2010) Designing activated carbons from natural and synthetic raw materials for pollutants adsorption. Mater Sci Forum 636-637:1404–1409. doi:10.4028/www.scientific.net/MSF.636-637.1404
44. Cansado IPP, Galacho C, Nunes AS, Carrott MLR, Carrott PJM (2010) Adsorption properties of activated carbons prepared from recycled PET in the removal of organic pollutants from aqueous solutions. Adsorpt Sci Technol 28(8–9):807–821
45. Swiatkowski A, Padee A (2007) Possibility of preparation of activated carbons from poly (ethylene terephtalate) waste. Ecol Chem Eng-Chemia I Inzynieria Ekologiczna 14(S2):199–206
46. Ciesinska W, Makomaski G, Zielinski J, Brzozowska T (2011) Preparation of sorbents from selected polymers. Polish J Chem Technol 13(1):51–54
47. Bratek W, Świątkowski A, Pakuła M, Biniak S, Bystrzejewski M, Szmigielski R (2013) Characteristics of activated carbon prepared from waste PET by carbon dioxide activation. J Anal Appl Pyrolysis 100:192–198
48. Lorenc-Grabowska E, Gryglewicz G, Machnikowski J, Díez MA, Barriocanal C (2009) Activated carbons from coal/pitch and polyethylene terephthalate blends for the removal of phenols from aqueous solutions. Energy Fuels 23(5):2675–2683
49. Barriocanal C, Díez MA, Álvarez R (2005) PET recycling for the modification of precursors in carbon materials manufacture. J Anal Appl Pyrolysis 73(1):45–51
50. Hirogaki K, Tabata I, Hisada K, Hori T (2010) Preparation of a porous polyester fiber by foaming with supercritical carbon dioxide. Sen-I Gakkaishi 繊維学会誌 66(7):163–167
51. Zhang FS, Itoh H (2003) Adsorbents made from waste ashes and post-consumer PET and their potential utilization in wastewater treatment. J Hazard Mater 101(3):323–337
52. Bach C, Dauchy X, Severin I, Munoz J-F, Etienne S, Chagnon M-C (2013) Effect of temperature on the release of intentionally and non-intentionally added substances from polyethylene terephthalate (PET) bottles into water: chemical analysis and potential toxicity. Food Chem 139(1–4):672–680
53. Cheng X, Shi H, Adams CD, Ma Y (2010) Assessment of metal contaminations leaching out from recycling plastic bottles upon treatments. Environ Sci Pollut Res 17(7):1323–1330
54. Bhaskar T, Mitan NM, Onwudili J, Muto A, Williams P, Sakata Y (2010) Effect of polyethylene terephthalate (PET) on the pyrolysis of brominated flame retardant-containing high-impact polystyrene (HIPS-Br). J Mater Cycles Waste Manage 10(4):332–340
55. Bóta A, László K, Nagy LGCT (1997) Comparative study of active carbons from different precursors. Langmuir 13(24):6502–6509
56. László K, Bóta A, Nagy LG (2000) Comparative adsorption study on carbons from polymer precursors. Carbon 38(14):1965–1976
57. László K, Tombácz E, Josepovits K (2001) Effect of activation on the surface chemistry of carbons from polymer precursors. Carbon 39(8):1217–1228

58. László K, Szűcs A (2001) Surface characterization of polyethyleneterephthalate (PET) based activated carbon and the effect of pH on its adsorption capacity from aqueous phenol and 2,3,4-trichlorophenol solutions. Carbon 39(13):1945–1953

59. Podkościelny P, László K (2007) Heterogeneity of activated carbons in adsorption of aniline from aqueous solutions. Appl Surf Sci 253(21):8762–8771

60. László K, Bota A, Dekany I (2003) Effect of heat treatment on synthetic carbon precursors. Carbon 41(6):1205–1214

61. László K (2005) Adsorption from aqueous phenol and aniline solutions on activated carbons with different surface chemistry. Colloids Surfaces A Physicochem Eng Aspects 265:32–39

62. László K, Marthi K, Rochas C, Ehrburger-Dolle F, Livet F, Geissler E (2004) Morphological investigation of chemically treated poly(ethylene terephthalate)-based activated carbons. Langmuir 20(4):1321–1328

63. Tóth A, Novák C, László K (2009) The effect of ionic environment on the TG response of phenol loaded PET-based porous carbons. J Therm Anal Calorim 97:273–280

64. Sych NV, Kartel NT, Tsyba NN, Strelko VV (2006) Effect of combined activation on the preparation of high porous active carbons from granulated post-consumer polyethyleneterephthalate. Appl Surf Sci 252(23):8062–8066

65. Kartel N, Gerasimenko N, Tsyba N, Nikolaychuk A, Kovtun G (2001) Obtaining and investigation of carbon adsorbent from polyethyleneterephthalate. Russ J Appl Chem 74(10):1711–1713

66. Kartel MT, Sych NV, Tsyba MM, Strelko VV (2006) Preparation of porous carbons by chemical activation of polyethyleneterephthalate. Carbon 44(5):1019–1022

67. Tamon H, Nakagawa K, Suzuki T, Nagano S (1999) Improvement of mesoporosity of activated carbons from PET by novel pre-treatment for steam activation. Carbon 37(10):1643–1645

68. Nakagawa K, Mukai SR, Suzuki T, Tamon H (2003) Gas adsorption on activated carbons from PET mixtures with a metal salt. Carbon 41(4):823–831

69. Nakagawa K, Namba A, Mukai SR, Tamon H, Ariyadejwanich P, Tanthapanichakoon W (2004) Adsorption of phenol and reactive dye from aqueous solution on activated carbons derived from solid wastes. Water Res 38(7):1791–1798

70. Almazán-Almazán MC, Pérez-Mendoza M, Domingo-García M, Fernández-Moralesa I, López FJ, López-Garzón FJ (2010) The influence of the process conditions on the characteristics of activated carbons obtained from PET de-polymerisation. Fuel Process Technol 91(2):236–242

71. Almazán-Almazán MC, Paredes JI, Pérez-Mendoza M, Domingo-García M, Fernández-Morales I, Martínez-Alonso A, López-Garzón FJ (2006) Surface characteristics of activated carbons obtained by pyrolysis of plasma pretreated PET. J Phys Chem B 110(23):11327–11333

72. Domingo-García M, Fernández JA, Almazán-Almazán MC, López-Garzón FJ, Stoeckli F, Centeno TA (2010) Poly(ethylene terephthalate)-based carbons as electrode material in supercapacitors. J Power Sources 195(12):3810–3813

73. Parra JB, Ania CO, Arenillas A, Pís JJ (2002) Textural characterisation of activated carbons obtained from poly(ethylene terephthalate) by carbon dioxide activation. Stud Surf Sci Catal 144:537–543

74. Parra JB, Ania CO, Arenillas A, Rubiera F, Pís JJ, Palacios JM (2006) Structural changes in polyethylene terephthalate (PET) waste materials caused by pyrolysis and CO_2 activation. Adsorpt Sci Technol 24(5):439–449

75. Arenillas A, Rubiera F, Parra JB, Ania CO, Pís JJ (2005) Surface modification of low cost carbons for their application in the environmental protection. Appl Surf Sci 252(3):619–624

76. Cansado IPP, Mourão PAM, Falcão AI, Ribeiro Carrott MML, Carrott PJM (2012) The influence of the activated carbon post-treatment on the phenolic compounds removal. Fuel Process Technol 103:64–70

77. Fernández-Morales I, Almazán-Almazán MC, Pérez-Mendoza MJ, Domingo-García M, López-Garzón FJ (2005) PET as precursor of microporous carbons: preparation and characterization. Micropor Mesopor Mater 80(1–3):107–115

78. Marco-Lozar J, Kunowsky M, Suárez-García F, Carruthers J, Linares-Solano A (2012) Activated carbon monoliths for gas storage at room temperature. Energy Environ Sci 5: 9833–9842

79. Parra JB, Ania CO, Arenillas A, Rubiera F, Pís JJ (2004) High value carbon materials from PET recycling. Appl Surf Sci 238(1–4):304–308

80. Parra JB, Ania CO, Arenillas A, Rubiera F, Palacios JM, Pís JJ (2004) Textural development and hydrogen adsorption of carbon materials from PET waste. J Alloys Compd 379:280–289

81. Mestre AS, Pires J, Nogueira JMF, Parra JB, Carvalho AP, Ani CO (2009) Waste-derived activated carbons for removal of ibuprofen from solution: role of surface chemistry and pore structure. Bioresour Technol 100(5):1720–1726

82. Montes-Moran MA, Menendez JA, Fuente E, Suarez D (1998) Contribution of the basal planes to carbon basicity: an ab-initio study of the H3O+ −pi interaction in cluster models. J Phys Chem B 102:5595–5601

83. Esfandiari A, Kaghazchi T, Soleimani M (2011) Preparation of high surface area activated carbon from polyethyleneterephthalate (PET) waste by physical activation. Res J Chem Environ 15(2):433–437

84. Esfandiari A, Kaghazchi T, Soleimani M (2012) Preparation and evaluation of activated carbons obtained by physical activation of polyethyleneterephthalate (PET) wastes. J Taiwan Inst Chem Eng 43:631–637

85. Lee J, Kim J, Hyeon T (2006) Recent progress in the synthesis of porous carbon materials. Adv Mater 18(16):2073–2094

86. Li Z, Song D, Zhi J, Hu A (2011) Synthesis of ultrathin ordered porous carbon through Bergman cyclization of enediyne self-assembled monolayers on silica nanoparticles. J Phys Chem C 115(32):15829–15833

87. Morishita T, Tsumura T, Toyoda M, Przepiorski J, Morawski AW, Konno H, Inagaki M (2010) A review of the control of pore structure in MgO-templated nanoporous carbons. Carbon 48(10):2690–2707

88. Morishita T, Soneda Y, Tsumura T, Inagaki M (2006) Preparation of porous carbons from thermoplastic precursors and their performance for electric double layer capacitors. Carbon 44(12):2360–2367

89. Morishita T, Wang L, Tsumura T, Toyoda M, Konno H, Inagaki M (2010) Pore structure and application of MgO-templated carbons. TANSO 2010(242):60–68

90. Seredych M, Bandosz TJ (2007) Surface properties of porous carbons obtained from polystyrene-based polymers within inorganic templates: role of polymer chemistry and inorganic template pore structure. Micropor Mesopor Mater 100(1–3):45–54

91. Walendziewski J (2006) Thermal and catalytic conversion of polyolefins. In: Scheirs J, Kaminsky W (eds) Feedstock recycling and pyrolysis of waste plastics: converting waste plastics into diesel and other fuels. Wiley, Chichester, pp 111–127

92. Pol VG, Pol SV, Calderon-Moreno J, Gedanken A (2006) High yield one-step synthesis of carbon spheres produced by dissociating individual hydrocarbons at their autogenic pressure at low temperatures. Carbon 44(15):3285–3292

93. Pol VG, Pol SV, Gedanken A, Sung M-G, Asai S (2004) Magnetic field guided formation of long carbon filaments (sausages). Carbon 42(12–13):2738–2741

94. Pol VG, Pol SV, Calderon-Moreno JM, Sung M-G, Asai S, Gedanken A (2006) The dependence of the oriented growth of carbon filaments on the intensity of a magnetic field. Carbon 44(10):1913–1918

95. Pol VG, Pol SV, Thackeray MM (2011) Autogenic pressure reactions for battery materials manufacture. US Patent 2011/0,104,553 A1

96. Pol VG (2010) Upcycling: converting waste plastics into paramagnetic, conducting, solid, pure carbon microspheres. Environ Sci Technol 44(12):4753–4759

97. Inagaki M, Park KC, Endo M (2010) Carbonization under pressure. New Carbon Mater 25(6):409–420
98. Inagaki M, Kuroda K, Sakai M (1981) Formation of carbon spherules from polyethylene under pressure. High Temp High Press 13:207–213
99. Inagaki M, Kuroda K, Sakai M (1983) Pressure carbonization of polyethylene-polyvinylchloride mixtures. Carbon 21(3):231–235
100. Inagaki M, Urata M, Sakai M (1989) Morphology change in carbons prepared from pitch-polyvinylchloride mixtures under pressure. J Mater Sci 24:2781–2786
101. Inagaki M, Washiyama M, Sakai M (1988) Production of carbon spherules and their graphitization. Carbon 26(2):169–172
102. Ayache J, Oberlin A (1990) Mechanism of carbonization under pressure, part II: influence of impurities. Carbon 28(2–3):353–362
103. Murata K, Sato K, Sakata Y (2004) Effect of pressure on thermal degradation of polyethylene. J Anal Appl Pyrolysis 71(2):569–589
104. Onwudili JA, Insura N, Williams PT (2009) Composition of products from the pyrolysis of polyethylene and polystyrene in a closed batch reactor: Effects of temperature and residence time. J Anal Appl Pyrolysis 86(2):293–303
105. Wei L, Yan N, Chen Q (2011) Converting poly(ethylene terephthalate) waste into carbon microspheres in a supercritical CO_2 System. Environ Sci Technol 45(2):534–539
106. Jia Z, Peng K, Li Y, Zhu R (2011) Preparation and application of novel magnetically separable γ-Fe_2O_3/activated carbon sphere adsorbent. Mater Sci Eng B 176(11):861–865
107. Nieto-Márquez A, Romero R, Romero A, Valverde JL (2011) Carbon nanospheres: synthesis, physicochemical properties and applications. J Mater Chem 21:1664–1672
108. Yuan D, Chen JX, Zeng J, Tan S (2008) Preparation of monodisperse carbon nanospheres for electrochemical capacitors. Electrochem Commun 10(7):1067–1070
109. Li M, Li W, Liu S (2011) Hydrothermal synthesis, characterization, and KOH activation of carbon spheres from glucose. Carbohydr Res 346(8):999–1004
110. Song X, Gunawan P, Jiang R, Leong SSJ, Wang K, Xu R (2011) Surface activated carbon nanospheres for fast adsorption of silver ions from aqueous solutions. J Hazard Mater 194:162–168
111. Funke A, Ziegler F (2010) Hydrothermal carbonization of biomass: a summary and discussion of chemical mecha nisms for process engineering. Biofuels Bioporducs Biorefining 4:160–177
112. Hu B, Wang K, Wu L, Yu S-H, Antonietti M, Titirici M-M (2010) Engineering carbon materials from the hydrothermal carbonization process of biomass. Adv Mater 22:813–828
113. Pol VG, Thackeray MM (2011) Spherical carbon particles and carbon nanotubes prepared by autogenic reactions: Evaluation as anodes in lithium electrochemical cells. Energy Environ Sci 4:1904–1912
114. Zhang JH, Li J, Cao J, Qian YT (2008) Synthesis and characterization of larger diameter carbon nanotubes from catalytic pyrolysis of polypropylene. Mater Lett 62(12–13):1839–1842
115. Li H, Sang J, Zhao J, Fu A, Liu H, Xu M, Pang G, Zhao XS (2012) Preparation of magnetically separable mesoporous Co@carbon/silica composites by the RAPET method. New J Chem 36:2308–2315
116. Zhao JH, Li HL, Lin Q, Li KX, Peng Z, Zhao XS (2010) Mesoporous carbon preparation by in-situ carbonization via a reaction under autogenic pressure at elevated temperature. Gaodeng Xuexiao Huaxue Xuebao/Chem J Chin Univ 31(6):1088–1092

Aromatic Hyperbranched Polymers: Synthesis and Application

Anindita Ghosh, Susanta Banerjee, and Brigitte Voit

Abstract Hyperbranched (hb) polymers have been receiving increasing attention because of their unique architecture that results in an interesting set of unusual chemical and physical properties. Over the past decade quite a number of excellent reviews on hb polymers have been published by different research groups, covering various aspects of this class of polymers. This review will highlight the work on aromatic hb polymers of the last decade, emphasizing general synthetic strategies and recent development of alternative synthetic strategies, and discussing various aspects of hb polymers to demonstrate their wide range of applications.

Keywords Hyperbranched polymers · Polymer applications · Polymer synthesis

Contents

A. Ghosh (✉)
Department of Applied Science, Symbiosis Institute of Technology (SIT), Symbiosis International University (SIU), Lavale, Pune 412115, India
e-mail: andy.iitkgp@gmail.com

S. Banerjee
Materials Science Centre, Indian Institute of Technology, Kharagpur 721302, India

B. Voit
Leibniz-Institut für Polymerforschung Dresden e. V., Hohe Strasse 6, 01069 Dresden, Germany

Abbreviations

6F-BPA	4,4′-(Hexafluoroisopropylidene)diphenol
AFM	Atomic force microscopy
BPA	4,4′-Isopropylidenediphenol
BPADA	2,2-Bis[4-(3,4-dicarboxyphenoxy) phenyl]propane dianhydride
BTDA	3,3′,4,4′-Benzophenonetetracarboxylic dianhydride
C-BPA	4,4′-(9-Fluorenylidene)diphenol
$CHCl_3$	Chloroform
Đ	Dispersity (M_w/M_n)
DB	Degree of branching
DMAc	Dimethyl acetamide
DMF	Dimethylformamide
DMSO	Dimethyl sulfoxide
DSC	Differential scanning calorimetry
EB	Elongation at break
FTIR	Fourier transform infra-red spectroscopy
GPC	Gel permeation chromatography
HQDPA	1,4-Bis(3,4-dicarboxyphenoxy)benzene dianhydride
hb	Hyperbranched
M_n	Number average molecular weight
M_w	Weight average molecular weight
NMP	N-Methylpyrrolidinone
NMR	Nuclear magnetic resonance
ODA	4,4′-Oxydianiline
ODPA	4,4′-Oxydiphthalic dianhydride
PAA	Polyamic acid
PL	Photoluminescence
PMDA	Pyromellitic dianhydride
SEM	Scanning electron microscopy
T_c	Crystallization temperature
T_d	Onset decomposition temperature
$T_{d,5\%}$	5% weight loss temperature
$T_{d,10\%}$	10% weight loss temperature
TEM	Transmission electron microscopy
T_g	Glass transition temperature
TGA	Thermogravimetric analysis
THF	Tetrahydrofuran
T_m	Melting temperature
UV	Ultraviolet

1 Introduction to Hyperbranched Polymers

The research activities in the field of hyperbranched (hb) polymers have generated an innovative and impressive number of new hb polymers, together with first applications of these materials. With the availability of synthetic strategies from a wide range of building blocks and with precise control over polymer architecture and functionality, hb polymers have attracted a great deal of attention during the past decade for many interesting applications. New synthetic methodologies have allowed the preparation of highly branched molecules under controlled conditions, and new analytical techniques have allowed the characterization of these materials [1–8]. Numerous unusual and novel properties have been noted for hb and dendritic macromolecules [9–11], and new applications are now appearing at a rapid pace [12–15].

Hyperbranched polymers are promising in practical applications due to their one-pot synthetic route on a large scale, as compared to dendrimers, which require multistep synthesis. Compared with linear polymers, hb polymers have lower viscosity and better solubility due to their abundant functional groups and globular shape. The ease of preparation of hb polymers has led to their incorporation into many copolymers [3, 16]. Copolymerization of linear monomer with branched monomer as a random component generates material with controlled branching that can enhance the properties of linear polymers [17, 18] and also lead to products that have added flexibility [19–22]. Hyperbranched polymers are frequently used as the core of core–shell block copolymers, with the shell block grown from the functional groups of the hb polymer [23–26]. They have also been grown from linear polymers to form diblock [27], triblock [28–30], and graft copolymers [31–33]. It is believed that the terminal groups of hb polymers can greatly affect the macromolecular properties, such as the glass transition temperature, solubility, dielectric properties, hydrophobicity, and thermal stability [34].

Of particular interest from an industrial point of view are the impressive advances that have been made using hb polymers for rheology modifiers, processing aids and, more recently, as functional materials in coatings, catalysts, sensors, biomaterials, emitting materials, nanotemplating applications, and piezo-electric sensors [35–42]. Many hb polymers have already been used as modifiers for different matrix polymers, especially for large-scale engineering plastics. Polymer blending is also a useful approach for combining the advantages of individual components [43]. The different structures of the hb polymers influence the properties of the blends in different ways.

This review is organized in the following way: In the first part, recent developments in the synthesis of various aromatic hb polymers are discussed. In the second part, the applications of hb polymers in polymer processing, including melt modifiers, additives, and blend components as classical examples, are discussed. In addition, the review includes a detailed discussion of new areas that are being explored for the use of hb polymers, such as materials for fuel cell applications, gas separation, optics, and electronics.

## 2 Synthesis of Aromatic Hyperbranched Polymers

Hyperbranched polymers have attracted increasing attention because of their ease of synthesis, high degree of functionality, and material properties. Many strategies have been developed for the preparation of polymers with highly branched structure; in particular, the convenient and cheap one-step polycondensation of AB_x monomer has received significant attention [44, 45]. Many hb polymers have also been prepared via the $A_2 + B_3$ synthetic approach [46, 47]. Kim has reported the synthesis of aromatic hb polyamides from AB_2 and A_2B-type monomers [48]. Monticelli et al. [49] have reported the synthesis of hb aromatic polyamides from an AB_2 monomer, namely 5-(4-aminobenzoylamino) isophthalic acid. Polymerizations were carried out in *N*-methylpyrrolidinone (NMP) using triphenylphosphite/pyridine as condensing agent. Yamakawa and Ueda developed a 'one-pot–multistep' strategy for the synthesis of aromatic hb polyamides with relatively low dispersities (*Đ*) of 1.1–1.5 and very high degree of branching (DB) of 80–90% [50, 51]. Their strategy consisted of a repetitive sequence of in situ carboxyl group activation and condensation reactions. Kakimoto and coworkers synthesized hb polyamides [52] using *p*-phenylenediamine or 4,4′-oxyphenylenediamine as A_2 monomer and trimesic acid as B_3 building block. The structures of these A_2 and B_3 monomers are shown in Scheme 1.

Russo and coworkers have extensively investigated hb polyamides prepared by homopolymerization of 5-(4-aminobenzamido) isophthalic acid or copolymerization of *p*-phenylenediamine and trimesic acid as supports for the preparation of Pd and Pt nanoparticles [53, 54]. Fang et al. [47, 55] first reported the synthesis of hb polyimides (hb-PIs) from a triamine, tris(4-aminophenyl)amine, and commercially available dianhydrides. The hb-PIs showed a combination of the excellent high temperature characteristics of linear polyimides together with high solubility, low viscosity, and noncrystallinity resulting from the hb structure. Melt polycondensation has been applied for the synthesis of aromatic and aromatic–aliphatic based hb polyesters, leading to broad molar mass distributions and limited molecular weights [56, 57]. Carboxylic acid chloride end-functionalized all-aromatic hb polyesters were prepared from the AB_2 monomer 5-(trimethylsiloxy) isophthaloyl dichloride [56] and the structure of this AB_2 monomer (**1–1**) is shown in Scheme 2.

The hb aromatic polyesters prepared via melt condensation reaction resulted in materials with a very high glass transition temperature (T_g) due to rigidity of the polymer backbones. However, the synthesis of hb polymers with much more facile techniques is still desirable. Kricheldorf et al. [58] synthesized highly branched aromatic polyesters from 3,5-bis(trimethylsiloxy)-benzoyl chloride as an AB_2 type monomer (**1–2**, Scheme 2). Moore and Stupp synthesized linear polyesters [59] by solution condensation using a condensing agent such as 1,3-dicyclohexylcarbodiimide (DCC) and a catalyst [4-(*N*,*N*-dimethylamino) pyridinium 4-tosylate] and the method was further utilized for the synthesis of hb polyesters. Blencowe and coworkers reported the synthesis of a rigid hb polyester using coupling agents such as DCC and 1,3-diisopropylcarbodiimide with an AB_2
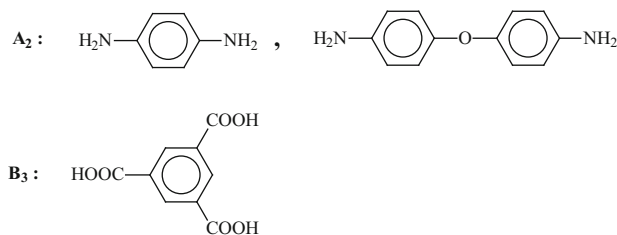
Scheme 1 Structures of A$_2$ and B$_3$ monomers used for preparation of hb polyamides [52]
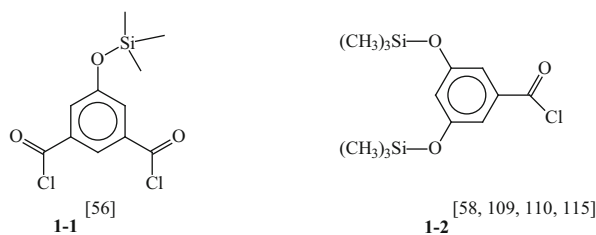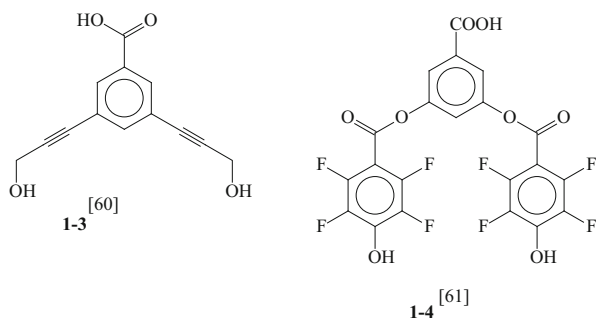

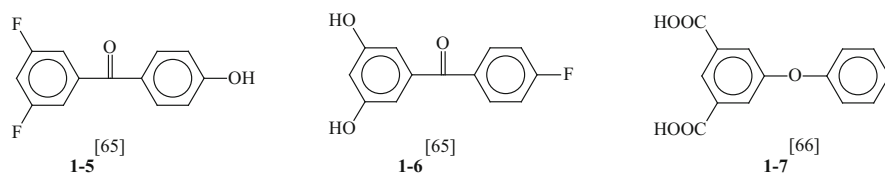**Scheme 2** Structures of AB$_2$ monomers used for preparing hb aromatic polyesters

monomer, namely 3,5-bis (3-hydroxylprop-1-ynyl)-benzoic acid [60] (**1–3**, Scheme 3). Jen and colleagues [61] reported a fluorinated hb aromatic polyester that was prepared by mild one-step polyesterification of an AB$_2$-type monomer, namely 3,5-bis(4-hydroxy-2,3,5,6-tetrafluorobenzoate)benzoic acid (**1–4**, Scheme 3), at room temperature using DCC and 4-(dimethylamino)pyridium 4-toluenesulfonate as the condensing agents.

Nucleophilic displacement of an activated dihalo or dinitro compound with an activated bisphenoxide salt at high temperatures has been the most explored method of poly(aryl ether) synthesis [62]. These synthetic strategies were further extended for the preparation of hb poly(aryl ether)s in one-step polymerization from AB$_2$ monomers containing a phenolic group and two aryl fluorides, which were activated toward nucleophilic displacement by a sulfone, ketone, imide, or heterocycle [63–65]. Miller et al. [63], Hawker and Chu [65], and Shu and Leu [66] reported the synthesis of hb poly(aryl ether ketone)s (hb-PAEKs) via the AB$_x$ method. The structures of AB$_2$ monomers reported by Hawker and Chu [65] are shown in Scheme 4 (**1–5** and **1–6**). The structures of AB$_2$ monomers reported by Shu and Leu [66] are shown in **1–7**, Scheme 4.

The synthesis of hb-PAEKs via the A$_2$ + B$_3$ approach has been reported by many research groups [67, 68]. Choi et al. [69] reported a self-controlled synthesis of hb-PAEKs from diphenyl ether (or 1,4-diphenoxybenene, B$_2$) and trimesic acid (A$_3$) via the Friedel–Crafts reaction. Baek and coworkers developed optimized conditions for Friedel–Crafts acylation in poly(phosphoric acid)/phosphorus pent-oxide (PPA/P$_2$O$_5$) medium for the preparation of hb-PAEKs [70, 71]. Martinez and Hay [72, 73] proposed the efficient synthesis and characterization of hb poly(aryl ether sulfone)s with a K$_2$CO$_3$/Mg(OH)$_2$ catalyst system for nucleophilic aromatic substitution. Kim et al. [74] reported the controlled nucleophilic aromatic

Scheme 3 Structures of AB$_2$ monomers used for preparation of hb polyesters [60, 61]

**Scheme 4** Structures of AB$_2$ monomers used for preparation of hb-PAEKs [65, 66]

substitution reaction (S$_N$Ar) of BC-type monomer, namely 5-fluoro-2-nitrobenzo-trifluoride [where the reactivity of B (fluoro group) > C (nitro group)], with A or A$_2$-type phenolate for the formation of two aromatic ether linkages. The nitro group activated by the trifluoromethyl group at the *ortho* position had a strong electron-withdrawing capability, enabling the displacement of other leaving groups at the *para* position before it was displaced.

The authors also investigated unusual growth of hb poly(arylene ether)s using 1,1,1-tris(4-hydroxyphenyl ethane as A$_3$-type and 5-fluoro-2-nitrobenzotrifluoride as BC-type monomer by one-pot synthesis with stepwise fluorine displacement followed by nitro displacement [75].

The *trans*-etherification reaction was realized during the polymerization of the above A$_3$ + BC system, leading to various types of growing species whose functional groups were dynamically exchanged during the polymerization. The monomer combination A$_3$ + BC is shown in Scheme 5.

Kim and Webster first prepared hb polyphenylenes from 3,5-dibromophenyl 4-boronic acid and dihalophenyl Grignard reagents by palladium-catalyzed and nickel-catalyzed aryl–aryl coupling reactions, respectively [76]. The structures of 3,5-dibromophenyl 4-boronic acid (**1–8**) and dihalophenyl Grignard reagents (**1–9**) are shown in Scheme 6.

Tang and coworkers [77] used cobalt-catalyzed polycyclotrimerization of aromatic diynes for the preparation of hb polyphenylenes. The representative structures of aromatic diynes used for homopolycyclotrimerizations are shown in Scheme 7.
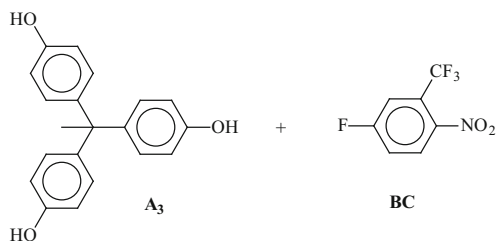
Scheme 5 Monomer combination $A_3 + BC$ used for the synthesis of hb poly(arylene ether)s
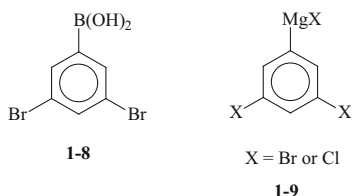
Scheme 6 Structures of 3,5-dibromophenyl 4-boronic acid and dihalophenyl Grignard reagents [76]
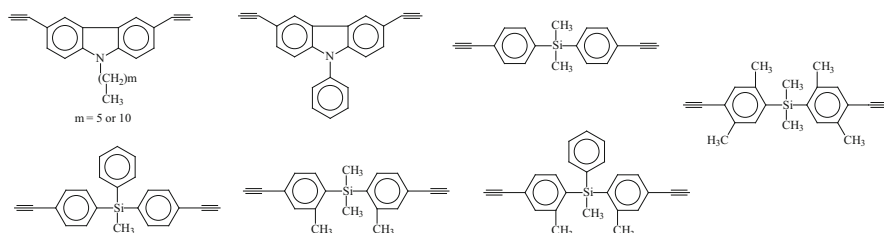
Scheme 7 Representative structures of aromatic diynes used for homopolycyclotrimerizations [77]

2.1 General Synthetic Approaches and Theoretical Aspects

Hyperbranched polymers are more promising for industrial applications than dendrimers because of single-step polymerizations, which are convenient for large-scale production. Hyperbranched polymers were first introduced by Flory in 1952 [78]. Flory presented hb polymers from a theoretical point of view, describing the intermolecular condensation of AB_x-type monomers. There are three types of repeating units, classified as dendritic (D), linear (L), and terminal (T), depending on the number of unreacted B functional groups in the structure of the hb polymers obtained from AB_x or $A_2 + B_x$ type monomers. In 1991, Hawker and Fréchet [79] described the degree of branching (DB) of AB_2 products as a factor for explaining the structure of the hb polymers:

$$DB = (D + T)/(D + L + T). \tag{1}$$

Because the number of dendritic units is theoretically equal to the number of terminal units at high molecular weights, Hawker and Chu [65] and Frey and coworkers [80] modified the definition as follows:

$$DB = 2D/(2D + L), \tag{2}$$

$DB = 0$ for a linear polymer because there is no branching and $DB = 1$ for a perfect dendrimer because it is completely branched.

Copolymerization has been widely used with polycondensation reactions to alter or enhance the physical properties and improve the processability of the final polymer. The introduction of the AB monomer allows control of the content of branching units. There are numerous reports in which an AB monomer has been copolymerized with an AB_x type monomer to afford copolymers with varying DB values, where DB is a typical characteristic frequently used to evaluate the irregularity of the structure of hb polymers.

The DB of the hb polymers resulting from the copolymerization of AB_2 with AB monomers depends on the fraction of branching unit AB_2 according to Eq. (3):

$$DB = 2rx/\left[r(1 - x) + (1 + r)^2\right], \tag{3}$$

where x represents the conversion ratio of A groups and r represents the feed fraction of AB_2 monomers in the total.

The maximum value the DB can reach is 0.5 when the reaction is close to completion for the AB_2 polycondensation system. The DB of the hb polymers resulting from the copolymerization of AB_2 and AB monomers depends greatly on the initial fraction of AB_2 monomer in the total feed. At the end of the reaction, when $x = 1$, Eq. (3) reduces to $DB = 2r/(1 + r)^2$.

Highly branched polymeric structures are also attainable through the polymerization of $A_2 + B_3$ monomers, but at a functional equivalence, when three-dimensional (3D) structures are developed, the polymer becomes a gel or highly crosslinked material that is insoluble in any organic solvent [78, 81]. Hence, polymerization requires careful control of the reaction to produce soluble hb polymers. The polycondensation to prepare hb polymers utilizing the $A_2 + B_3$ approach leads to gelation at the later stage of reactions (at a specific critical conversion and critical concentration) and affects the structure and properties of the final products. The gelation occurs because of the nonlinear propagation of macromolecules through the intermolecular reaction, which depends on the monomer reactivity and molecular steric elements. By choosing the appropriate monomer concentration and composition ratio, or controlling the reaction conversion, the crosslinking can be effectively avoided. A deeper understanding of the kinetics of $A_2 + B_3$ polymerization is valuable for both academic and practical application. Recently, Yang et al. [82] applied a 3D reactive bond fluctuation lattice model to study the kinetics of nonideal $A_2 + B_3$-type hb polymerization with consideration of the intramolecular cyclization, monomer reactivity, and steric elements. This model was further

used to simulate a realistic example of an $A_2 + B_3$ polycondensation system from the work of Voit and colleagues [83, 84], utilizing fitting approximations.

It is well known that avoidance of gelation is crucial in the synthesis of hb polymers. Hence, low monomer concentration, intense stirring, and slow addition speed are used to maintain the lowest local concentration in order to prevent gelation for $A_2 + B_3$-type hb polymerization. Flory's theory of gelation in the polymerization of $A_2 + B_3$ monomers is based on the following requirements for gelation: the equal reactivity of all A groups as well as B groups, the exclusive reactivity of A groups with B groups, and no intramolecular cyclization or chain termination in the process [85]. Thus, if an $A_2 + B_3$ polymerization does not obey these assumptions, gelation can be avoided. Recently, the more facile synthetic approach of $A_2 + BB'_2$ was developed [86–90] because of the more effective avoidance of gelation in this system compared with $A_2 + B_3$. In this approach, monomers are used that contain the same functional groups but with different reactivities, allowing for the formation of an intermediate AB_2 type monomer that is further polymerized to an hb polymer [91].

Litvinenko and coworkers [92, 93], Beginn et al. [94], Dusek et al. [95], Cameron et al. [96], and Galina et al. [97] have discussed the theoretical aspects of the related polycondensation systems in detail. Recently, Zhou et al. investigated the kinetics of the co-polycondensation of AB_2 and AB-type monomers in the presence of multifunctional cores [98].
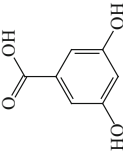
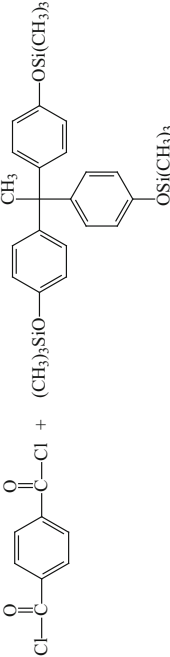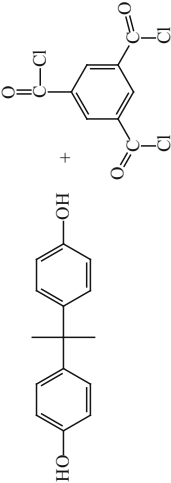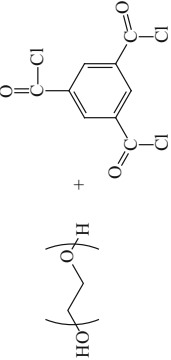## 2.2 Synthesis of Selected Aromatic hb Polymers

Unlike linear polymers, hb polymers are highly branched 3D macromolecules and have inherent internal cavities and abundant terminal groups, which often lead to better processability, compatibility, and solubility [99]. The terminal groups of hb polymers can greatly affect the macromolecular properties, such as the T_g, solubility, dielectric properties, hydrophobicity, and thermal stability. For example, aromatic polyamides (aramids) are well known as high-performance polymers [100]. However, hb structures are introduced [101, 102] in order to improve the poor processability caused by the rigid repeating unit in aramids. As an important engineering plastic, poly(phenylene oxide) has outstanding thermal, mechanical, and dielectric properties [103, 104]. However, its poor moldability, poor solubility, and inadequate adhesive strength limit its application. Compared with linear polymers, hb polymers show lower viscosity and better solubility due to the branching and their abundant functional groups and, therefore, hb poly(phenylene oxide)s, which combine the merits of poly(phenyl oxide) and hb polymers, have been synthesized to expand their application. Linear polyphenylenes [105] are found to be only partially soluble in most common organic solvents as they tend to aggregate in the solid state because of interchain π–π stacking interactions. Introducing the highly branched structure of these materials has made them attractive because of improved solubility and reduced or eliminated strong intermolecular interactions

and aggregation [106]. We will now discuss the synthesis of selected hb polymers such as hb poly(aryl ester)s, hb poly(aryl amide)s, hb polyimides, hb poly(aryl ether)s, hb poly(phenylene oxide)s, hb poly(phenylene sulfide)s, and hb poly (phenylene)s.

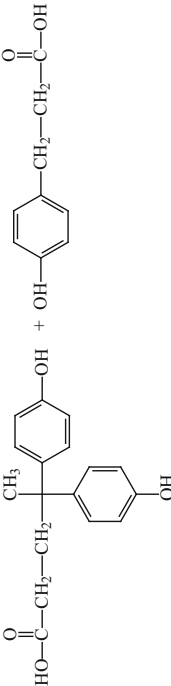### 2.2.1 Hyperbranched Poly(aryl ester)s

Melt polymerization is widely used in preparation of hb poly(aryl ester)s in industry because of the easy one-step process, but the solution polymerization route is more attractive because of the mild polymerization conditions, which reduce the potential for side reactions. Voit and coworkers [107] performed one-pot solution polycondensation of commercially available 3,5-dihydroxybenzoic acid as AB_2 monomer (Table 1, entry **1**), at room temperature in the presence of 4-(dimethylamino) pyridinium-4-tosylate as catalyst to suppress the formation of N-acylurea. Different carbodiimides as coupling agents were investigated to find the optimal esterification conditions. To compare the properties of the AB_2 aromatic polyesters produced by different pathways, the solution polycondensation was compared with their well-known analogs synthesized in melt [78, 108]. Because of the mild reaction conditions, completely colorless fully OH-terminated hb aromatic polyester with narrow Đ was obtained. The degree of polymerization could be simply controlled by the reaction time, in contrast to melt polycondensation. The product showed a DB of 60%, which was similar to that of the product previously reported by melt polymerization of 3,5-bis(trimethylsiloxy) benzoyl chloride [78] and was higher in comparison with ideal statistically branched polymers from AB_2 monomers (which should posses a theoretical DB of 50%). The authors attributed the high DB to the activation or deactivation of different reaction sites as a result of different electron densities caused by different substituents formed during the course of the reaction in both melt and solution. Thermal analysis indicated that the hb polyesters were amorphous in nature in contrast to the linear analog poly(m-hydroxybenzoate), which is semicrystalline with a T_g of 145°C and a melting point T_m of 183°C [58]. Previously, Schmaljohann and coworkers [109, 110] used quantitative NMR to analyze the kinetics of the melt polycondensation of 3,5-bis(trimethylsiloxy)benzoyl chloride in detail using the contents of different structural units at different degrees of conversion. A major accelerating effect was a result of preferred formation of the most stable phenolate, which favored the formation of dendritic units as per the previous findings reported in literature [111, 112]. Recently, Khalyavina et al. [113] studied the effect of the DB on the T_g of hb polyesters and observed that the DB did not show much influence on the T_g of the polymers with an identical amount of phenolic –OH groups per unit. For example, the T_g and M_n values of OH-terminated polymers with DB = 8% (M_n = 14,500 Da, T_g = 155°C) and DB = 50% (M_n = 17,000 g/mol, T_g = 152°C), were close to each other. This finding was also in accordance with that observed previously by Wooley et al. [114], where linear, hb, and dendritic polyesters containing an identical amount of phenolic –OH groups per unit showed similar T_g values in the range 197–204°C.

Table 1 Monomer structures and monomer combinations used for the synthesis of hb poly(aryl ester)s

Entry no.	Monomer structures and monomer combinations	Polymerization type	References
1		AB$_2$	[107]
2		A$_2$ + B$_3$	[115]
3		A$_2$ + B$_3$	[116]
4		A$_2$ + B$_3$	[117]

(continued)

Table 1 (continued)

Entry no.	Monomer structures and monomer combinations	Polymerization type	References
5		$A_2 + B_3$	[118]

Voit and coworkers [115] prepared hb polyesters by solution polycondensation at room temperature from the previously reported monomer, namely 3,5-bis (trimethylsilyloxy)-benzoyl chloride (Scheme 2, **1–2**) [109, 110]. Fully soluble aromatic AB$_2$ hb polyesters with a DB of about 55% in very high yield (~98 %) and of high molar mass ($M_w = 45,000$ Da) were achieved, which was in accordance with results previously reported in the literature [79, 108]. The hb polyesters showed high T_g of 220°C and $T_{d,5}$ of ~380°C. The hb aromatic polyesters prepared by the A$_2$ + B$_3$ approach were also prepared by Voit and coworkers [115], where the A$_2$ monomer was terephthaloyl chloride (TCl) and the B$_3$ monomer was 1,1,1-tris (4-hydroxyphenyl)-ethane (THPE) or THPE modified with 1,1,1-tris(4-trimethylsiloxyphenyl)ethane (TMS) (see Table 1, entry **2** for monomer combination). All the polymerization reactions were conducted at room temperature due to the high reactivity of the TCl. In order to avoid gelation, the polycondensation of TCl (A$_2$) and THPE (B$_3$) was performed in dilute solution by slowly adding TCI solution to the THPE solution. The synthesis was carried out using different monomer ratios (A$_2$:B$_3$ = 3:2, 1:1, 3:4, and 1:2). The structures of the A$_2$ + B$_3$ hb polyesters as well as the DB were calculated from the NMR spectra. Well-separated signals corresponding to the different subunits confirmed the hb structure of the A$_2$ + B$_3$ hb polyester. In general, on approaching the stoichiometric ratio of the functionalities, the molecular weight of the resulting hb polymers increased and, as a result, the T_g and DB also showed an increasing trend. However, at the same time, gelation could not be avoided with higher monomer concentration or when high molar mass products were aimed for. Gelation was observed for higher A$_2$ ratios (3:2 and 1:1 at a monomer concentration of 57 mmol/L), resulting in insoluble polymers and, hence, gel permeation chromatography (GPC) could not be performed. The T_g values of the polymers obtained were in the range of 199–268°C, which showed an increasing trend with increasing molecular weight. A high T_g of 268°C was realized for M_w as high as 28,500 Da, at an A$_2$:B$_3$ molar ratio of 1:1. Interestingly, the melt rheology of A$_2$ + B$_3$ (3:4) hb polyester from solution polymerization indicated viscous behavior with a shear thinning effect, whereas AB$_2$ polyester behaved as a completely elastic material.

Hyperbranched poly(aryl ester)s via the polycondensation of A$_2$ and B$_3$ monomers were also prepared utilizing the A$_2$ + B$_3$ approach by Lin and Long [116]. A dilute bisphenol A (A$_2$) solution was added slowly to a dilute 1,3,5-benzenetricarbonyl trichloride (B$_3$) solution at 25°C to prepare hb poly(aryl ester)s in the absence of gelation (see Table 1, entry **3** for monomer combination). The molar ratio of A$_2$:B$_3$ was maintained at 1:1, and the maximum final monomer concentration was maintained at 0.08 M to avoid gelation. Gelation was not observed, even at longer reaction times of 72 h. Moderate values of M_w of the hb poly(aryl ester)s were obtained in the range of 10,000 and 22,000 Da, with Đ values ranging from 2.45 to 3.48. The molecular weights did not show any increase on increasing the reaction time. The DB was determined to be in the range 47–55%. The hb polymers exhibited lower solution viscosities, as expected, and also exhibited lower T_g values than the linear analogs, ranging from 130 to 150°C,

depending on molecular weight. The authors attributed this to poor chain entangle-ment of the hb polymers in comparison to the linear analogs.

Tailoring the DB through the synthesis of hb poly(ether ester)s was accom-plished by Unal et al. [117]. The polymerizations were conducted at room temper-ature using the $A_2 + B_3$ approach for the reaction of an acid chloride (1,3,5-benzenetricarbonyltrichloride) with poly(ethylene glycol) (PEG) (see Table 1, entry **4** for monomer combination) in the presence of anhydrous triethylamine (TEA) and using chloroform as solvent. In general, reactions were allowed to proceed for 24 h to ensure complete conversion. When a dilute solution of B_3 monomer was added to a dilute solution of A_2 oligomer, highly crosslinked products were obtained regardless of the rate of addition. In contrast, slow addition of the oligomeric A_2 solution to the B_3 solution yielded branched polymers. The monomer concentration did not show much influence on the molar mass and the $Đ$ of the final products. Commercially available PEG diols of various number-average molecular weights (M_n) controlled the DB. ^{1}H NMR spectroscopy indicated a DB of 69% for a highly branched poly(ether ester) derived from 200 g/mol PEG diol. In general, the molar mass increased with increasing monomer concentration for PEG-600, decreased with increasing monomer concentration for PEG-2000, and changed nonsystematically for the samples derived from PEG-200. Decrease in molar mass with increased monomer concentration for hb poly(ether ester) derived from PEG-2000 was attributed to the limited solubility of the A_2 oligomer and the branched products at higher concentrations. Gelation during the polymerization was also observed at higher monomer concentration for various PEG-diols of M_n 200, 600, and 2,000 g/mol. Molar mass distributions broadened with increasing weight-average molar mass (M_w). The effects of branching and the length of the PEG segments also showed interesting thermal properties of the highly branched polymers, as detected by differential scanning calorimetry (DSC). The branched poly(ether ester)s based on PEG-2000 showed T_g values ranging from -42 to $-51°C$ and a depressed T_m of 40°C, relative to both the A_2 oligomer (PEG-2000) and the linear poly(ether ester) based on PEG-2000, consistent with the reduced crystallization behavior of branched polymers.

A one-pot solution polymerization was performed at room temperature using partially aromatic monomers, namely 4,4-bis(4′-hydroxyphenyl)valeric acid as AB_2 and 3-(4-hydroxyphenyl)propionic acid as AB [118] (see Table 1, entry **5** for monomer combination), in the presence of 4-(N,N dimethylamino) pyridinium 4-tosylate (DPTS) as catalyst and dicyclohexylcarbodiimide (DCC). The depen-dencies of the DB and the thermal properties of the polymers on the AB:AB_2 monomer ratio were studied. Polyesters with statistical dendritic topology, con-trolled DB, and $M_w > 35,000$ g/mol were obtained. The DB was found to decrease with an increase in the amount of AB monomers and increasing comonomer ratio in the polymer (r_p = ratio of AB to AB_2) as shown in Fig. 1. Interestingly, the DB for hb homopolyester and branched copolyester at $r_p = 0.46$ was similar (see Fig. 1a), because of the fact that on adding the small-sized linear AB to the more voluminous AB_2 monomers in the reaction mixture, the steric effects decreased, which pro-moted the formation of dendritic units formed by the AB_2 monomer. The thermal
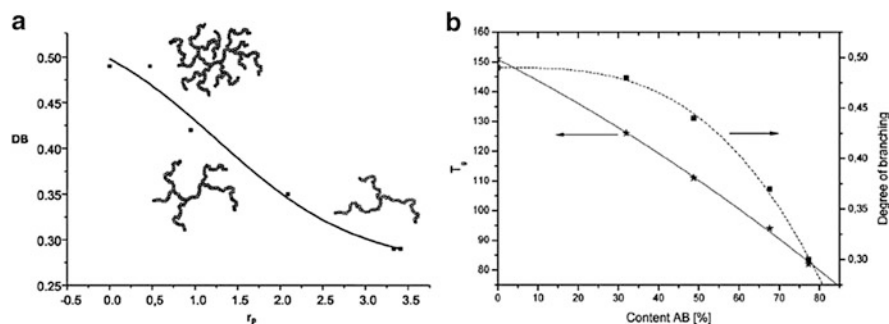
Fig. 1 (**a**) Degree of branching (DB) versus ratio of AB to AB$_2$ (r_p). (**b**) Influence of the content of AB units on DB and T_g. Reproduced with permission from [118]

behavior strongly depended on the branching of the polymers. Theoretically, with increasing DB, the T_g should decrease but an opposite behavior was observed. The T_g value is also dependent on the flexibility of the polymers. DSC measurements showed a decrease in the T_g with a decrease in the DB, which was ascribed to the higher flexibility of the polymer structures containing an increasing amount of AB units. The T_g of homopolymer resulting from AB$_2$ monomer was 151°C and that of copolymer resulting from AB + AB$_2$ monomer combinations with $r_p = 0.46$ was 125°C. The hb homopolyester and copolyesters ($r_p = 0$, 0.46, and 0.94–2.00) showed an amorphous behavior. However, the decrease in the DB and increase in the number of linear units in the polymers enabled the formation of crystalline sections. For this reason, the hb copolyester with $r_p = 3.44$ showed a broad melting region, and the T_g ranged from 150 to 220°C with a maximum at 178°C. The dependence of the T_g on the DB and the content of AB units in the copolymer is shown in Fig. 1b. The T_g decreased from 150 to 81°C with increasing AB content in the copolymer as the flexibility of the chains increased, which in turn decreased the T_g. Thermogravimetric analysis (TGA) showed a higher thermal stability for the branched copolyesters, with maximum decomposition temperature in the range 430–450°C, in comparison with the maximum decomposition temperature of 400°C for the hb homopolyester.

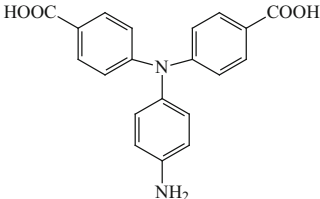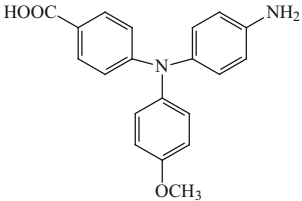### 2.2.2 Hyperbranched Poly(aryl amide)s and Poly(arylether amide)s

Polymers containing arylamide units have been prepared by forming the amide bonds directly during polymerization or by using monomers that contain amide units and linking them, e.g. by nucleophilic substitution, to form poly(arylether amide)s. for example, Baek and Harris [119] prepared two self-polymerizable AB$_2$ amide monomers, namely N,N'-bis(4-fluorobenzoyl)-3,4-diamino-4'-hydroxydiphenylether (Table 2, entry **1**) and N,N'-bis(4-fluorobenzoyl)-3,5-diamino-4'-hydroxybenzophenone (Table 2, entry **2**), and polymerized them to afford a hb poly(aryl ether amide) and a hb poly(aryl ether ketone amide). The aryl fluoride-

Table 2 Structures of monomers used for the synthesis of hb poly(aryl ether amide)s and poly (aryl amide)s

Entry no.	Monomer structures	Type of monomer	References
1		AB$_2$	[119]
2		AB$_2$	[119]
3		AB$_2$	[120]
4		A$_2$B	[120]
5		B$_3$	[121]
6		AB$_2$	[122]

(continued)

Table 2 (continued)

Entry no.	Monomer structures	Type of monomer	References
7		A$_2$B	[123]
8		AB	[125]

terminated hb poly(aryl ether amide) and poly(aryl ether ketone amide) were amorphous and soluble in many common organic solvents, including THF and CHCl$_3$. However, hb poly(aryl ether ketone amide) showed a higher T_g of 269°C compared with that of poly(aryl ether amide), which showed a T_g value of 210°C. The thermal stability evaluated by TGA also showed a similar trend. The $T_{d,5\%}$ values in N$_2$ were recorded as 323°C and 433°C for hb poly(aryl ether amide) and poly(aryl ether ketone amide), respectively. The authors attributed the drastic weight loss at 323°C to the intramolecular formation of imidazole moieties with a concomitant loss of 4-fluorobenzoic acid.

Hyperbranched poly(aryl ether amides) with fluorine or hydroxy end groups were synthesized by In and Kim [120] from AB$_2$ (Table 2, entry 3) or A$_2$B (Table 2, entry 4) type monomers via a nucleophilic aromatic substitution (S$_N$Ar) reaction. Monomer syntheses were facilitated by chemoselective amidation reactions, and even a direct synthesis of hb polymer was possible without isolation of the monomer. The resulting hb poly(aryl ether amide)s showed highly branched characteristics, with DB ranging from 43 to 53%. All hb polymers were readily soluble in polar aprotic solvents such as DMF, DMSO, and NMP, regardless of the end groups, due to the high amide contents and longer branching distances between adjacent branching points in the hb polymer backbones. The M_n values measured by GPC were in the range of 46,200 to 112,400 Da. The polymers showed a high T_g of over 220°C and high thermal stability, with $T_{d,10\%}$ over 420°C.

Shabbir et al. [121] aimed to prepare aromatic and semi-aromatic amine-terminated hb polyamides without gelation via direct polymerization of triamine as B$_3$ monomer with different aliphatic and aromatic diacid chlorides (terephthaloyl chloride, isophthaloyl chloride, sebacoyl chloride, and adipoyl chloride) as A$_2$ monomers. An aromatic triamine (B$_3$), 1,3,5-tris(4′-aminophenylcarbamoyl)benzene (TAPCB) (Table 2, entry 5), was reacted with two aromatic and two aliphatic

diacid chlorides (terephthaloyl chloride, isophthaloyl chloride, sebacoyl chloride, and adipoyl chloride) to yield four hb polyamides. In this work, the ratio $A_2:B_3$ was set to 2:3 to control the polymerization without catalyst by consideration of reactants and reaction conditions; no free acid chloride groups existed in the polymers, making these amine-terminated polymers. No gelation occurred for the selected reaction temperature and time (0°C for 3 h) with a monomer concentration of 10 mmol. Products containing a large amount of terminal amine groups resulted. The polymers were soluble in polar aprotic solvents at room temperature. The hb polyamides in general showed low molecular weights in the range of 13,000–27,000 Da and DB in the range of 51–55%. Higher molar masses could not be achieved because of the off-stoichiometry chosen to prevent gelation. The T_g values for hb polyamides were in the range of 138–198°C, depending on the rigidity of the polymer structure, the highest being for the hb polyamide containing rigid benzamide units and the lowest for the hb polymer with an alkyl–amide chain. The $T_{d,5\%}$ values recorded in nitrogen for the hb polyamides were in the range of 262–331°C, indicating moderate thermal stability. The hb polyamides studied by X-ray diffraction showed no crystallinity, indicating an amorphous nature that was attributed to the highly branched architecture preventing the packing of macromolecules through hydrogen bonding between the amide groups.

Ohta et al. [122] reported a new approach for controlling the polymerization of AB_2 monomers from a core initiator by utilizing the change in substituent effects between monomer and polymer to suppress statistical self-condensation but favor a type of chain growth. The polymerization of AB_2 monomer (Table 2, entry 6) was carried out utilizing a mixture of 1.1 equivalents of lithium 1,1,1,3,3,3-hexamethyldisilazide (LiHMDS) and 6.7 mol% of core initiator in the presence of lithium chloride (LiCl), where LiCl helped in reducing the reactivity of the intermediate amide anion. The obtained hb polyamides showed controlled molecular weight and narrow dispersity, $Đ \sim 1.11$, indicating that the controlled polymerization of AB_2 monomer was not only governed by slow monomer addition, but also by the change in substituent effects between the monomer and polymer to suppress self-polymerization.

Liou and coworkers [123] synthesized A_2B type monomer (Table 2, entry 7) by chemical modification of end functional groups incorporating *para*-methoxy-substituted triphenylamine groups [124], which lowered the oxidation potentials and afforded different electrochromic characteristics. Furthermore, the content of branching units could also be tuned by copolymerization of the A_2B with AB type monomer (Table 2, entry 8), namely 4-amino-4′-carboxy-4″-methoxytiphenylamine [125]. The aromatic hb polyamide formed by self-condensation of A_2B monomer and the copolymer formed by utilizing the monomer combination A_2B + AB were prepared by the usual polycondensation method using triphenyl phosphite and pyridine. The hb polyamide formed by self-condensation of A_2B monomer was post-functionalized with an amino monomer as the end-capping agent. The high solubility of the hb polyamides in polar aprotic solvents such as NMP, DMAc, DMF, and DMSO and also in THF was attributed to the incorporation of bulky, 3D triphenylamine moieties along the polymer backbone, which

resulted in a high steric hindrance for close packing, and thus reduced their tendency to crystallize. A high T_g in the range of 193–211°C was recorded, depending upon the stiffness of the polymer chain, and DSC thermograms indicated the amorphous nature of the hb polyamides. The $T_{d,10\%}$ of these polymers in nitrogen and air were recorded as 505–550°C and 510–535°C, respectively, indicating good thermal stability.

2.2.3 Hyperbranched Polyimides

Aromatic polyimides represent an important class of high-performance polymeric materials because of their many outstanding key properties, such as high mechanical strength, high modulus, unusual thermoxidative stability, excellent electrical properties, and superior chemical resistance [126, 127]. Hyperbranched polyimides (hb-PIs) show high T_g and superior solubility due to their 3D architecture as well as excellent physical and chemical properties.

Similarly to hb poly(aryl amide)s, the imide function in hyperbranched polyimides can be formed directly through imidation of the respective anhydride (acid)- and amine-containing AB_2 monomers or $A_2 + B_3$ monomer combinations or by polymerization of imide function-containing monomers leading, e.g., to poly (ester imide)s or poly(ether imide)s. Kricheldorf et al. synthesized a poly(ester imide) from a trifunctional imide monomer [128]. Maier et al. synthesized a heterocyclic hb-PI from a monomer containing a maleimide group (A) and an azine group (B_2) through a crisscross cycloaddition polymerization [129]. Moore and coworkers [130] reported the preparation of aromatic hb-PIs through the nucleophilic etherification of a protected AB_2 monomer (**1–10**, Scheme **8**). The self-polycondensation was carried out through the nucleophilic etherification of silylated phenol and aryl fluoride in diphenylsulfone at 240°C in the presence of cesium fluoride. Other AB_2-type monomers were also prepared for the synthesis of hb-PIs via nucleophilic etherification, as shown in **1–11**, Scheme **8** [131].

An AB_2-type monomer (**1–12**, Scheme **8**) was prepared by Hao et al. [132] by multistep synthesis. The AB_2 monomer was self-condensed to form five hb-PIs by variation of the concentration and reaction temperature. The synthesized hb-PIs showed good solubility in polar aprotic solvents such as in DMF, DMAc, DMSO, and NMP with a DB around 50%. The hb-PIs prepared from the new AB_2 monomer were observed to be soluble in polar aprotic solvents like NMP, DMF, and DMSO. The self-condensation of AB_2 monomer at room temperature, carried out at a dilute concentration of 0.06–0.16, led to low molecular weight oligomers of ~11,100 Da and, hence, polymerization was investigated at higher solution concentration and at a temperature of 50°C. Increasing the solution concentration from 0.06 to 0.32 g/ mL showed a limited increase in molecular weight up to 25,500 Da; however, increasing the temperature to 50°C at a dilute concentration of 0.08 g/mL resulted in a marked increase in molecular weight to 173,000 Da. The T_g values of the hb-PIs were found to be in the range of 155–161°C and showed an increasing trend with
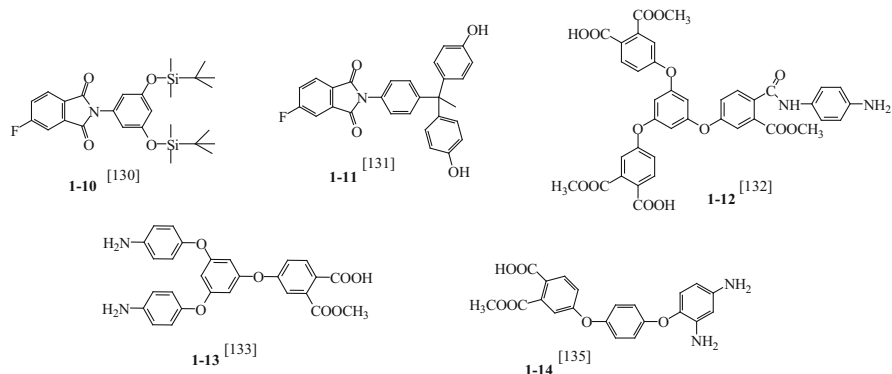
Scheme 8 Structures of some AB_2 monomers used for the synthesis of hb-PIs

increase in molecular weight. The $T_{d,5\%}$ values for the hb-PIs were 445–460°C, indicating high thermal stability.

An AB_2-type monomer (**1–13**, Scheme 8), was synthesized by Yamanaka et al. [133] starting from 3,5-dimethoxyphenol via a polyamic acid methyl ester precursor. The aromatic hb-PIs were prepared by chemical imidization in the presence of acetic anhydride and pyridine. The synthesized polyimides were soluble in polar aprotic solvents and showed thermal stability, with a $T_{d,10\%}$ of 470°C in nitrogen and a T_g of 193°C. In another work by Yamanaka et al. [134], the same AB_2 monomer containing free amine end groups of the precursor was end-capped with acetyl, *n*-heptanoyl chloride, and 4-methylphthalic anhydride. By chemical imidization of these precursors in the presence of acetic anhydride and pyridine, hb-PIs were prepared. The DB of the hb-PIs was ~50% as expected. The hb-PIs showed a $T_{d,5\%}$ above 395°C, and T_g values of 189, 138, and 186°C for the end groups of acetoamide, *n*-heptanoamide, and 4-methylphthalimide, respectively.

Wang et al. [135] prepared a novel ABB′ monomer (**1–14**, Scheme 8), namely 4-[4-(2,4-diaminophenoxy)phenoxy] phthalic acid 2-methyl ester, which was polymerized to form the precursor polyamic acid monomethyl ester. The direct polycondensation of the ABB′ monomer was carried out to form polyamic acid monomethyl ester as a precursor and had a M_n of 12,000 Da. Chemical imidization in the presence of acetic anhydride and pyridine gave hb-PIs with low DB. The DB of the precursor, as determined by the ¹H NMR spectra, was only 7%. They ascribed the low DB to the differences in the reactivities of the amino groups. End modification reactions were accomplished with acetyl chloride, benzoyl chloride, and phthalic anhydride to form end-capped polyimides. The end-group-modified polyimides were soluble in polar aprotic solvents such as DMSO, DMF, and NMP. TGA measurements showed $T_{d,5\%}$ in the range of 400–520°C, and T_g of 200–258°C. The hb-PIs showed film-forming ability, but they were more brittle than analogous linear polymers.

Shen et al. [136] prepared several hb-PIs from a BB′₂-like aromatic triamine monomer, namely 2,4,6-tris[3-(4-aminophenoxy)phenyl]pyridine (TAPPP) (**1–15**

Scheme 9a), with commercial aromatic dianhydrides [4,4′-oxydiphthalic dianhydride (ODPA), 3,3′,4,4′-benzophenonetetracarboxylic dianhydride (BTDA), and 2,2-bis[4-(3,4-dicarboxyphenoxy) phenyl]propane dianhydride (BPADA)] as A_2 type monomers by the $A_2 + B_3$ approach. A different monomer addition order and changes in monomer molar ratios resulted in different hb-PIs. The addition of dianhydride into triamine TAPPP with a monomer molar ratio of 1:1 yielded the amine-terminated hb-PIs, whereas the reverse monomer addition order with a molar ratio of 2:1 gave the anhydride-terminated hb-PIs. The monomer was added slowly to avoid any high local concentration. The amine-terminated hb polyamic acids (hb-PAAs) were thermally imidized in solution at 180°C for 24 h, whereas the anhydride-terminated hb-PAAs were chemically converted into hb-PIs using a mixture of excess acetic anhydride and pyridine. The hb-PIs were obtained in high yields (95–98%). The DB for anhydride-terminated hb-PIs based on ODPA (1–20, Scheme 9b), BTDA (1–21, Scheme 9b), or BPADA (1–22, Scheme 9b) with TAPPP was 100%, indicating a completely branched structure. For amine-terminated hb-PIs, it was impossible to determine the DB by ^{1}H-NMR because the peaks of linear units and terminal units were always in the same range. For the amine-terminated and anhydride-terminated hb-PIs based on BPADA with TAPPP, the M_w was 92,000 and 32,000 Da, respectively. The DSC measurements of the amine-terminated hb-PIs showed T_g in the range of 232–258.5°C and the anhydride-terminated hb-PIs showed T_g in the range of 219–273.5°C. The highest T_g was recorded for BTDA-based hb-PIs and the lowest T_g in the series was detected for BPADA-based hb-PIs because of the flexible ether linkages present in the structure. In the dynamic mechanical analysis (DMA), the T_g values of obtained hb-PI films were in the range of 214–270°C, showing similar values to those detected by DSC. The $T_{d,10\%}$ values for the hb-PIs were in the range of 532–575°C for the amine- and anhydride-terminated hb-PIs, indicating high thermal stability. The hb-PI films showed film-forming ability. Their mechanical properties were evaluated and showed high tensile strength of 83–96 MPa, tensile modulus of 1.8–2.4 GPa, and low elongation at break (EB) of 5–7%.

Chen et al. [137] employed microwave irradiation for the preparation of amine- or anhydride-terminated hb-PIs. A BB'_2-type triamine monomer, namely 2,4,6-tris (4-aminophenyl)pyridine (TAPP) (1–16, Scheme 9a), was synthesized under microwave irradiation to prepare a series of amine- and anhydride-terminated triphenylpyridine-containing hb-PIs by $A_2 + BB'_2$ polymerization. Several commercially available aromatic dianhydrides, namely pyromellitic dianhydride (PMDA, 1–23, Scheme 9b), BTDA, and ODPA, were used as A_2 type monomers to react with the BB'_2 type aromatic triamine (TAPP). The addition of dianhydride to triamine with a monomer molar ratio of 1:1 yielded the amine-terminated polymer, whereas the reverse monomer addition order with a molar ratio of 2:1 gave the anhydride-terminated polymer. Slow monomer addition was used to avoid any high local concentration. The authors kept the total solid content below 0.08 mol/L for the amine-terminated polymer and 0.06 mol/L for the anhydride-terminated polymer to prevent insoluble gels. During the whole polymerization, continuous microwave irradiation was employed to enhance the reactivity and

a Triamines as B₃ monomers:

b Dianhydrides as A₂ monomers:
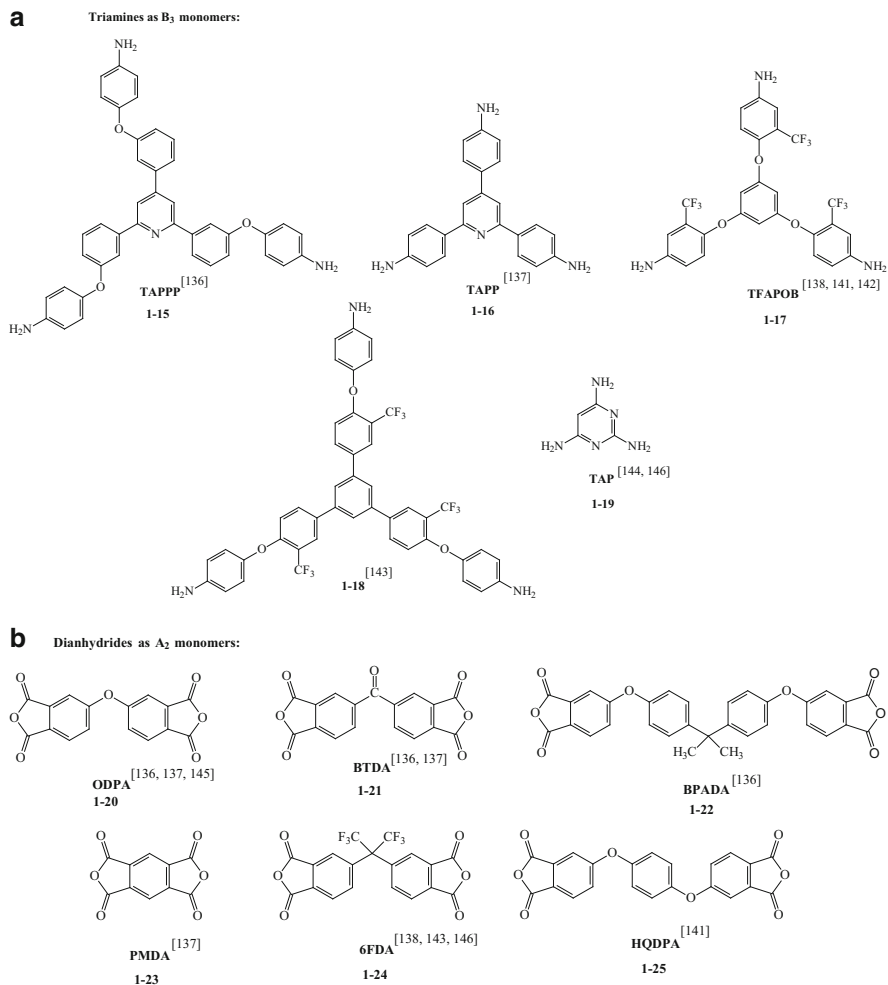
Scheme 9 Structures of (**a**) triamines as B_3 monomers and (**b**) dianhydrides as A_2 monomers commonly used for the synthesis of hb-PIs

shorten the reaction time. The amine-terminated hb-PAAs were thermally imidized in solution in the presence of *m*-xylene at 170°C, whereas the anhydride-terminated hb-PAAs were chemically converted into hb-PIs using a mixture of excess acetic anhydride and pyridine at 40°C. All resulting hb-PIs were obtained in high yields (95–98 wt%). The model compounds of terminal and linear analogous units were not easy to obtain separately because of their multiple isomers and it was difficult to determine the DB. The amorphous polyimides were soluble in polar aprotic solvents at room temperature or upon heating. The amino- and anhydride-terminated hb-PIs showed $T_{d,10\%}$ values of 568–583°C, indicating high thermal stability. The BTDA- and ODPA-based hb-PIs showed high T_g values of 311–339°C. The

thermally cured solution-cast films evaluated for mechanical properties showed tensile strength and modulus of 53–89 MPa, and 1.0–1.2 GPa, respectively, with low EB of up to 7%.

Gao et al. [138] synthesized fluorinated hb-PIs from a triamine monomer, namely 1,3,5-tris(2-trifluoromethyl-4-aminophenoxy)benzene (TFAPOB) (**1–17**, Scheme 9a), as B_3 monomer (shown in Scheme 2) and 4,4-(hexafluoroisopropylidene)diphthalic anhydride (6FDA, **1–24**, Scheme 9b) as A_2 monomer to form fluorinated hb-PIs by the $A_2 + B_3$ approach. Here, 3,5-ditrifluoromethylphenyl was used as an end-capping reagent. The synthesis route was similar to the conventional two-step method for the synthesis of linear polyimides, but with a different monomer addition order. Molar ratios of the dianhydride monomer and triamine monomer resulted in different hb polymers. The addition of dianhydride to triamine TFAPOB with a monomer molar ratio of 1:1 yielded the amine-terminated polymers, whereas the reverse monomer addition order with a molar ratio of 2:1 gave the anhydride-terminated polymers, as also reported by Chen et al. [137]. All hb-PIs exhibited moderate molecular weights with broad distributions. The anhydride-terminated hb-PI and amine-terminated hb-PI showed T_g values of 232°C and 243°C, respectively, in DSC. They ascribed the difference in T_g values to the appearance of hydrogen bonds in amine-terminated hb-PI and the different content of 6FDA residues in the two polymers [139]. The authors observed that hb-PI showed a birefringence as low as 0.002 at 650 nm, which was attributed to the presence of triamine monomers that reduced the orientation of the bonds in the polymer backbone and thereby reduced the birefringence. Liu et al. [140] used a nonideal $A_2 + B_3$ polymerization approach to obtain fluorinated hb-PIs based on TFAPOB. A series of aromatic ether dianhydride monomers with different flexible linear lengths were used to overcome the poor mechanical properties of globular branched macromolecules. In general, by increasing the linear part of the dianhydride monomer, the entanglements of polymer chains were enhanced and the mechanical properties of fluorinated hb-PIs were further improved.

Gao et al. [141] synthesized –CF$_3$-terminated hb-PI by condensation of a triamine monomer, 1,3,5-tris(2-trifluoromethyl-4-aminophenoxy) benzene (TFAPOB) (**1–17** Scheme 9a), and a commercially available dianhydride mono-mer, 1,4-bis(3,4-dicarboxyphenoxy) benzene dianhydride (HQDPA, **1–25**, Scheme 9b), using the $A_2 + B_3$ approach. Here, 3,5-ditrifluoromethylaniline was used as an end-capping reagent. In addition, the physical and gas transport proper-ties of CF$_3$-HQDPA were compared with those of the non-trifluoromethyl-termi-nated fluorinated hb-PI analog. The authors found that the introduction of –CF$_3$ groups at the end of hb polyimide increased oxygen and nitrogen permeability, whereas the selectivity decreased in the presence of the terminal groups. The B_3 monomer TFAPOB (**1–17**, Scheme 9a) was further utilized by Zhang and col-leagues [142] together with 4,4′-oxydiphthalic anhydride (ODPA) as A_2 monomer to form fluorinated hb-PIs by the $A_2 + B_3$ approach. Fluorinated hb-PIs end-capped with metallophthalocyanines were prepared by the reaction of dicyanophenyl end-capped fluorinated hb-PI with excessive amounts of 1,2-dicyanobenzene and

the corresponding metal (Cu, Zn, Ni) salt in quinoline. Because of the paramagnetic copper and nickel ions, ^{1}H-NMR analysis was not possible for structural elucidation; however, the UV–vis absorption spectrum supported the chemical structure of metallophthalocyanine-containing hb-PIs. The metallophthalocyanine-containing hb-PIs also showed good solubility in polar aprotic solvents and $CHCl_3$ and their M_n varied from 25,300 to 31,800 Da. The T_g values of these polymers were in the range of 217–225°C and the $T_{d,5\%}$ varied from 440 to 487°C.

Banerjee et al. [143] synthesized a triamine monomer B_3 (**1–18**, Scheme 9a) with the aim of preparing fluorinated hb-PIs by the $A_2 + B_3$ approach using commercially available dianhydrides as A_2 monomers. However, during solution imidization of the amide acids that formed by the reaction of the dianhydrides and B_3 monomer, an appreciable amount of gelation was observed for all the molar ratios, except when 6FDA was used as dianhydride for reaction molar ratio of 1:1 and the solution concentration was maintained at 2.7 wt%. Due to the considerable amount of gelation during solution imidization, further characterization was not explored.

Previously, Park et al. [144] prepared hb-PIs by the polymerization of $A_2 + B_2B'$ monomers. No gelation occurred during the polymerization although the monomer conversions surpassed the theoretical gel points, which was attributed to the unequal reactivity of the amino groups present in 2,4,6-triaminopyrimidine TAP as B_2B' monomer (**1–19**, Scheme 9a). Peter et al. [145] prepared a series of hb-PI membranes by copolymerization of 4,4'-oxydiphthalic anhydride (ODPA), 2,4,6-triaminopyrimidine (TAP), and 4,4'-oxydianiline (ODA) at various molar ratios of comonomers. No gelation occurred during polymerizations, probably because of the different reactivities of the amino groups at the 2- and 4-/6- positions in TAP. These hb-PIs were further explored for gas separation studies.

Recently, Chen et al. [146] also prepared a series of free-standing transparent hb-PI membranes by the $A_2 + B_2B' + B_2$ polymerization approach using 6FDA as A_2 monomer, TAP as B_2B' monomer, and ODA as B_2 monomer. Here too, no gelation occurred during polymerization because of the different reactivities of the amino groups present in the TAP monomer. The DB of the prepared hb-PIs increased from 0 to 69% with increase in the content of branching unit TAP. The T_g decreased in the range of 313–266°C with increasing the content of TAP, which the authors attributed to a lowering of molecular weight [147] with increasing TAP content, which in turn led to higher segment mobility of the macromolecules and, hence, lower T_g values. The TGA measurements revealed that the $T_{d,5\%}$ decreased from 559 to 432°C with increase in the TAP content. These hb-PI membranes were further studied for gas separation applications.

2.2.4 Hyperbranched Poly(aryl ether)s

High molecular weight poly(aryl ether)s can be prepared typically from arylhalogenides and phenols in the presence of weak bases such as potassium carbonate in dipolar aprotic solvents [148–150]. The water formed during the

reaction is removed azeotropically with toluene to promote the polymerization. The S_NAr reaction generally requires a leaving group activated with an electron-withdrawing group at the *ortho* or *para* position. Typical leaving groups are fluorine, chlorine, and nitro groups. Fluorine as a leaving group shows good reactivity due to its small size and high electronegativity.
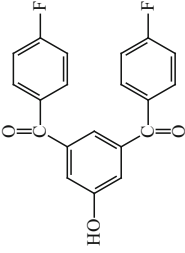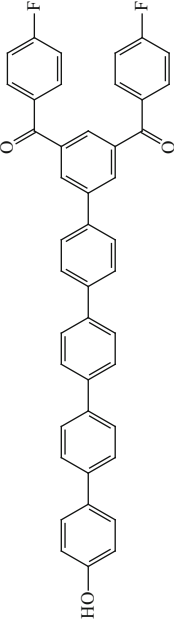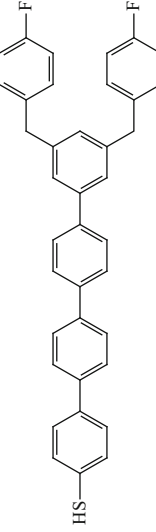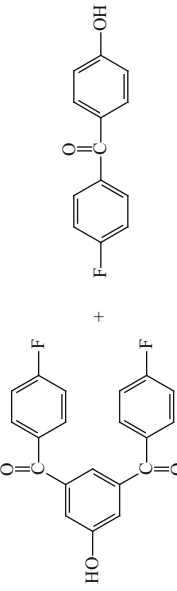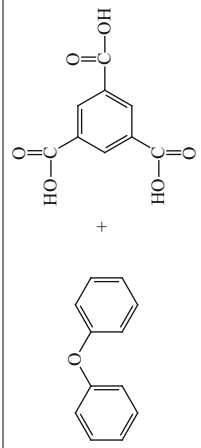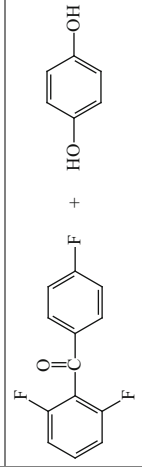
Hyperbranched Poly(aryl ether)s with a Ketone Moiety

Kricheldorf et al. [151] prepared 3,5-bis(4-fluorobenzoyl)phenol from 5-hydroxyisophthalic acid and 5-methoxyisophthalic acid via Friedel–Crafts acylation of fluorobenzene with 5-methoxyisophthaloyl chloride. The 3,5-bis (4-fluorobenzoyl)phenol as AB_2 monomer (Table 3, entry **1**) was polycondensed under various reaction conditions utilizing different solvent mixtures and temperature ranges (DMSO + toluene/140–145°C, NMP + toluene/150–155°C, sulfolane + toluene/150–155°C, sulfolane + xylene/170–175°C). In NMP, the molecular weights of the poly(aryl ether ketone)s were slightly lower than those obtained in DMSO. With sulfolane and either toluene or xylene, the reaction temperature could be raised to 150–155 or 170–175°C, respectively, but the lowest molecular weights were obtained using this solvent. The M_w values were in the range of 7,000 to 12,500 Da. Copolymerizations were carried out using 4,4′-difluordiphenyl sulfone (DFBP) as a comonomer in varying ratios, leading to the formation of star-shaped polymers with a diphenyl sulfone star center. The results were compared with those obtained from 'linear polycondensations' based on DFBP and 4-*tert*-butylcatechol or bisphenol A. The hb poly(aryl ether ketones) (hb-PAEKs) prepared from DFBP had low molecular weights and contained high fractions of cyclic poly(ether ketone)s. The authors concluded that for hb polymers, cyclization competes with propagation at any stage of the polycondensation at any concentration and that for polycondensations with AB_n-type monomers, in general, star-shaped polymers having a cyclic core and hb star arms are formed.

Previously, Morikawa [152] prepared hb-PAEKs with various numbers of phenylene units in the backbone. A representative structure of the AB_2 monomer containing phenylene units is shown in Table 3, entry **2**. The values of T_g for the hb-PAEKs were in the range of 188–218°C and increased with an increasing number of the phenylene units.

Recently, Maken and coworkers [153] prepared AB_2-type monomers, namely 4-thio-3′,5′-bis(4-fluorobenzal)biphenyl,4-thio-3″,5″-bis(4-fluorobenzal)-*p*-terphenyl and 4-thio-3‴,5‴-bis(4-fluorobenzal)-*p*-quarterphenyl (Table 3, entry **3**), starting from 3,5-bis(4-fluorobenzoyl)phenol. The AB_2 monomers were prepared by repeating a series of conversions of the hydroxy group to the triflate, crosscoupling of the triflate with (*p*-methoxythiophenyl) boronic acid, reduction of the carbonyl groups, and subsequent conversion of the methylthio group to a thiol group. The AB_2 monomers self-condensed to form different hb-PAEKs and the T_g was 175, 197, or 215°C, depending on whether the repeat unit structure contained biphenyl, terphenyl, or quadriphenyl units in the polymer backbone.

Table 3 Monomer structures and monomer combinations used for the synthesis of hb poly(aryl ether ketone)s

Entry no.	Monomer structures and monomer combinations	Type of polymerization	References
1		AB$_2$	[151]
2		AB$_2$	[152]
3		AB$_2$	[153]
4		AB$_2$ + AB	[154]

| 5 | | (structure: diphenyl ether + benzene-1,3,5-tricarboxylic acid, HO–C=O, HO–C=O, HO–C=O) | $A_2 + B_3$ | [155] |
| 6 | | (structure: 2,6-difluorobenzophenone with F substituents + hydroquinone, HO– –OH) | $A_2 + BB'_2$ | [156] |

Baek and Tan [154] improved the procedure for preparation of 3,5-bis (4-fluorobenzoyl)phenol (AB_2 monomer) at the intermediate step by the use of an acetyl group instead of a methyl group as the protecting group for the hydroxyl function of the AB_2 monomer. Alkaline hydrolysis of the intermediate 3,5-bis (4-fluorobenzoyl)phenyloxyacetate led to the desired AB_2 monomer, 3,5-bis (4-fluorobenzoyl)phenol. High molecular weight products ($M_w = 23{,}900$–$49{,}800$ Da) were obtained from that monomer. The T_g value of the hb-PAEK was recorded to be 159°C, which was higher than the previously reported T_g by Miller et al. (140–143°C) [63]. The hb homopolymer showed a bimodal molecular weight distribution that was also observed for other related linear hb systems. The AB_2 monomer was also copolymerized with AB monomer, namely 4-fluoro-4'-hydroxybenzophenone, in weight ratios AB_2:AB of 1:3, 1:1, and 3:1 to afford the respective hb-PAEKs with variable degrees of branching. The monomer combination AB_2 + AB is shown in Table 3, entry **4.** For 1:1 and 3:1 copolymers, the T_g value was 213°C and 164°C, respectively, indicating an increase in T_g with increase in the AB monomer content. The 1:3 copolymer (i.e., at 75 wt% of AB content) was semicrystalline in nature and showed a well-defined melting endotherm at 340°C, but no T_g was observed.

Trimesic acid and phenyl ether were in-situ polymerized as A_2 and B_3 monomers, respectively, in a Friedel–Crafts acylation in the presence of 10 wt% multiwalled carbon nanotubes (MWCNTs) by Baek and coworkers [155] to afford nanocomposites of hb-PAEK and MWCNT (hb-PAEK-*g*-MWNT). The feed ratios of A_2 and B_3 monomers varied from 2:3 to 2:1 in a mildly acidic medium. The monomer combination A_2 + B_3 is shown in Table 3, entry **5**. By simply varying the A_2:B_3 monomer feed ratio, the polarity of the resulting nanocomposites was altered, changing from highly ionizable (theoretically 100% COOH end groups when A_2:$B_3 = 1:1$) to relatively nonpolar (theoretically 100% phenoxy end groups when A_2:$B_3 = 2:1$). Because of the globular molecular architecture of hb polymers, the morphology of the nanocomposites resembled 'mushroom-like clusters on MWCNT stalks.' The hb-PAEK-*g*-MWCNT nanocomposites showed good solubility in polar aprotic solvents. The T_g of the nanocomposites was 276–325°C and $T_{d,10\%}$ was recorded to be 477–498°C in air, indicating high temperature stability.
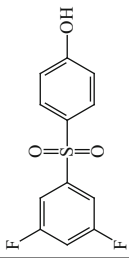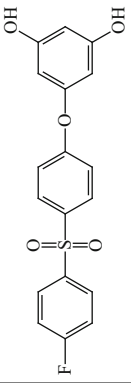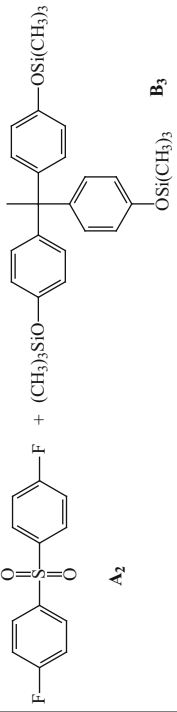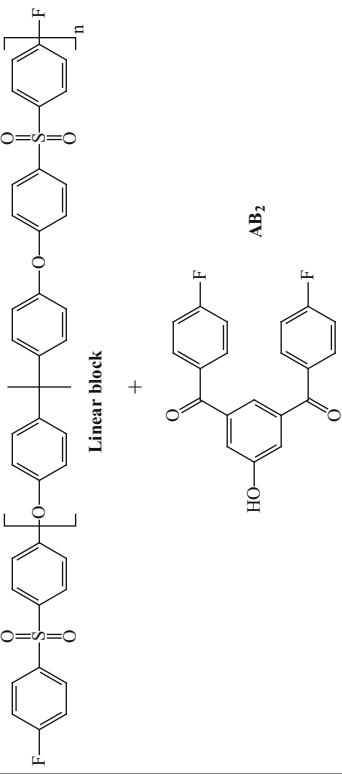
Li et al. [156] prepared hb poly(aryl ether ketone)s by the A_2 + BB'_2 approach using hydroquinone (A_2 monomer) and 2,4',6-trifluorobenzophenone (BB'_2 monomer). The monomer combination A_2 + BB'_2 is shown in Table 3, entry **6**. When the feed molar ratio of A_2 to BB'_2 was less than or equal to 1 (A_2:$BB'_2 \leq 1$ or OH:F ≤ 0.67), aryl fluoro-terminated hb poly(aryl ether ketone) (F-hb-PAEK) was obtained. When the feed molar ratio of A_2 to BB'_2 was greater than or equal to 2 (A_2:$BB'_2 \geq 2$ or OH:F ≥ 1.33), phenolic –OH terminated hb poly(aryl ether ketone) (OH-hb-PAEK) was obtained. The chemical structure of F-hb-PAEK and HO-hb-PAEK was confirmed using FTIR and ^{1}H-NMR spectroscopy. In the A_2 + BB'_2 approach, the reaction of the B group (fluorine located at *para* position of the C=O group) of BB'_2 and the A group of A_2 monomer was much faster than that of B' group (fluorine located at *ortho* position of the C=O group) of BB'_2 and the A group of A_2 monomer. Hence, in the initial stage of the reaction, the dimers

AB'_2 were formed predominantly as new monomers, and such dimers further polymerized with each other to form the hb polymer. The DB of F-hb-PAEK was more than 50%, whereas that of OH-hb-PAEK was 100%. Other copolymers were also prepared by using 4,4'-oxydiphenol, bisphenol A, or dihydroxydiphenyl as A_2 monomers. All the hb polymers exhibited good solubility in common organic solvents. The T_g values of the hb polymers varied in the range of 146–176°C, depending on the structure of the A_2 monomers. The T_g of OH-hb-PAEK was higher than that of F-hb-PAEK. This difference was attributed to the appearance of hydrogen bonds and the different contents of hydroquinone in the two types of hb polymers. The highest T_g was recorded for the copolymer containing the rigid diphenyl moiety and the lowest T_g was recorded for the copolymer containing isopropylidene groups on account of the flexibility and increased free volume in the polymer. The $T_{d,5\%}$ values of all the hb polymers were above 500°C in nitrogen, indicating high thermal stability.

Hyperbranched Poly(aryl ether)s with a Sulfone Moiety

Himmelberg and Fossum [157] synthesized a new AB_2 monomer, namely 3,5-difluoro-4'-hydroxydiphenyl sulfone) (Table 4, entry 1), by the reaction of 3,5-difluorophenylmagnesium bromide with 4-methoxyphenylsulfonyl chloride, followed by deprotection of the phenol group with HBr in acetic acid. The polymerization of AB_2 in the presence of core molecules, namely 3,4,5-trifluorophenylsulfonyl benzene or tris(3,4,5-trifluorophenyl)phosphine oxide, yielded hb poly(aryl ether sulfone)s, (hb-PAESs) with M_n values ranging from 3,400 to 8,400 Da and Đ values ranging from 1.5 to 4.8. The DB of the hb-PAESs was determined by ^{19}F-NMR spectra of the polymers and found to be in the range 51–70%, which was higher than the 50% usually observed for AB_2-type polymers. No satisfactory explanation was provided by the authors for the higher DB values. The polymerizations were accomplished using two different solvents, namely DMSO and NMP. The hb-PAESs synthesized using DMSO or NMP showed relatively low M_n values of 4,070 Da (Đ = 4.00) and 7,170 Da (Đ = 2.84), respectively. The presence of cyclic oligomeric species, formed by an intramolecular cyclization process, was a contributing factor for the relatively low molecular weights, which were attributed to the tetrahedral geometry of the AB_2 monomer. The intramolecular cyclization was restricted by conducting polymerization at higher concentration, leading to higher Đ values. However, all the M_n values observed for the polymerization reactions of 3,5-difluoro-4'-hydroxydiphenyl sulfone were also relatively low in comparison with the M_n values of the polymers prepared from a similar monomer with a ketone analog [65]. The authors were of the opinion that the low M_n values were due to the presence of core molecules that placed an upper limit on the molecular weight, or due to the formation of small cyclic structures that consumed monomer leading to additional core molecules. The T_g values for the hb-PAESs were in the range of 205–222°C with $T_{d,10\%}$ as high as 500°C under nitrogen.

Table 4 Monomer structures and monomer combinations used for the synthesis of hb poly(aryl ether sulfone)s

Entry no.	Monomer structures and monomer combinations	Type of polymerization	References
1		AB_2	[157]
2		AB_2	[158]
3		$A_2 + B_3$	[160]
4		Linear block + AB_2	[162]
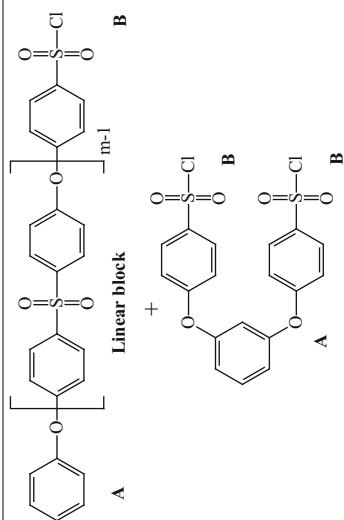
| 5 | | AB + AB$_2$ | [163] |

Jikei et al. [158] reported the synthesis of a new AB_2 monomer (Table 4, entry **2**) with a sulfone linkage and prepared hb-PAESs and studied their properties. It was found that the reaction conditions affected the DB of the resulting polymers. Self-condensation of the AB_2 monomer to form hb-PAES was explored in three different ways: First, self-condensation of the AB_2 monomer was performed in the presence of a base such as K_2CO_3 in a DMAc/toluene solvent system. Second, the AB_2 monomer was polymerized using cesium fluoride (CsF) in DMAc as solvent by stirring the mixture at 160°C for 10 h. Third, self-condensation of the AB_2 monomer was performed by using low monomer concentration in the presence of DMAc as solvent in a highly diluted solution. The structure of the AB_2 monomer was elucidated by ^{1}H-NMR and ^{13}C-NMR spectra and the peaks confirmed the proposed structure.

The self-condensed polymer prepared in three different ways showed an absolute M_w (determined by GPC-MALLS in NMP) in the range 27,000–270,000 Da. The DB of the hb-PAES prepared at a temperature of 160°C with CsF was higher (DB = 39%) than that of hb-PAES prepared with K_2CO_3 (DB = 17%) although both showed the same T_g value of 217°C. The difference in DB was attributed to the difference between the solubility of dissociated phenolate anions mediated by K_2CO_3 and that of phenolate-ion-like intermediates mediated by CsF [159] for the polymerization reaction. Both the hydroxyl groups of the AB_2 monomer were converted to the corresponding phenolates but the solubility of the diphenolates in the reaction medium was very low compared with the monophenolate. This increased the possibility of reaction between the monophenolate and the AB_2 monomer resulting in the formation of the linear units and causing a lower DB of 17%. In comparison, the phenolate-ion-like intermediates showed better solubility in the reaction medium, leading to a higher DB of 39%. Interestingly, when the heating–cooling scan of the hydroxyl-terminated hb-PAES (DB = 39%) was carried out five times in air at temperatures ranging from 50 to 300°C, the T_g increased from 217 to 236°C and the polymer sample became insoluble in all of the organic solvents, indicating thermal crosslinking. The hb-PAES prepared with K_2CO_3 with DB = 17% also showed an increase in the T_g, but the effect on the increasing trend of T_g was predominantly weaker than for the hb-PAES with DB = 39%. This finding indicated that the increasing trend in T_g was dependent on the DB of hb-PAES. However, the nitrobenzene-terminated hb-PAES did not show the increase in T_g after the heating–cooling scans from 50 to 260°C (repeated five times) in air. The hydroxyl-terminated hb-PAES prepared with CsF showed an improvement in thermal stability after heating at 300°C for 30 min in air and the $T_{d,5\%}$ and $T_{d,10\%}$ were recorded as 406 and 424°C, respectively, due to thermal crosslinking reactions at high temperature. The hydroxyl groups in the hb-PAES were end-functionalized by p-fluoro nitrobenzene to yield nitrobenzene-terminated hb-PAES, which showed a T_g value of 183°C that was lower than the T_g of the hydroxyl-terminated hb-PAES (T_g = 217°C). This difference was attributed to the strong intra-and intermolecular interactions occurring between the hydroxyl groups present in hydroxyl-terminated hb-PAES.

Kricheldorf et al. [160] prepared hb-PAESs from 1,1,1-tris(4-hydroxyphenyl) ethane (THPE) as B_3 and 4,4'-difluorodiphenyl sulfone (DFDPS) as A_2 monomers, either by polycondensation in DMSO with the elimination of water or via the silyl method in NMP. All polycondensations based on silylated THPE were conducted in NMP. The monomer combination of $A_2 + B_3$ monomers is shown in Table 3, entry **3**. The reaction temperature of most experiments was kept at 140–145°C to allow for a comparison with the experiments performed in DMSO and to keep minimum chain scission. The silyl method required longer reaction times than the standard method because the concentration of active end groups (phenoxide ions activated by K_2CO_3) was significantly lower when silylated monomers were used. However, when an exact 1:1 stoichiometry was used, an increase in reaction time from 24 to 48 h did not significantly enhance the molecular weight, whereas a higher temperature for 24 h was more successful. With an exact 1:1 stoichiometry, crosslinking was avoidable. For the silyl method, even an excess of DFDPS of 10 mol% did not result in crosslinking, but larger excess of DFDPS yielded gels after a short reaction time of 2 h.

Lin et al. [161] reported the preparation of hb polymers, with moderately branched, slightly branched, and linear topologies by phenol end-capped telechelic poly(arylene ether sulfone) oligomers as A_2 and tris(4-fluorophenyl) phosphine oxide as trifunctional monomer B_3. When bisphenol A and low molar mass oligomers were used as A_2, pronounced cyclic reactions led to branched products without gelation. The significance of the cyclic reactions decreased as the molar mass of the A_2 oligomers was increased. When moderate molar mass oligomers were used as A_2 monomers, a kinetic excluded volume effect resulted in a low branching efficiency. An increase in the concentration of A_2 oligomer significantly improved the branching efficiency.

Osano et al. [162] reported the synthesis of hybrid linear–dendritic 'ABA'-type architectures, where A and B were hb poly(ether ketone)s and linear poly(ether sulfone)s, respectively. They prepared an AB_2 monomer [3,5-bis(4'-fluorobenzoyl) phenol] to construct the hb segments, in an attempt to provide better control of the resultant hb structures than by utilizing the $A_2 + B_3$ approach. The monomer combination of linear block and AB_2 monomer for the formation of ABA-type architecture are shown in Table 4, entry **4**. Unreacted terminal groups of the ABA polymers were capped by *tert*-butylphenol and sodium 4-hydroxybenzene sulfonate. Such a flexible approach could allow different functional groups on the polymer chain ends simply by replacing the functional group on the phenol in the last part of the synthesis.

Kakimoto and coworkers [163] prepared multiblock linear–hb copolymers by a two-step method involving polymerization of the AB monomer, namely [4-(phenoxy)benzenesulfonyl chloride], to generate the linear block followed by addition of the AB_2 monomer 4,4'-(*m*-phenylene-dioxy)-bis(benzenesulfonyl chloride) in large molar excess (AB_2:AB = 19:1) to generate the hb block. The monomer combinations of linear block AB and AB_2 are shown in Table 4, entry **5**. The thermal properties of multiblock linear–hb polymers were compared with the homo-linear and homo-hb polymers.

The advantage of such a multiblock linear–hb architecture lies in its simplicity, ability to control the ratio of linear to hb blocks, and the avoidance of the potential degradation of the macromonomer sulfonyl chloride by clean-up procedures. The DB of such polymers was difficult to calculate from the ^{1}H-NMR spectra because of the broad, overlapping peaks. The overall AB_2:AB monomer molar feed ratio for the entire procedure was 1.35 for 15 min and 0.39 for 1 h for linear–hb block polymerization. The thermal stability of the multiblock hb–linear polymers was intermediate to that of the homo-linear and homo-hb polymers. The linear polymers showed $T_{d,10\%}$ at nearly 500°C, independent of molecular weight, and the hb polymer showed $T_{d,10\%}$ above 343°C. The multiblock hb–linear polymers showed $T_{d,10\%}$ values between 500 and 343°C, based on the weight ratio of linear to hb polymer. The DSC thermograms showed a single T_g of ~200°C for all multiblock hb–linear polymers, which was higher than that measured for the linear homopolymers ($T_g = 133–154$°C), indicating a homogenous product formation with no phase separation. A homo-hb polymer of molecular weight 30,000 Da showed no indication of a T_g below 250°C; however, a homo-hb polymer of only 8,400 Da showed a T_g at 181°C. Multiblock hb–linear products prepared with a linear reaction time of 15 min and hb reaction time of 6–12.5 h had $M_w = 26,600–34,600$ Da and did not showed any film-forming ability, similar to homo-hb polymers. Multiblock hb–linear products prepared with a linear reaction time of 1 h and longer hb reaction time (6–12.5 h) had $M_w = 53,500–145,600$ Da and showed film-forming ability, but the mechanical properties could not be evaluated due to brittleness of the hb polymer films.

Hyperbranched Poly(aryl ether)s with a Phosphine Oxide Moiety

The phosphine oxide group is an exceptionally good electron-donating group and facilitates the subsequent coordination with various metal ions or the formation of relatively strong hydrogen bonds. In addition, polymers incorporating phosphorus are known to have flame retardance and oxygen plasma resistance.

Lee et al. [164] prepared AB_2 and BA_2 monomers, namely bis(4-fluorophenyl)-4′-hydroxyphenylphosphine oxide and bis(4-hydroxyphenyl)-4′-fluorophenyl-phosphine oxide, that were converted to the corresponding hb poly(arylene ether phosphine oxide)s (hb-PAEPOs) with hydroxyphenyl and fluorophenyl end functional groups. The hb polymers were prepared by self-condensation of AB_2 (**1–26**, Scheme 10) or BA_2 monomers (**1–27**, Scheme 10) utilizing NMP/toluene as solvent in the presence of K_2CO_3 as base. The hb-PAEPO with hydroxyphenyl end functional groups showed a lower intrinsic viscosity ($\eta = 0.15$ dL/g), and thus a lower molecular weight, in comparison to the hb-PAEPO with fluorophenyl end functional groups ($\eta = 0.44$ dL/g) because of the low solubility of the phenolate ion during polymerization. The T_g values for the obtained polymers were 230 and 266°C, which showed an increasing trend with increase in η values. The fluorophenyl-terminated hb polymer was soluble in $CHCl_3$, but the hydroxyphenyl-terminated polymer was not soluble in $CHCl_3$ even though it had
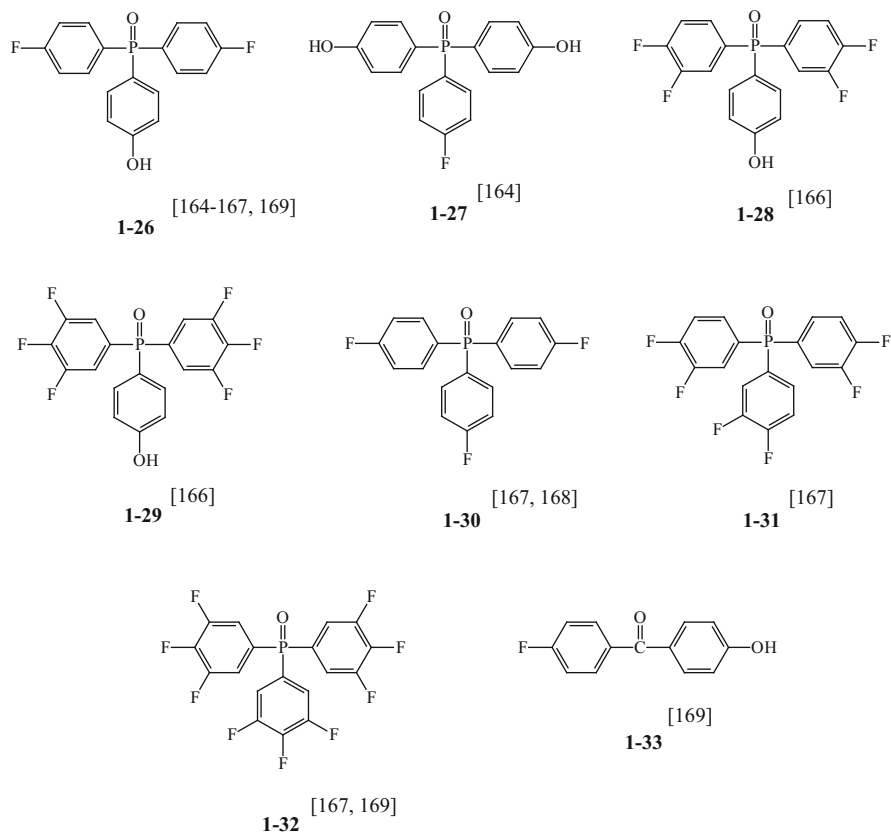
Scheme 10 Structures of monomers and core molecules used for the synthesis of hb-PAEPOs

a lower molecular weight than the fluorophenyl-terminated polymer, indicating that the properties of the hb polymers were dependent on the end functional groups as well as on their molecular weight. The prolonged polymerization of the AB_2 monomer yielded insoluble product, presumably due to the intermolecular reaction. However, the polymerization of BA_2 monomer at the same polymerization conditions produced relatively low molecular weight polymer due to the poor solubility of the corresponding phenoxide salt.

The AB_2 monomer, 4-(fluorophenyl)-4′,4″-(bishydroxyphenyl) phosphine oxide (**1–26**, Scheme 10), was synthesized by Lin and Long [165] by polymerizing the AB_2 monomer with various catalysts, such as K_2CO_3 or Cs_2CO_3/Mg(OH)$_2$, in the presence of dry and distilled DMSO as a solvent. All hb-PAEPOs were readily soluble at room temperature in polar aprotic solvents and basic water. Because of the highly irregular, branched 3D structures, gel permeation chromatography (GPC) did not provide an accurate measurement of molecular weight. Higher monomer concentrations in DMSO resulted in higher molecular weight but with

lower yields. The $Cs_2CO_3/Mg(OH)_2$ catalyst resulted in higher molecular weights than similar reaction conditions employing K_2CO_3 but resulted in lower yields of about 45%, which the authors attributed to the formation of insoluble, high molecular weight products. DSC measurements indicated no thermal transitions for the hb-PAEPO below 350°C, with the exception of a transition at 100°C that the authors attributed to the presence of residual water. They were of the opinion that the abundance of phenolic end groups was capable of efficient hydrogen bonding with other polar compounds.

A series of AB_2 monomers, namely bis-(4-fluorophenyl)-(4-hydroxyphenyl) phosphine oxide (**1–26**, Scheme 10), bis-(3,4-difluorophenyl)-(4-hydroxyphenyl) phosphine oxide (**1–28**, Scheme 10), and 4-hydroxyphenyl-bis-(3,4,5-trifluorophenyl)phosphine oxide (**1–29**, Scheme 10), were synthesized and characterized by Bernal et al. [166]. The AB_x monomers were self-condensed to form hb-PAEPOs according to the procedure reported by Hawker and Chu [65]. Spectral analysis of the resulting polymers indicated DB of 57% with M_w ranging from 22,400 to 52,500 Da and $Đ$ in the range of 2.44–3.60. The polymerization time required to achieve reasonable molecular weights was decreased from 20 h to less than 6 h and then to 4.5 h by the introduction of additional fluorine atoms to some of the monomers, and a M_w of 33,000–22,400 Da was obtained. The hb-PAEPOs showed only a very weak endothermic baseline shift at approximately 300°C in DSC scans up to 450°C. TGA measurements of hb-PAEPOs showed high thermal stability at 545–590°C under nitrogen atmosphere and 475–480°C in air atmosphere.

Bernal et al. [167] further extended their work and prepared hb-PAEPOs with controlled molecular weights and narrow $Đ$ by the polymerization of bis-(4-fluorophenyl)-(4-hydroxyphenyl)phosphine oxide in the presence of three core molecules. Polymerization reactions of bis-(4-fluorophenyl)-(4-hydroxyphenyl)phosphine oxide (**1–26**, Scheme 10) in the presence of 3, 5, and 10 mol% of tris(4-fluorophenyl)phosphine oxide (**1–30**, Scheme 10), tris(3,4-difluorophenyl)phosphine oxide (**1–31**, Scheme 10), and tris(3,4,5-trifluorophenyl)phosphine oxide (**1–32**, Scheme 10), respectively, were carried out in NMP at reflux in the presence of K_2CO_3, with reaction times of 8 h. The more reactive the core toward nucleophilic aromatic substitution, the more control was provided over the final molecular weight and the resultant $Đ$. Polymers showed M_n values ranging from 3,270 to 8,100 Da for polymerization reactions in the presence of core molecules. The highly fluorinated core, tris(3,4,5-trifluorophenyl) phosphine oxide (**1–32**, Scheme 10), yielded polymers with molecular weights approaching the theoretical values and narrow $Đ$ values as low as 1.25 were obtained. The DB also decreased significantly with increase in concentration of the core molecule from 3.5 to 10 mol%.

Czupik and Fossum [168] prepared hb-PAEPOs via an $A_2 + B_3$ polymerization technique with tris(4-fluorophenyl) phosphine oxide (**1–30**, Scheme 10) as B_3 monomer, using a variety of bisphenols, namely 4,4′-isopropylidenediphenol (BPA), 4,4′- dihydroxybiphenyl (DHB), and 4,4′-dihydroxybiphenyl ether

(DHBE), as A_2 monomers. They studied the effects of the reactivity of the A_2 monomer, the A:B ratio, the mode of addition, the solvent, and the concentration on the final molecular weight, Đ, and DB. Soluble hb-PAEPOs with M_w up to 299,000 Da were obtained. When BPA was added to a solution of tris (4-fluorophenyl) phosphine oxide over a period of 5.7 h, the M_w of the resulting polymer increased slowly until all of the BPA was added, and then the M_w increased dramatically to 299,000 Da with a Đ of 24.2. If a solution of tris(4-fluorophenyl) phosphine oxide was slowly added to a solution of BPA over a period about 4 h, only 85% of tris(4-fluorophenyl) phosphine oxide could be added before the gel point was reached. If tris(4-fluorophenyl) phosphine oxide was added slowly to BPA over 3.5 h at twice the concentration (i.e., A_2:B_3 = 2:1), the entire solution of tris(4-fluorophenyl) phosphine oxide could be added before the gel point was reached. These results indicated that soluble, moderate molecular weight hb-PAEPOs with Đ values of about 3.0 were achieved with a molar ratio of 2:1 (A_2:B_3) if the reaction was stopped at an appropriate time. Slow addition of DHB to a solution of tris(4-fluorophenyl) phosphine oxide and of tris(4-fluorophenyl) phosphine oxide to a solution of DHB resulted in significantly lower molecular weight products, with M_w values ranging from 7,800 to 12,600 Da and Đ of about 2. When DHBE was added slowly to a solution of tris(4-fluorophenyl) phosphine oxide, M_w values were similar to those observed for BPA and DHB, which increased with an increase in reaction time. Reactions in which the A_2 component was added slowly resulted in lower DBs, ranging from 20 to 50%, whereas the slow addition of the B_3 component provided samples with DBs of approximately 75%. Reactions performed under highly diluted conditions were independent of the mode of monomer addition and afforded completely soluble products with M_w values in the range of 9,000–12,100 Da and Đ values as low as 2.2.

Fossum and coworkers [169] reported the synthesis and characterization of soluble, branched copoly(aryl ether ketones) with a phosphine oxide moiety with controlled molecular weights and relatively low Đ values, prepared via the copolymerization reactions of AB (**1–33**, Scheme 10) and AB$_2$ (**1–26**, Scheme 10) in the presence of a highly reactive core molecule, tris-(3,4,5-trifluorophenyl)phosphine oxide (**1–32**, Scheme 10). Many of their findings were compared with previously reported results [170]. Initial reactions were performed with AB:AB$_2$ molar ratios of 75:25, 90:10, and 95.5 in the presence of 3 mol% of core molecule, at a final reaction temperature of 200°C. The final molecular weight could be easily controlled by varying the amount of core molecule added to the reaction mixture. For example, for AB:AB$_2$ with 95:5 mol%, when 5 mol% of core molecule was utilized in the polymerization reaction compared to 3 mol%, a corresponding decrease in the M_n value (4,010 Da compared with 6,820 Da) was observed for the same polymerization temperature of 200°C. At each polymerization temperature, the ratio of AB:AB$_2$ also showed a significant impact on the Đ of the samples. Samples prepared at the same reaction temperature, for example at 200°C, with AB:AB$_2$ ratios of 75:25, 90:10, and 95:5 possessed Đ values of 2.2, 2.6, and 4.1, respectively. The combined effects of reaction temperature, the ratio of AB:AB$_2$, and the
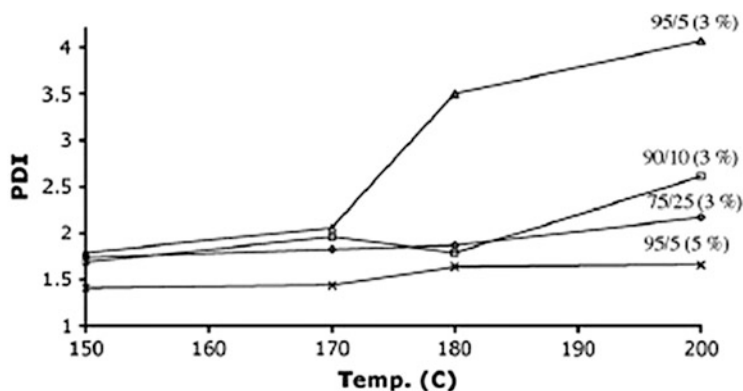
Fig. 2 The combined effects of reaction temperature, the ratio of AB to AB_2, and the mol% of the core molecule on the final polydispersity (*PDI*) of hb-PEK copolymers. Reproduced with permission from [169]

percentage of core molecule on the final $Đ$ of hb-PEK copolymers are shown in Fig. 2.

The substantial increase in $Đ$ values with the increase of AB_2 in the ratio of AB: AB_2 was attributed to the greater number of end groups present in the growing polymer chains, thus favoring the reaction of monomer with growing polymer rather than starting a new polymer chain. Fossum and coworkers also observed that the effect of reaction temperature was not that significant for 5 mol% of core molecule in comparison to that observed at 3 mol%. This finding was attributed to the fact that the total number of end groups in the system was higher when a higher mol% of core was utilized. Furthermore, for hb polymer prepared under similar reaction conditions, with AB:AB_2 molar ratio of 75:25 mol% containing 3 mol% of core molecule, both T_c (229°C) and T_m (278°C) were measurable in comparison to a similar polymer product prepared without a core molecule, which was completely amorphous. Samples prepared under the same reaction temperature of 200°C, with AB:AB_2 ratios of 75:25 containing 3 mol% of core molecule, showed much lower M_n and dispersity ($M_n = 5,400$ Da, $Đ = 2.2$) compared with a similar polymer sample prepared without the presence of a core molecule ($M_n = 13,000$ Da, $Đ = 11$). Fossum and coworkers assumed that the polymer samples prepared in the presence of core molecule were more homogeneous in nature, leading to better packing into crystalline regions and, hence, a T_m of 205°C. A similar polymer sample prepared under the same reaction conditions without the core molecule was completely amorphous in nature and did not show any T_m, which the authors attributed to self-plasticification, thus preventing the formation of crystalline regions. The M_n values of these systems could be controlled by altering the percentage content of core molecule, providing an efficient method for generating materials for a thorough study of structure–property relationships.

Scheme 11 Structure of AB$_2$ monomer with ketone-imide moiety [131]
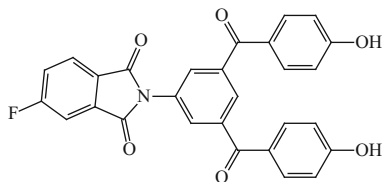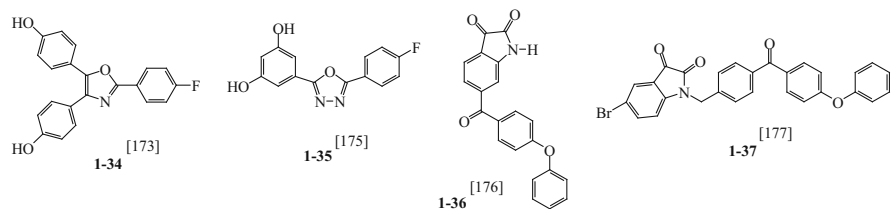

Hyperbranched Poly(aryl ether) with a Keto-imide Moiety

Baek et al. [131] synthesized an AB$_2$ monomer containing a preformed aromatic imide moiety and *para*-carbonyl functions to facilitate the formation of phenolate nucleophiles using K$_2$CO$_3$ as base. The AB$_2$ monomer, *N*-[3,5-bis (4-hydroxybenzoyl)benzene]-4-fluorophthalimide (shown in Scheme 11) was prepared from 4-fluoroisophthalic anhydride and 3,5-bis(4-hydroxybenzoyl)aniline. The AB$_2$ monomer was then polymerized via the aromatic fluoride-displacement reaction to afford the corresponding hydroxyl-terminated hb poly(aryl ether keto-imide) (hb-PAEKI). Functionalization of the resulting hb poly(arylene-ether-ketone-imide) was accomplished by modifying the chain ends with allyl bromide, propargyl bromide, or epichlorohydrin to afford allyl-terminated, propargyl-terminated, or epoxy (glycidyl)-terminated hb polymers, respectively. All hb-PAEKIs were soluble in common organic solvents. The hydroxyl-terminated hb PAEKI showed a T_g of 224°C due to hydrogen bonding whereas its derivatives exhibited lower T_g values that ranged from 122 to 174°C. Preliminary thermal study of the allyl ether-terminated hb polymer as a toughening additive for high-performance thermosets was conducted. The allyl-terminated hb-PAEKI was blended with a bisphenol A-based bis(maleimide) in various weight ratios. The results from DSC studies indicated that the presence of allyl-terminated hb-PAEKI significantly affected the T_g and cure behavior of bisphenol A-based bis(maleimide) when added up to 32 wt%.

Baek and coworkers [171] also synthesized a phthalonitrile-terminated hb-PAEKI that was end-functionalized with allyl groups, which could serve as a good processing aid and property enhancer for a bismaleimide resin. Furthermore, the authors blended it with a phthalonitrile (PN) resin based on [4,4′-bis (3,4-dicyanophenoxy)biphenyl] because PN resins are known to show excellent thermal and oxidative stability, together with flame retardant properties, and have attracted a great deal of attention as matrices for composite applications in the vicinity of an aircraft or submarine engine.

Fossum and coworkers were very curious to prepare hb-PAEKIs from the same AB$_2$ monomer [172] on an industrial scale via a cost-effective route. They concluded that the introduction of phenol groups via the nucleophilic aromatic substitution reaction of aryl fluorides with K$_2$CO$_3$ afforded a very low-cost and efficient alternative to demethylation of the methoxy groups using either pyridine hydrochloride or BBr$_3$ when a large excess of reagent is used. The yields and selectivity of the reactions were also improved significantly utilizing the nucleophilic aromatic

Scheme 12 Structures of monomers containing oxazole, oxadiazole, and oxindole moieties

substitution reaction of aryl fluorides with potassium hydroxide as a low cost reagent.

Hyperbranched Poly(aryl ether)s with Oxazole, Oxadiazole, and Oxindole Moieties

Gong et al. [173] synthesized and characterized an ABB′-type monomer containing a pair of phenolic groups and an aryl fluoride, which was activated toward displacement by the attached oxazole ring. The ABB′ monomer (**1–34**, Scheme 12) was self-condensed to form a hb poly(aryl ether oxazole) (hb-PAE-Ox) with terminal phenolic groups. The DB of hb-PAE-Ox was approximately 50%. The polymer was thermally stable and readily soluble in polar organic solvents. The terminal phenolic groups were easily functionalized, yielding hb hb-PAE-Oxs with a variety of ester-terminated and ether-terminated chain ends using different end-capping agents. Physical properties such as the T_g and solubility of the hb-PAE-Oxs depended significantly on the nature of the chain ends. It is known that for hb polymers the transition from the polar hydroxyl function to nonpolar aliphatic end groups results in a decrease in T_g because of the reduction in the extent of intermolecular interactions in the polymeric molecules [174]. The hb-PAE-Ox, which has polar hydroxyl terminal groups, showed a T_g value of 274°C. Polymers with less polar terminal groups, such as ester and ether groups, showed T_g values of 197 and 154°C, respectively. A further decrease in T_g to 124 and 119°C was observed for polymers when the length of the alkoxyl chain of the terminal ester or ether groups increased. The different chain ends also led to differences in solubility. The phenolic-terminated polymers were soluble in polar solvents such as DMSO and DMF, whereas the ester-terminated polymers were only partially soluble in DMF and insoluble in DMSO; the ether-terminated polymers were totally insoluble in both polar solvents. Conversely, in relatively nonpolar solvents such as CH_2Cl_2 and $CHCl_3$ polymers with ester- and ether-terminated chain ends were very soluble, whereas the polymers with a hydroxyl-terminated chain end were insoluble.

An AB_2 monomer (**1–35**, Scheme 12) was synthesized by Wu and Shu [175] for preparation of a hb poly(aryl ether oxadiazole) (hb-PAE-Oxd) with terminal phenol functionalities. The AB_2 monomer contained two phenolic groups and a single aryl

fluoride group that was activated toward nucleophilic displacement by the attached oxadiazole ring. The hb-PAE-Oxd showed a DB of 44%. The terminal phenolic groups were further post-functionalized with ether and ester chain ends using different end-capping agents to yield hb-PAE-Oxds. The nature of the chain-end groups showed a significant influence on the T_g and solubility. The hb-PAE-Oxd containing polar hydroxyl terminal groups showed T_g of 286°C, whereas the T_g values of hb-PAE-Oxds that contained less polar terminal groups, namely ether and ester groups, were 183 and 220°C, respectively. A further decrease in T_g to 121 and 146°C was observed for polymers with increasing length of the alkoxyl chain of the terminal ether or ester groups.

Hyperbranched poly(aryl ether oxindole)s (hb-PAE-Oxns) with a DB of 100% were prepared by Fu et al. [176] from an isatin-based AB$_2$ monomer (**1–36**, Scheme 12) by one-pot polymerization without using toxic organometallics nor chromatographic purification. The hb-PAE-Oxns soluble in apolar solvents were able to encapsulate a hydrophilic dye from the same polymer.

Kowalczuk et al. [177] synthesized an AB$_2$-type monomer (**1–37**, Scheme 12) that was self-condensed to give the hb poly(aryl ether oxindole) (hb-PAE-Oxn) with a DB of 100% and showed good solubility in common organic solvents such as CHCl$_3$ and THF. In general, the synthesis of the monomers for the preparation of hb-PAE-Oxn required toxic chemicals. However, in this work, the AB$_2$ monomer was prepared by only three steps: Friedel–Crafts acylation of 4-methylbenzoyl chloride with diphenyl ether to yield benzophenone, which was brominated by treatment with N-bromosuccinimide leading to benzyl bromide, and alkylation with 5-bromoisatin to yield the respective AB$_2$ monomer purified simply by precipitation from diisopropyl ether. The isatin functional groups were then end-capped with phenol and acylated using 2-bromoisobutyryl bromide, yielding a macroinitiator that was used for the synthesis of star polymers. The molar mass and dispersity of the synthesized bromopropionyl-functionalized poly(arylene oxindole) core showed $M_n = 20{,}000$ Da and $Đ = 1.7$. The hb core polymer exhibited a high T_g of about 250°C, which was similar to the previously obtained linear analogs ($T_g \sim 250$–300°C) [178].

Hyperbranched Poly(aryl ether)s with a Phenylquinoxaline Moiety

Baek and Harris prepared AB$_2$ (**1–38**, Scheme 13) and A$_2$B (**1–39**, Scheme 13) monomers [179] and self-polymerized them to very high molecular weight hb poly (phenylquinoxaline)s (hb-PPQs). The phenol-terminated hb-PPQs were only soluble in strong organic acids, whereas the aryl fluoride-terminated hb-PPQs were soluble in most common organic solvents. The hb-PPQs were treated with allyl bromide to afford an allyl ether-terminated hb-PPQ, which was also soluble in most organic solvents. The aryl fluoride hb-PPQs had a much higher M_w of ~2,643,000 Da and a much broader molecular weight distribution ($Đ \sim 60$) than the phenol-terminated hb-PPQs ($M_w = 322{,}000$ Da, $Đ = 3.7$) and allyl-terminated hb-PPQs ($M_w = 243{,}000$ Da, $Đ \sim 4$). The results indicated that phenol-terminated

1-38 [179, 180]   **1-39** [179, 180]   **1-42** [181]

1-40 [180]   **1-41** [180]
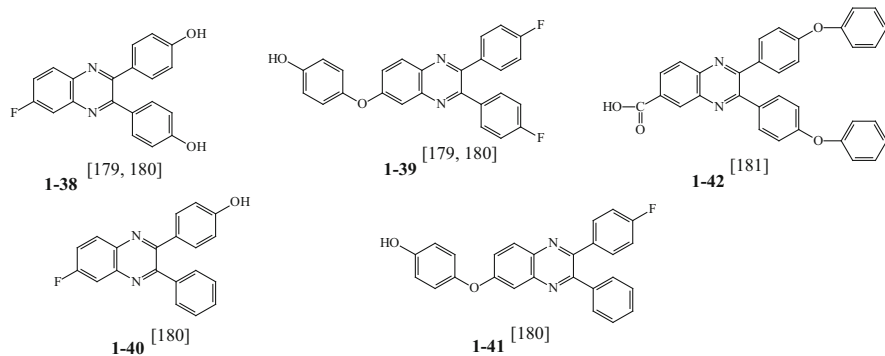
Scheme 13 Structures of monomers used for the synthesis of hb-PPQs

hb-PPQs formed aggregates in solution due to the formation of hydrogen bonding and showed limited solubility in organic solvents. The aryl fluoride-terminated hb-PPQs, on the other hand, had a much more extended and open conformation and showed good solubility in most common organic solvents. The lower T_g (225°C) of aryl fluoride-terminated hb-PPQs compared with phenol-terminated hb-PPQs ($T_g = 255$°C) was attributed to the extra flexible units in the repeating unit, no hydrogen bonding, and its apparent extended and open conformation. The phenol-terminated hb-PPQ and the aryl fluoride-terminated hb-PPQ showed $T_{d,5\%}$ at 511 and 575°C, respectively, in nitrogen, indicating high thermal stability. The reduced thermal stability of phenol-terminated hb-PPQs was attributed to the lower stability of the terminal phenol groups.

Baek and Harris also synthesized AB (**1–40**, Scheme 13) and BA (**1–41**, Scheme 13) monomers [180] in addition to the previously synthesized AB$_2$ and A$_2$B monomers [179]. The AB and AB$_2$ monomers were copolymerized to afford different degrees of linear units in hydroxyl-terminated hb-PPQs. Similarly, BA and A$_2$B monomers were copolymerized to afford different types of fluorine-terminated hb-PPQs. In the case of hydroxyl-terminated hb-PPQs, properties such as solubility, solution viscosity, T_g, and polymer degradation temperature were greatly influenced by the number of hydroxyl groups on the surface. However, the properties of fluorine-terminated hb-PPQs were much less influenced by the number of fluorines on the surface. The copolymers of AB and AB$_2$ were soluble in most aprotic solvents and phenolic solvents and T_g values ranged from 239 to 274°C. Copolymers of BA and A$_2$B were also soluble in most aprotic solvents and phenolic solvents. The hydroxyl- and fluorine-terminated hb-PPQs showed $T_{d,5\%}$ values ranging from 511 to 568°C in air and from 556 to 588°C in nitrogen, respectively, indicating that thermal degradation depended on the surface functional groups at the chain ends. The enhanced thermal stabilities of fluorine terminated hb-PPQs could be attributed to the fluorine terminal groups on the macromolecule surfaces.

A new phenylquinoxaline-containing AB$_2$ monomer (**1–42**, Scheme 13) was designed and synthesized by Baek and Tan [181] and the corresponding polymer

was synthesized at the optimal temperature of ~130°C using PPA and P_2O_5 (4:1). During the optimization study, the evolution of polymer density was realized by visualizing the existence of a changeover in the macromolecular architecture from a 'fanlike' conformation at the early stage of polymerization to a denser, globular conformation at higher molecular weights. The authors also showed that the subsequent chain-end functionality transformation for the resulting hb-PPQ could be performed either in a one-pot process or a batch process. The resultant hb-PPQs were thermally stable, with a $T_{d,5\%}$ of over 500°C in air.

Fluorinated hb Poly(arylene ether)s

Fluorine-containing polymers [182] are of special interest because they provide attractive properties such as low optical loss, birefringence, dielectric constant, and moisture absorption. On the other hand, poly(arylene ether)s are well-known aromatic polymers of high T_g, excellent thermal stability, and mechanical strength. Researchers have reported that perfluoroalkyl groups as a pendant unit or in the main chain activate fluoro displacement by phenoxides [183]. Since electron-withdrawing perfluoroalkyl groups cannot participate in resonance stabilization, activation by this group is expected due to the stabilization of the negative charges at the 2- or 4-position by a negative inductive effect [184, 185]. The steric congestion due to the bulky trifluoromethyl group ($-CF_3$) may also facilitate the formation of a stable Meisenheimer complex with the release of steric strain [186]. The presence of a pendent $-CF_3$ group in polymers increases the fractional free volume and lowers the dielectric constant while increasing its solubility without forfeiture of thermal stability [187–190]. The pendent $–CF_3$ group also decreases the crystallinity and serves to increase the free volume of the polymers, thereby improving gas permeability [191, 192] and electrical insulating properties [193]. The continued search for new activating groups for nucleophilic aromatic substitution leading to the formation of poly(arylene ether)s has been a very active area of polymer research, and in this regard fluorinated hb poly(arylene ether)s (F-hb-PAEs) with pendant $–CF_3$ groups are noteworthy in terms of their interesting properties observed.

An AB_2 monomer containing pendent $-CF_3$ groups (**1–43**, Scheme 14), namely 2,4 bis-(4-fluoro-trifluoromethylphenyl)phenol, was synthesized by Banerjee [194] utilizing Pd-initiated coupling, which was self-condensed to yield fluorinated hb poly(arylene ether) (F-hb-PAE) with an $M_n = 8,200$ Da and $Đ = 1.2$, indicating a highly regular structure. The F-hb-PAE was soluble in a wide variety of organic solvents and also in acetone. F-hb-PAE showed reasonable thermal stability, with $T_{d,5\%}$ in air of about 379°C and a T_g of 132°C. However, it was not possible to calculate the DB from NMR spectra due to several aromatic units between the branching points that restricted the analysis between a linear and a terminal unit.

An AB_2 monomer containing pendent $-CF_3$ groups (**1–44**, Scheme 14), namely bis-(4-fluoro-3-trifluoromethylphenyl)-4′-hydroxyphenylphosphine oxide, was synthesized by Satpathi et al. [195]. On self-condensation, this AB_2 monomer led
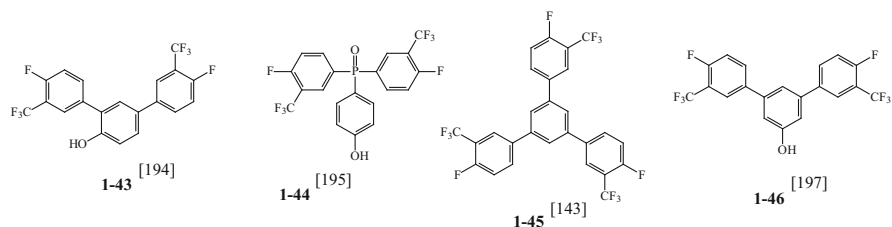
Scheme 14 Structures of monomers used for the synthesis of F-hb-PAEs

to fluorinated hb poly(arylene ether phosphine oxide) (F-hb-PAEPO) of much higher molar mass ($M_w \sim 6{,}16{,}000$ Da).The F-hb-PAEPO showed a T_g value of 225°C; the $T_{d,10\%}$ in nitrogen and air were found to be 508°C and 448°C, respectively. Due to missing entanglements, no free-standing films could be prepared from the F-hb-PAEPO and no mechanical properties could be recorded. An interesting finding was observed from ^{19}F-NMR spectra that indicated partial loss of 4-fluoro groups from unreacted B sites, as also observed previously by Fossum and coworkers [167] but was not explained. This effect was also manifested on the DB of the F-hb-PAEPO, which was approximated to 53 or 59% using the equations given by Frechét or Frey, respectively, but the DB should be ~50% without unwanted side reactions. Satpathi and coworkers ascribed this to the lability of these activated fluorine atoms under basic polymerization conditions. Under basic conditions of the polycondensation reaction, this fluorine was not only replaced by the phenolate under formation of ether bonds but probably also by the water that was generated by the deprotonation of the hydroxyl groups, which was not removed fast enough by azeotropic distillation, and this finding was supported by a model reaction. Herbert et al. showed that activation of the fluorine by the phosphine oxide group in the *para* position could further accelerate this reaction [196].

Banerjee et al. synthesized a new trifluoromethyl-activated trifluoro monomer by Pd-initiated coupling of 1,3,5-tribromobenzene with 4-fluoro-3-trifluoromethyl-phenylboronic acid to afford 1,3,5-tris(4-fluoro-3-trifluoromethylphenyl)benzene as B$_3$ monomer (**1–45**, Scheme 14) [143]. The B$_3$ monomer was reacted with three different bisphenols, namely 4,4′-isopropylidenediphenol (BPA), 4,4-′-(hexafluoroisopropylidene) diphenol (6F-BPA), and 4,4′-(9-fluorenylidene) diphenol (C-BPA), as A$_2$ monomers in different molar ratios (A$_2$:B$_3$ = 1:1, 1.5:1, or 2:1) leading to several fluorinated hb poly(arylene ether)s (F-hb-PAEs). At a functional equivalence of A$_2$:B$_3$ (i.e., 3:2 molar product) very high molecular weight products were obtained without significant gelation. In order to prevent gelation, a slow mode of addition of B$_3$ monomer for a period of 3 h was adopted to prevent any high local concentration at any time during polymerization, and the solid content was kept as low as 2.7 wt%. For 1:1 and 2:1 (A$_2$:B$_3$) molar ratios, reactions proceeded smoothly without any noticeable gel formation since both contained a significant excess of one type of functionality. However, despite the highest reactivity of BPA (strongly nucleophilic) toward the B$_3$ monomer in the

series, there was no gelation even at a functional equivalence ($A_2:B_3 = 1.5:1$). Theoretically, the gel point is reached in such a system at a functional group conversion of about 71% whereas, interestingly, a very high molar mass product (714,200 Da) was achieved in high yields, which clearly indicated a high monomer conversion and this was also manifested by spectral analysis. Polymerization in a highly diluted system, as well as slow monomer addition, helps to prevent macroscopic gelation to some extent according to the previous findings in literature [83, 84]; however, there could be a tendency to intramolecular cyclization due to favorable monomer configuration, which might help in shifting the gel point to higher conversion or prevented it totally. Some gelation was observed in the case of F-hb-PAEs resulting from 6F-BPA or C-BPA towards B_3 monomer (i.e., $A_2:B_3 = 2:1$ molar ratio) under similar reaction conditions. It was also observed that the gel content increased with increase in reaction time, particularly when the reaction temperature was 180°C. To avoid the problem of gelation, the F-hb-PAEs based on 6F-BPA or C-BPA with $A_2:B_3 = 1.5:1$ were prepared by maintaining the reaction temperature at only 165°C. All the polymers were soluble at room temperature in common organic solvents such as NMP, DMF, and DMAc, but were insoluble in DMSO. The ^{19}F-NMR signals revealed very high DB for these F-hb-PAEs (>70% and approaching almost 100%). GPC analysis of the F-hb-PAEs polymers prepared from 1:1 or 2:1 molar reaction of A_2 and B_3 monomers showed relatively low molar masses with values as low as 10,900 Da and narrow Đ values as low as 1.45 due to the presence of excess reactive functional groups, resulting in termination of the polycondensation. The 1.5:1 molar reaction resulted in very high molecular weight polymers, up to 2,840,000 Da, with Đ as high as 7.94. The 1.5:1 and 2:1 molar F-hb-PAEs exhibited higher T_gs than the 1:1 molar products. The phenoxy-terminated products, i.e., the 2:1 molar reaction products, showed a higher T_g (180–249°C) than the 1:1 molar reaction products (T_g ~147–232°C). The F-hb-PAE prepared from C-BPA and B_3 monomer with 1.5:1 molar ratio of $A_2:B_3$ did not show any T_g up to 350°C and showed a $T_{d,10\%}$ as high as 595°C, indicating very high thermal stability. Besides, the polymers showed more than 50% char residue even above 700°C under nitrogen atmosphere.

A new AB_2 monomer [3,5-bis(4-fluoro-3-trifluoromethylphenyl)phenol] containing pendent –CF_3 groups (1–46, Scheme 14) was prepared by Ghosh et al. [197] utilizing Suzuki coupling of 4-fluoro-3-trifluoromethylphenylboronic acid and 3,5-dibromophenol. The self-condensation of the AB_2 monomer led to F-hb-PAEs of low molecular weight and high molecular weight (see Scheme 15 for hb structures), depending on the solution concentration and reaction time. In general, a high solution concentration and long reaction time led to high molecular weight products. The M_w of the AB_2 self-condensation product was further increased to 231,300 Da with a Đ of 2.0 when the solution concentration was increased to 10 wt%. The fluorinated hb copoly(arylene ether)s **2a**, **2b**, **2c**, **3a**, **3b**, and **3c** (see Scheme 15 for hb structures) were prepared by the $AB_2 + A_2$ approach. The synthesized AB_2 monomer was reacted with two different commercial bisphenols, namely BPA and 6 F-BPA, at three different molar ratios ($AB_2: A_2 = 1:1, 3:2, 2:1$) to form fluorinated hb copoly(arylene ether)s. Here, the reactions
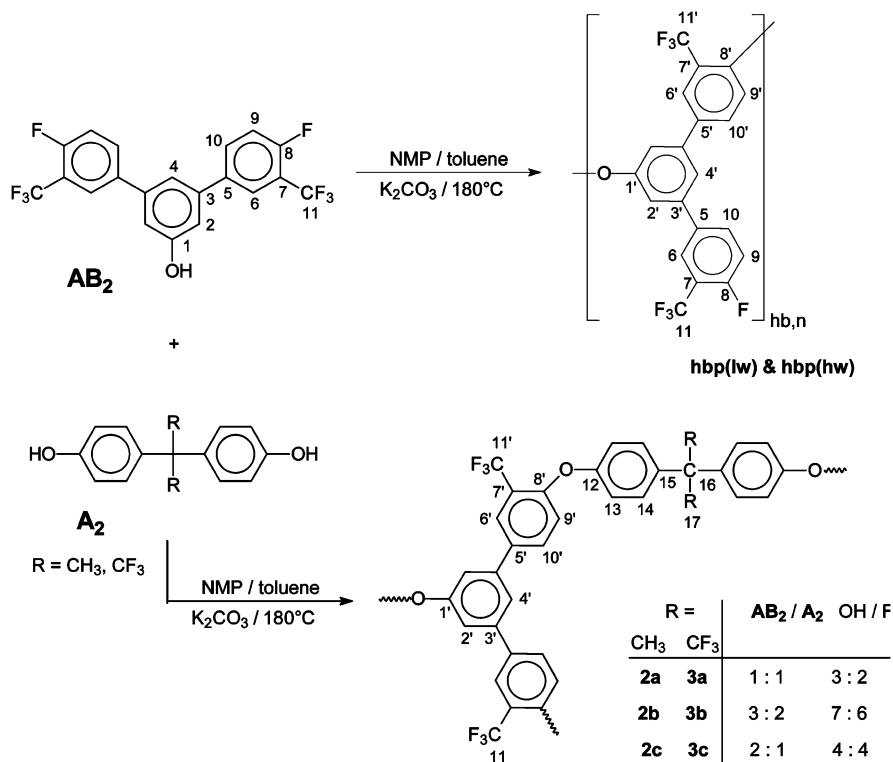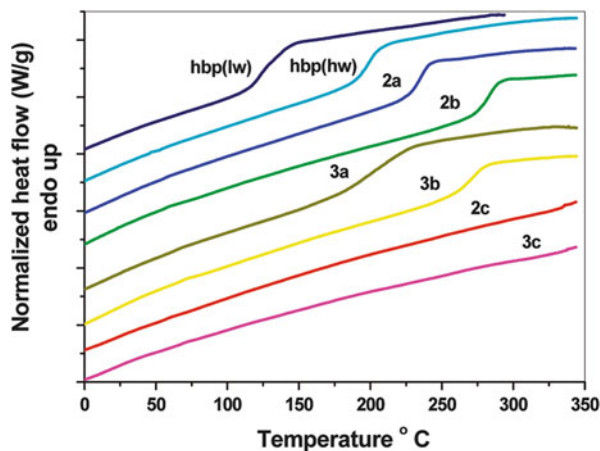
Scheme 15 Reaction scheme and structure of the hb poly(arylene ether)s. Reproduced with permission from [197]

were carried out at lower solution concentration of about 4 wt% to avoid any gelation, and some changes were also made in terms of reaction temperature and reaction time, such as 150°C for 8 h and then at 180°C for another 3 h. These changes were required to avoid any gelation in the 2:1 molar reactions of AB_2 and A_2. The calculation from ^{1}H-NMR spectra for hbp(lw) showed $DB_{Frechet}$ value of 0.5, whereas DB_{Frey} gave a value of 0.44. As the molecular weight increased for high molecular weight F-hb-PAE, broadening of the ^{1}H-NMR signals prevented an accurate determination of the content of linear, dendritic, and terminal subunits. For the polymers **2c** and **3c**, there were broad and overlapping signals; however, the copolymer structures could be confirmed. For the fluorinated hb copoly(arylene ether) samples with excess of A groups (**2a, 2b, 3a,** and **3b**), additional signals due to unreacted A sites of the AB_2 and A_2 monomer, respectively, were observed.

Both refractive index (RI) and multi-angle laser light scattering (MALLS) detectors were used in GPC measurements to determine the molecular weight of the F-hb-PAEs synthesized using different monomer ratios. Extremely high molecular weight products were obtained without gelation for 2:1 molar reactions, with M_w values of ~3,730,000 and ~4,470,000 Da using BPA and 6 F-BPA as A_2

monomers, respectively. The authors stated that for the molar ratio $AB_2:A_2 = 2:1$, i.e., at a stoichiometric equivalence, only half of the A functional groups contributed to potential gelation whereas the other half underwent self-condensation of the AB_2 monomer, and shifted the critical conversion from ~70% to nearly 90% without affecting the molar mass of the product. This observation was somewhat in accordance with the previous theoretical finding by Voit and coworkers on the 'diluting' effect on the critical functionality ratio of adding A_x to AB_2 [198]. The F-hb-PAEs showed excellent thermal stability and very high T_g values. The AB_2 self-condensed F-hb-PAE showed a T_g as high as 199°C and $T_{d,10\%}$ as high as 573°C in N_2, whereas the extremely high molar mass products of the $AB_2 + A_2$ approach did not show any T_g up to 350°C and $T_{d,10\%}$.as high as 554°C.The DSC plots of the fluorinated hb homopoly(aryl ether)s and copoly(aryl ether)s are shown in Fig. 3.

2.2.5 Hyperbranched Poly(aryl amine)s with a Triazine Moiety

Mahapatra and Karak [199] prepared triazine-containing hb polyamines (hb-PAms) by the $A_2 + B_3$ polymerization approach. The methylene-containing hb-PAm (the monomer combination is shown in Scheme 16a) showed a lower T_g of 230°C due to the presence of the flexible methylene linkage compared with the sulfone-containing hb-PAm (monomer combination shown in Scheme 16b), with a T_g of 240°C as per DSC measurements. The solubility studies revealed that the hb-PAms were soluble only in polar aprotic solvents, which the authors attributed to the presence of polar –NH– groups and rigid triazine moieties. Flame retardancy studies revealed that the resulting sulfone-containing hb-PAm showed higher flame retardancy in terms of the limiting oxygen index (LOI), with a value as high as 42 compared with that of the methylene-containing hb-PAm with a LOI value of 32. The authors attributed the higher LOI of the sulfone-containing hb polyamine to the presence of sulfur as a nonflammable element compared to the
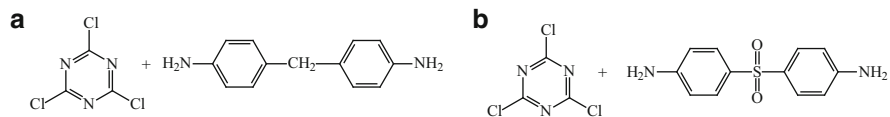
Scheme 16 Structures of monomer combinations used for the synthesis of triazine-containing hb-PAms [199]
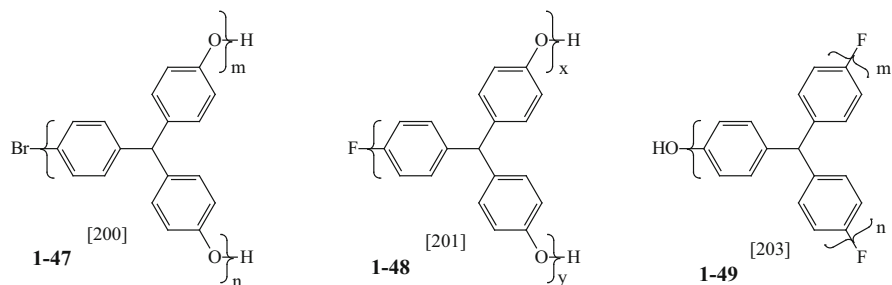
Scheme 17 Structures of hb-PPOs with different end-functionalities

methylene-containing hb-PAm, which might form flammable methane, ethane or similar type of flammable molecule upon combustion.

2.2.6 Hyperbranched Poly(phenylene oxide)s

Zhang et al. [200] prepared an AB_2 monomer, namely 4-bromo-4′,4″-dihydroxytriphenylmethane, through a modified Ullmann reaction. The monomer was treated with K_2CO_3 or NaOH as a base and copper chloride (CuCl) as a catalyst in solvents such as DMSO or sulfolane to form hb poly(phenylene oxide)s (hb-PPOs) with phenolic terminal groups (1–47, Scheme 17). The sulfolane/NaOH system at a higher temperature of ~210°C led to more rapid polymerization with a higher DB (71%), in comparison to polymers prepared in the presence of DMSO/K_2CO_3 at a temperature of 170°C, which showed a DB of 48%. The phenolic terminal groups were modified into a variety of functional chain ends, namely methoxy, 1-butoxy, ethyleneoxy, or diethyleneoxy units, which were coupled with the aryl hydroxyl branch-end. The nature of the chain-end groups showed significant influence on the solubility of the hb-PPOs. The hb-PPOs were insoluble in chloroform, whereas the modified hb-PPOs were soluble in chloroform. Due to the presence of the branched structure and the large number of polar phenolic terminal groups, the resulting samples exhibited higher T_g values, between 130°C and 153°C, compared to linear PPOs with T_g values of about 95°C. The resulting hb polymers showed high thermal stability, with $T_{d,5\%}$ above 258°C in N_2 and above 280°C in air.

Lv et al. [201] designed and synthesized an AB_2-type monomer, namely 4-fluoro-4′,4″-dihydroxy triphenyl methane. Through the homopolymerization of

the monomer, hb-PPO with terminal phenolic groups (**1–48**, Scheme 17) was obtained. Here, the aryl bromide was replaced with aryl fluoride group because in the previous studies [200], hb-PPOs prepared from 4-bromo-4′,4″-dihydroxyltriphenylmethane by the Ullmann reaction had some limitations such as promotion of branching via Ar–CH_3 groups during high temperature processing by the unreacted amine and copper salts and also difficulty in removal of copper salts [202]. Hence, the aromatic nucleophilic substitution reaction was used to replace the Ullmann reaction to synthesize hb-PPO free of the amine and copper salts for environmental safety. Aromatic nucleophilic substitution (S_NAr) is a very effective method among the various reactions that involve a leaving group activated with an electron-withdrawing group that produces an aromatic ether linkage [74, 120]. The fluorine was chosen as a leaving group due to its good reactivity on account of its small size and high electronegativity. Moreover, the fluorine group can offer many desirable properties such as low polarity, low moisture absorption, and good solubility.

A new AB_2 monomer, namely 4-hydroxyl-4′,4″-difluorotriphenylmethane, was successfully synthesized by Luo et al. [203] via a Friedel–Crafts alkylation of phenol from 4,4′-difluorodiphenylmethanol. A series of fluoro-terminated hb-PPOs (F-hb-PPOs, **1–49**, Scheme 17) was prepared by self-condensation leading to different molecular weights, with M_n values varying from 2,000 to 6,800 Da and Đ of 1.7–4.8. It was found that the molecular weight and Đ of the F-hb-PPOs increased with monomer concentration and reaction time. The solubility of the F-hb-PPO was different from the hb-PPO synthesized in a previous study [200], which the authors attributed to the large number of terminal groups leading to the greater solubility of hb polymers. The DB of the F-hb-PPOs decreased from 0.63 to 0.53 as the molecular weight increased. This was attributed to differences in reactivity between the two B groups of AB_2 monomer due to the steric hindrance. The authors were of the opinion that one B group of the AB_2 monomer reacted with an A group and the other B group in the same AB_2 had lesser chance of reacting with the A group. As the molecular weight increased, the hb architecture became larger and the terminal B groups on the outside surface became increasingly crowded. The crowding or the steric hindrance inhibited the reaction between the second B group and the A group, resulting in a more linear architecture and thus lowered the DB. The T_g of the F-hb-PPOs increased with increasing molecular weight, up to 164°C when the M_n was over 6,800 Da. The increase in T_g was ascribed to the highly branched molecular architecture, which could inhibit the mobility of chain segments. The F-hb-PPOs showed excellent thermal stability, with $T_{d,5\%}$ values up to 559°C.

The trifluoromethyl group can act as an effective activating group for fluoro displacement. Ghosh et al. synthesized a new trifluoromethyl-substituted AB-type monomer, namely 4-fluoro-3-trifluoromethylphenyl phenol [204], which was copolymerized with the AB_2 monomer [197] in molar ratio 1:1 to yield a fluorinated hb copolymer by the AB + AB_2 polymerization approach. The representative structure of the hb copolymer is shown in Scheme 18. The DB could not be evaluated from spectral analysis; however, assuming a random copolymerization of the

Scheme 18 Representative
structure of the fluorinated
hb copolymer [204]
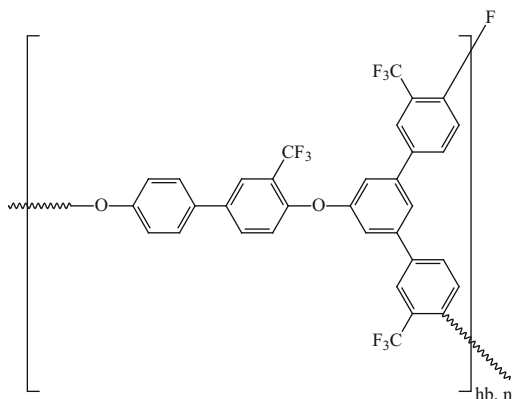
monomers and a full conversion of A groups, the DB should be approximately 44%
as calculated theoretically by Frey and Holter for a 1:1 molar ratio of AB:AB$_2$
[205]. The hb copolymer exhibited M_w of 144,100 Da. The hb copolymers
exhibited good solubility in common organic solvents such as in THF, CH$_2$Cl$_2$,
and CHCl$_3$ compared with a linear polymer that was prepared by self-condensation
of the AB monomer for comparison. The hb copolymers showed excellent thermal
stability, with $T_{d,10\%}$ up to 522°C in air and T_gs as high as 187°C.

2.2.7 Hyperbranched Poly(phenylene sulfide)s

Mellace et al. [206] reported the preparation and characterization of hb poly
(phenylene sulfide) (hb-PPS) utilizing 3,4-dichlorobenzenethiol as the AB$_2$ mono-
mer. Furthermore, polymerization of 3,4-dichlorobenzenethiol as AB$_2$ monomer
with 1,3,5-trichlorobenzene as a multifunctional core (B$_3$ monomer) was utilized to
prepare hb-PPS by the AB$_2$ + B$_3$ approach. Polymerization of commercially avail-
able 3,4-dichlorobenzenethiol was accomplished utilizing anhydrous K$_2$CO$_3$ as a
base in the presence of DMF or NMP as solvent. The monomer combination is
presented in Scheme 19. When DMF was used as solvent, the reaction was carried
out at 100°C for 24 h and in NMP the reaction was carried out at 150°C for 8.5 h.

The polymer resulting from AB$_2$ monomer (see structure of AB$_2$ monomer in
Scheme 19) showed a reasonably high M_w (~17,000 Da), with a Đ value of 2.0
when polymerization was accomplished in DMF as solvent. Addition of 1 core
molecule for every 50 monomers gave a polymer with a M_w of 8,400 Da and Đ of
1.2 in DMF, and a polymer with a M_w of 13,000 Da and Đ of 1.3 in NMP. DSC
revealed that the hb-PPS was amorphous, with a T_g between 60 and 90°C in
comparison to linear PPS with a T_g value of 85°C. No T_m was observed up to
375°C for hb-PPS. They attributed the low T_g values (similar to the linear analogs)
to a change in the nature of the intermolecular interactions as a result of the large
number of terminal chlorines, or to the nonsymmetrical branching [207, 208]. The

Scheme 19 $AB_2 + B_3$ monomer combination for preparation of hb-PPS [206]
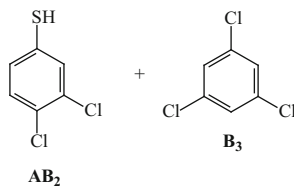
hb-PPSs reported by Mellace and co-workers had both nonsymmetrical branching and a nonsymmetrical arrangement of the chlorines on the terminal groups, which might have resulted in the reduction in T_g. A crystallization temperature T_c was not observed for hb-PPSs by annealing, even when the polymer samples were heated to 300°C, in contrast to the linear PPS that showed T_c of ~225°C. The lack of crystallinity was due to the highly branched nature of hb-PPS. The hb-PPS samples showed an onset temperature for decomposition (T_d) between 400 and 445°C, compared to 480°C for linear PPS. The author attributed the slightly reduced thermal stability to the large numbers of chain ends, which had a tendency to evolve volatiles at a lower temperature, or to effect of chlorination of the terminal and linear groups in the polymer, leading to more rapid chain-cleavage.

A detailed study on the thermal degradation of hb-PPS was accomplished by Bo et al. [209] utilizing thermal decomposition kinetics by applying the Kissinger [210], Friedman [211, 212], and Ozawa–Flynn methods [213]. The values of activation energy were constant with increasing degree of conversion. Through analyzing the activation energies obtained by the three methods, it was found that the values were close to each other for Kissinger, Friedman, and Flynn–Wall–Ozawa methods and the values were 183, 189, and 194 kJ mol^{-1}, respectively. The Coats–Redern method [214–216] was also chosen for determining the activation energy and showed a value of 184 kJ mol^{-1}. These values strongly suggest that the solid-state thermal degradation mechanism followed by hb-PPS is a phase boundary controlled reaction mechanism. Oxidation of the hb-PPS to hb poly(phenylene sulfone) was also accomplished by Mellace et al. [206] with hydrogen peroxide in acetic acid. The resulting sulfone polymers were insoluble in all common solvents. DSC analysis of the hb poly(phenylene sulfone) polymer revealed a T_g of ~155°C, which was higher than for hb-PPS ($T_g = 85$°C) and lower than for the linear aromatic polysulfones, which usually show high T_g values of above 200°C. The hb poly(phenylene sulfone) did not show any detectable T_m due to its branched architecture.

Xu et al. [217] decorated the core of hb-PPS with benzyl, phenyl, and naphthyl groups and investigated the effects of the core structures on the fluorescence properties of hb-PPS. Two hb-PPSs were synthesized (batch 1: polymerization time = 7 h, $M_n = 1,900$ Da, and $Đ = 1.4$; batch 2: polymerization time = 16 h, $M_n = 4,500$ Da, and $Đ = 1.2$). Under the same reaction conditions, three different molecules naphthyl, phenyl, or benzyl were attached to the central thiol (−SH) group as shown in Scheme 20.
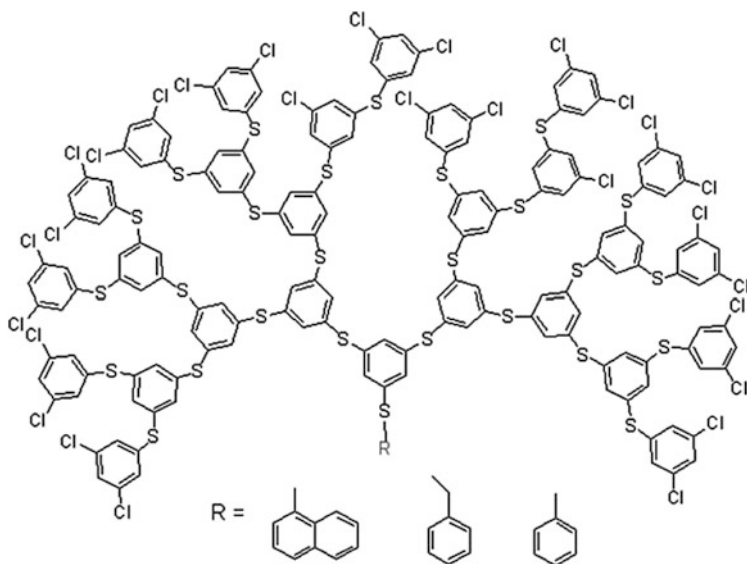
Scheme 20 Schematic structure of core-functionalized hb-PPS. Reproduced with permission from [217]

Both the phenyl-cored and the naphthyl-cored hb-PPS gave rise to a fluorescence peak at about 500 nm due to excimers formed by intermolecular packing, which results in a high degree of fluorescence polarization due to encumbered molecular rotation. Phenyl and naphthyl groups could form conjugated structures with the hb-PPS backbones through sulfide bridges, whereas the benzyl group showed almost no effect on the fluorescence properties of hb-PPS. The naphthyl-cored hb-PPS showed drastic fluorescence enhancement of about 10- to 18-fold higher than the original hb-PPS, indicating that the core structures are conjugated with the hb backbones and might have important effects on the structural rigidity of the hb backbones [218]. The naphthyl core was more restricted in its intramolecular rotations in comparison to the phenyl core, which could easily rotate. DSC analysis showed that the T_g of naphthyl-cored hb-PPS increased to 93°C in comparison with the T_g of 55°C for neat hb-PPS; however, no significant change in T_g was found for benzyl- or phenyl-cored hb-PPS. DSC results indicated that naphthyl-cored hb-PPS showed a higher T_g because of the strengthened intermolecular packing, leading to strengthened planar rigidity, proving that the focal group might have an important effect on the electronic structure of highly branched hb-PPS conjugated polymers.

2.2.8 Hyperbranched Polyarylenes

Acetylene cyclotrimerization is a well-established method for the effective transformation of triple bonds to benzene rings. Acetylenic polymerization has emerged

as a useful technique for the synthesis of advanced specialty polymers with novel molecular structures and unique functional properties. Polycyclotrimerizations of diyne molecules are anticipated to result in the formation of hb polyarylenes [219–221]. The polycyclotrimerization of aromatic diyne uses only a single A_2-type monomer. The A_2-type diyne monomers are stable at room temperature in the absence of a catalytic species. The polymers have been found to exhibit a variety of unique properties such as high luminescence with fluorescence quantum yields up to unity and high thermal stability up to 500°C [222]. Triple bond-mediated metathesis or insertion, coupling, addition, and cyclization have also been explored for synthesis of acetylenic polymers with different chain structures and dimension-alities such as poly(arylene ethynylene), polydiacetylene, polyarylene, and poly (1,2,3-triazole) as well as their substituted derivatives [223, 224].

Hyperbranched Polyphenylenes

Hyperbranched polyphenylenes (hb PPhs) are nonconducting polymers because extended π-conjugation is hindered due to their tightly packed and strongly twisted phenylene units. Different linear or branched PPh have been explored by several research groups [76, 225–227]. The polymers are synthesized utilizing Diels–Alder cycloaddition [228] of phenylated cyclopentadienones with phenylated alkynes and subsequent decarbonylation leading to hb structures with high thermal stability and better processability. Previously, Tang and colleagues prepared hb-PPhs using diyne polycyclotrimerization initiated by transition metal catalysts [229] and base-catalyzed alkyne polycyclization [230].

Hyperbranched PPhs were synthesized by Voit and coworkers [231] utilizing the Diels–Alder reaction with subsequent decarbonylation based on the $A_2 + B_3$, AB $+ AB_2$, and AB_2 approaches. All the polymer backbones were based on hexaphenylbenzene units that were linked in different ways depending on the monomer structure and the Diels–Alder adduct that was formed during the course of the polymerization reaction, which was conducted for 48 h. The structures of the monomers and monomer combinations are shown in Scheme 21. For structural characterization of different hb-PPhs, ^{1}H-NMR and ^{13}C-NMR was carried out. It was difficult to assign terminal, linear, and dendritic substructures due to signal overlap for AB_2 and $AB_2 + AB$-type polymers. For $A_2 + B_3$ polymers, signals for both ^{1}H-NMR and ^{13}C-NMR spectra were clearly distinguishable and it was possible to assign terminal, linear, and dendritic substructures.

The $A_2 + B_3$ polymerization was carried out at different molar ratios of A_2 and B_3 monomers (A_2:B_3 = 1:1, 3:2, 2:1, and 3:1). The molar masses of polymers obtained by the $A_2 + B_3$ approach were lower (M_w = 2,500–68,000 Da, as recorded by refractive index detector) than those of AB_2 polymers (M_w = 47,000–660,000 Da, as recorded by light scattering detector) due to the off-stoichiometric functional ratios. For AB_2-type polymerization, a higher molar mass was attained at longer reaction times. All the AB_2 polymers showed a bimodal weight distribution whereas all the polyphenylenes derived from the A_2 and B_3 monomers showed a
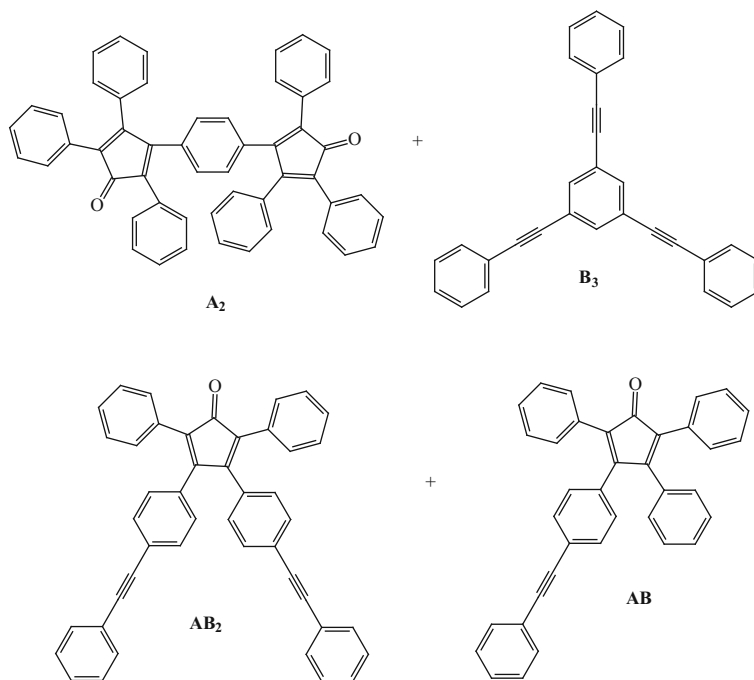
Scheme 21 Structures of monomers and monomer combinations used for the synthesis of hb-PPhs [231]

monomodal distribution. The molar masses of polymers resulting from the $AB_2 + AB$ approach (AB_2:$AB = 3$:1 and 1:1) decreased with an increase in the AB monomer content ($M_w = 74{,}000$–$20{,}000$ Da, as recorded by light scattering detector). All the hb-PPhs showed good solubility in common organic solvents, including chloroform and toluene. The polymer of molar mass $M_w = 95{,}800$ Da and Đ of 9.5 synthesized by self-condensation of AB_2 monomer also showed film-forming ability using very slow evaporation from a chloroform solution over several weeks [232]. Scheme 22 shows the structure of hb-PPh from AB_2 monomer and of a small rolled-up film of hb-PPh. It is noteworthy that the $A_2 + B_3$ system showed no crosslinking at functional equivalence (A_2:$B_3 = 3$:2) although the monomer conversions crossed the theoretical gel points. Voit and colleagues ascribed this behavior to the steric hindrance of the bulky hexaphenylbenzene units after two of the B groups of monomer B_3 were converted, resulting in polymers with a high percentage of linear units. The synthesized hb-PPhs did not show any T_g up to 360°C and TGA measurements showed $T_{d,10\%}$ of 550–600°C, indicating high thermal stability.

Suitable crosslinking chemistry for the hb-PPh with reactive alkynyl functionalities derived from the AB_2 approach, utilizing azide–alkyne click reaction by 1,3-dipolar cycloaddition, was utilized to check the suitability of such polymers as dielectric material in microelectronics. For polymers to be used for optoelectronic
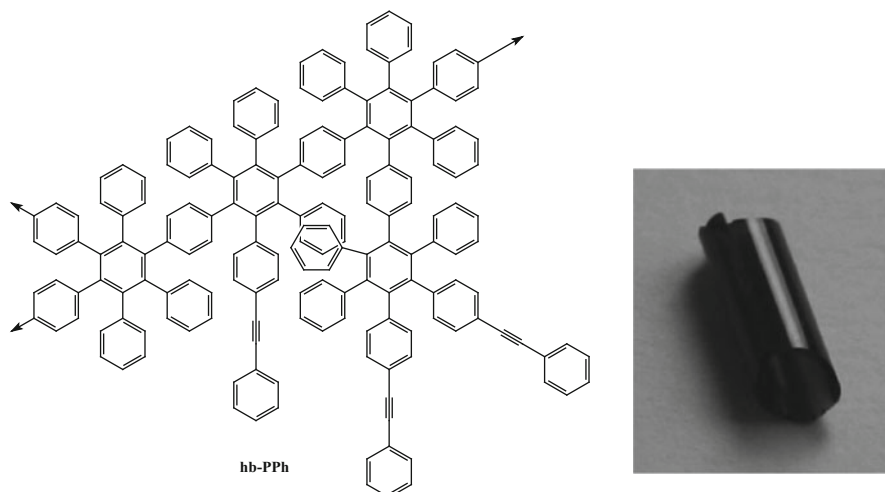
Scheme 22 Structure of hb-PPh from an AB$_2$ monomer (*left*) [231]. Small rolled-up film of hb-PPh of wall thickness ~0.5 mm (*right*). Reproduced with permission from [232]

application a metal-free reaction for curing is the preferred route because the removal of the Cu residues after click coupling of alkyne–azide moieties using Cu(I) catalyst is quite difficult, and small residues might be detrimental for a material to be used in microelectronic applications. Again, high temperatures for curing, such as above 200°C, should be avoided because of potential degradation of some active substances. In this regard, a small molecule, namely 1,3,5-tris (azidomethyl)benzene (TAMB), was prepared by Pötzsch and Voit [233] and successfully used to crosslink the hb-PPh matrix both thermally and photochemically. The mechanisms of these two crosslinking reactions were different; in thermal curing, triazole units were formed between the acetylene groups of hb-PPh and the azide group of the crosslinker in a 1,3-dipolar cycloaddition reaction. In the photochemical curing, a reactive nitrene group was formed upon photolysis of the azide group, which further reacted with the benzene rings in hb-PPh to form an azanorcaradiene derivate and after rearrangement an azepine unit. Films of hb-PPh and TAMB (9:1) were made by drop-casting the 5 wt% toluene solution onto glass substrates and either thermally crosslinking at 180°C for 6 h or exposing to UV light for 2 h. Scheme 23c shows neat hb-PPh film , where immediate film dissolution is observed in CHCl$_3$ yielding a greenish solution that is typical for hb-PPh. In comparison, for the thermally or photochemically crosslinked films, no film dissolution in CHCl$_3$ took place even after several days, indicating that these films were sufficiently crosslinked. Atomic force microscopy (AFM) in tapping mode revealed homogeneous surfaces of thin film, which explains why the thin film morphology remained unaffected by the crosslinking reactions.

The selectivity of thiol addition to a diphenylacetylene (DPA) system was studied recently by Voit and coworkers [234]. When thiophenol was used, no trace of bis-adduct was observed even when a large excess was used, which was
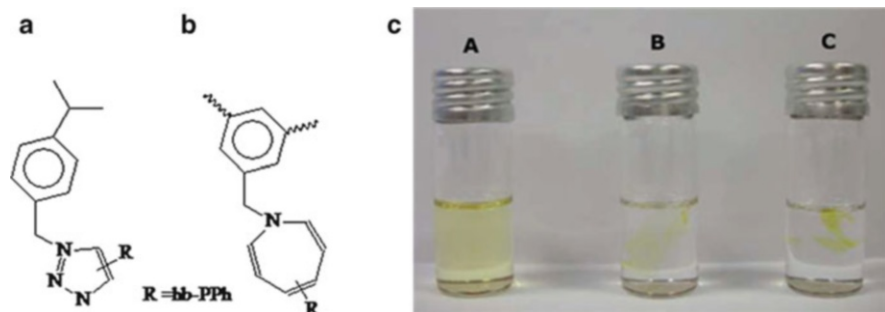
Scheme 23 (**a**) Thermal curing by formation of triazole unit. (**b**) UV curing by formation of azepine unit. (**c**) Films of hb–PPh in CHCl$_3$: pristine film (*A*); thermally crosslinked film (*B*); and UV crosslinked film (*C*). Reproduced with permission from [233]
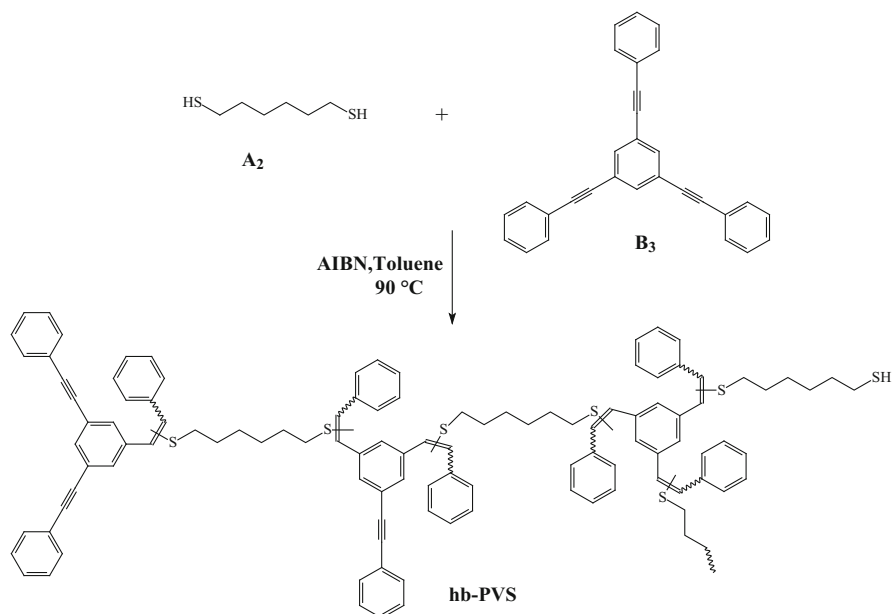
Scheme 24 Synthesis of hb poly(vinyl sulfide) (hb-PVS) with a sketch of the hyperbranched structure showing all potential units that may appear in the final polymer, depending on the molar ratio of A$_2$ and B$_3$. Reproduced with permission from [234]

attributed to the steric hindrance of a second thiol addition to the vinyl sulfide. This selective and efficient mono-addition reaction was applied for the preparation of hb poly(vinyl sulfide)s (hb-PVSs) via the A$_2$ + B$_3$ approach starting from 1,3,5-tris (phenylethynyl)benzene B$_3$ monomer and hexane-1,6- dithiol as A$_2$ monomer (as shown in Scheme 24). Polymerization was therefore conducted with a 1:1 molar ratio of thiol and alkyne functional groups using thermal initiation. The hb-PVS showed $T_{d,5\%}$ of 350°C and T_g of 68°C. The resulting polymer exhibited

excellent solubility in common organic solvents and showed a high refractive index of 1.70 at 589 nm, which was attributed to the presence of sulfur and phenyl rings in the (hb-PVS) [235]. The vinyl sulfides and residual end groups also provided suitable crosslinking sites. The authors concluded that such interesting properties, including good processability and the potential for secondary crosslinking, might be useful for application as suitable coating materials for optical devices.

Utilizing the methodology of selective thiol radical mono-addition to phenyl–acetylene derivatives, Voit and coworkers [236] recently synthesized a series of high refractive index hb polymers (refractive index of 1.68–1.75 with low optical dispersions of 0.004) by using different dithiol and trialkyne monomers. The hb structures produced materials with better performance in terms of light reflection and chromatic dispersion compared with linear analogs that were also synthesized for comparison.
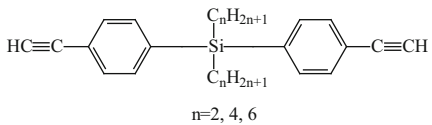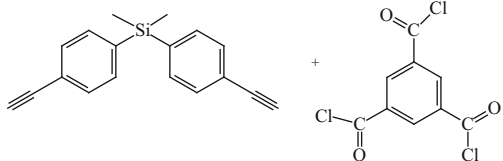
Conjugated Hyperbranched Polyarylenes

A variety of potential optical and electronic applications have been proposed for conjugated polymers, and the perspective has stimulated dynamic research activities on macromolecules with extended π-conjugations [237]. The frontier of research on conjugated polymers is now moving from linear to dendritic and hb structures [238, 239]. In general, such polymers are prepared by transition-metal-catalyzed alkynepolycyclotrimerization involving a single monomer species, such as acetylenic monomers, and do not suffer from stoichiometric imbalance [240]. Tang and coworkers explored polycyclotrimerization of aromatic diynes and succeeded in the homopolycyclotrimerization of organic and organometallic diynes and their copolycyclotrimerization with aromatic and aliphatic monoynes [241, 242].

Liu et al. [243] prepared soluble and processable hb poly(silylenephenylene)s (hb-PSPs) (Table 5, entry 1) by the polycyclotrimerization of A_2-type monomers initiated by a single-component catalyst $TaBr_5$. Spectroscopic analyses assisted by mathematical modeling revealed that ~75% of the triple bonds were cyclotrimerized into benzene rings via a [2+2+2] cyclotrimerization mechanism. The hb-PSPs were completely soluble in common organic solvents. The polymers showed $T_{d,5\%}$ of 480°C, possessed a unique σ–π conjugated electronic structure, and emitted strong violet-blue light upon photoexcitation. The triple bonds on the peripheries allowed the thin films of the polymers to be readily photocrosslinked, generating fluorescent photoimages in high resolutions.

Tang and coworkers [244] further synthesized a series of conjugated hb polyarylenes (hb-PAs) containing carbazole and/or fluorene chromophores by the homo- and copolycyclotrimerization of diynes with monoyne by different transition-metal catalysts and investigated their thermal and optical properties. Alkyne polycyclotrimerizations are effected by TaX_5-Ph_4Sn (X = Cl, Br) and $C_pCo(CO)_2$-$h\nu$ catalysts, yielding soluble hb-PAs with high molecular weights (M_w up to ~1.6×10^5 Da). The homopolymer showed $T_{d,5\%}$ as high as 560°C. All

**Table 5** Monomer structures and monomer combination used for the synthesis of conjugated hb polyarylenes

Entry no.	Monomer structures and monomer combination	References
1	$HC{\equiv}C-\!\!\!\!\!\text{⬡}\!\!\!\!\!-\underset{C_nH_{2n+1}}{\overset{C_nH_{2n+1}}{Si}}-\!\!\!\!\!\text{⬡}\!\!\!\!\!-C{\equiv}CH$ n=2, 4, 6	[243]
2		[246]

the copolymers started degrading at slightly lower temperatures due to the incorporation of aliphatic 1-octyne into the polymer structure. In general, the hb-PAs prepared from $TaCl_5$-Ph_4Sn and $C_pCo(CO)_2$ showed quantum yield values of 50 and 53%, respectively, whereas the hb-PAs obtained from $TaBr_5$-Ph_4Sn showed a quantum yield value as high as 90%. The authors suggested that the poorer π-conjugation along the all-*meta*-substituted benzene ring might partially block the radiative decay pathways of the excited species and, consequently, lower the quantum yield value.

Organometallic hb-PPhs containing ferrocene groups to be utilized for magnetic ceramics were synthesized by Tang and colleagues [245] by designing a diyne monomer carrying a ferrocene moiety as single crystals. Scheme 25 shows the reaction scheme and structures of the monomer and hb-PPh. The authors successfully developed ruthenium- and rhodium-based catalysts to bring the polymerization reactions under control. The hb-PPh recorded by DSC showed a peak at 240°C during the first heating scan due to the thermally induced crosslinking associated with the alkyne polymerization; however, during the second heating scan no exothermic peak was realized indicating that the thermal curing process was irreversible. The (hb-PPh) started to lose weight at temperatures above 300°C.

For metallization, hb-PPh was admixed with octacarbonyldicobalt to form a cobalt complex. Refractive index values were measured for the neat hb-PPh and for the hb-PPh cobalt complex, indicating refractive index values of 1.704–1.681 together with low optical dispersion for the hb-PPh-cobalt complex, as verified by the high value of the Abbe number. The authors concluded that these materials could act as precursors to magnetic ceramics with high magnetizabilities.

Recently, Tang and coworkers [246] reported a new method for the formation of conjugated hb polymers with diyne monomer [bis(4-ethynylphenyl)dimethylsilane] and benzene-1,3,5-tricarbonyl trichloride as branching unit using the $A_2 + B_3$ polymerization approach (Table 5, entry **2**) by the rhodium (Rh)-catalyzed decarbonylative reaction for the formation of hb poly(arylene chloro-vinylene)s. The molar ratio selected for polymerization of A_2:B_3 was 4:3 (A:B = 8:9) so as to
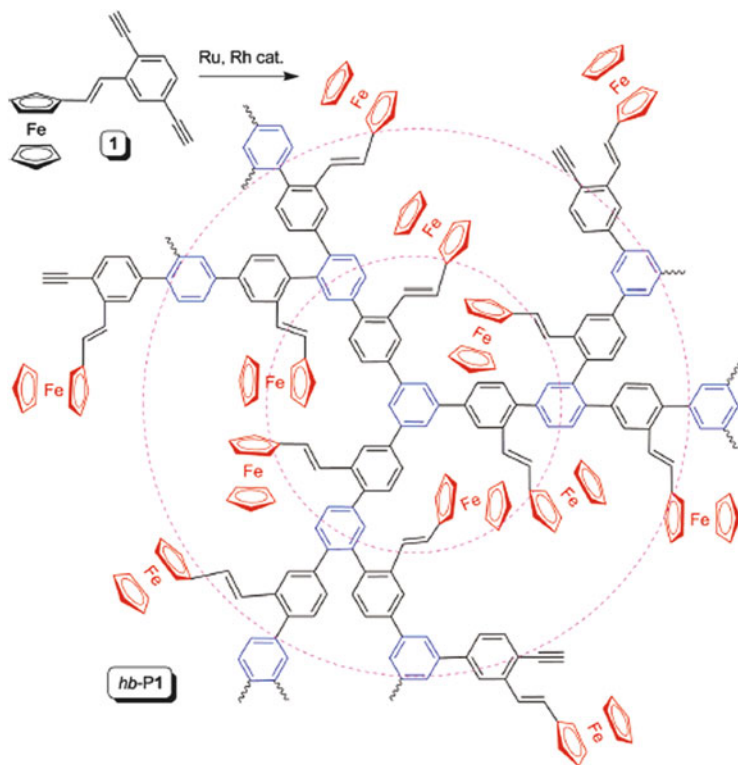
Scheme 25 Polymerization of (*E*)-1-[2-(2,5-diethynylphenyl)vinyl]ferrocene (*1*) to hyperbranched polyphenylene (*hb-P1*) with ferrocenyl groups attached to its repeat branches as pendant groups. Reproduced with permission from [245]

render an excess of alkyne functionalities at its peripheries for post-functionalization. The polymers showed good solubility in common organic solvents. The DB value of hb polymer was determined to be 30%. The authors attributed the low DB to the stoichiometric imbalance of the two mutually reactive groups during polymerization and to structural crowding of the branching unit (benzene-1,3,5-tricarbonyl trichloride). Thus, the reaction of the remaining acyl chloride moiety was difficult after the first two were consumed, leading to the formation of a large fraction of linear units and, hence, a lower DB. DSC measurements showed no thermal transitions in the hb polymer in both first and second heating cycles. The authors assumed that the hb polymer did not undergo any crosslinking reaction or post-polymerization due to its spatially branched structure, which restricted the probability for the vinyl chloride groups to approach each other. The $T_{d,5\%}$ of ~350°C indicated good thermal stability.

3 Applications

Hyperbranched polymers show lower viscosity and better solubility due to the branching and abundant functional groups and therefore they are good for use as additives. The aromatic hb polymers combine good miscibility and are thermally stable enough to allow melt processing.

3.1 *Additives and Rheology Modifier*

Schmaljohann et al. [247] used hb polyesters with alkyl-modified end groups as dye carriers in polyolefins. The use of hb polyesters resulted in a reduced melt viscosity of the polyolefin and a much better distribution of the dye in the polyolefin matrix. Jang et al. [248] showed that a small amount of hb polyester with hydroxyl end groups could greatly reduce the relative crystallinity of a semicrystalline polyethylene terephthalate (PET) through hydrogen bonds between the –OH groups of the hb polymer and the carbonyl groups of PET. Simon and coworkers [249] discovered that the lower-generation hb polyesters (Boltorn™-type) showed shear-thinning, whereas higher-generation polyesters exhibited Newtonian dependency, which was also found in the blends if at least one blend component showed Newtonian behavior. The study of Nunez et al. [250] on the rheological behavior of hb polyesters and their blends with linear polymers observed a drastic decrease in viscosity depending on the hb polymer concentration in the blends. More recently, Li et al. [251] employed hb poly(ether ether ketone) (hb-PEEK) at 1–5 wt% as a rheology modifier towards linear poly(ether ether ketone) (LPEEK) for improving the melt processability. Interestingly, the crystallization temperatures (T_c) of LPEEK/hb-PEEK blends were higher than that of pure LPEEK ($T_c = 283°C$), and the T_c of LPEEK/hb-PEEK blends gradually increased from 288 to 294°C with increasing hb-PEEK content in the blends. The increase in T_c of the blends was attributed to the enhanced crystallization capacity of LPEEK because incorporation of branched polymer resulted in a lower melt viscosity of the LPEEK/hb-PEEK blends compared to pure LPEEK, thus improving the mobility of LPEEK segments and leading to the increase in the crystallization capacity of LPEEK. Figure 4 shows the effect of hb-PEEK concentration on nonisothermal crystallization of LPEEK, indicating an increase in the crystallization capacity of LPEEK in the blends due to the presence of hb-PEEK as a rheology modifier in the crystallizing process of LPEEK.

Bismaleimide (BMI) resin is one of the most important thermosetting polymers due to its superior thermal resistance, outstanding dielectric property, and good fatigue resistance at high humidity. However, being a thermosetting resin, original BMI resins suffer from brittleness and poor processing features, such as high melting point and narrow work life, so toughening and improving the processing characteristics have been the main targets of the investigation of BMI resins. Recently, Tang et al. [252] synthesized allyl-terminated hb-PAEK and incorporated it into the BMI matrix with the aim of improving the toughness. BMI resins

Fig. 4 Effect of hyperbranched poly(ether ether ketone) (*HPEEK*) concentration on nonisothermal crystallization of linear poly (ether ether ketone) (*LPEEK*) at 10°C/min. Reproduced with permission from [251]
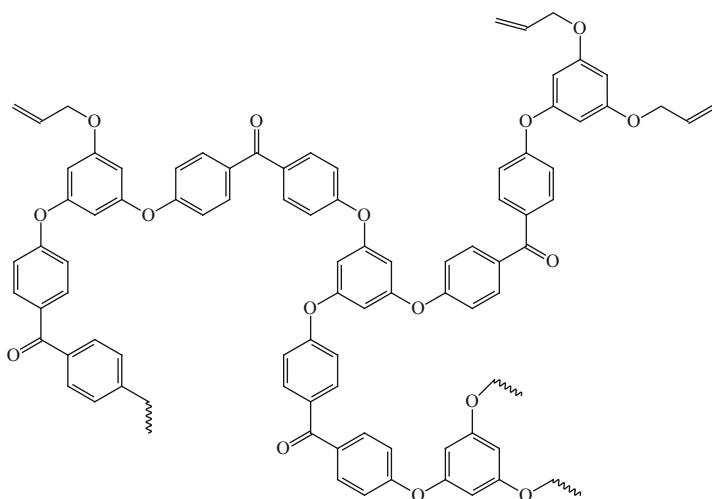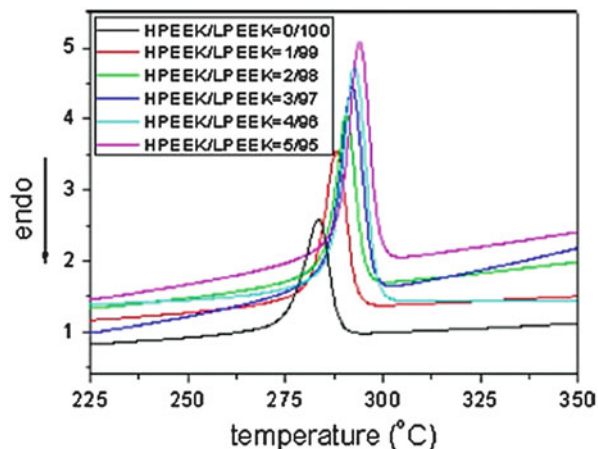
Scheme 26 Structure of allyl-terminated hb-PAEK [252]

modified by allyl-terminated hb-PAEK (see structure in Scheme 26) showed good processability, with viscosities below 0.6 Pa s at 110°C. An increase in impact strength from 9.5 kJ/m^2 to about 14 kJ/m^2 was realized, indicating improvement in the toughness of the cured BMI resins due to the presence of allyl-terminated hb-PAEK.

Aromatic hb polyamides have been used to modify the thermal, dielectric, viscoelastic, and rheological properties of linear polyamides [253, 254]. The characteristic architecture of these macromolecules makes them interesting candidates as a blend component with commercial linear polymers. A hb poly(ether amide) was blended with commercially available polyamide-6 (PA6) by Huber et al. [255] and Clausnitzer and coworkers [256]. The complex melt viscosity of the new materials was reduced, even at small amounts of the hb polymer, whereas the
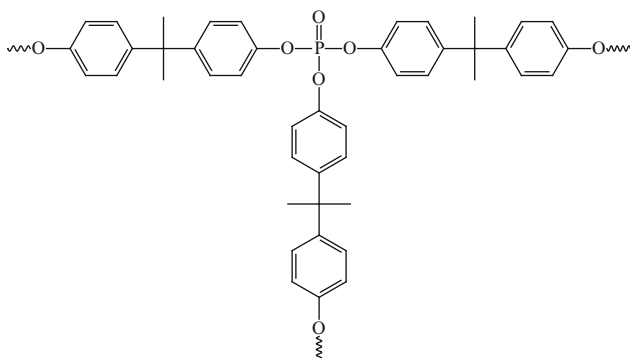
Scheme 27 Structure of dendritic unit of hb polyphosphate ester [258]

mechanical properties of the blends remained nearly constant. This was explained by the formation of hydrogen bonds between the hb polymer with the large number of hydroxyl groups and the polyamide. Hyperbranched polyphenylenes synthesized from AB_2 monomers were blended with linear polystyrene (PS) [76]. The resulting materials exhibited a reduced viscosity at high temperatures and an improved thermal stability compared with pure PS.

PA6 is one of the most important engineering plastics and is widely used as fibers, molded articles, and binders for composites. However, the applications of PA6 are still restricted in many fields owing to its poor flame retardant property and low limiting oxygen index (LOI) ~21, and because it burns easily. Fang et al. [257] synthesized hb polyphosphate bisphenol-S ester to improve the flame retardancy of PA6. Chen et al. [258] synthesized hb polyphosphate ester (Scheme 27) and used it as curing agent and flame retardant in epoxy resins.

Polypropylene shows an interesting set of mechanical and physical properties but it lacks dyeability and is not usually regarded as a textile fiber. Many efforts have been made to improve the dyeability of polypropylene. Recently, Sari et al. [259] utilized a poly(ester amide)-based hb polymer (Scheme 28) in fiber-grade polypropylene (PP) to study the nanostructure of the hb-modified PP and its correlation with macromechanical behavior. The study revealed an enhancement in mechanical properties due to the grafting reactions of hb poly(ester amide), leading to the formation of a crosslinked nanostructure of dendritic domains. The domains were capable of penetrating into the amorphous phase of the semicrystalline structure of the PP matrix and behaving as a toughener.

In order to improve the toughness of epoxy materials, hb polymers, having a 3D globular architecture and a large number of functional groups, were used for improving the toughness [260] and reducing the dielectric constant [203] by blending with epoxy resin lacking such qualities.

Qiang et al. used hb polymer with a terminal carboxyl group as an additive in auxiliary tanning of natural leather to improve the moisture absorption and permeability to water vapor of microfiber synthetic leather [261]. Recently, Ren et al. [262] prepared amino-terminated hb polyamide and grafted the same onto the polyamide microfiber synthetic leather employed for clothing, and organic
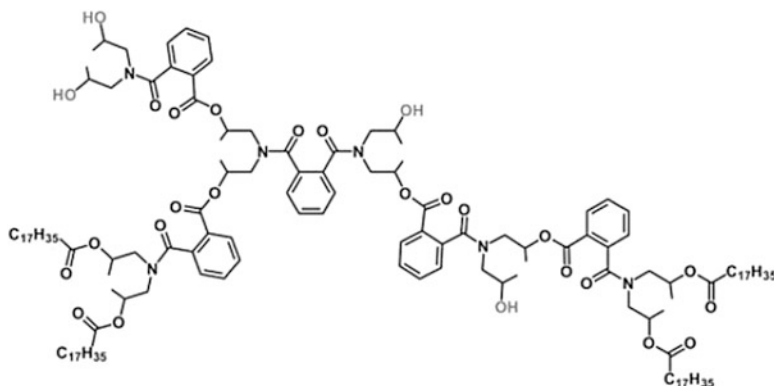
Scheme 28 Structure of hb poly(ester amide) (DSM Hybrane PS2550). Reproduced with permission from [259]

phosphine was used as a crosslinking agent to improve the content of the active groups and enhance the dyeing rate and color fastness. Wang and colleagues [263] synthesized hb poly(aryl ether ketone) terminated with cobalt phthalocyanine (CoPc-hb-PAEK) and studied its catalytic activity in oxidative decomposition of 2,4,6-trichlorophenol (TCP); the results were compared with those for the linear poly(aryl ether ketone) terminated with cobalt phthalocyanine [264, 265]. CoPc-hb-PAEK decomposed 75% of initial TCP within 7 h, whereas linear analogs decomposed only 68–70% within 7 h. This indicated that the efficiency of CoPc-hb-PAEK was better than the linear analogs due to highly branched structure of CoPc-hb-PAEK, followed by the high density and good dispersion of cobalt phthalocyanines compared to the linear analogs.

Hence, because of their unique 3D structure and the large number of functional groups, hb polymers provide high chances for possible interactions and, therefore, are expected to result in novel materials with improved properties upon compounding with other components. Thus, hb polymers are considered good candidates for use as additives and rheology modifiers.

3.1.1 Hyperbranched Phenylene Oxide as a Low Temperature Curing Agent

An epoxy-functionalized hb-PPO (epoxy-hb-PPO) (see structure in Scheme 29) was synthesized by Huang et al. [266] and the effect of adding 2.5–15% of epoxy-hb-PPO on the curing mechanism and kinetics of cyanate ester (CE) was studied.

Each prepolymer showed one exothermic peak; however, interestingly, all peaks of CE/epoxy-hb-PPO prepolymers appeared at a significantly lower temperature than those of CE prepolymer, demonstrating that an additional reaction took place in the CE/epoxy-hb-PPO resin system. The curing mechanism of CE was the cyclotrimerization of CE, whereas that of CE/epoxy-hb-PPO included the cyclotrimerization of CE under the catalytic role of –OH groups in epoxy-hb-PPO, the

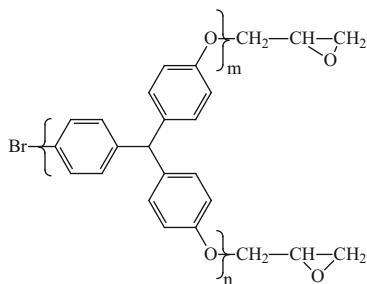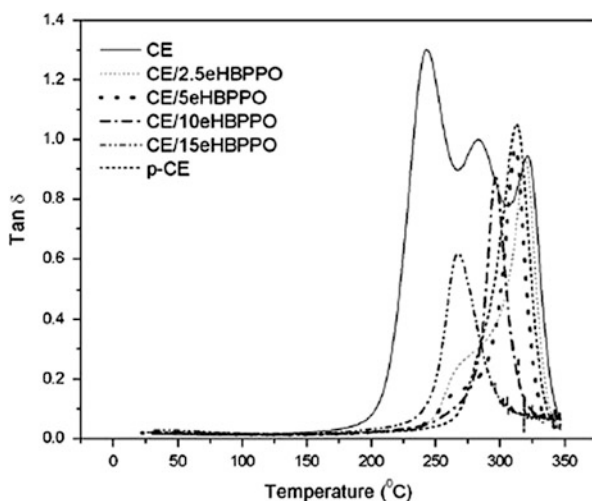**Scheme 29** Structure of epoxy-functionalized hb-PPO [266]

Fig. 5 Overlay plots of tan ∂ versus temperature for cured cyanate ester (*CE*), cured CE resin post-cured at 230°C (*p-CE*), and epoxy-functionalized hyperbranched poly (phenylene oxide) (*CE/ eHBPPO*) resins. Reproduced with permission from [266]

copolymerization between epoxy and –OCN groups as well as triazine rings of CE, and the self-polymerization of epoxy-hb-PPO. Moreover, CE/epoxy-hb-PPO showed a slightly smaller apparent activation energy (55–57 kJ mol^{-1}) than CE (58 kJ mol^{-1}), indicating the ease of the curing reaction of CE/epoxy-hb-PPO with the addition of epoxy-hb-PPO to CE. On the other hand, CE/epoxy-hb-PPO molecules less easily to collide with each other for curing because of the more branched architecture of epoxy-hb-PPO compared with neat CE. The incorporation of 10 and 15% of epoxy-hb-PPO to CE yielded CE/10epoxy-hb-PPO or CE/15epoxy-hb-PPO resin systems and their thermal properties were studied. Because the T_g of the cured CE ranged from 243 to 321°C and was difficult to compare with the resin systems containing epoxy-hb-PPO, the authors compared the thermal properties of the resins with p-CE (cured CE resin post-cured at 230°C), which showed a single T_g value of 314°C, as recorded from the plot of tan ∂ versus temperature. The T_g values observed for CE/10epoxy-hb-PPO and CE/15epoxy-hb-PPO resin system were 296 and 266°C, respectively, which were lower than the T_g value of the p-CE, indicating that the CE/epoxy-hb-PPO resin systems cured at lower temperatures than p-CE. Figure 5 shows the tan ∂–temperature plots for cured CE, p-CE, and CE/eHBPPO resins.
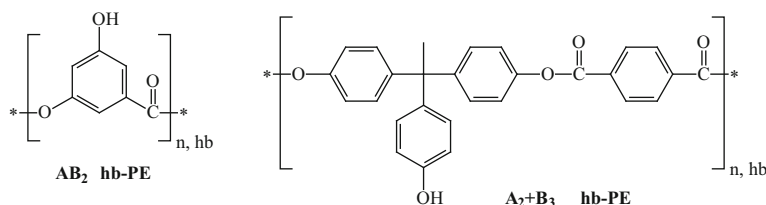
Scheme 30 Structures of hb-PEs from AB$_2$ and A$_2$ + B$_3$ approaches [267]

3.1.2 Hyperbranched Poly(aryl ester)s as Rheology Modifiers for Linear Polyamides

Voit and coworkers utilized high T_g hb aromatic polyesters [115] as additives for modification of the most important engineering thermoplastics, namely polyamides, in terms of their thermal properties and melt rheological behavior by blending. A lowering of the melt viscosity and, thus, an improvement in the processing properties is of high interest, especially for the partially aromatic polyamide PA6T/6, which requires a processing temperature above 310°C. Different amounts of the two hb polyesters, from 1 up to 20 wt%, were added to the linear thermoplastic polyamides by melt mixing. Two different polyamide grades, either partly aromatic polyamide-6 (PA6) or aliphatic polyamide-6 T-type (PA6T/6), were used for blending with hb aromatic polyesters [267]. Scheme 30 shows the structures of the AB$_2$ and A$_2$ + B$_3$-type polyesters that were used for blending. The influence of the addition of AB$_2$ and A$_2$ + B$_3$-type polyesters on the rheological behavior of linear polyamides was investigated. Miscible blends were formed in all cases, as was confirmed by a single T_g in DSC measurements.

The –OH group density in AB$_2$ hb polyesters (hb-PEs) was higher than that of A$_2$ + B$_3$ hb-PEs. The hb-PEs were compounded in the melt with the partly aromatic polyamide PA6 and the aliphatic polyamide PA6T/6 to obtain polyamide blends. Melt mixing was carried out at 320°C for PA6T/6 and at 250°C for PA6. As control samples, pure matrix polyamides and pure hb polyesters were also processed under the same conditions for comparison with the blends. All of the blends showed both T_g and T_m, indicating the semicrystalline nature of the polymer blends. The T_m as well as the crystallinity of the blends of PA6T/6 and hb-PE containing the AB$_2$ hb-PE was decreased from 297 to 258°C with increasing the amount of hb polymer from 1 to 20 wt%. The T_m as well as the crystallinity of the PA6/hb-PE blends containing the AB$_2$ hb-PE was decreased from 221 to 205°C with increasing the amount of hb polymer from 1 to 20 wt%. The T_g of the blends increased from 103 to 119°C for polyamide PA6T/6 as matrix material and from 56 to 72°C in the blends for polyamide PA6 as matrix material with increasing the content of AB$_2$ hb-PE from 1 to 20 wt% in the blends. With respect to the structures of the hb polyester and the polyamides, the increase in T_g was favored due to the formation of strong hydrogen bonding between the hydroxyl groups of AB$_2$ hb-PE and the carbonyl groups of the polyamides.

The addition of 1–10 wt% of $A_2 + B_3$ hb-PEs to polyamide PA6T/6 showed negligible effect on the T_g of the blends, the value of 101°C being the same as that for the polyamide PA6T/6. This was attributed to the influence of the temperature selected for compounding. At high processing temperatures (320°C) for the PA6T/6 blends, the $A_2 + B_3$ hb-PEs might undergo side reactions such as post-polymerization, leading to crosslinking, which prevent the formation of miscible blends. Gas chromatography/mass spectrometry (GC/MS) investigations of $A_2 + B_3$ hb-PE showed a release of phenol at temperatures above 250°C due to decomposition of terminal groups derived from the B_3 monomer [115], thus reducing the number of free phenolic groups responsible for the interactions with the polyamide.

The modification of PA6T/6 with AB_2 hb-PE led to a reduction in the complex viscosity, even at low concentrations of AB_2 hb-PE. After adding 1 wt% of AB_2 hb-PE, the zero-shear viscosity of PA6T/6 changed from 500 Pa s (0 wt% of AB_2 hb-PE) to 340 Pa s (1 wt% of AB_2 hb-PE). By increasing the amount of AB_2 hb-PE in the blends, a continuous reduction in the viscosity was observed until a concentration of 10 wt% was reached. Further increase in the AB_2 hb-PE content of the blends did not further affect the complex viscosity. The decreased melt viscosity of the resulting blends indicated improved processability of polyamides by the addition of AB_2 hb-PE. Adding 1 wt% of $A_2 + B_3$ hb-PE to PA6T/6 resulted in a comparable complex viscosity to that of the processed matrix polyamide. However, a larger amount of $A_2 + B_3$ hb-PE (10 wt%) in the blends resulted in a reduction in viscosity, especially in the region of higher frequencies. Generally, for the same concentration (e.g., 10 wt%) of hb polymers in the blends, the addition of AB_2 hb-PE resulted in a much more significant reduction in the complex viscosity of the final material than addition of $A_2 + B_3$ hb-PE.

All of the blends of PA6 and the hb polyesters exhibited Newtonian behavior. Only at a high content of AB_2 hb-PE was a decrease in the complex viscosity of the blends observed. The addition of $A_2 + B_3$ hb-PE to PA6 resulted in a continuously increased zero-shear viscosity from 380 to 920 Pa s with increase in the content of $A_2 + B_3$ hb-PE from 0 to 15 wt% in the blends, which is in contrast to previous findings [49, 247, 254, 268]. This was attributed to the existence of a heterogeneous system in which a phase with a higher viscosity ($A_2 + B_3$ hb-PE) was dispersed in the continuous phase (PA6) possessing a lower complex viscosity, and this was also manifested in the scanning electron microscopy (SEM) images. The hb polymer phase behaved like reactive filler. Also, $A_2 + B_3$ hb-PE distributed in the blend might behave as a coupling agent, connecting the polyamide chains at different positions through strong physical interactions that result in effects similar to a material being reinforced, causing an increase in the complex viscosity. In general, the addition of AB_2 hb-PE to the polyamides showed a more pronounced effect on the improvement of T_g and the processability of both the polyamides. However, the gelation tendency of $A_2 + B_3$ hb-PE at higher processing temperatures and the larger nonpolar branching unit and lower branching density lead to a lower miscibility of $A_2 + B_3$ hb-PE within the polyamide matrix. Besides, the lower density of –OH groups in $A_2 + B_3$ hb-PE induce a lower possibility for hydrogen bonding between $A_2 + B_3$ hb-PE and polyamides. Hence, AB_2 hb polyesters show a much higher
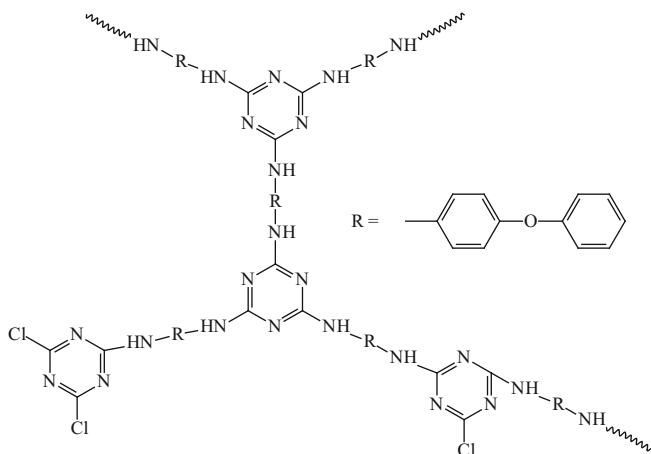
Scheme 31 Representative structure of hb-PAm used as flame retardant for PA6 [269]

potential for use as processing additives in linear thermoplastic polyamides compared to $A_2 + B_3$ hb polyesters because of the potential post-polymerization at the processing temperatures.

3.1.3 Hyperbranched Poly(aryl amine) as Flame Retardant for PA6

A hb polyamine (hb-PAm) was prepared by Ke et al. [269] utilizing the $A_2 + B_3$ approach where s-triazine was the B_3 monomer and ODA was the A_2 monomer. The representative hb-PAm structure is shown Scheme 31. The resulting hb-PAm acted as a hb charing and foaming agent (HCFA) in combination with ammonium polyphosphate (APP) to form a new intumescent flame retardant (IFR) system for PA6, abbreviated as IFR-PA6. The effect of HCFA on the flame retardance and thermal degradation properties of IFR-PA6 was investigated by the limiting oxygen index (LOI), UL-94 vertical burning, cone calorimetry, and thermogravimetric analysis (TGA).

The experimental results of UL-94 vertical burning indicated that all the IFR-PA6 composites gave a V-0 rating when the weight ratio of HCFA to APP was between 1:3 and 3:2. The IFR system showed the most effective flame retardancy in PA6 when the weight ratio of HCFA to APP was 1:2. The LOI value of IFR-PA6 could reach 36.5 with a V-0 rating when the IFR loading was 30 wt%. Additionally, even with 25 wt% loading of the IFR (where HCFA: APP = 1:2), a V-0 rating could be still maintained with an LOI value of 31. The interaction between APP and HCFA improved the char formation ability of the IFR system. Much more char was formed for the PA6/HCFA/APP composite than for the PA6/APP system, indicating better flame retardancy with incorporation of HCFA. The char acted as a barrier that prevented the transfer of gas and heat flow during combustion and, hence, the flame retardancy of PA6 resin was greatly

improved by adding HCFA to the system. The average heat release rate (Av-HRR), peak heat release rate (PHRR), and total heat release (THR) values were recorded by a cone calorimeter. In general, for effective flame retardant materials, the heat release in tests should reduce drastically. The results of cone calorimetry also showed HCFA/APP as an effective IFR system for PA6. Neat PA6 showed the following values: Av-HRR 310 KW/m^2, PHRR 490 KW/m^2, and THR 106.5 MJ/m^2. For the PA6/APP system, the values were reduced: Av-HRR 133 KW/m^2, PHRR 420 KW/m^2, and THR 43.7 MJ/m^2. The PA6/HCFA/APP showed Av-HRR 76 KW/m^2, PHRR 343 KW/m^2, and THR 31 MJ/m^{2}values, which were lower than the values recorded for neat PA6 and indicated that PA6/HCFA/APP is an effective flame retardant system. TGA results showed higher char residue at 700°C for the PA6/HCFA/APP composite system (24% char residue) compared to the PA6/APP composite system (15% char residue) because when HCFA was added the polyphosphoric acid not only interacted with PA6 but also with HCFA, decreasing the amount of evaporated excess polyphosphoric acid and enhancing the char formation ability.

3.1.4 Hyperbranched Polyphenylene Sulfide as Textile Dyeing Agent for Polypropylene

The hb-PPS prepared from previously synthesized AB$_2$ monomer [206] was utilized for studying the dye uptake by PP in the presence of a monoazo-type of disperse dye, namely CI Disperse Red 202 [270]. The hb-PPS at various concentrations was added to PP granules followed by melt mixing to form hb-PPS/PP spun fibers. Due to the presence of polar groups and aromatic rings in hb-PPS, the hb-PPS/PP spun fibers showed the potential to interact with the dye. The neat PP fibers were dyed to a pale depth and the modified PP fibers were dyed to a deeper depth, indicating the presence of hb-PPS in the modified PP. In the case of the modified PP fibers, the dye uptake increased with increased hb-PPS content from 1 to 3 w/w%, which was attributed to the increased introduction of polar groups and aromatic rings that acted as active sites for the dye molecules. With hb-PPS dispersed in PP matrix, the chlorides formed intermolecular hydrogen bonding with the proton-supplying groups (such as −OH and −NH$_2$) present in the dye structure. Aromatic rings, present in hb-PPS, formed π bonds with the groups in the dye molecules supplying protons, which also helped to produce deeper shades of color. There was no increase in the depth of shade in hb-PPS modified PP fibers with increasing the dye concentration from 4 to 6%, which Yan's group attributed to the saturation of dye sites in hb-PPS-modified PP fiber. The hb-PPS/PP blends showed only one T_g, corresponding to the T_g of PP, because of the very low content of hb-PPS present in the blend. Interestingly, with increasing the hb-PPS content, the T_g of the PP phase showed a tendency to shift towards higher temperatures, indicating that the blends were partially miscible.

3.2 Membranes

Aromatic hb polymers have been found to fulfill the broad material needs for membrane-based separation applications due to their large free volume. Some selected examples will be highlighted to demonstrate the potential of hb polymers for membrane-based applications.

In recent years, there has been increasing interest in reverse osmosis (RO) membranes for desalination. Thin film composite polyamide membranes are currently used in commercial RO membranes [271]. Among these materials, m-phenylenediamine- and trimesoyl chloride-based polyamides prepared by interfacial polymerization are available as commercial products [272, 273]. Ideally, RO membranes should possess high flux and high salt rejection, in addition to excellent chlorine and fouling resistance, mechanical durability, and low cost. Chiang et al. [274] synthesized nanofiltration membranes based on hb polyethyleneimine ($M_w = 2,000$ Da) with two acyl chlorides, namely trimesoyl chloride and terephthaloyl chloride. They observed that highly branched polyamides showed higher flux and higher salt rejection to sodium chloride, which the authors attributed to the presence of pendant amine groups that interact with the ions in the pathway and thus hinder ion transport. Recently, Park et al. [275] prepared hb aromatic polyamide-grafted silica and disulfonated 4,4-bis(3-aminophenoxy)phenyl sulfone composite membranes to enhance the chlorination resistance of RO membranes for desalination. After the chlorination test, salt rejection was decreased by 36.2% and water permeation was increased by only 5.6% compared with performance before chlorination measurement.

Fuel cells are regarded as efficient and clean energy sources as alternatives to limited fossil fuel resources. For proton exchange membranes for fuel cell (PEMFC) applications, high proton conductivity, mechanical properties, and oxidative stability are the basic requirements. DuPont's Nafion is a commercially available perfluoro sulfonated polymer membrane and is the current state-of-the-art proton exchange membrane [276]. However, Nafion has the drawbacks of low operational temperature ($<80°C$) and being very costly due to its complex preparative technique. These deficiencies have produced great research interest in developing alternative polymer electrolyte membranes based on ethoxysiloxane [277]. The proton conductivities of these membranes are comparable to Nafion 115 in humid state. In a separate study, Gode et al. synthesized a novel sulfated hb polymer for the PEMFC [278], such as sulfonated poly[3-ethyl-3-(hydroxy-methyl] oxetane. The hb polymer-containing PEMFC showed higher proton conductivity compared to Nafion 117 in humid state. The hb sulfonated poly(3-ethyl-3-(hydroxy-methyl) oxetane-modified membrane was more flexible and exhibited better mechanical properties than the chemically crosslinked membranes, such as the Nafion series. Recently, Itoh et al. synthesized two novel hb polymers with sulfonic acid or acryloyl groups at the end of chains [279]. It was reported that the ionic conductivity of these two novel hb polymers increased with increasing

temperature and that the thermal stability of these materials was perfect up to 200°C.

Membrane-based gas separation has attracted much attention during the last two decades. Compared with traditional separation processes it has many significant advantages, such as low investment cost, low energy consumption, simple operation, etc. Gas separation processes using polyimide gas separation membranes have been developed and are of great interest because of their excellent thermal, mechanical, and gas transport properties [280]. The high gas permeability of polyimides is generally attributed to the large fractional free volume, which is closely related to their highly rigid structure, whereas the high selectivity is due to the high diffusion selectivity and/or the high solubility selectivity. On the other hand, it is reported that there are many open and accessible cavities in a rigid hb polymer that are formed due to the periphery of neighboring branches. These cavities may function as the pathways for the transport of gas molecules, resulting in high gas permeability [281–286].

3.2.1 Sulfonated hb Poly(aryl ether ketone) for PEMFC

Wang et al. [287] prepared sulfonated linear poly(aryl ether ketone) (S-LPAEK)/ sulfonated hb poly(aryl ether ketone)s (S-hb-PAEKs) blend membranes and focused on the influence of the IEC and the content of S-hb-PAEKs on the properties of the blend membranes. The S-LPAEK membranes with varying content of sulfonated groups were synthesized and characterized. Three S-hb-PAEKs were synthesized based on varying degrees of sulfonation by post-functionalization of fluoro-terminated hb poly(aryl ether ketone) (F-hb-PAEK) with concentrated sulfuric acid at different temperatures and reaction times to afford S-hb-PAEKs with three different ion exchange capacities (IECs); these were named S-hb-PAEK-20, S-hb-PAEK-40, and S-hb-PAEK-60. The monomer combinations for the synthesis of S-LPAEK and S-hb-PAEK are shown in Scheme 32. The, S-hb-PAEKs and S-LPAEKs were blended and cast into membranes. The blend membranes were prepared using DMAc as solvent and S-hb-PAEK content was 15, 20, 25, and 30 wt% in the S-hb-PAEK/S-LPAEK blends.

The T_g of F-hb-PAEK was 124°C, whereas no T_g was found up to 300°C for S-hb-PAEKs due to the ionic effects that produced increased intermolecular interaction, followed by the difficulty of the internal rotations. The thermal stability of F-hb-PAEK was better than that of the S-hb-PAEKs, and the thermal stability of S-hb-PAEKs gradually decreased with increasing IEC value because of the increase in sulfonated groups.

The T_g values of all S-hb-PAEK/S-LPAEK blend membranes were lower than 214°C (the T_g of the sulfonated linear analog, S-LPAEK was 214°C) and gradually decreased with the increase in S-hb-PAEK content. The T_g values of these membranes were 214, 199, 188, 184, and 180°C for blend composition S-hb-PAEK-XX/ S-LPAEK with S-hb-PAEK-XX contents of 0, 15, 20, 25, and 30 wt%, respectively. Besides, S-hb-PAEK-40/S-LPAEK and S-hb-PAEK-60/S-LPAEK membranes
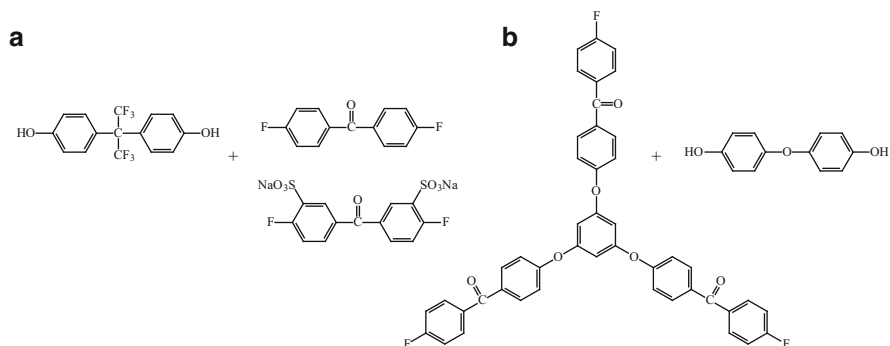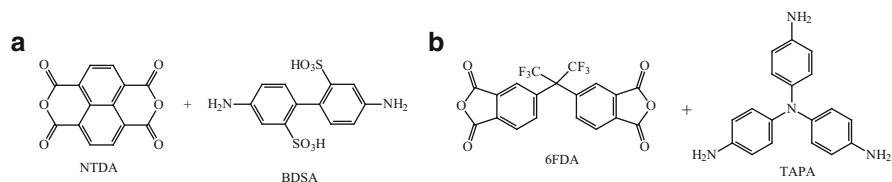
Scheme 32 (**a**) Monomer combinations for the synthesis of S-LPAEK. (**b**) Monomer combination for the synthesis of S-hb-PAEK [287]

showed similar a trend. The blend membranes exhibited second and third weight loss at ~350°C and 500°C, corresponding to the loss of sulfonated groups and the actual thermal decomposition of the polymer backbone, respectively, indicating high thermal stability. The water uptake and proton conductivity of all the blend membranes increased with the IEC and content of S-hb-PAEK in the blend membranes compared to neat S-LPAEK. This was a result of the formation of larger and more continuous ion networks as well as an increase in the free volume arising from the introduction of the branched structure. The membranes exhibited enhanced proton conductivity at lower temperatures (20 and 40°C).

3.2.2 Sulfonated Star Hyperbranched Polyimide for PEMFC

Suda et al. [288] reported the synthesis and characterization of a series of sulfonated star-hb polyimides (S-hb-PIs) without any crosslinking for use as proton exchange membranes. Sulfonated anhydride-terminated polyimides with different molecular weights (M_w = 59,000, 200,000 and 300,000 Da) based on monomer combination 1,4,5,8-naphthalene tetracarboxylic dianhydride/4,4′-diaminobiphenyl 2,2′-disulfonic acid (NTDA/BDSA) were synthesized using different molar ratios of BDSA:NTDA. The amine-terminated hb-PI based on monomer combination 4,4-(hexafluoroisopropylidene)diphthalic anhydride/tris(4-aminophenyl)amine (6FDA/TAPA) was also prepared. Scheme 33 shows the monomer combinations used for the preparation of (S-hb-PI).

The amine-terminated polyimide solution in m-cresol was added dropwise to sulfonated anhydride-terminated polyimide and stirred following a temperature profile of 70°C for 4 h and 180°C for 24 h to form S-hb-PI with a core–shell structure. The hb polymer based on 6FDA/TAPA formed the core and linear polymer based on NTDA/BDSA formed the shell. The S-hb-PI membranes was soluble in aprotic polar solvents such as in DMAc, DMSO, DMF, and NMP. The

Scheme 33 (**a**) Monomer combination NTDA and BDSA used for the synthesis of sulfonated anhydride-terminated polyimide. (**b**) Monomer combination 6FDA and TAPA used for the synthesis of amine-terminated hb-PI [288]

S-hb-PI membranes showed film-forming ability because of the enhanced entanglement between linear polymers. The M_w values of the S-hb-PI membranes were 320,000, 500,000, and 830,000 Da, respectively, which corresponded to the increase in the molecular weights of sulfonated anhydride terminated polyimides. The onset temperature of decomposition T_d started above 280°C due to the desulfonation of the S-hb-PI membranes. The weight loss above 550°C was due to decomposition of the polymer backbone. The proton conductivities of the S-hb-PI membranes were in the range of 0.34–0.51 S/cm at 80°C and relative humidity ~98%, indicating higher values than that of Nafion (proton conductivity ~0.15 S/cm) under the same conditions. Suda and coworkers suggested that the S-hb-PI membrane containing sulfonic acid groups as a linear hydrophilic domain at the core surface might have formed ionic channels. However, the S-hb-PI membranes broke within 1 h in the presence of Fenton's reagent, indicating that oxidative stability should be improved from an application point of view.

3.2.3 Hyperbranched Polyimide–Silica as a Gas Separation Membrane

The gas transport properties of hb-PI blend membranes of 4,4′-(hexafluoroisopropylidene) diphthalic anhydride/1,3,5-tris(4-aminophenoxy)benzene (6FDA/TAPOB) and 4,4′(hexafluoroisopropylidene) diphthalic anhydride/3,3′-dihydroxybenzidine (6FDA/HAB) blends and their silica hybrid membranes were investigated by Suzuki et al. [289]. The formation of a hb-PI blend silica hybrid membrane is presented in Scheme 34 in a simplified manner. Polymer blending is also a useful approach for combining the advantages of individual components. A number of polyimide-based polymer blends have been studied to develop high-performance gas separation membranes [43, 290–292]. DMAc solutions of the amine-terminated 6FDA/TAPOB-based hb-PAA and 6FDA/HAB hydroxyl-PAA were mixed at room temperature in ratios of 40:60 or 20:80 wt%. Then, 3-(triethoxysilyl)propylsuccinic anhydride (TEOSPSA) was added as a coupling agent and imidization carried out under nitrogen flow to obtain (6FDA/TAPOB)/(6FDA/HAB) blend silica hybrid membranes of 20–25 μm thickness. Neat blended membranes without silica were also prepared in a similar manner for comparison.
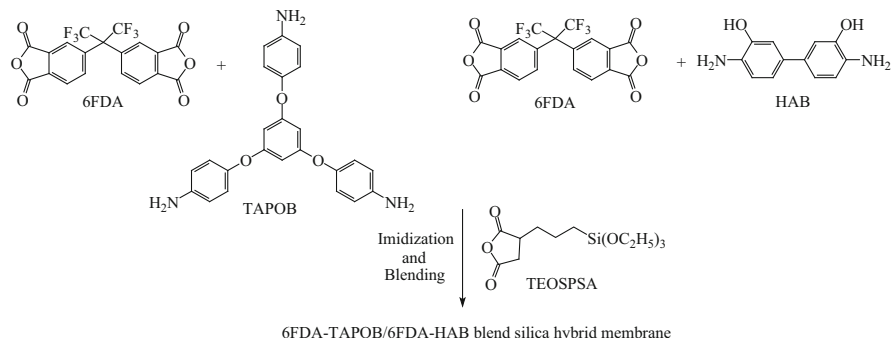
Scheme 34 Monomer combinations used for the formation of hb blend silica hybrid membranes in the presence of coupling agent [289]

In general, gas permeability and selectivity of a binary polymer blend are described by the semilogarithmic additive rule [293]. Gas permeability coefficients of hb-PI (6FDA/TAPOB)/(6FDA/HAB) blend membranes showed positive deviation from the semilogarithmic additive rule. The enhanced gas permeabilities resulted from the increase in free volume elements caused by the intermolecular interaction, disrupting molecular chain packing between terminal amine groups of hb-PI (6FDA/TAPOB) and hydroxyl groups coming from the (6FDA/HAB) backbone. Ideal the CO_2/CH_4 selectivity of hb-PI(6FDA/TAPOB)/(6FDA/HAB) blend silica hybrid membranes showed a tendency to exceed the upper limit for CO_2/CH_4 separation with increasing silica content, that is CO_2 permeability, comparing the results reported by Robeson [294, 295]. The remarkable CO_2/CH_4 separation behavior was considered to be due to the characteristic distribution and interconnectivity of free volume elements created by the incorporation of silica. For the hb-PI (6FDA/TAPOB)/(6FDA/HAB) blend system, the polymer blending and hybridization with silica synergetically induced the enhancement of free volume elements, which provided the prominent CO_2/CH_4 separation ability. This finding was also supported by SEM images, where silica particles showed poor interfacial adhesion with sharp and clear boundaries, indicating the induction of free space around the polymer–silica interfacial area. The T_g values of the hybrid membranes could not be detected by DSC, whereas the blend membranes without silica showed T_g values in the range of 332–329°C. This behavior was attributed to a strong inhibition of segmental mobility of molecular chains by silica. On the other hand, the $T_{d,5\%}$ increased up to 486–496°C with increasing silica content in comparison to the blend membranes without silica that showed values of ~479°C, indicating higher thermal stability by the hybridization with silica. The gas permeability coefficients of the hybrid membranes also increased with increasing silica content.

3.3   Optoelectronic Materials

Photosensitive polymers are well-known polymer materials that play important roles in the field of semiconductor manufacturing as protection and insulation layers. The applications of hb polymers as photoresist materials seem to be very promising. Hyperbranched polymers with compact molecular chains and low chain entanglement offer some advantages over linear polymers for those attempting to pattern feature sizes that are on the order of the molecular dimensions. In addition, the peripheral location of the photosensitive groups at the polymer framework is expected to produce high sensitivity to exposure to light. Fréchet and coworkers [296] reported a hb polymer as the first example of a chemically amplified resist. Ueda and coworkers [297] reported a new negative working photoresist based on resorcinol-terminated hb poly(ether imide) with 4,4′-methylenebis[2,6-bis (hydroxymethyl)]phenol as a crosslinker (**1–50**, Scheme 35) and diphenyliodonium 9,10-dimethoxyanthracene-2-sulfonate as a photoacid generator; it exhibited a feature resolution of 4.5 μm when exposed to 365-nm UV light.

   In et al. [298] reported a hydroxy-terminated hb poly(arylene ether phosphine oxide) (**1–51**, Scheme 35) containing 10 wt% diphenyliodonium-9,10-dimethoxyanthracene-2-sulfonate as a photoacid generator and 25 wt% 4,4′-methylenebis-[2,6-bis(hydroxymethylphenyl)phenol] as a crosslinker. It had a sensitivity of 9 mJ/cm^2 and a contrast of 1.6 under 365-nm UV light exposure. Kakimoto and coworkers [299] described a kind of chemically amplified photosensitive polybenzoxazole based on a *tert*-butoxycarbonyl-protected hb poly(*o*-hydroxyamide) (**1–52**, Scheme 35). The resist showed a sensitivity of 115 mJ/cm^2 and a contrast of 2.2 with 365-nm light exposure. A series of benzophenone-containing hb polyimides (hb-PIs) were prepared by Chen and Yin [300, 301] via the end-capping modification of the terminal anhydride groups by *ortho*-alkyl aniline. The hb-PIs were characterized as inherently photosensitive to UV exposure, giving a patterning resolution greater than 3 μm. Chen and Yin [302] also prepared hb-PIs with terminal phenol groups that were modified by acyl chloride compounds (acryloyl chloride, methylacryloyl chloride, and cinnamoyl chloride) to yield photosensitive hb-PIs. Photosensitive property studies revealed good photolithographic properties with a resolution greater than 3 μm and a sensitivity of 650–680 mJ/cm^2. A series of autophotosensitive semi-aromatic hb-PIs end-capped with 3-aminophenylacetylene (**1–53**, Scheme 35) were prepared by Liu et al. [303]. Photosensitivities of hb-PIs were obtained in the range of 80–162 mJ/cm^2, and they showed a clear negative image with a line width of 8 μm when exposed to UV light of 365 nm. Scheme 35 shows some structures of hb polymers used as photoresist materials.

   Second-order nonlinear optical (NLO) organic polymer materials have also attracted much attention because of their potential applications in the fields of high-speed electro-optic (EO) modulators, optical data transmission, and optical information processing [304, 305]. Organic polymers have been conceived as a suitable material for these optical devices due to their large optical nonlinearity and
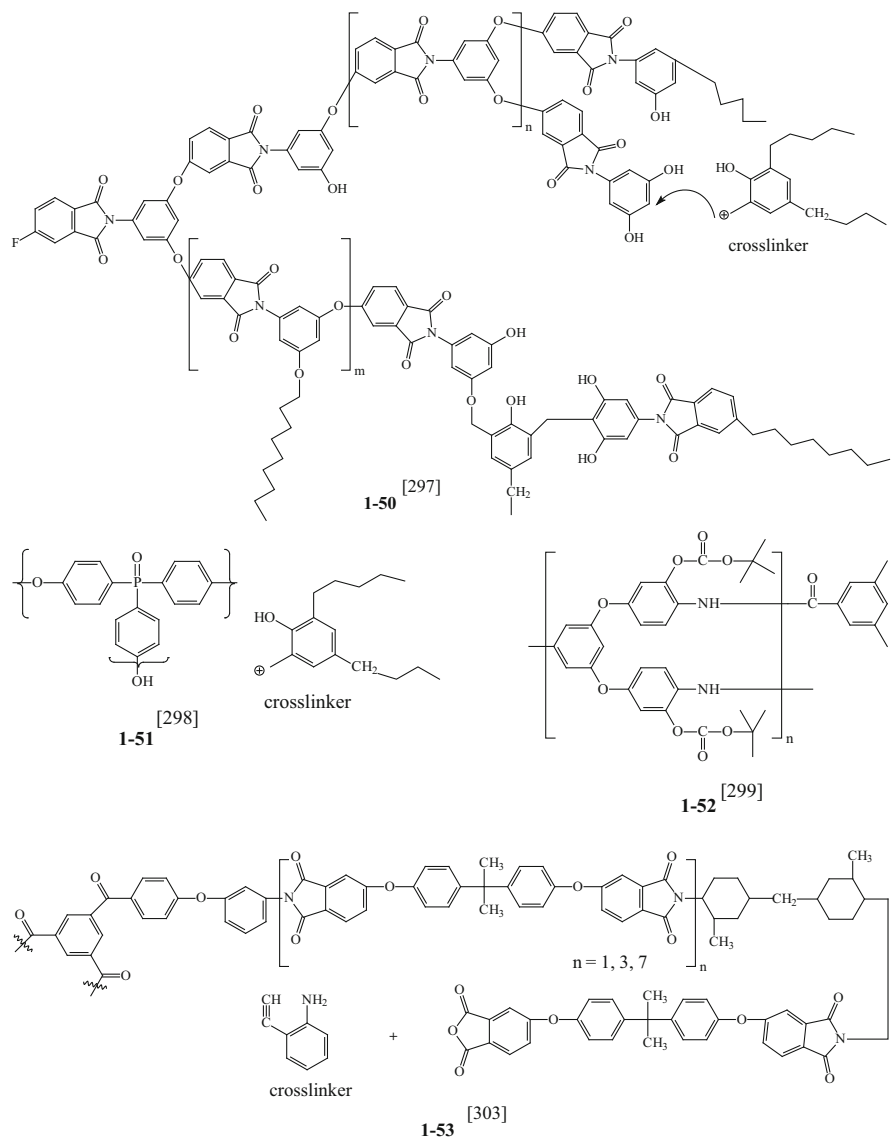
**Scheme 35** Representative structures of hb photosensitive polymers

easy fabrication. NLO polymers have many advantages over conventional inorganic polymers, such as light weight, low cost, ultrafast response, wide response wave band, high optical damage threshold, and good processability to form optical devices. A potential NLO polymer must contain highly polarizable conjugated electronic systems and has to be mechanically very strong and thermally stable with a high T_g, together with stabilization of electrically induced dipole alignment.

To exhibit an EO effect, the active moieties (NLO chromophores) should be generally poled under an electric field to form a highly ordered noncentrosymmetric alignment. A proportional relationship between chromophore concentration and optical nonlinearity is observed at low chromophore content. Furthermore, intermolecular dipole interactions at high chromophore content cause obvious decrement in optical nonlinearity. The design of a chemical structure that suppresses the dipole interactions is a promising approach for improving the optical nonlinearity. Hence, there is a need to design and synthesize new chromophores to produce better optical nonlinearity. Hyperbranched polymers with 3D spatial separation of the chromophore moieties endows them with favorable site isolation effects, while their void-rich topological structure could minimize optical loss in the NLO process [306–309]. Therefore, macromolecules with branched architectures are alternative promising candidates for NLO materials with large bulk EO activities. Chang et al. [310] synthesized hb polymers via a ring-opening addition reaction between azetidine-2,4-dione and primary amine. All the obtained polymers showed EO coefficients in the range of 6–16 pm/V with temporal stability at 60°C. The monomer combination used for the synthesis of hb NLO polymer is shown in Scheme 36.

Hyperbranched polymers with methyl ester or epoxy as terminal groups containing pendant azobenzene chromophores (**1–54**, Scheme 37) were prepared by Xie et al. [311]. The poled films exhibited EO coefficients (>50 pm/V) due to the 3D spatial isolation effect resulting from their highly branched structures. Bai et al. [312] prepared thermally crosslinkable, hb oligomer containing NLO chromophores and blended it with linear host polymer. They obtained large and stable EO coefficients up to 65 pm/V, which are suitable for device development in terms of improved poling efficiency and temporal stability. Xie et al. [313] synthesized an hb polytriazole (**1–55**, Scheme 37) and compared the results with a linear analog. The poled film of hb polytriazole showed a much higher second-harmonic coefficient (96.8 pm/V) than the linear analog (23.5 pm/V). They proposed that the 3D spatial isolation effect resulting from the highly branched structure and crosslinking of the terminal acetylene groups at moderate temperature led to the enhancement of optical nonlinearity.

Jiang's group [68] prepared fluorinated hb-PAEK end-capped with nickel phthalocyanine and checked the material for NLO applications. The third-order nonlinear coefficient was found to have a value of 0.98×10^{-11} esu, which the authors attributed to the dual contributions of nonlinear absorption and refraction of the molecules. Moreover, the obtained value was found to be almost five times larger than that of other metallophthalocyanines [314] due to presence of the hyperbranched structure, the aromatic backbone, and the number of end-functionalities.

Hyperbranched polymers, are good candidates for both core and cladding materials in photonic device applications [315, 316] due to excellent processability and good optical properties in terms of low optical losses, low birefringence and high T_g. Gao et al. [317] developed ZnO/hb-PI nanohybrid films and investigated the optical properties and fluorescence mechanisms. An efficient energy transfer from
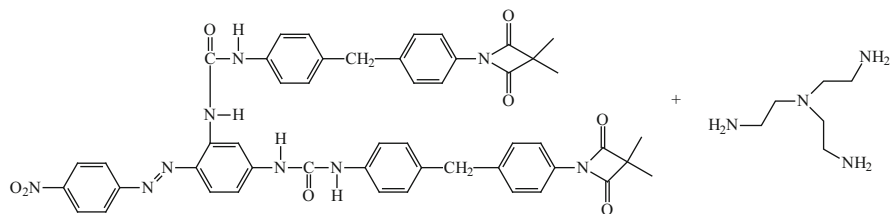
Scheme 36 Monomer combination used for the synthesis of hb NLO polymer [310]

R = ![epoxide] or -OH

[311]
1-54

[313]
1-55
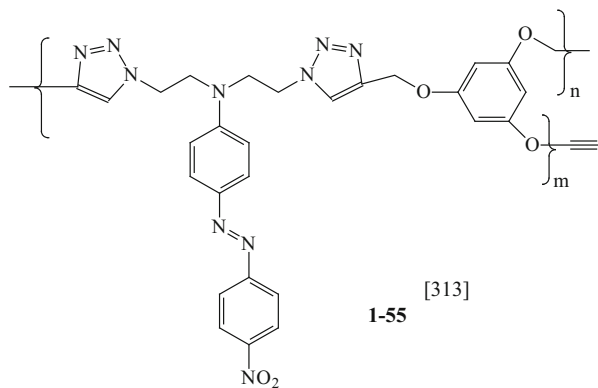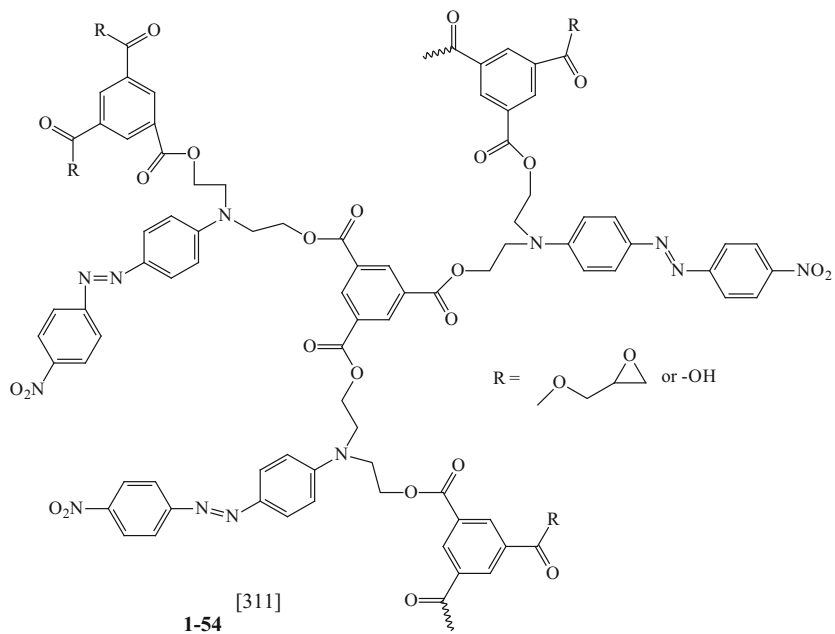
Scheme 37 Representative hb architectures used as NLO polymers

the excited donor (ZnO) to the accepter (hb-PI) occurred in this unique hybrid system and originated from the sufficiently short distance between the ZnO surface and hb-PI chains. All the films exhibited good optical transparency in the range of 450–800 nm, as detected by UV–vis absorption spectra. Chen et al. [137] synthesized both amine- and anhydride-terminated hb-PIs and investigated them using UV–vis spectra and fluorescence spectroscopy. The hb-PIs showed UV–vis absorptions in the region 200–400 nm and also displayed strong purple and blue fluorescence at 400 and 460 nm, respectively, indicating their possible utilization in organic photoluminescence and photoelectricity. Zhang and colleagues [142] prepared hb-PIs end-capped with metallophthalocyanines that showed different colors in chloroform ($CHCl_3$) solution depending on the type of metal present in the hb-PI, i.e., brown, dark green, and green colored for Cu, Zn, and Ni, respectively. The absorption maxima as detected by UV–vis spectra of the three polymers in chloroform solution were 672, 701, and 665 nm, respectively. A fluoro-terminated hb poly (aryl ether ketone) end-capped by azobenzene chromophores was prepared by Jiang et al. [318]. The UV-visible absorption spectrum of azo-hb-PAEK in DMF solution exhibited two absorption bands in the range of 300–650 nm, centered around 347 and 445 nm, which revealed the π–π* and n–π* electronic transitions of the azo-chromophoric moieties. The azo-hb-PAEK films were investigated for surface relief grating (SRG) and birefringence measurements. The SRGs of the azo-hb-PAEK film showed good thermal shape stability and could not be totally erased by even heating up to 300°C, which the authors attributed to the rigidity of the azo-hb-PAEK structure. The azo-hb-PAEK showed a large photoinduced birefringence intensity and good reversible optical storage upon irradiation with 532 nm light using a Nd:YAG laser. Such azo-hb-PAEKs show potential application in holographic memory, reversible high-density optical storage, optical switches, and other photodriven devices.

Multilevel interconnection technology is essential for realization of high density and ultralarge scale integrated circuits (ULSIs). The interlayer dielectric film technology is one of the most important keys for fabrication of multilevel interconnections [319]. Dielectric materials must meet stringent material property requirements for successful integration into the interconnect structures. The desired electrical properties are low dielectric constant, high T_g, high thermal and chemical stability, and good mechanical properties. The linear polyimide made from PMDA and ODA was the first to be commercialized by DuPont under the trade name Kapton®, and it is still the most widely used dielectric material in microelectronics. It has a high T_g of 377–400°C and dielectric constant of 3.1–3.5. With microelectronic devices becoming smaller and lighter during the past decades, a low dielectric constant has become one of the most crucial factors for minimizing electrical power loss and delay in signal transmission in microelectronic applications and, hence, there is a great need for materials exhibiting low dielectric constants for application as insulating materials around the interconnecting wires in these devices [320].

One of the developments in low-dielectric-constant polymers has been an increase in the free volume in the structure. Dubois et al. prepared hb carbosiloxane

thin films by sol–gel processing and reported dielectric constants ranging from 2.6 to 3.1. The Dow Chemical Company has already commercialized a polyphenylene-based product under the trade name SiLK™ with dielectric constant value of 2.65 [321]. Somboonsub et al. [322] prepared multilayer hb-PI/POSS nanocomposites synthesized by the incorporation of POSS into the side chains of polyimide. The lowest dielectric constant value attained was 2.54 in the hb-PI/POSS nanocomposite because of the large free volume and loose polyimide structures. The fluorinated hb poly(aryl ether)s (F-hb-PAEs) synthesized [143, 197] could be used for dielectric coatings, which require crosslinked films on a substrate after high-temperature baking. The dielectric constant values ($\varepsilon = 2.67 \pm 0.2$) obtained for the analogous linear poly(aryl ether)s [323] support the fact that these F-hb-PAEs exhibit even lower dielectric constants due to the increased free volume arising from the highly branched architecture and to the –CF_3 pendant groups on these polymers. Hyperbranched polyphenylenes have been shown to exhibit low dielectric constants due to their branched and twisted nonpolar all-phenylene structure. Hyperbranched PPhs are promising candidates for application as insulating materials in microelectronics, where features like high thermal stability, good processability and solubility, and low moisture absorption are required. The dielectric constant value of the synthesized hb-PPh from an AB_2 monomer prepared by Voit and colleagues showed a value of 2.1 [232] at low frequencies, indicating that hb-PPh is a very promising insulating material, even without the presence of pores. The introduction of nanopores into a low dielectric matrix [324, 325] can offer further advantages because a very low dielectric value might be obtained in combination with greater mechanical strength and greater thermal conductivity.

3.3.1 Hyperbranched Poly(arylene ethynylene) as NLO Material

A hb poly(arylene ethynylene) was prepared by Li et al. [326] via a Sonogashira coupling reaction, in which the chromophore moieties were in the main chain rather than in the side chains. The structure of the hb poly(arylene ethynylene) is shown in Scheme 38. A linear analog was also prepared for comparison.

Both hb and linear poly(aryleneethynylene) exhibited good film-forming ability, and their poled thin films showed second harmonic generation coefficient values ($d33$) of 144 and 53 pm/V, respectively, at the 1,064 nm fundamental wavelength. The values indicated that the incorporation of hb polymer together with the chromophoric groups in the main chain showed very high $d33$, implying large optical nonlinearity and high stabilization of dipole moments compared to the linear analog. The onset temperature for decay of hb polymer was found to be 153°C, which was higher than for the linear polymer (onset temperature for decay was 119°C), indicating long term temporal stability of the hb polymer as shown in Fig. 6. These results clearly revealed that the hb polymer had greatly enhanced poling efficiency, making it a promising candidate for optoelectronic applications.
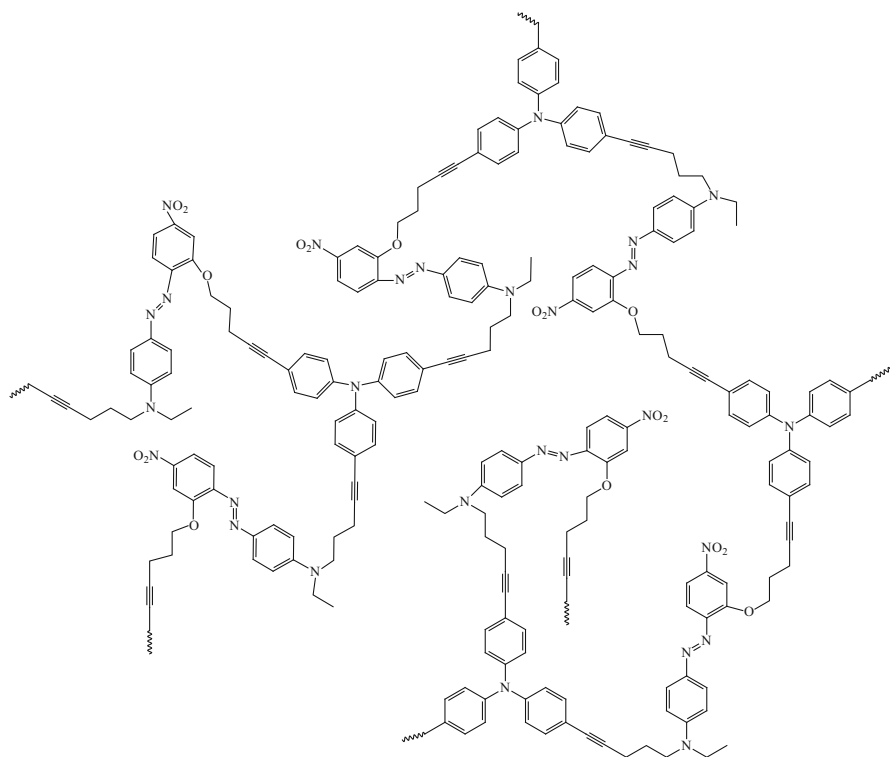
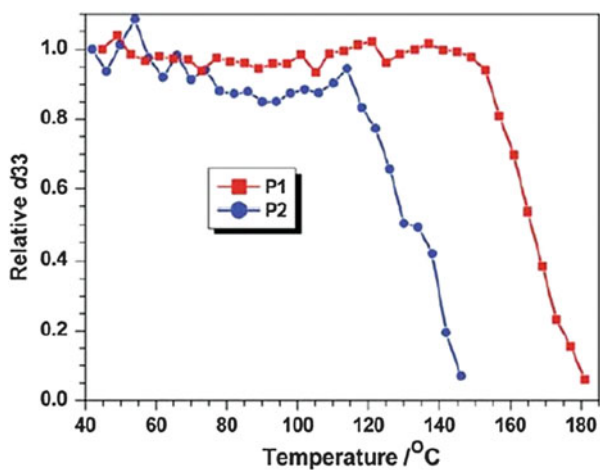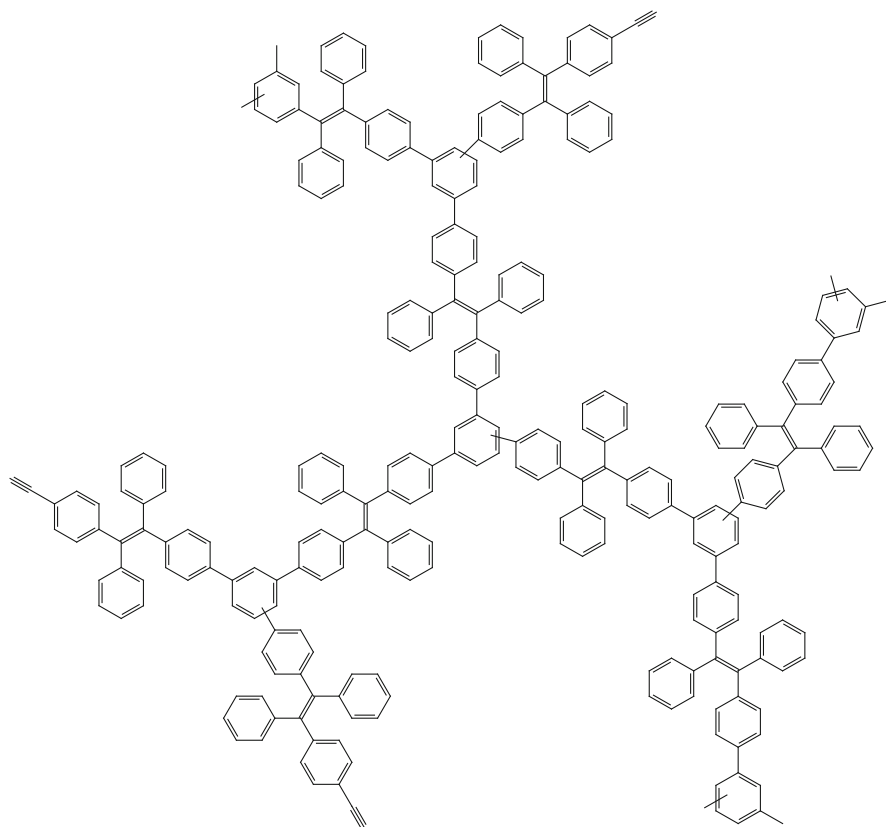**Scheme 38** Structure of hb poly(arylene ethynylene) used as NLO material [326]

Fig. 6 Decay curves of second harmonic generation (SHG) coefficient of hb poly(arylene ethynylene) (*P1*)and linear poly(arylene ethynylene) (*P2*) as a function of temperature. Reproduced with permission from [326]

Scheme 39 Structure of hb poly(tetraphenylethene) used as fluorescent chemosensor [327]

3.3.2 Hyperbranched Poly(tetraphenylethene) as Fluorescent Chemosensor for Detection of Explosives

Hu et al. [327] synthesized hb conjugated polymers containing tetraphenylethene units. Tetraphenylethene (TPE) is a well-known building block for aggregation-induced emission (AIE) luminogens. By cyclotrimerization of a TPE-functionalized diyne in the presence of TaBr$_5$ as catalyst, using toluene as solvent at room temperature, hb poly(tetraphenylethene) (hb-TPE) was afforded. The structure of hb-TPE is shown in Scheme 39. The hb-TPE showed good solubility in common organic solvents such as toluene, CH$_2$Cl$_2$, CHCl$_3$, and THF, which the authors attributed to the twisted conformation of the TPE unit, which in turn led to large intermolecular distances and free volume for interaction with the solvent molecules. The hb-TPE also showed good film-forming ability by spin-coating or solution-casting techniques.

The onset decomposition temperatures (T_d) of hb-TPE were 462°C in nitrogen atmosphere and 417°C in air, indicating high thermal stability. The remaining triple

bonds on the periphery of hb-TPE provided suitable sites for photocrosslinking, generating photopatterns. The polymer showed a superamplification effect in the emission quenching of the polymer nanoaggregates by picric acid (used as a model explosive in their work), indicating hb-TPE as a promising fluorescent chemosensor for detection of explosives.

Concluding Remarks

Hyperbranched polymers are characterized by high solubility, low melt and solution viscosity, and excellent thermal properties. They can be tailored for various end-use applications and many of these branched architectures have already been commercialized by the chemical industry. New monomers and hb polymers have been more recently developed to result in materials for various applications, where the branching allows more easy processability and better solubility than the corresponding linear polymers. Typical approaches developed for linear polymers can be used to prepare hb polymers [e.g., poly(aryl ester)s, poly(aryl amide)s, poly(aryl ether), poly(imide)s, and poly(arylene)s] by employing monomers such as AB_2 and A_2B that allow branching and also by copolymerization with AB monomers to adjust the degree of branching. In particular, $A_2 + B_3$-type polymerizations are widely used because of the more easily accessible monomers and the ability to prevent gelation by controlling factors such as the rate of monomer addition, monomer molar ratio, and percentage solid content. New synthetic strategies such as the $AB_2 + A_2$ approach for synthesis of high molecular weight hb poly (aryl ether)s have been identified. The high molecular weight products show significant advantages with regard to thermal stability and film-forming ability. Small amounts of hb polymer can be incorporated into linear polymers to improve the processability, melt flow properties, and various other material properties. For example, hb poly(phenylene sulfide)s exhibits dyeability in commercially available polypropylene, hence opening a new gateway towards the application of polypropylene as a textile fiber. Triazine-based hb polyamines show good flame retardancy in which the limiting oxygen index value can be tailored by incorporating different moieties in the structure. Sulfonated hb poly(aryl ether ketone)s have been incorporated into linear analogs to prepare blend membranes that could be used as proton exchange membranes. Fluorinated hb poly(arylene ether)s may find application as dielectric materials and as optical waveguide materials. Nanohybrid materials based on hb polyimides have also been explored recently for fluorescence applications. Thus, the future of hb polymers seems to be very promising for a wide range of applications.

References

1. Voit BI, Lederer A (2009) Hyperbranched and highly branched polymer architectures-synthetic strategies and major characterization aspects. Chem Rev 109:5924–5973
2. Voit BI, Komber H, Lederer A (2013) Hyperbranched polymers: synthesis and characterization aspects. Mater Sci Technol. doi:10.1002/9783527603978.mst043
3. Gao C, Yan D (2004) Hyperbranched polymers: from synthesis to applications. Prog Polym Sci 29:183–275
4. Ishizu K, Tsubaki K, Mori A, Uchida S (2002) Architecture of nanostructured polymers. Prog Polym Sci 28:27–54
5. Voit B (2000) New developments in hyperbranched polymers. J Polym Sci A Polym Chem 38:2505–2525
6. Schluter AD, Rabe JP (2000) Dendronized polymers: synthesis, characterization, assembly at interfaces, and manipulation. Angew Chem Int Ed 39:864–883
7. Roovers J, Comanita B (1999) Dendrimers and dendrimer-polymer hybrids. Adv Polym Sci 142:179–228
8. Moore JS (1997) Shape-persistent molecular architectures of nanoscale dimension. Acc Chem Res 30:402–413
9. Newkome GR, Moorefield CN, Vogtle F (2001) Dendrimers and dendrons. Wiley-VCH, Weinheim
10. Peerlings HWI, Meijer EW (1997) Chirality in dendritic architectures. Chem Eur J 3:1563–1570
11. Jang JG, Bae YC (1999) Phase behaviors of hyperbranched polymer solutions. Polymer 40:6761–6768
12. Pirrung FOH, Loen EM, Noordam A (2002) Hyperbranched polymers as a novel class of pigment dispersants. Macromol Symp 187:683–694
13. Striba SE, Frey H, Haag R (2002) Dendritic polymers in biomedical applications: from potential to clinical use in diagnostics and therapy. Angew Chem Int Ed 41:1329–1334
14. Mezzenga R, Boogh L, Manson JAE (2001) A review of dendritic hyperbranched polymer as modifiers in epoxy composites. Compos Sci Technol 61:787–795
15. Haag R (2001) Dendrimers and hyperbranched polymers as high-loading supports for organic synthesis. Chem Eur J 7:327–335
16. Hirao A, Hayashi M, Loykulnant S, Sugiyami K, Ryu SW, Haraguchi N, Matsuo A, Higashihara T (2005) Precise syntheses of chain-multi-functionalized polymers, star-branched polymers, star-linear block polymers, densely branched polymers, and dendritic branched polymers based on iterative approach using functionalized 1,1-diphenylethylene derivatives. Prog Polym Sci 30:111–182
17. Unal S, Long TE (2006) Highly branched poly(ether ester)s via cyclization-free melt condensation of A_2 oligomers and B_3 monomers. Macromolecules 39:2788–2793
18. McKee MG, Park T, Unal S, Yilgor I, Long TE (2005) Electrospinning of linear and highly branched segmented poly(urethane urea)s. Polymer 46:2011–2015
19. Nomura R, Matsuno T, Endo T (1999) Synthesis and polymerization of a self-condensable macromonomer. Polym Bull 42:251–256
20. Yamada B, Konosu O, Tanaka K, Oku F (2000) Preparation of branched polymer by radical polymerization using polymerizable chain transfer agent. Polymer 41:5625–5631
21. Trollsas M, Kelly MA, Claesson H, Seimens R, Hedrik JL (1999) Highly branched block copolymers: design, synthesis, and morphology. Macromolecules 32:4917–4924
22. Peleshanko S, Gunawidjaja R, Petrash S, Tsukruk VV (2006) Synthesis and interfacial behavior of amphiphilic hyperbranched polymers: poly(ethylene oxide)−polystyrene hyperbranches. Macromolecules 39:4756–4766
23. Bernard J, Schappacher M, Viville P, Lazzaroni R, Deffieux A (2005) Synthesis and properties of PS–PEO core–shell amphiphilic dendrigrafts. Polymer 46:6767–6776

24. Ishizu K, Ochi K (2006) Architecture of star−block copolymers consisting of triblock arms via a *N,N*-diethyldithiocarbamate-mediated living radical photo-polymerization and application for nanocomposites by using as fillers. Macromolecules 39:3238–3244

25. Kreutzer G, Ternat C, Nguyen TQ, Plummer CJG, Manson JAE, Castelletto V, Hamley IW, Sun F, Sheiko SS, Herrmann A, Ouali L, Sommer H, Fieber W, Velazco MI, Klok HA (2006) water-soluble unimolecular containers based on amphiphilic multiarm star block copolymers. Macromolecules 39:4507–4516

26. Magnusson H, Malmstrom E, Hult A (1999) Synthesis of hyperbranched aliphatic polyethers via cationic ring-opening polymerization of 3-ethyl-3-(hydroxymethyl)oxetane. Macromol Rapid Commun 20:453–457

27. Istratov V, Kautz H, Kim YK, Schubert R, Frey H (2003) Linear-dendritic nonionic poly (propylene oxide)–polyglycerol surfactants. Tetrahedron 59:4017–4024

28. An SG, Cho CG (2004) Synthesis and characterization of Dumbbell type amphiphilic block copolymers via ATRP. Polym Bull 51:255–262

29. Kwak SY, Ahn DU, Choi J, Song HJ, Lee SH (2004) Amelioration of mechanical brittleness in hyperbranched polymer. 1. Macroscopic evaluation by dynamic viscoelastic relaxation. Polymer 45:6889–6896

30. Okrasa L, Zigon M, Zagar E, Czech P, Boiteux G (2005) Molecular dynamics of linear and hyperbranched polyurethanes and their blends. J Non-Cryst Solids 351:2753–2758

31. Seino M, Hayakawa T, Ishida Y, Kakimoto M (2006) Synthesis and characterization of crystalline hyperbranched polysiloxysilane with POSS groups at the terminal position. Macromolecules 39:8892–8894

32. Fanghond G, Tang H, Liu C, Jiang B, Ren Q, Yang Y (2006) Preparation of hyperbranched polymers through ATRP of in situ formed AB* monomer. J Appl Polym Sci 101:850–856

33. Zhu X, Chen L, Yan D, Chen Q, Yao Y, Xiao Y, Hou J, Li J (2004) Supramolecular self-assembly of inclusion complexes of a multiarm hyperbranched polyether with cyclodextrins. langmuir 20:484–490

34. Yan D, Gao C, Frey H (eds) (2011) Hyperbranched polymers: synthesis, properties, and applications. Wiley, Hoboken

35. Peleshanko S, Tsukruk V (2011) Grafting and surface properties of hyperbranched polymers. In: Yan D, Gao C, Frey H (eds) Hyperbranched polymers: synthesis, properties and applications, 1st edn. Wiley, Hoboken, pp 369–386. doi:10.1002/9780470929001.ch14

36. Bruchmann B, Voit B (2011) Applications of hyperbranched polymers in coatings, as additives, and in nanotechnology. In: Yan D, Gao C, Frey H (eds) Hyperbranched polymers: synthesis, properties, and applications. Wiley, Hoboken, pp. 415–440. doi:10.1002/9780470929001.ch16

37. Zhang D, Liang E, Li T, Chen S, Zhang J, Cheng X, Zhou J, Zhang A (2013) Environment-friendly synthesis and performance of a novel hyperbranched epoxy resin with a silicone skeleton. RSC Adv 3:3095–3102

38. Zhu Q, Qiu F, Zhu B, Zhu X (2013) Hyperbranched polymers for bioimaging. RSC Adv 3:2071–2083

39. Wang D, Chen H, Su Y, Qiu F, Zhu L, Huan X, Zhu B, Yan D, Guo F, Zhu X (2013) Supramolecular amphiphilic multiarm hyperbranched copolymer: synthesis, self-assembly and drug delivery applications. Polym Chem 4:85–94

40. Hartmann-Thompson C, Hu J, Kaganove SN, Keinath SN, Keeley DL, Dvornic PR (2004) Hydrogen-bond acidic hyperbranched polymers for surface acoustic wave (SAW) sensors. Chem Mater 16:5357–5364

41. Kricheldorf HR, Stukenbrock T (1998) New polymer syntheses XCIII. Hyperbranched homo- and copolyesters derived from gallic acid and β-(4-hydroxyphenyl)-propionic acid. J Polym Sci A Polym Chem 36:2347–2357

42. Li J, Bo Z (2004) "AB2 + AB" approach to hyperbranched polymers used as polymer blue light emitting materials. Macromolecules 37:2013–2015

43. Robeson LM (2010) Polymer blends in membrane transport processes. Ind Eng Chem Res 49:11859–11865
44. Newkome GR, Moorefield CN, Vogtle F (2008) Dendritic molecules: concepts, syntheses, perspectives. VCH, New York, pp 49–161
45. Astruc D, Chardac F (2001) Dendritic catalysts and dendrimers in catalysis. Chem Rev 101:2991–3024
46. Emrick T, Chang HT, Fréchet JMJ (2000) The preparation of hyperbranched aromatic and aliphatic polyether epoxies by chloride-catalyzed proton transfer polymerization from AB_n and $A_2 + B_3$ monomers. J Polym Sci A Polym Chem 38:4850–4869
47. Fang J, Kita H, Okamoto K (2000) Hyperbranched polyimides for gas separation applications. 1. Synthesis and characterization. Macromolecules 33:4639–4646
48. Kim YH (1992) Lyotropic liquid crystalline hyperbranched aromatic polyamides. J Am Chem Soc 114:4947–4948
49. Monticelli O, Russo S, Campagna R, Voit B (2005) Preparation and characterisation of blends based on polyamide 6 and hyperbranched aramids as palladium nanoparticle supports. Polymer 46:3597–3606
50. Yamakawa Y, Ueda M, Takeuchi K, Asai M (1999) One-pot synthesis of dendritic polyamide. J Polym Sci A Polym Chem 37:3638–3645
51. Yamakawa Y, Ueda M, Takeuchi K, Asai M (1999) One-pot synthesis of dendritic polyamide. 2. Dendritic polyamide from 5-[3-(4-aminophenyl)propionylamino]isophthalic acid hydrochloride. Macromolecules 32:8363–8369
52. Jikei M, Chon SH, Kakimoto MA, Kawauchi S, Imase T, Watanebe J (1999) Synthesis of hyperbranched aromatic polyamide from aromatic diamines and trimesic acid. Macromolecules 32:2061–2064
53. Tabuani D, Monticelli O, Chincarini A, Bianchini C, Vizza F, Moneti S, Russo S (2003) Palladium nanoparticles supported on hyperbranched aramids: synthesis, characterization, and some applications in the hydrogenation of unsaturated substrates. Macromolecules 36:4294–4301
54. Tabuani D, Monticelli O, Komber H, Russo S (2003) Preparation and characterisation of Pd nanoclusters in hyperbranched aramid templates to be used in homogeneous catalysis. Macromol Chem Phys 204:1576–1583
55. Fang J, Kita H, Okamoto K (2001) Gas permeation properties of hyperbranched polyimide membranes. J Membr Sci 182:245–256
56. Yamaguchi N, Wang JS, Hewitt JM, Lenhart WC, Mourey TH (2002) Acid chloride-functionalized hyperbranched polyester for facile and quantitative chain-end modification: one-pot synthesis and structure characterization. J Polym Sci A Polym Chem 40:2855–2867
57. Kricheldorf HR, Hobzova R, Schwarz G (2003) Cyclic hyperbranched polyesters derived from 4,4-bis(4′-hydroxyphenyl)valeric acid. Polymer 44:7361–7368
58. Kricheldorf HR, Zang QZ, Schwarz G (1982) New polymer syntheses: 6. Linear and branched poly(3-hydroxy-benzoates). Polymer 23:1821–1829
59. Moore JS, Stupp SI (1990) Room temperature polyesterification. Macromolecules 23:65–70
60. Blencowe A, Davidson L, Hayes A (2003) Synthesis and characterization of hyperbranched polyesters incorporating the AB_2 monomer 3,5-bis(3-hydroxylprop-1-ynyl)benzoic acid. Eur Polym J 39:1955–1963
61. Kang SH, Luo J, Ma H, Barto RR, Frank CW, Dalton LR, Jen AKY (2003) Hyperbranched aromatic fluoropolyester for photonic applications. Macromolecules 36:4355–4359
62. Jayakannan M, Ramakrishnan S (2001) Recent developments in polyether synthesis. Macromol Rapid Comm 22:1463–1473
63. Miller TM, Neenan TX, Kwock EW, Stein SM (1993) Dendritic analogs of engineering plastics: a general one-step synthesis of dendritic polyaryl ethers. J Am Chem Soc 115:356–357
64. Chu F, Hawker CJ (1993) A versatile synthesis of isomeric hyperbranched polyetherketones. Polym Bull 30:265–272

65. Hawker CJ, Chu F (1996) Hyperbranched poly(ether ketones): manipulation of structure and physical properties. Macromolecules 29:4370–4380
66. Shu CF, Leu CM (1999) Hyperbranched poly(ether ketone) with carboxylic acid terminal groups: synthesis, characterization, and derivatization. Macromolecules 32:100–105
67. Mu JX, Zhang CL, Chen J, Jiang ZH, Kireev VV (2006) Synthesis of functionalized fluorine-containing hyperbranched poly(aryl ether ketones) for optical applications. Polym Sci Ser A 48:1035–1040
68. Wang D, Zhang SL, Zhang YH, Wang H, Mu JX, Wang GB, Jiang Z (2008) Preparation and nonlinear optical characterization of a novel hyperbranched poly(aryl ether ketone) end-functionalized with nickel phthalocyanine. Dyes Pigments 79:217–223
69. Choi JY, Tan LS, Baek JB (2006) Self-controlled synthesis of hyperbranched poly(ether ketone)s from A3 + B2 approach via different solubilities of monomers in the reaction medium. Macromolecules 39:9057–9063
70. Baek JB, Tan LS (2003) Improved syntheses of poly(oxy-1,3-phenylenecarbonyl-1,4-phenylene) and related poly(ether–ketones) using polyphosphoric acid/P_2O_5 as polymerization medium. Polymer 44:4135–4147
71. Baek JB, Park SY, Price GE, Lyons CB, Tan LS (2005) Unusual thermal relaxation of viscosity-and-shear-induced strain in poly(ether-ketones) synthesized in highly viscous polyphosphoric acid/P_2O_5 medium. Polymer 46:1543–1552
72. Martinez CA, Hay AS (1997) Preparation of hyperbranched macromolecules with aryl fluoride and phenol terminal functionalities using new monomers and Cs_2CO_3 or $Mg(OH)_2$ as the condensation agent. J Polym Sci A Polym Chem 35:2015–2033
73. Martinez CA, Hay AS (1998) Synthesis of hyperbranched oligomers with activated aryl chloride and phenol terminal groups. J Macromol Sci Pure Appl Chem 35:57–90
74. Kim YJ, Chung IS, Kim SY (2003) Synthesis of poly(phenylene oxide) containing trifluoromethyl groups via selective and sequential nucleophilic aromatic substitution reaction. Macromolecules 36:3809–3811
75. Kim YJ, Kakimoto MA, Kim SY (2006) Synthesis of hyperbranched poly(arylene ether) from monomer containing nitro group: kinetically controlled growth of polymer chain through dynamic exchange of end functional groups. Macromolecules 39:7190–7192
76. Kim YH, Webster OW (1992) Hyperbranched polyphenylenes. Macromolecules 25:5561–5572
77. Häußler M, Lam JWY, Zheng R, Peng H, Luo J, Chen J, Charles CCW, Tang BZ (2003) Hyperbranched polyarylenes. Chimie 6:833–842
78. Flory PJ (1952) Molecular size distribution in three dimensional polymers. VI. Branched polymers containing A-R-B_{f-1} type units. J Am Chem Soc 74:2718–2723
79. Hawker, CJ, Fréchet, JMJ (1991) One-step synthesis of hyperbranched dendritic polyesters. J Am Chem Soc 113:4583–4588
80. Holter D, Burgath A, Frey H (1997) Degree of branching in hyperbranched polymers. Acta Polym 48:30–35
81. Odian G (1991) Principles of polymerization. Wiley, New York
82. Yang X, Wang L, He X (2010) Kinetics of nonideal hyperbranched $A_2 + B_3$ polycondensation: Simulation and comparison with experiments. J Polym Sci A Polym Chem 48:5072–5082
83. Reisch A (2005) Untersuchungen zur Strukturentwicklung in Hochverzweigten Polymeren auf der Basis von A_2+B_3 Systemen. Diploma Thesis, Technische Universität Dresden, Dresden
84. Reisch A, Komber H, Voit B (2007) Kinetic analysis of two hyperbranched $A_2 + B_3$ polycondensation reactions by NMR spectroscopy. Macromolecules 40:6846–6858
85. Yan DY, Gao C (2000) Hyperbranched polymers made from A_2 and BB'_2 type monomers. 1. Polyaddition of 1-(2-aminoethyl)piperazine to divinyl sulfone. Macromolecules 33:7693–7699

86. Gao C, Yan DY (2001) Polyaddition of B_2 and BB'_2 type monomers to A_2 type monomer. 1. Synthesis of highly branched copoly(sulfone–amine)s. Macromolecules 34:156–161

87. Gao C, Tang W, Yan DY, Zhu PF, Tao P (2001) Hyperbranched polymers made from A_2, B_2 and BB'_2 type monomers, 2. Preparation of hyperbranched copoly(sulfone-amine)s by polyaddition of N-ethylethylenediamine and piperazine to divinylsulfone. Polymer 42:3437–3443

88. Gao C, Yan DY, Zhu X, Huang W (2001) Preparation of water-soluble hyperbranched poly (sulfone-amine)s by polyaddition of N-ethylethylenediamine to divinyl sulfone. Polymer 42:7603–7610

89. Liu Y, Chung TS (2002) Facile synthesis of hyperbranched polyimides from $A_2 + BB'_2$ monomers. J Polym Sci A Polym Chem 40:4563–4569

90. Chang YT, Shu CF (2003) Synthesis of hyperbranched aromatic poly(amide–imide): Copolymerization of B'B2 monomer with A2 monomer. Macromolecules 36:661–666

91. Abdelrehim M, Komber H, Langenwalter J, Voit B, Bruchmann B (2004) Synthesis and characterization of hyperbranched poly(urea-urethane)s based on AA* and B_2B* monomers. J Polym Sci A Polym Chem 42:3062–3081

92. Radke W, Litvinenko G, Müller AHE (1998) Effect of core-forming molecules on molecular weight distribution and degree of branching in the synthesis of hyperbranched polymers. Macromolecules 31:239–248

93. Litvinenko G, Simon PFW, Müller AHE (2001) Molecular parameters of hyperbranched copolymers obtained by self-condensing vinyl copolymerization, 2. Non Equal Rate Constants Macromolecules 34:2418–2426

94. Beginn U, Drohman C, Moller M (1997) Conversion dependence of the branching density for the polycondensation of AB_n monomers. Macromolecules 30:4112–4116

95. Dusek K, Somvarsky J, Smrckova M, Simonsick WJ, Wilczek L (1999) Role of cyclization in the degree-of-polymerization distribution of hyperbranched polymers modelling and experiments. Polym Bull 42:489–496

96. Cameron C, Fawcett AH, Hetherington CR, Mee RAW, McBride FV (1997) Cycles frustrating fractal formation in an AB_2 stepgrowth polymerization. Chem Commun 1997(18):1801–1802. doi:10.1039/A703567E

97. Galina H, Lechowicz JB, Kaczmarski K (2001) Kinetic models of the polymerization of an AB2 monomer. Macromol Theory Simul 10:174–178

98. Zhou Z, Jia Z, Yan D (2010) Kinetic analysis of co-polycondensation of AB_2 and AB type monomers in presence of multi-functional cores. Polymer 51:2763–2768

99. Voit B (2005) Hyperbranched polymers – all problems solved after 15 years of research? J Polym Sci A Polym Chem 43:2679–2699

100. Liaw DJ, Chang FC, Leung MK, Chou MY, Muellen K (2005) High thermal stability and rigid rod of novel organosoluble polyimides and polyamides based on bulky and noncoplanar naphthalene–biphenyldiamine. Macromolecules 38:4024–4029

101. Scholl M, Kadlecova Z, Klok HA (2009) Dendritic and hyperbranched polyamides. Prog Polym Sci 34:24–61

102. Chao D, He L, Berda EB, Wang S, Jia X, Wang C (2013) Multifunctional hyperbranched polyamide: synthesis and properties. Polymer 54:3223–3229

103. Seike Y, Okude Y, Iwakura I, Chiba I, Ikeno T, Yamada T (2003) Synthesis of polyphenylene ether derivatives: estimation of their dielectric constants. Macromol Chem Phys 204:1876–1881

104. Chiang C, Chang F (1998) Polymer blends of polyamide-6 (PA6) and poly(phenylene ether) (PPE) compatibilized by a multifunctional epoxy coupler. J Polym Sci B Polym Phys 36:1805–1819

105. Wegner G (1981) Polymers with metal-like conductivity-a review of their synthesis, structure and properties. Angew Chem Int Ed Engl 20:361–381

106. Peng H, Dong Y, Jia D, Tang B (2004) Syntheses of readily processable, thermally stable, and light-emitting hyperbranched polyphenylenes. Chinese Sci Bull 49:2637–2639

107. Erber M, Boye S, Hartmann T, Voit B, Lederer A (2009) A convenient room temperature polycondensation toward hyperbranched AB$_2$-type all-aromatic polyesters with phenol terminal groups. J Polym Sci A Polym Chem 47:5158–5168

108. Turner SR, Voit BI, Mourey TH (1993) All-aromatic hyperbranched polyesters with phenol and acetate end groups: synthesis and characterization. Macromolecules 26:4617–4623

109. Schmaljohann D (1998) Funktionalisierung von Hochverzweigten Polyestern fur den Einsatzals Beschichtungs- und Blend material. Ph.D. thesis, TU Munchen, Munchen

110. Schmaljohann D, Komber H, Barratt JG, Appelhans D, Voit B (2003) Kinetics of nonideal hyperbranched polymerizations. 2. Kinetic analysis of the polycondensation of 3,5-Bis (trimethylsiloxy)benzoyl chloride using NMR spectroscopy. Macromolecules 36:97–108

111. Magnusson H, Malmstrom E, Hult A (2000) Structure buildup in hyperbranched polymers from 2,2-Bis(hydroxymethyl)propionic acid. Macromolecules 33:3099–3104

112. Thompson DS, Markoski LJ, Moore JS (1999) Rapid synthesis of hyperbranched aromatic polyetherimides. Macromolecules 32:4764–4768

113. Khalyavina A, Häußler L, Lederer A (2012) Effect of the degree of branching on the glass transition temperature of polyesters. Polymer 53:1049–1053

114. Wooley KL, Hawker CJ, Pochan JM, Frechet JMJ (1993) Physical properties of dendritic macromolecules: a study of glass transition temperature. Macromolecules 26:1514–1519

115. Fan Z, Lederer A, Voit B (2009) Synthesis and characterization of A2 + B3-type hyperbranched aromatic polyesters with phenolic end groups. Polymer 50:3431–3439

116. Lin Q, Long TE (2003) Polymerization of A2 with B3 Monomers: a facile approach to hyperbranched poly(aryl ester)s. Macromolecules 36:9809–9816

117. Unal S, Lin Q, Mourey TH, Long TE (2005) Tailoring the degree of branching: preparation of poly(ether ester)s via copolymerization of poly(ethylene glycol) oligomers (A$_2$) and 1,3,5-benzenetricarbonyl trichloride (B$_3$). Macromolecules 38:3246–3254

118. Schallausky F, Erber M, Komber H, Lederer A (2008) An easy strategy for the synthesis of well-defined aliphatic-aromatic hyperbranched polyesters. Macromol Chem Phys 209:2331–2338

119. Baek JB, Harris FW (2003) Poly(arylether amides) and poly(aryletherketone amides) via aromatic nucleophilic substitution reactions of self-polymerizable AB and AB$_2$ monomers. J Polym Sci A Polym Chem 41:2374–2389

120. In I, Kim SY (2005) Hyperbranched poly(arylene ether amide) via nucleophilic aromatic substitution reaction. Macromol Chem Phys 206:1862–1869

121. Shabbir S, Zulfiqar S, Sarwar MI (2011) Amine-terminated aromatic and semi-aromatic hyperbranched polyamides: synthesis and characterization. J Polym Res 18:1919–1929

122. Ohta Y, Fujii S, Yokoyama A, Furuyama T, Uchiyama M, Yokozawa T (2009) Synthesis of well-defined hyperbranched polyamides by condensation polymerization of AB$_2$ monomer through changed substituent effects. Angew Chem Int Ed 48:5942–5945

123. Liou GS, Lin HY, Yen HJ (2009) Synthesis and characterization of electroactive hyperbranched aromatic polyamides based on A$_2$B-type triphenylamine moieties. Mater Chem 19:7666–7673

124. Liou GS, Chang CW (2008) Highly stable anodic electrochromic aromatic polyamides containing N, N, N′, N′-tetraphenyl-p-phenylenediamine moieties: synthesis, electrochemical, and electrochromic properties. Macromolecules 41:1667–1674

125. Liou GS, Lin KH (2009) Synthesis and characterization of a novel electrochromic aromatic polyamide from AB-type triphenylamine-based monomer. J Polym Sci Part A Polym Chem 47:1988–2001

126. Mittal KL (ed) (2009) Polyimides and other high temperature polymers, vol. 5. VSP/Brill, Leiden

127. Ghosh A, Sen SK, Banerjee S, Voit B (2012) Solubility improvements in aromatic polyimides by macromolecular engineering. RSC Adv 2:5900–5926

128. Kricheldorf HR, Bolender O, Wollheim T (1998) New polymer synthesis 99. Hyperbranched poly(ester-imide)s derived from 4,5-dichlorophthalic acid. High Perform Polym 10:217–229

129. Maier G, Zech C, Voit B, Komber H (1998) An approach to hyperbranched polymers with a degree of branching of 100%. Macromol Chem Phys 199:2655–2664
130. Orlicki JA, Thompson JL, Markoski LJ, Sill KN, Moore JS (2002) Synthesis and characterization of end-group modified hyperbranched polyetherimides. J Polym Sci A Polym Chem 40:936–946
131. Baek JB, Qin H, Mather PT, Tan LS (2002) A new hyperbranched poly(arylene–ether–ketone − imide): synthesis, chain-end functionalization, and blending with a bis(maleimide). Macromolecules 35:4951–4959
132. Hao J, Jikei M, Kakimoto M (2003) Synthesis and comparison of hyperbranched aromatic polyimides having the same repeating unit by AB2 self-polymerization and A2 + B3 polymerization. Macromolecules 36:3519–3528
133. Yamanaka K, Jikei M, Kakimoto MA (2000) Synthesis of hyperbranched aromatic polyimides via polyamic acid methyl ester precursor. Macromolecules 33:1111–1114
134. Yamanaka K, Jikei M, Kakimoto MA (2000) Preparation and properties of hyperbranched aromatic polyimides via polyamic acid methyl ester precursors. Macromolecules 33:6937–6944
135. Wang KL, Jikei M, Kakimoto MA (2004) Synthesis of soluble branched polyimides derived from an ABB′ monomer. J Polym Sci A Polym Chem 42:3200–3211
136. Shen J, Zhang Y, Chen W, Wang W, Xu Z, Yeung KWK, Yi C (2013) Synthesis and properties of hyperbranched polyimides derived from novel triamine with prolonged chain segments. J Polym Sci A Polym Chem 51:2425–2437
137. Chen W, Yan W, Wu S, Xu Z, Yeung KWK, Yi C (2010) Preparation and properties of novel triphenylpyridine-containing hyperbranched polyimides derived from 2,4,6-tris (4-aminophenyl)pyridine under microwave irradiation. Macromol Chem Phys 211:1803–1813
138. Gao H, Wang D, Guan S, Wi J, Jiang Z, Gao W, Zhang D (2007) Fluorinated hyperbranched polyimide for optical waveguides. Macromol Rapid Commun 28:252–259
139. Kaino T (1987) Preparation of plastic optical fibers for near-IR region transmission. J Polym Sci A Polym Chem 25:37–46
140. Liu Y, Zhang Y, Guan S, Zhang H, Yue X, Jiang Z (2009) Synthesis of novel fluorinated hyperbranched polyimides with excellent optical properties. J Polym Sci A Polym Chem 47:6269–6279
141. Gao H, Wang D, Jiang W, Guan S, Jiang Z (2008) Gas permeability of fluorinated hyperbranched polyimide. J Appl Polym Sci 109:2341–2346
142. Zhao L, Yao H, Liu Y, Zhang Y, Jiang Z (2013) Synthesis and properties of novel hyperbranched polyimides end-capped with metallophthalocyanines. J Appl Polym Sci 128:3405–3410
143. Banerjee S, Komber H, Häußler L, Voit B (2009) Synthesis and characterization of hyperbranched poly(arylene ether)s from a new activated trifluoro B3 monomer adopting an A2 + B3 approach. Macromol Chem Phys 210:1272–1282
144. Park SJ, Li K, Jin FL (2008) Synthesis and characterization of hyperbranched polyimides from 2,4,6-triaminopyrimidine and dianhydrides system. Mater Chem Phys 108:214–219
145. Peter J, Khalyavina A, Kriz J, Bleha M (2009) Synthesis and gas transport properties of ODPA–TAP–ODA hyperbranched polyimides with various comonomer ratios. Eur Polym J 45:1716–1727
146. Chen Y, Zhang Q, Sun W, Lei XF, Yao P (2014) Synthesis and gas permeation properties of hyperbranched polyimides membranes from a novel (A₂ + B₂B′ + B₂)-type method. J Membr Sci 450:138–146
147. Hawthorne DG, Hodgkin JH (1999) Amine reactivity changes in imide formation from heterocyclic bases. High Perform Polym 11:315–329
148. Riley D, Gungor A, Srinivasan SA, McGrath JE (1997) Synthesis and characterization of flame resistant poly(arylene ether)s. Polym Eng Sci 37:1501–1511

149. Smith CD, Grubbs H, Gungor A, Webster HF, Wightman JP, McGrath JE (1991) Unique characteristics derived from poly(arylene ether phosphine oxide)s. High Perform Polym 3:211–229
150. Yang J, Gibson HW (1999) A polyketone synthesis involving nucleophilic substitution via carbanions derived from bis(α-aminonitrile)s. 5. A new, well-controlled route to "long" bisphenol and activated aromatic dihalide monomers. Macromolecules 32:8740–8746
151. Kricheldorf HR, Vakhtangishvili L, Schwarz G, Kruger RP (2003) Cyclic hyperbranched poly(ether ketone)s derived from 3,5-bis(4-fluorobenzoyl)phenol. Macromolecules 36:5551–5558
152. Morikawa A (1998) Preparation and properties of hyperbranched poly(ether ketones) with a various number of phenylene units. Macromolecules 31:5999–6009
153. Agarwal S, Kumar S, Maken S (2012) Synthesis and characterization of new hyperbranched poly(ether ketones) with various number of phenylene units. J Ind Eng Chem 18:1489–1495
154. Baek JB, Tan LS (2003) Linear-hyperbranched copolymerization as a tool to modulate thermal properties and crystallinity of a *para*-poly(ether-ketone). Polymer 44:3451–3459
155. Choi JY, Oh SJ, Lee HJ, Wang DH, Tan LS, Baek JB (2007) In-situ grafting of hyperbranched poly(ether ketone)s onto multiwalled carbon nanotubes via the $A_3 + B_2$ approach. Macromolecules 40:4474–4480
156. Li X, Zhang S, Wang H, Pang J, Sun D, Mu J, Wang G, Jiang Z (2010) Facile synthesis and characterization of hyperbranched poly(aryl ether ketone)s obtained via an $A_2 + BB'_2$ approach. Polym Int 59:1360–1366
157. Himmelberg P, Fossum E (2005) Development of an efficient route to hyperbranched poly (arylene ether sulfone)s. J Polym Sci A Polym Chem 43:3178–3187
158. Jikei M, Uchida D, Haruta Y, Takahashi Y, Matsumoto K (2012) Synthesis and properties of hyperbranched poly(ether sulfone)s prepared by self-polycondensation of novel AB_2 monomer. J Polym Sci A Polym Chem 50:3830–3839
159. Imai Y, Ishikawa H, Park KH, Kakimoto M (1997) A facile cesium fluoride-mediated synthesis of aromatic polyethers from bisphenols and activated aromatic dihalides. J Polym Sci Part A Polym Chem 35:2055–2061
160. Kricheldorf HR, Vakhtangisgvili L, Fritsch D (2002) Synthesis and functionalization of poly (ether sulfone)s based on 1,1,1-tris(4-hydroxyphenyl)ethane. J Polym Sci Part A Polym Chem 40:2967–2978
161. Lin Q, Unal S, Fornof AR, Yilgor I, Long TE (2006) Highly branched poly(arylene ether)s via oligomeric A2 + B3 strategies. Macromol Chem Phys 207:576–586
162. Osano K, Force L, Turner SR (2010) Synthesis and properties of linear poly(ether sulfone)s with hyperbranched terminal groups. Ind Eng Chem Res 49:12098–12103
163. Grunzinger SJ, Hayakawa T, Kakimoto MA (2008) Synthesis of multiblock hyperbranched-linear poly(ether sulfone) copolymers. J Polym Sci Part A Polym Chem 46:4785–4793
164. Lee HS, Takeuchi M, Kakimoto MA, Kim SY (2000) Hyperbranched poly(arylene ether phosphine oxide)s. Polym Bull 45:319–326
165. Lin Q, Long TE (2000) Synthesis and characterization of a novel AB_2 monomer and corresponding hyperbranched poly(arylene ether phosphine oxide)s. J Polym Sci A Polym Chem 38:3736–3741
166. Bernal DP, Bankey N, Cockayne RC, Fossum E (2002) Fluoride-terminated hyperbranched poly(arylene ether phosphine oxide)s via nucleophilic aromatic substitution. J Polym Sci A Polym Chem 40:1456–1467
167. Bernal DP, Bedrossian L, Collins K, Fossum E (2003) Effect of core reactivity on the molecular weight, polydispersity, and degree of branching of hyperbranched poly(arylene ether phosphine oxide)s. Macromolecules 36:333–338
168. Czupik M, Fossum E (2003) Manipulation of the molecular weight and branching structure of hyperbranched poly(arylene ether phosphine oxide)s prepared via an $A_2 + B_3$ approach. J Polym Sci A Polym Chem 41:3871–3881

169. Sennet L, Fossum E, Tan LS (2008) Branched poly(arylene ether ketone)s with tailored thermal properties: effects of AB/AB_2 ratio, core (B_3) percentage, and reaction temperature. Polymer 49:3731–3736

170. Fossum E, Tan LS (2005) Geometrical influence of AB_n monomer structure on the thermal properties of linear-hyperbranched ether–ketone copolymers prepared via an $AB + AB_n$ route. Polymer 46:9686–9693

171. Wang DH, Baek JB, Tan LS (2005) Phthalonitrile-terminated hyperbranched poly(arylene-ether-ketone-imide): synthesis and its blending with 4,4′-bis(3,4-dicyanophenoxy)biphenyl, phthalonitrile-terminated hyperbranched poly(arylene-ether-ketone-imide): synthesis and its blending with 4,4′-Bis(3,4-dicyanophenoxy)biphenyl. Polym Prepr 46:727–728

172. Yu Z, Fossum E, Wang DH, Tan LS (2008) Alternative approach to an AB_2 monomer for hyperbranched poly(arylene ether ketone imide)s. Syn Commun 38:419–427

173. Gong ZH, Leu CM, Wu FI, Shu CF (2000) Hyperbranched poly(aryl ether oxazole)s: synthesis, characterization, and modification. Macromolecules 33:8527–8533

174. Schmaljohann D, Haussler L, Potschke P, Voit BI, Loontjens TJA (2000) Modification with alkyl chains and the influence on thermal and mechanical properties of aromatic hyperbranched polyesters. Macromol Chem Phys 201:49–57

175. Wu FI, Shu CF (2001) Synthesis and characterization of new hyperbranched poly(aryl ether oxadiazole)s. J Polym Sci A Polym Chem 39:3851–3860

176. Fu Y, Oosterwijck CV, Vandendriessche A, Kowalczuk-Bleja A, Zhang X, Dworak A, Dehaen W, Smet M (2008) Hyperbranched poly(arylene oxindole)s with a degree of branching of 100% for the construction of nanocontainers by orthogonal modification. Macromolecules 41:2388–2393

177. Kowalczuk A, Vandendriessche A, Trzebicka B, Mendrek B, Szeluga U, Cholenwiński G, Smet M, Dworak A, Dehaen W (2009) Core-shell nanoparticles with hyperbranched poly (arylene-oxindole) interiors. J Polym Sci A Polym Chem 47:1120–1135

178. Colquhoun H, Zolotukhin M, Khalolov L, Dzhemilev U (2001) Superelectrophiles in aromatic polymer chemistry. Macromolecules 34:1122–1124

179. Baek JB, Harris FW (2005) Hyperbranched polyphenylquinoxalines from self-polymerizable AB_2 and A_2B monomers. Macromolecules 38:297–306

180. Baek JB, Harris FW (2005) Fluorine- and hydroxyl-terminated hyperbranched poly (phenylquinoxalines) (PPQs) from copolymerization of self-polymerizable AB and AB_2, BA, and BA_2 monomers. Macromolecules 38:1131–1140

181. Baek JB, Tan LS (2006) Hyperbranched poly(phenylquinoxaline–ether–ketone) synthesis in poly(phosphoric acid)/P_2O_5 medium: optimization and some interesting observations. Macromolecules 39:2794–2803

182. Dhara M, Banerjee S (2010) Fluorinated high-performance polymers: poly(arylene ether)s and aromatic polyimides containing trifluoromethyl groups. Prog Polym Sci 35:1022–1077

183. Labadie JW, Hedrick JL (1990) Perfluoroalkylene-activated poly(aryl ether) synthesis. Macromolecules 23:5371–5373

184. Yang H, Hay AS (1993) Fluorine substitutent effects on poly(2,6-diphenylphenylene ether). J Polym Sci A Polym Chem 31:2015–2029

185. Maier G, Hecht R (1995) Poly(aryl ether thiazole)s with pendent trifluoromethyl groups. Macromolecules 28:7558–7565

186. Park SK, Kim SY (1998) Synthesis of poly(arylene ether ketone)s containing trifluoromethyl groups via nitro displacement reaction. Macromolecules 31:3385–3387

187. Mohanty AK, Sen SK, Ghosh A, Maji S, Banerjee S (2010) Synthesis, characterization, and comparison of properties of new fluorinated poly(arylene ether)s containing phthalimidine moiety in the main chain. Polym Adv Technol 21:767–773

188. Aggarwal M, Maji S, Sen SK, Dasgupta B, Chatterjee S, Ghosh A, Banerjee S (2009) New poly(arylene ether)s containing phthalimidine group in the main chain. J Appl Polym Sci 112:1226–1233

189. Salunke AK, Ghosh A, Banerjee S (2007) Synthesis and characterization of novel poly (arylene ether)s based on 9,10-bis-(4-fluoro-3-trifluoromethylphenyl) anthracene and 2,7-bis-(4-fluoro-3-trifluoromethylphenyl) fluorine. J Appl Polym Sci 106:664–672

190. Digal AK, Ghosh A, Banerjee S (2008) Synthesis and characterization of novel poly(Arylene Ether)s from 4,4′-thiodiphenol. J Macromol Sci A Pure and Appl Chem 45:212–217

191. Banerjee S, Maier G, Dannenberg C, Spinger J (2004) Gas permeabilities of novel poly (arylene ether)s with terphenyl unit in the main chain. J Membr Sci 229:63–71

192. Xu ZK, Dannenberg C, Springer J, Banerjee S, Maier G (2002) Novel poly(arylene ether) as membranes for gas separation. J Membr Sci 205:23–31

193. Ghosh A, Banerjee S (2009) Synthesis and characterization of new fluorinated polyimides derived from 9, 10-bis[3′-trifluoromethyl-4′ (4″-aminobenzoxy) benzyl] anthracene. High Perform Polym 21:173–186

194. Banerjee S (2007) Synthesis and characterization of novel hyperbranched poly(arylene ether) from a AB_2 monomer. J Polym Mater 24:247–254

195. Satpathi H, Ghosh A, Banerjee S, Komber H, Voit B (2011) Synthesis and characterization of new semifluorinated linear and hyperbranched poly(arylene ether phosphine oxide)s through $B_2 + A_2$ and AB_2 approaches. Eur Polym J 47:196–207

196. Herbert CG, Bass RG, Watson KA, Connell JW (1996) Preparation of poly(arylene ether pyrimidine)s by aromatic nucleophilic substitution reactions. Macromolecules 29:7709–7716

197. Ghosh A, Banerjee S, Komber H, Voit B (2010) Extremely high molar mass hyperbranched poly(arylene ether)s from a new semifluorinated AB_2 monomer by an unusual $AB_2 + A_2$ polymerization approach. Macromolecules 43:2846–2854

198. Dusek K, Duskova-Smrckova M, Voit B (2005) Highly-branched off-stoichiometric functional polymers as polymer networks precursors. Polymer 46:4265–4282

199. Mahapatra SS, Karak N (2007) Hyperbranched aromatic polyamines with *s*-triazine rings. J Appl Polym Sci 106:95–102

200. Zhang J, Wang H, Li X (2006) Novel hyperbranched poly(phenylene oxide)s with phenolic terminal groups: synthesis, characterization, and modification. Polymer 47:1511–1518

201. Lv J, Meng Y, He L, Qiu T, Li X, Wang H (2013) Novel epoxidized hyperbranched poly (phenylene oxide): synthesis and application as a modifier for diglycidyl ether of bisphenol A. J Appl Polym Sci 128:907–914

202. Theil F (1999) Synthesis of diaryl ethers: a long-standing problem has been solved. Angew Chem Int Ed 38:2345–2347

203. Luo L, Qiu T, Meng Y, Guo L, Yang J, Li Z, Cao X, Li X (2013) A novel fluoro-terminated hyperbranched poly(phenylene oxide) (FHPPO): synthesis, characterization, and application in low-*k* epoxy materials. RSC Adv 3:14509–14520

204. Ghosh A, Chatterjee S, Banerjee S, Komber H, Voit B (2011) Linear and hyperbranched poly (arylene ether)s from a new semifluorinated AB monomer. J Macromol Sci A Pure and Appl Chem 48:509–517

205. Frey H, Holter D (1999) Degree of branching in hyperbranched polymers. 3 Copolymerization of AB_m-monomers with AB and AB_n-monomers. Acta Polym 50:67–76

206. Mellace A, Hanson JE, Griepenburg J (2005) Hyperbranched poly(phenylene sulfide) and poly(phenylene sulfone). Chem Mater 17:1812–1817

207. Brandrup J, Immergut EH, Grulke EA (eds) (1999) Polymer handbook, 4th edn. Wiley, New York

208. De Girolamo Del Mauro A, Loffredo F, Venditto V, Longo P, Guerra G (2003) Polymorphic behavior of syndiotactic poly(*p*-chlorostyrene) and styrene/*p*-chlorostyrene cosyndiotactic random copolymers. Macromolecules 36:7577–7584

209. Bo Y, Yanmo C, Hao Y, Bin S, Meifang Z (2009) Kinetics of the thermal degradation of hyperbranched poly(phenylene sulfide). J Appl Polym Sci 111:1900–1904

210. Day M, Budgell DR (1992) Kinetics of the thermal degradation of poly(phenylene sulfide). Thermochim Acta 203:465–474

211. Yang MH (2002) On the thermal degradation of poly(styrene sulfone)s. V Thermogravimetric kinetic simulation of polyacrylamide pyrolysis. J Appl Polym Sci 86:1540–1548
212. Li XG, Huang MR (1999) Thermal decomposition kinetics of thermotropic poly(oxybenzoate-co-oxynaphthoate) Vectra copolyester. Polym Degrad Stab 64:81–90
213. Popescu C (1996) Integral method to analyze the kinetics of heterogeneous reactions under non-isothermal conditions A variant on the Ozawa–Flynn–Wall method. Thermochim Acta 285:309–323
214. Sun JT, Huang YD, Gong GF, Cao HL (2006) Thermal degradation kinetics of poly(methylphenylsiloxane) containing methacryloyl groups. Polym Degrad Stab 91:339–346
215. Núñez L, Fraga F, Núñez MR, Villanueva M (2000) Thermogravimetric study of the decomposition process of the system BADGE ($n=0$)/1,2 DCH. Polymer 41:4635–4641
216. Montserrat S, Málek J, Colomer P (1998) Thermal degradation kinetics of epoxy–anhydride resins: I.: influence of a silica filler. Thermochim Acta 313:83–95
217. Xu R, Liu H, Liu S, Li Y, Shi W (2008) Effect of core structure on the fluorescence properties of hyperbranched poly(phenylene sulfide). J Appl Polym Sci 107:1857–1864
218. Zeng Q, Li Z, Dong Y, Di C, Qin A, Hong Y, Ji L, Zhu Z, Jim CKW, Yu G, Li Q, Li Z, Liu Y, Qin J, Tang BZ (2007) Fluorescence enhancements of benzene-cored luminophors by restricted intramolecular rotations: AIE and AIEE effects. Chem Commun 2007(1):70–72. doi:10.1039/B613522F
219. Lam JWY, Chen J, Law CCW, Peng H, Xie Z, Cheuk KKL, Kwork HS, Tang BZ (2003) Silole-containing linear and hyperbranched polymers: synthesis, thermal stability, light emission, nano-dimensional aggregation, and optical power limiting. Macromol Symp 196:289–300
220. Tang BZ (2008) Construction of functional polymers from acetylenic triple-bond building blocks. Macromol Chem Phys 209:1303–1307
221. Haussler M, Qin A, Tang BZ (2007) Acetylenes with multiple triple bonds: a group of versatile A_n-type building blocks for the construction of functional hyperbranched polymers. Polymer 48:6181–6204
222. Peng H, Lam JWY, Tang BZ (2005) Hyperbranched poly(aryleneethynylene)s: synthesis, thermal stability and optical properties. Macromol Rapid Commun 26:673–677
223. Hong Y, Lam JWY, Tang BZ (2009) Aggregation-induced emission: phenomenon, mechanism and applications. Chem Commun 2009(29): 4332–4353. doi:10.1039/B904665H
224. Qin A, Lam JWY, Tang BZ (2010) Click polymerization. Chem Soc Rev 39:2522–2544
225. Mukamal H, Harris FW, Stille JK (1967) Diels–Alder polymers. III. Polymers containing phenylated phenylene units. J Polym Sci A Polym Chem 5:2721–2729
226. Loi S, Butt HJ, Hampel C, Bauer R, Wiesler UM, Müllen K (2002) Two-dimensional structure of self-assembled alkyl-substituted polyphenylene dendrimers on graphite. Langmuir 18:2398–2405
227. Andreitchenko EV, Clark CG Jr, Bauer RE, Lieser G, Müllen K (2005) Pushing the synthetic limit: polyphenylene dendrimers with "exploded" branching units—22-nm-diameter, monodisperse, stiff macromolecules. Angew Chem Int Ed 44:6348–6354
228. Tasdelen MA (2011) Diels–Alder "click" reactions: recent applications in polymer and material science. Polym Chem 2:2133–2145
229. Xu K, Peng H, Sun Q, Dong Y, Salhi F, Luo J, Chen J, Huang Y, Zhang D, Xu Z, Tang BZ (2002) Polycyclotrimerization of diynes: synthesis and properties of hyperbranched polyphenylenes. Macromolecules 35:5821–5834
230. Dong H, Zheng R, Lam JWY, Häussler M, Tang BZ (2005) A new route to hyperbranched macromolecules: syntheses of photosensitive poly(aroylarylene)s via 1,3,5-regioselective polycyclotrimerization of bis(aroylacetylene)s. Macromolecules 38:6382–6391
231. Stumpe K, Komber H, Voit B (2006) Novel branched polyphenylenes based on A_2/B_3 and AB_2/AB monomers via Diels–Alder cycloaddition. Macromol Chem Phys 207:1825–1833

232. Stumpe K, Eichhorn KJ, Voit B (2008) Characterisation of thin composite films from hyperbranched polyphenylene and thermolabile hyperbranched polycarbonate. Macromol Chem Phys 209:1787–1796

233. Pötzsch R, Voit B (2012) Thermal and photochemical crosslinking of hyperbranched polyphenylene with organic azides. Macromol Rapid Commun 33:635–639

234. Pötzsch R, Komber H, Stahl BC, Hawker CJ, Voit BI (2013) Radical thiol-yne chemistry on diphenylacetylene: selective and quantitative addition enabling the synthesis of hyperbranched poly(vinyl sulfide)s. Macromol Rapid Commun 34:1772–1778

235. Liu JG, Ueda M (2009) High refractive index polymers: fundamental research and practical applications. J Mater Chem 19:8907–8919

236. Pötzsch R, Stahl BC, Komber H, Hawker CJ, Voit BI (2014) High refractive index polyvinylsulfide materials prepared by selective radical mono-addition thiol–yne chemistry. Polym Chem 5:2911–2921

237. Lam JWY, Tang BZ (2005) Functional polyacetylenes. Acc Chem Res 38:745–754

238. Schluter AD, Wegner G (1993) Palladium and nickel catalyzed polycondensation – the key to structurally defined polyarylenes and other aromatic polymers. Acta Polym 44:59–69

239. Tour JM (1994) Soluble oligo- and polyphenylenes. Adv Mater 6:190–198

240. Watson MD, Fechtenkotter A, Mullen K (2001) Big is beautiful – "aromaticity" revisited from the viewpoint of macromolecular and supramolecular benzene chemistry. Chem Rev 101:1267–1300

241. Zheng R, Dong H, Peng H, Lam JWY, Tang BZ (2004) Construction of hyperbranched poly (alkenephenylene)s by Diyne polycyclotrimerization: single-component catalyst, glycogen-like macromolecular structure, facile thermal curing, and strong thermolysis resistance. Macromolecules 37:5196–5210

242. Zheng R, Haussler M, Dong H, Lam JWY, Tang BZ (2006) Synthesis, structural character-ization, and thermal and optical properties of hyperbranched poly(aminoarylene)s. Macro-molecules 39:7973–7984

243. Liu J, Zheng R, Tang Y, Haussler M, Lam JWY, Qin A, Ye M, Hong Y, Gao P, Tang BZ (2007) Hyperbranched poly(silylenephenylenes) from polycyclotrimerization of A2-type diyne monomers: synthesis, characterization, structural modeling, thermal stability, and fluorescent patterning. Macromolecules 40:7473–7486

244. Haussler M, Liu J, Zheng R, Lam JWY, Qin A, Tang BZ (2007) Synthesis, thermal stability, and linear and nonlinear optical properties of hyperbranched polyarylenes containing carba-zole and/or fluorene moieties. Macromolecules 40:1914–1925

245. Shi J, Jim CJW, Mahtab F, Liu J, Lam JWY, Sung HHY, Williams ID, Dong Y, Tang BZ (2010) Ferrocene-functionalized hyperbranched polyphenylenes: synthesis, redox activity, light refraction, transition-metal complexation, and precursors to magnetic ceramics. Mac-romolecules 43:680–690

246. Liu J, Deng C, Tseng NW, Chan CYK, Yue Y, Ng JCY, Lam JWY, Wang J, Hong Y, Sung HHY, Williams ID, Tang BZ (2011) A new polymerisation route to conjugated polymers: regio- and stereoselective synthesis of linear and hyperbranched poly(arylene chlorovinylene)s by decarbonylative polyaddition of aroyl chlorides and alkynes. Chem Sci 2:1850–1859

247. Schmaljohann D, Pötschke P, Haussler R, Voit BI, Froehling PE, Mostert B, Loontjens JA (1999) Blends of amphiphilic, hyperbranched polyesters and different polyolefins. Macro-molecules 32:6333–6339

248. Jang J, Hak Oh J, Moon SI (2000) Crystallization behavior of poly(ethylene terephthalate) blended with hyperbranched polymers: the effect of terminal groups and composition of hyperbranched polymers. Macromolecules 33:1864–1870

249. Hsieh TT, Tiu C, Simon GP (2001) Rheological behaviour of polymer blends containing only hyperbranched polyesters of varying generation number. Polymer 42:7635–7638

250. Nunez CM, Chiou BS, Andrady AL, Khan SA (2000) Solution rheology of hyperbranched polyesters and their blends with linear polymers. Rheological behaviour of polymer blends

containing only hyperbranched polyesters of varying generation number. Macromolecules 33:1720–1726

251. Li X, Zhang S, Wang H, Zhang C, Pang J, Mu J, Ma G, Wang G, Jiang Z (2011) Study of blends of linear poly(ether ether ketone) of high melt viscosity and hyperbranched poly(ether ether ketone). Polym Int 60:607–612

252. Tang H, Fan X, Shen Z, Zhou Q (2013) One-pot synthesis of hyperbranched poly(aryl ether ketone)s for the modification of bismaleimide resins. Polym Eng Sci 54:1675–1685

253. Hakme C, Stevenson I, Fulchiron R, Seytre G, Clement F, Odoni L, Rochat S, Varlet J (2005) Dielectric studies of hyperbranched aromatic polyamide and polyamide-6,6 blends. J Appl Polym Sci 97:1522–1537

254. Monticelli O, Oliva D, Russo S, Clausnitzer C, Potschke P, Voit B (2003) On blends of polyamide 6 and a hyperbranched aramid. Macromol Mater Eng 288:318–325

255. Huber T, Pötschke P, Pompe G, Häßler R, Voit B, Grutke S, Gruber F (2000) Blends of hyperbranched poly(ether amide)s and polyamide-6. Macromol Mater Eng 280–281:33–40

256. Böhme F, Clausnitzer C, Gruber F, Grutke S, Huber T, Potschke P, Voit B (2001) Hyperbranched poly(ether amide)s via nucleophilic ring opening reaction of oxazolines. High Perform Polym 13:S21–S31

257. Fang K, Li J, Ke C, Zhu Q, Zhu J, Yan Q (2010) Synergistic effect between a novel hyperbranched flame retardant and melamine pyrophosphate on the char forming of polyamide 6. Polym Plastics Technol Eng 49:1489–1497

258. Chen X, Jiao C, Li S, Sun J (2011) Flame retardant epoxy resins from bisphenol-A epoxy cured with hyperbranched polyphosphate ester. J Polym Res 18:2229–2237

259. Sari MG, Stribeck N, Moradian S, Zeinolebadi A, Bastani S, Botta S (2013) Correlation of nanostructural parameters and macromechanical behaviour of hyperbranched-modified polypropylene using time-resolved small-angle X-ray scattering measurements. Polym Int 62:1101–1111

260. Foix D, Ramis X, Ferrando F, Serra A (2012) Improvement of epoxy thermosets using a thiol-ene based polyester hyperbranched polymer as modifier. Polym Int 61:727–734

261. Qiang TT, Wang X (2007) Study on synthesis of hyperbranched polymer with terminal carboxyl and its effect of chrome-tanning assistant. PhD Thesis, Shanxi University of Science and Technology, China

262. Ren L, Zhao G, Qiang T, Wang X, Wang N (2013) Synthesis of amino-terminated hyperbranched polymers and their application in microfiber synthetic leather base dyeing. Textile Res J 83:381–395

263. Lei L, Wang H, Zhang Y, Li X, Mu J, Wang G, Jiang Z, Zhang S (2010) Preparation and characterization of a novel hyperbranched poly(aryl ether ketone) terminated with cobalt phthalocyanine to be used for oxidative decomposition of 2,4,6-trichlorophenol. Macromol Res 18:331–335

264. Zhang YH, Niu YM, Xu R, Wang GB, Jiang ZH (2006) Synthesis and characterization of poly(aryl ether sulfone)s with metallophthalocyanine pendant unit. J Appl Polym Sci 102:3457–3461

265. Zhang YH, Sun XB, Niu YM, Xu R, Wang GB, Jiang ZH (2006) Synthesis and characterization of novel poly(aryl ether ketone)s with metallophthalocyanine pendant unit from a new bisphenol containing dicyanophenyl side group. Polymer 47:1569–1574

266. Huang P, Gu A, Liang G, Yuan L (2012) Synthesis of epoxy-functionalized hyperbranched poly(phenylene oxide) and its modification of cyanate ester resin. J Appl Polym Sci 123:2351–2359

267. Fan Z, Jaehnichen K, Desbois P, Haussler L, Vogel R, Voit B (2009) Blends of different linear polyamides with hyperbranched aromatic AB$_2$ and A$_2$+B$_3$ polyesters. J Polym Sci A Polym Chem 47:3558–3572

268. Mulkern TJ, Beck Tan NC (2000) Processing and characterization of reactive polystyrene/hyperbranched polyester blends. Polymer 41:3193–3203

269. Ke C, Li J, Fang K, Zhu Q, Zhu J, Yan Q (2011) Enhancement of a hyperbranched charring and foaming agent on flame retardancy of polyamide 6. Polym Adv Technol 22:2237–2243
270. Yan H, Chen Y (2010) Blends of polypropylene and hyperbranched poly(phenylene sulphide) for production of dyeable PP fibres. Iran Polym J 19:791–799
271. Lau WJ, Ismail AF, Misdan N, Kassim MA (2012) A recent progress in thin film composite membrane: a review. Desalination 287:190–199
272. Tang CY, Kwon YN, Leckie JO (2007) Probing the nano- and micro-scales of reverse osmosis membranes—a comprehensive characterization of physiochemical properties of uncoated and coated membranes by XPS, TEM, ATR-FTIR, and streaming potential measurements. J Membr Sci 287:146–156
273. Jadav GL, Singh PS (2009) Synthesis of novel silica-polyamide nanocomposite membrane with enhanced properties. J Membr Sci 328:257–267
274. Chiang YC, Hsub YZ, Ruaan RC, Chuang CJ, Tung KL (2009) Nanofiltration membranes synthesized from hyperbranched polyethyleneimine. J Membr Sci 326:19–26
275. Park SY, Kim SG, Chun JH, Chun BH, Kim SH (2012) Fabrication and characterization of the chlorine-tolerant disulfonated poly(arylene ether sulfone)/hyperbranched aromatic polyamide-grafted silica composite reverse osmosis membrane. Desalin Water Treat 43:221–229
276. Peighambardoust SJ, Rowshanzamir S, Amjadi M (2010) Review of the proton exchange membranes for fuel cell applications. Int J Hydrogen Energy 35:9349–9384
277. Colicchio I, Keul H, Sanders D, Simon U, Weirich TE, Moeller M (2006) Development of hybrid polymer electrolyte membranes based on the semi-interpenetrating network concept. Fuel Cells 6:225–236
278. Gode P, Hult A, Jannasch P, Johansson M, Karlsson LE, Lindbergh G, Malmström E, Sandquist D (2006) A novel sulfonated dendritic polymer as the acidic component in proton conducting membranes. Solid State Ionics 177:787–794
279. Itoh T, Hamaguchi Y, Uno T, Kubo M, Aihara Y, Sonai A (2006) Synthesis, ionic conductivity, and thermal properties of proton conducting polymer electrolyte for high temperature fuel cell. Solid State Ionics 177:185–189
280. Ghosh A, Sen SK, Dasgupta B, Banerjee S, Voit B (2010) Synthesis, characterization and gas transport properties of new poly(imide siloxane) copolymers from 4,4′-(4,4′-isopropylidenediphenoxy)bis(phthalic anhydride). J Membr Sci 364:211–218
281. Cornelius CJ, Marand E (2002) Hybrid silica-polyimide composite membranes: gas transport properties. J Membr Sci 202:97–118
282. Hibshman C, Cornelius CJ, Marand E (2003) The gas separation effects of annealing polyimide–organosilicate hybrid membranes. J Membr Sci 211:25–40
283. Hibshman C, Mager M (2004) Marand E (2004) Effects of feed pressure on fluorinated polyimide–organosilicate hybrid membranes. J Membr Sci 229:73–80
284. Suzuki T, Yamada Y (2006) Characterization of 6FDA-based hyperbranched and linear polyimide–silica hybrid membranes by gas permeation and ^{129}Xe NMR measurements. J Polym Sci B Polym Phys 44:291–298
285. Suzuki T, Yamada Y (2007) Effect of end group modification on gas transport properties of 6FDA-TAPOB hyperbranched polyimide—silica hybrid membranes. High Perform Polym 19:553–564
286. Suzuki T, Yamada Y, Itahashi K (2008) 6FDA-TAPOB hyperbranched polyimide-silica hybrids for gas separation membranes. J Appl Polym Sci 109:813–819
287. Wang H, Pang J, Zhou F, Zhang H, Jiang Z, Zhang S (2013) Synthesis and preparation of sulfonated hyperbranched poly(aryl ether ketone)–sulfonated linear poly(aryl ether ketone) blend membranes for proton exchange membranes. High Perform Polym 25:759–768
288. Suda T, Yamazaki K, Kawakami H (2010) Syntheses of sulfonated star-hyperbranched polyimides and their proton exchange membrane properties. J Power Sources 195:4641–4646
289. Suzuki T, Miki M, Yamada Y (2012) Gas transport properties of hyperbranched polyimide/hydroxy polyimide blend membranes. Eur Polym J 48:1504–1512

290. Hosseini SS, Teoh MM, Chung TS (2008) Hydrogen separation and purification in membranes of miscible polymer blends with interpenetration networks. Polymer 49:1594–1603
291. Low BT, Chung TS, Chen H, Jean YC, Pramoda KP (2009) Tuning the free volume cavities of polyimide membranes via the construction of pseudo-interpenetrating networks for enhanced gas separation performance. Macromolecules 42:7042–7054
292. Im H, Kim H, Kim CK, Kim J (2009) Enhancement of gas selectivities of hexafluoroisopropylidene-based polyimides with poly(methylmethacrylate) blending. Ind Eng Chem Res 48:8663–8669
293. Morisato A, Shen HC, Sankar SS, Freeman BD, Pinnau I, Casillas CG (1996) Polymer characterization and gas permeability of poly(1-trimethylsilyl-1-propyne) [PTMSP], poly (1-phenyl-1-propyne) [PPP], and PTMSP/PPP blends. J Polym Sci B Polym Phys 34:2209–2222
294. Robeson LM (1991) Correlation of separation factor versus permeability for polymeric membranes. J Membr Sci 62:165–185
295. Robeson LM (2008) The upper bound revisited. J Membr Sci 320:390–400
296. Trimble AR, Tully DC, Fréchet JMJ, Medeiros DR, Angelopoulos M (2000) Patterning of hyperbranched resist materials by electron-beam lithography. Polym Prepr 41:325–326
297. Okazaki M, Shibasaki Y, Ueda M (2001) New negative-type photosensitive polyimide based on hyperbranched poly(ether imide), a cross-linker, and a photoacid generator. Chem Lett 8:762–763
298. In I, Lee H, Fujigaya T, Okazaki M, Ueda M, Kim SY (2003) A new photoresist based on hyperbranched poly(ary1ene ether phosphine oxide). Polym Bull 49:349–355
299. Hong CS, Jikei M, Kikuchi R, Kakimoto M (2003) Chemically amplified photosensitive polybenzoxazoles based on tert-butoxycarbonyl protected hyperbranched poly (o-hydroxyamide)s. Macromolecules 36:3174–3179
300. Chen H, Yin J (2003) Synthesis of autophotosensitive hyperbranched polyimides based on 3,3′,4,4′-benzophenonetetracarboxylic dianhydride and 1,3,5-tris(4-aminophenoxy)benzene via end capping of the terminal anhydride groups by *ortho*-alkyl aniline. J Polym Sci A Polym Chem 41:2026–2035
301. Chen H, Yin J (2003) Preparation of auto-photosensitive hyperbranched co-polyimide by the condensation of 4,4′-(hexafluoroisopropy1idene)diphthalic anhydride and 3,3′,4,4′-benzophenonetetracarboxylic dianhydride with 1,3,5-tris(4-aminophenoxy)benzene through a stage addition reaction method. Polym Bull 50:303–310
302. Chen H, Yin J (2004) Synthesis and characterization of negative-type photosensitive hyperbranched polyimides with excellent organosolubility from an $A_2 + B_3$ monomer system. J Polym Sci A Polym Chem 42:1735–1744
303. Liu C, Zhao X, Li Y, Yang D, Wang L, Jin L, Chen C, Zhou H (2013) New autophoto-sensitive semiaromatic hyperbranched polyimides with excellent thermal stabilities and low birefringences. High Perform Polym 25:301–311
304. Zyss J (1994) Molecular nonlinear optics: materials, physics and devices. Academic, Boston
305. Li Z, Dong S, Li P, Li Z, Ye C, Qin J (2008) New PVK-based nonlinear optical polymers: enhanced nonlinearity and improved transparency. J Polym Sci A Polym Chem 46:2983–2993
306. Czech P, Okrasa L, Méchin F, Boiteux G, Ulanski J (2006) Investigation of the polyurethane chain length influence on the molecular dynamics in networks crosslinked by hyperbranched polyester. Polymer 47:7207–7215
307. Ren Q, Gong F, Jiang B, Zhang D, Fang J, Guo F (2006) Preparation of hyperbranched copolymers of maleimide inimer and styrene by ATRP. Polymer 47:3382–3389
308. Zhou Z, Yan D (2006) Distribution function of hyperbranched polymers formed by AB_2 type polycondensation with substitution effect. Polymer 47:1473–1479
309. Zhu Z, Li Z, Tan Y, Li Z, Li Q, Zeng Q, Ye C, Qin J (2006) New hyperbranched polymers containing second-order nonlinear optical chromophores: synthesis and nonlinear optical characterization. Polymer 47:7881–7888

310. Chang HL, Chao TY, Yang CC, Dai SA, Jeng RJ (2007) Second-order nonlinear optical hyperbranched polymers via facile ring-opening addition reaction of azetidine-2,4-dione. Eur Polym J 43:3988–3996
311. Xie J, Deng X, Cao Z, Shen Q, Zhang W, Shi W (2007) Synthesis and second-order nonlinear optical properties of hyperbranched polymers containing pendant azobenzene chromophores. Polymer 48:5988–5993
312. Bai Y, Song N, Gao JP, Sun X, Wang X, Yu G, Wang ZY (2005) A new approach to highly electrooptically active materials using cross-linkable, hyperbranched chromophore-containing oligomers as a macromolecular dopant. J Am Chem Soc 127:2060–2061
313. Xie J, Hu L, Shi W, Deng X, Cao Z, Shen Q (2008) Synthesis and nonlinear optical properties of hyperbranched polytriazole containing second-order nonlinear optical chromophore. J Polym Sci B Polym Phys 46:1140–1148
314. He N, Chen Y, Doyle J, Liu Y, Blau WJ (2008) Optical and nonlinear optical properties of an octasubstituted liquid crystalline copper phthalocyanine. Dyes Pigments 76:569–573
315. Zhang Y, Wang L, Wada T, Sasabe H (1996) One-pot synthesis of a new hyperbranched polyester containing 3,6-di-acceptor-substituted carbazole chromophores for nonlinear optics. Macromol Chem Phys 197:667–676
316. Pitois C, Wiesmann D, Lindgren M, Hult A (2001) Functionalized fluorinated hyperbranched polymers for optical waveguide applications. Adv Mater 13:1483–1484
317. Gao H, Yorifuji D, Wakita J, Jiang Z-H, Ando S (2010) In situ preparation of nano ZnO/hyperbranched polyimide hybrid film and their optical properties. Polymer 51:3173–3180
318. Jiang X, Wang H, Chen X, Li X, Lei L, Mu J, Wang G, Zhang S (2010) A novel photoactive hyperbranched poly(aryl ether ketone) with azobenzene end groups for optical storage applications. React Funct Polym 70:699–705
319. Maier G (2001) Low dielectric constant polymers for microelectronics. Prog Polym Sci 26:3–65
320. Volksen W, Miller RD, Dubois G (2010) Low dielectric constant materials. Chem Rev 110:56–110
321. Martin SJ, Godschalx JP, Mills ME, Shaffer EO II, Townsend PH (2000) Development of a low-dielectric-constant polymer for the fabrication of integrated circuit interconnect. Adv Mater 12:1769–1778
322. Somboonsub B, Thongyai S, Praserthdam P (2009) Dielectric properties and solubility of multilayer hyperbranched polyimide/polyhedral oligomeric silsesquioxane nanocomposites. J Appl Polym Sci 114:3292–3302
323. Banerjee S, Maier G, Burger M (1999) Novel poly(arylene ether)s with pendent trifluoromethyl groups. Macromolecules 32:4279–4289
324. Hedrick JL et al (1993) US Patent 5,776,990
325. Zhong B (2001) US Patent 6,197,913
326. Li Z, Wu W, Ye C, Qin J, Li Z (2010) New hyperbranched polyaryleneethynylene containing azobenzene chromophore moieties in the main chain: facile synthesis, large optical nonlinearity and high thermal stability. Polym Chem 1:78–81
327. Hu R, Lam JWY, Liu J, Sung HHY, Williams ID, Yue Z, Wong KS, Yuen MMF, Tang BZ (2012) Hyperbranched conjugated poly(tetraphenylethene): synthesis, aggregation-induced emission, fluorescent photopatterning, optical limiting and explosive detection. Polym Chem 3:1481–1489

Changing Polymer Solvation by Electrochemical Means: Basics and Applications

Felix A. Plamper

Abstract Developments in the area of electrochemical manipulation of polymers are reviewed, with an emphasis on soft condensed matter (with some weight on aqueous systems). Electrochemical control of polymer solubility is a current issue, with applications in smart colloids, gels, and self-assembled systems. Electrode modification is addressed briefly. Different stimuli-responsive systems are categorized by highlighting the peculiarity of electrochemical switching. The review then categorizes different basic mechanisms for electrochemical switching of polymers: electrochemically induced solvation (switching of redox-active sites, which are strongly bound to the polymer), electrochemically induced complexation (free redox-active entities interact with complexation sites along the polymer), and mixed concepts. Further, features of different metallocene-based polymers are compared and ion-specific effects for the interaction of metallates with polyelectrolytes are addressed.

Keywords Electrochemistry · Polymer · Solution properties · Stimuli responsiveness

Contents

F.A. Plamper (✉)
Institute of Physical Chemistry, RWTH Aachen University, Landoltweg 2, 52056 Aachen, Germany
e-mail: plamper@pc.rwth-aachen.de

1   Introduction

Stimuli-responsive materials have attracted enormous interest in the fields of polymer, supramolecular, and colloidal science over the last few decades [1–5]. It can be anticipated that stimuli-sensitive systems in general and switchable polymers in particular will continue to be a thriving branch of chemistry. New applications can be envisioned, for instance, for controlled uptake and release, fine-tuning of mechanical properties, or actuating purposes.

1.1   Classification of Stimuli-Responsive Systems

Systems sensitive to different stimuli such as pH, salinity, solvent composition, and other chemical reactants have already been addressed. In these cases, the system is changed by adding chemicals (this behavior is termed a type I stimuli-responsivity). In contrast, external switching is possible by using magnetic/electric fields (including light) [6, 7] or temperature (type II). The latter is probably the most prominent stimulus in polymer science [8]. Significantly under-represented, electrochemical means for switching polymer properties is still a relatively undiscovered field, although redox-active polymers have been known for decades (Fig. 1). Recently, their study has gained new impetus, as highlighted by this review and other recent reviews with slightly different emphases [9–11]. The full possibilities of redox-active polymers can only vaguely be anticipated. Many unrevealed properties are still to be discovered, especially when considering the impact of rather simple-looking polymer complexes with fullerene, which gives a peculiar switching behavior [12]. Another possibility is that the marriage of artificial molecular machines [13, 14] with polymers might give unprecedented properties (Fig. 2). Still, the question remains: Why has electrochemical manipulation only recently found increased interest among the polymer community? As a possible answer, the last-century climax of redox-sensitive polymers (viologens, tetrathiafulvalenes, etc.) might already have been reached when controlled radical polymerization had its huge impact on polymer science at the end of the 1990s. Probably, controlled radical polymerization [15–17] led to a shift in research, with the focus moving more towards the generation of advanced macromolecular structures utilizing monomers that previously could not be polymerized by living techniques. Interestingly, controlled polymerization is indeed on its way to being re-united with electrochemistry, as highlighted in a related review [18]. Still, advanced polymeric
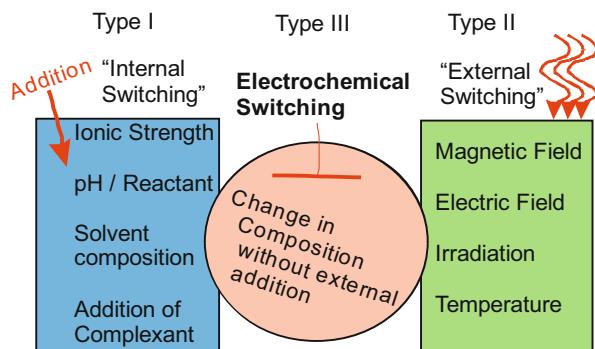
Fig. 1 Categories of stimuli-responsive systems
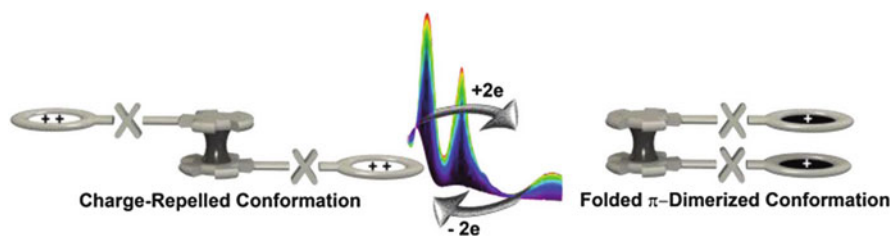
Fig. 2 Example of an electrochemically triggered conformation change of viologen-modified ferrocens (acting as a ball bearing for the viologenic rotors) (reprinted with permission from [14]. Copyright 2012 American Chemical Society)

architectures (e.g., block copolymers, branched macromolecules, and microgels) based on electrochemically active monomers are rare.

Electrochemical switching is peculiar because it has an intermediate position between the internal and external switching described above (see Fig. 1, type III). In principle, no chemicals are added to the system, but chemical reactions are triggered at the electrodes. Types I and II do not necessarily require "real" chemical reactions, although chemical reactions can be employed (e.g., for azobenzene-containing polymers or light-sensitive counterions) [4, 19–21]. In contrast, chemical conversion is always required for an electrochemical stimulus (type III reaction). Thus, by using a simple electrical switch, one can remotely and easily manipulate the chemical composition and, thereby, the properties of a system. Hence, there is no need to open the system to change its composition. In addition, electrochemical switching is rather independent of extrinsic variables such as temperature or light. Thus, it can be used preferentially on occasions where changes in temperature or illumination are detrimental. As a possible disadvantage, the electrochemical switching of bulk samples, as is the case for most of the other principles, is rarely instantaneous (typically in the time scale of minutes). However, by proper engineering of the electrochemical cell, shorter switching times are

possible. This is also illustrated by the short reaction times used, e.g., in cyclic voltammetry (reactions take place partly on the sub-second time scale). Here, the sample is converted only locally in the vicinity of the electrode. In consequence, electrode film switchability by electrochemical means can be instantaneous, although bulk electrolysis takes longer, even under stirring. If rapid bulk conversion is required, chemical redox (type I) might again become the switching principle of choice. Hence in some cases, there is a good argument for the use of conventional chemical redox reactions. Still, the potential of electrochemically responsive polymers is far from being exhausted, even though redox-sensitive polymers have been known for decades. This review will bridge the past to the future, while the main emphasis is on recent developments in this field.

1.2 Classification of Redox-Sensitive Systems in Terms of Application

The topics are classified phenomenologically (Fig. 3): (I) electrochemically addressable polymers in solution, (II) electrochemically induced micellization and demicellization (including vesicles and capsules with switchable porosity), (III) electrochemically addressable hydrogels and microgels, and (IV) thin films for electrode modification (without emphasizing classical electrochemical polymerization). An overview of polymerizations under electrochemical control is given elsewhere [18].

The scope of some publications touches several classes and therefore the publications cannot be sorted unambiguously. Topic IV is an especially vivid branch of research and only a short overview can be given (see Sect. 2.4). Further information can be found in the literature [22–25]. This review does not intend to give an exhaustive list of all research in this field. This is especially true for electronic devices that are based on polymers, i.e., organic (light-emitting) diodes, organic (field effect) transistors, organic photovoltaic cells, storage devices, organic batteries, etc. Reviews and articles on these devices can be found in literature [26–31]. The scope of this manuscript is primarily focused on the electrochemical manipulation of solution properties by electrochemical means (with some emphasis on aqueous media).

1.3 Classification of Redox-Sensitive Systems in Terms of Chemistry

For each of the areas of interest (topics I–IV; see Sects 2.1, 2.2, 2.3, and 2.4), it is reasonable to distinguish between at least two basic principles of electrochemical switching of polymers: electrochemically induced solvation and electrochemically

Fig. 3 Areas of interest
covered by this review
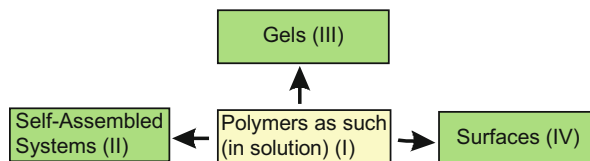
induced complexation. The systems are categorized in Sect. 2.1 according to this scheme. The first switching principle relies on the direct electrochemical switching of redox-sensitive units, which are bound to the polymeric backbone. Often, these redox reactions are coupled with generation or depletion of charges on the polymer. Then, the induced polyelectrolyte behavior enhances water compatibility and aggravates solubility in organic media. The second principle is realized by redox-sensitive units of low molecular weight, which can interact with the polymer depending on their respective oxidation state (co-assembly). In some rare cases, the interaction between polymer and electroactive species is not so important because the polymer can take the role of a viscosity modulator for a solution of redox-active species [32]. More relevant in our context are cases in which small species act as the redox-responsive entities, which interact with the polymer, e.g., electrostatical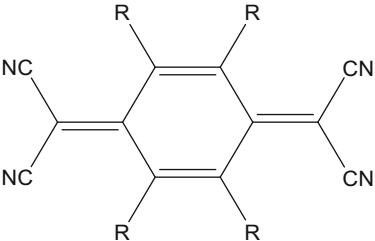ly. In some cases, electrochemically induced solvation and complexation compete with each other (Fig. 4). Then, strict categorization is not possible and a mixed concept is introduced (e.g., when complexants are present during an electrochemically induced solvation, both the solubility of the polymer per se and the complexation constant change).

1.4 General Remarks

Where applicable, chemical redox reactions (categorized as type I stimuli-responsive systems) are briefly addressed [33, 34]. Literature reports show a number of systems utilizing thiol/disulfide coupling chemistry [35, 36], which is especially appealing for biomedical applications [37]. Electrochemical control of this reaction is barely feasible, which is evidenced by a scarcity of reports on the subject. Reasons might include undesired electrode–thiol interactions and the coupled full oxidation of sulfur (for electrochemical detection special measures are often required [38, 39]). Still, some equilibrium potentials of thiol/disulfide couples have been reported [40]. In other cases, the literature is sometimes rather vague regarding the applicability of electrochemical means for changing polymer properties. Sometimes, chemical redox reactions are used and further electrochemical characterization is limited to methods such as cyclovoltammetry (CV). Still, if electrochemical analytics were used in a publication, the investigated system is regarded as electrochemically addressable and is emphasized in this review. If no electrochemical characterization is mentioned, the topic of the publication is mentioned if the case is of considerable interest. This review is not meant to be
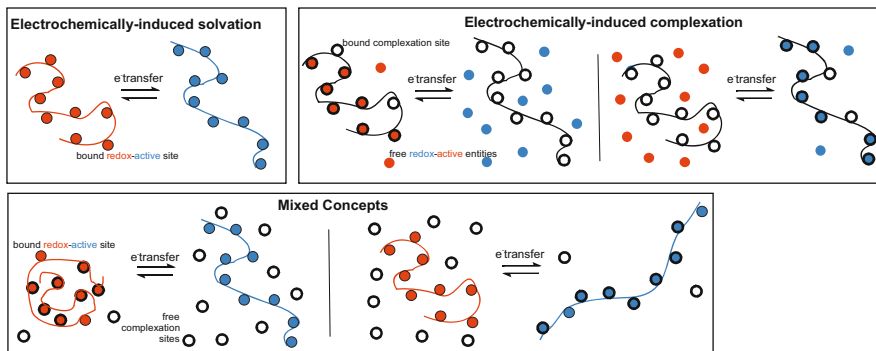
Fig. 4 General switching principles of redox-active polymers in solution, showing an increase in solvent contact and polymer expansion upon electrochemical stimulus (the *colored* polymer backbones indicate strongly bound redox-active sites and the *colored dots* indicate the redox-active entities in general; *blue* was arbitrarily chosen for the more soluble form; *black rings with thick wall* indicate the host entities for complexation: uncomplexed with *white interior*, complexed with *colored interior*)

exhaustive, especially as parts of the addressed topics are "busy" subjects in electrochemistry (e.g., electrode modification). Also, it is not easy to give a common picture: electrochemical processes are very dependent on the conditions, and changes in electrode material can alter electron transfer significantly. In several cases, the electrode material was not specified although CV had been conducted. Despite these complications, a proper overview of research on electrochemical manipulation of polymers has been attempted.

2 Main Part

2.1 Addressable Polymers in Solution

Electrochemical manipulation of polymers in solution can lead to conformational changes and finally to changes in their solubility. Naturally, this was found for electrochemically induced solvation, but also for electrochemically induced complexation. Changes in solubility can even lead to gelation, which will be covered further in Sect. 2.3. In any case, addressable polymers in solution are good examples for explaining the basic concepts behind the switching procedures.

2.1.1 Electrochemically Induced Solvation

This section deals with the changes in solvation of redox-active, polymer-bound units. It is worthwhile distinguishing between covalently bound moieties, which are

most often organic entities. But, "non-classical" coordination bonds can also provide stable connection of electroactive metal centers to the polymer backbone (almost irrespective of their oxidation state). Hence, this case is categorized as electrochemically induced solvation because the redox active groups are typically strongly bound, without much interference by decomplexation. For weaker complexation of metal centers to polymeric ligands, the switching principle can be regarded as a mixture of both extremes (electrochemically induced solvation and complexation).
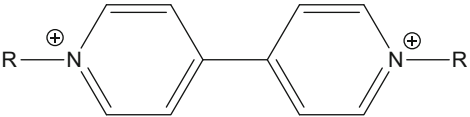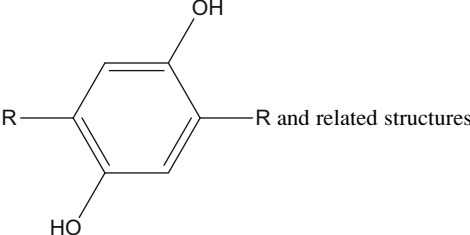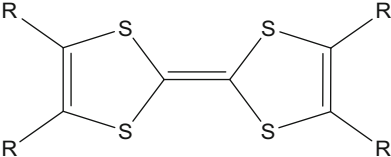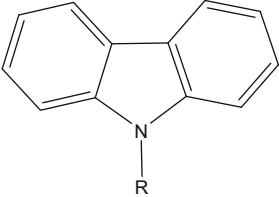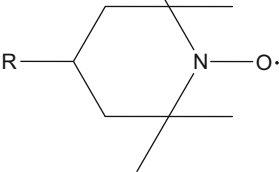
Covalently Bound Redox Centers

Different structural motifs are addressed in this section. Without being exhaustive, an overview is given in Table 1. Starting with viologens (fully quaternized 4,4′-bipyridines), they can be typically reduced from a dicationic species via a radical cation to a non-charged quinoidic moiety. They can then be arranged within the main chain [41–43], but side-chain viologens [44–46] or star-like viologens [47, 48] are also known. Viologen is poorly conducting, but by stopping the reduction at an intermediate state, mixed-valence assemblies (partially oxidized) can also conduct electrons in the dry state [49, 50]. Diffusion controlled, electrochemically reversible electron transfer kinetics have been found for viologen-modified poly (vinylphosphonic acid) [51]. The side-chain approach was also taken up for polysoaps [52]. For example, viologen derivatives can be attached via longer alkyl chains onto the backbone [53]. In contrast to the monomeric amphiphiles, the polymeric surfactants can cause a change in equilibrium potential, facilitating the initial reduction of the dicationic viologen species in response to relief of the high charge density.

It is reported that the redox reaction of the viologen unit is reversible (in a chemical sense) [53, 54], which might not be the case for side-chain viologens attached to a conjugated backbone [55, 56]. In the case of the viologenic polysoaps, adsorption processes were observed especially for the reduced species, indicating a solubility change upon reduction [54]. This can be utilized for redox-sensitive solubilization and release of hydrophobic substances [54]. Low molecular weight viologens allowed a reversible supramolecular polymerization into redox-active suprapolymers, which – upon stimulus – decomposed again into their monomers [57, 58]. Hence, this is referred to as the principle of inclusion complexation (see section "Inclusion Complexation"), which adds another level of manipulation of polymer interactions on top of the mere solubility changes. Hence, the radical state of a viologen could be utilized for the reversible dimerization of, e.g., dendrimers, facilitated by the presence of cucurbit[8]uril (Fig. 5) [59].

Polyhydroquinone [60], which is soluble in organic media [61], was prepared with a defined architecture [62]. In this case, hydroquinone is part of the main chain [63] although side-chain polyhydroquinones also exist [64, 65]. Anthraquinone-based polymers, which can be connected in various ways, are known [66–71]. These are rather peculiar examples of redox-sensitive polymers because

Table 1 Typical organic, redox-active units used for electroactive polymers

Name	Structure
Viologens	
Hydroquinones	R and related structures
Tetrathiafulvalenes	
Tetracyano-quinodimethanes	
Carbazoles, triarylamines, etc.	
Amine oxides	
Polyaniline, polypyrrol, polythiophenes	Conjugated polymers

R indicates a proper location for binding to a polymer

Fig. 5 Dimerization of dendrimers triggered by reduction of viologen units (reprinted with permission from [59]. Copyright 2004 Wiley)
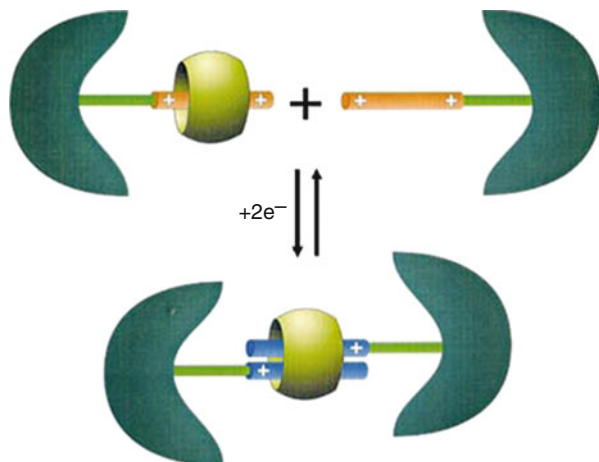
the electrochemical reaction does not necessarily change the polymer's net charge upon full oxidation/reduction (because the oxidized units release protons). However, the thin-film analogues of some polymers showed doping effects upon re-reduction and the necessary proton capture was assumed to be slower than salt insertion from the electrolyte [62]. Depending on the pH, this example is instructive in demonstrating that not necessarily every electrochemical reaction of a polymer needs to change the net charge of the macromolecule. At the same time, solubility changes are expected to be less affected by the change in the oxidation state, unless other effects play a role (e.g., hydrogen bonding). These quinone-related polymers have been described as possible energy storage materials [10, 71–75].

Rather exotically, nicotinamide has been introduced into polymers, but the solubility in aqueous solution was reduced considerably. Therefore, only the monomers were tested electrochemically, indicating the absence of chemical reversibility upon electrochemical switching [53, 76].

Tetrathiafulvalene (TTF) is known in supramolecular chemistry for its many charge-transfer complexes [77, 78]. TTF-containing polymers [79] or supramolecules have high impact as redox-sensitive molecules [80, 81] and their research has been a hot topic since the last century [82–89]. TTF can be attached to polymers via main-chain or side-chain connectivity [90–94]. A number of examples of the latter are known: TTF bound to fluorene polymer [95], polycarbazole [96], or even to polypyrrole/polythiophene derivatives [97–100]. In these examples, the interplay between the redox-active TTF group and the conjugated backbone is an issue [101, 102]. Main chain analogues have been studied [103] as well as TTF attached as an end group [104, 105]. Furthermore, polymeric derivatives of TTF such as dithiafulvenes are known [106–108].

Tetracyanoquinodimethane (TCNQ), which is famous for its supramolecular charge-transfer complexation, entered polymer science some time ago [109]. Here, main-chain polymers were introduced [110, 111], including TCNQ polymers decorated with dendrons [112].

Polymers with porphyrin units in the main chain and fullerene side groups are described as electroactive [113], as well as polymers with azo-groups in the main chain [114] and triarylamines in the side chain [115–118]. By proper functionalization and architecture, even poly(thiophene) [119] and oligoaniline [120–122] and derivatives [123] become soluble in different solvents. Also, electroactive polymers derived from 2,2,6,6-tetramethyl piperidinyloxyl (TEMPO) have drawn attention, especially with respect to energy storage applications [124–127].

Strongly Coordinating Metal Centers

As already implied by the last examples, redox-active groups were attached covalently to polymers, proteins and nanoparticles [128–131]. However, classical covalent linkages are not necessarily required in order to impart redox sensitivity to polymers [132]. Polymers with suitable ligands can bind redox-active metals by "inorganic" complexation [133]. This coordination concept is even used in a supramolecular sense [134, 135]. If this complexation is strong enough, then a real, classical covalent bond is mimicked by the coordination forces. Metallocene-based polymers comprise just one example in addition to ruthenium complexes, porphyrin-ligands and so on. This is in line with the fact that the equilibrium constant is far on the side of the complex, leaving the chemical structure almost unaffected by oxidation or reduction.

Metallocenes

Metallocene-containing polymers are often related to prominent ferrocene and cobaltocene [136–139]. Work in this area has been reviewed recently [140–142]. Therefore, the following serves as an overview.

The ferrocene moiety can be electrochemically oxidized and reduced reversibly, unless special polymers are considered that show an irreversible oxidation [143]. Hence, polyferrocenylsilane and its derivatives have attracted considerable interest [144]. Here, the ferrocene units are assembled along the main chain and are in close proximity, often leading to two reversible redox peaks because of the charge–charge repulsion along the backbone [145, 146]. This coupling decreases with an increasing number of spacer units between the ferrocenes [147]. The conformational changes upon oxidation have been used for studies on a redox-driven macromolecular motor [148, 149]. Not only are the electrochemical properties appealing, but also the controlled formation of micelles is a flourishing topic of research (crystallization-driven "living micellization") [150–152]. Other ferrocene-containing polymers are available, such as poly(vinylferrocene). Here, the electroactive groups are pendant along the backbone (as side chains). Prominently [153, 154], the theory of noninteracting redox centers was developed with the help of studies on poly(vinylferrocene) in organic media (in contrast to the interacting electron transfers for some polyferrocenylsilanes) [155]. Accordingly, other polymers did not show any interaction between the redox sites, such that the
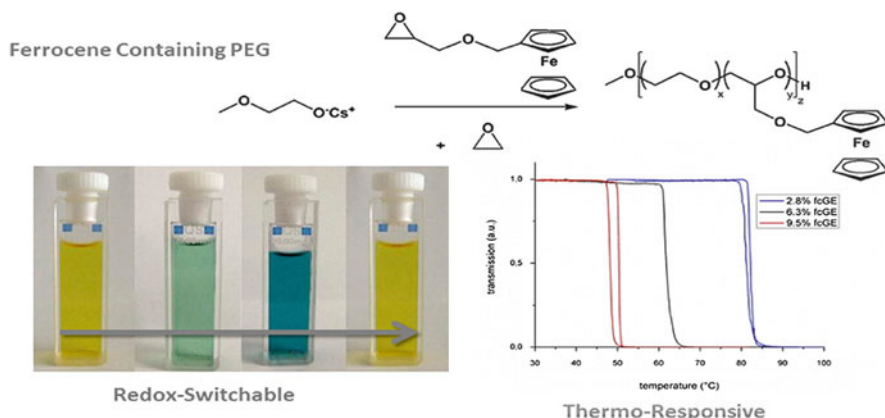
Fig. 6 Thermosensitive polymers with redox-switchable LCST properties; *fcGE* ferrocenyl glycidyl ether (reprinted with permission from [159]. Copyright 2013 American Chemical Society)

electrochemical behavior deviated from a one electron transfer reaction [156]. Under certain circumstances, the molecular weight of these polymers can be estimated electrochemically [154].

Regarding electroswitching, the most research on ferrocene-containing polymers was conducted on nonaqueous systems. The limited stability of the oxidized polymeric ferrocene units in aqueous surroundings, especially in the presence of oxygen, might play a role here [157, 158]. Thus, main chain ferrocene units (as for polyferrocenylsilanes) are somewhat disadvantageous because polymer degradation and chain scission might occur in its oxidized state in the presence of water. In contrast, side-chain ferrocene-containing polymers such as poly(vinylferrocene) are less affected because the polymer backbone stays intact even in the presence of some (minor amounts of) decomposed ferrocenium side groups [142]. Hence, there are a number of examples that suggest that ferrocenium is sufficiently stable in protic solvents (see below); e.g., polyethers with pendent ferrocene groups show an oxidation-dependent lower critical solution temperature (LCST) behavior in water (Fig. 6) [159].

For longer polymers, adsorption and film formation can take place in organic solvents, which are good solvents for the neutral ferrocene-based species but bad solvents for the oxidized species [153, 154, 160–165]. In this case, even diblock copolymers precipitate on the electrode, without indication of the formation of micellar structures upon electrochemical switching [166–168]. Co-precipitation with carbon nanotubes onto electrodes has been achieved [169]. As a matter of fact, common solvents for both redox states are seldom available, unless the hydrophobic ferrocene units are complexed by cyclodextrins (in this case, water is a good solvent) [170, 171]. As another example, dendritic ferrocene-based polymers are sufficiently solubilized, even after oxidation in organic media (probably, the insoluble units are shielded in the interior of the dendrimers) [172]. Star-like
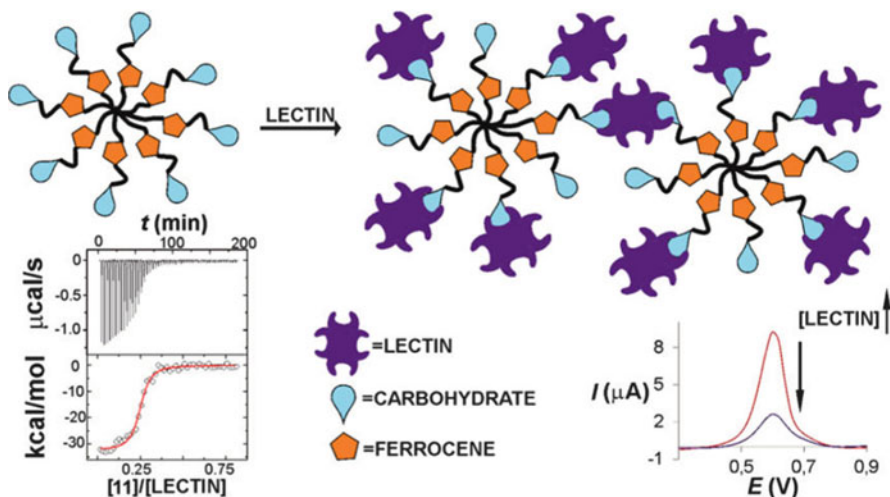
Fig. 7 Electrochemical switching of ferrocene units within a dendrimeric, sugar-based receptor molecule is impeded by conjugation with lectins (reprinted with permission from [174]. Copyright 2013 American Chemical Society)

polymers with block arms act similarly [173]. Apparently, the organic spacers assure solubility in organic media in both oxidation states, which allows the determination of the hydrodynamic radii by electrochemical means. Similarly, sugar-decoration provides solubility in aqueous media. These ferrocene-based dendrimers were used for detection of lectin binding (see Fig. 7) [174].

To mention a last example showing a common solvent, spherical brushes consisting of side-chain ferrocene-containing grafts [e.g., poly(ferrocenyl methacrylate) or poly(vinylferrocene)] displayed a pronounced increase in hydrodynamic radius upon chemical oxidation in nonpolar solvents, which was attributed to the electrostatic repulsion between the ferrocenium units (Fig. 8) [161, 175]. In addition, parts of the increase in hydrodynamic radius might be caused by the uptake of the bulky hexachloroantimonate counterions.

In certain cases, ferrocene-labeled polyelectrolytes show chemical irreversibility during electrochemical switching, unless redox mediators allow the efficient reduction of the hidden redox active site [176, 177]. This can be attributed to the strong interaction of the oxidized ferrocenium site with the anionic polyelectrolyte. At the same time, this polyelectrolyte shielding prevents ferrocenium reduction at the electrode interface. Consequently, this effect is not expected for neutral backbones such as polystyrene. Hence, chemical reversibility was detected for singly ferrocene-labeled polystyrene prepared by reversible addition fragmentation chain transfer (RAFT) polymerization [178]. Interestingly, a single cobaltocene label entails chemical irreversibility of the electrode reaction in DMF, when being attached to poly(styrene) or poly(methacrylates) prepared by atom transfer radical polymerization (ATRP; see Fig. 9) [179]. It could be reasoned that copper traces left after ATRP might cause such a behavior because there is indication of chemical reversibility for fully functionalized side-chain cobaltocene-containing polymers
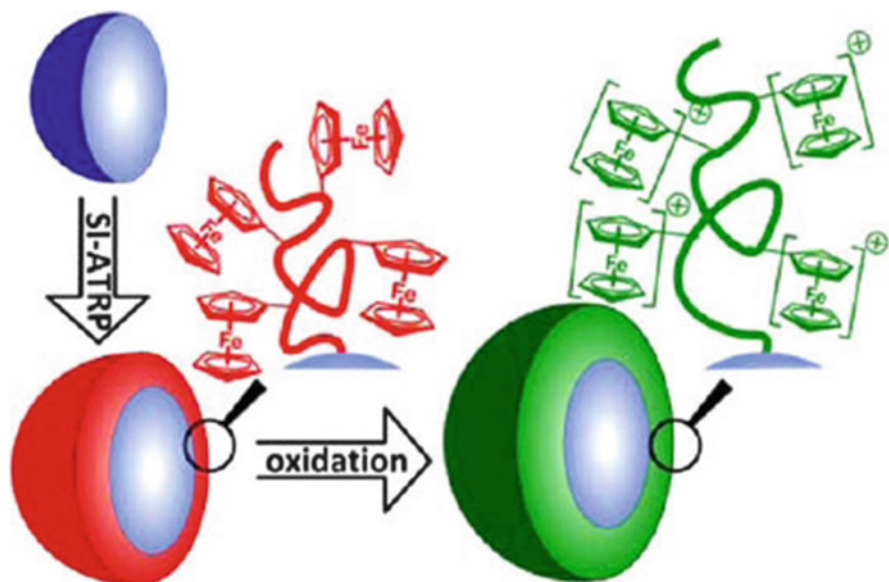
Fig. 8 Poly(vinylferrocene) brushes extend upon oxidation in hexachloroantimonate solutions of methylene chloride or tetrahydrofuran; *SI-ATRP* surface initiated atom transfer radical polymerization (reprinted with permission from [161]. Copyright 2012 American Chemical Society)

prepared by free radical polymerization, e.g., poly(acryloyloxyethyl cobaltocenniumcarboxylate hexafluorophosphate). These appear soluble in DMF both in the oxidized and reduced state [180]. Also, the oxidized form is water soluble, whereas the reduced form precipitates at the electrode. Even heterobimetallic block-like copolymers of ferrocene and cobaltocene have been prepared (Fig. 10) [181, 182], some of them exhibiting sensitivity towards decomposition of the ferrocene-containing block upon performing cyclovoltammetry in DMF [182]. The CV data on main-chain cobaltocene-based polymers, e.g., poly(cobaltocenophanes), again suggest solubility in water in one of the two redox states [183].

Advanced metallocene-based structures[162], including amphiphilic graft polymers, have been prepared by controlled radical polymerizations [184, 185]. In this respect, an interesting application is given for ferrocene-based block copolymers, which can undergo conjugation with amines in terms of an oxime function (Fig. 11) [186]. At the same time, this combination allows the determination of conjugation by electrochemical means because the half-wave potential shifts with increasing conjugation.

An acrylamide-based polymer was grafted from a poly(ferrocenylsilane) backbone, giving not only electroactive, but also thermosensitive bottle-brush polymers [187].

Arene complexes of hemimetallocenes are also known [165, 188, 189]. Ferrocene-based inclusion complexation have been described as a tool for
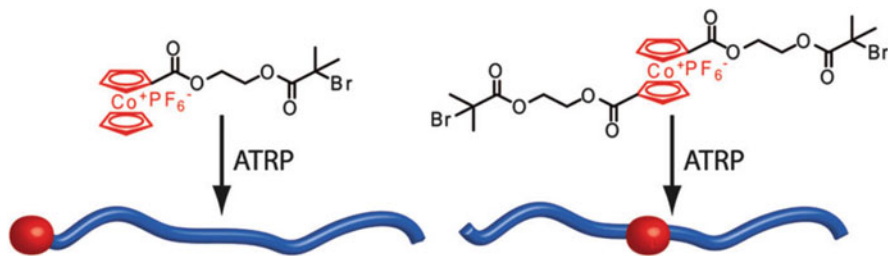
Fig. 9 Cobaltocenium-containing polymers obtained by atom transfer radical polymerization (*ATRP*) (reprinted with permission from [179]. Copyright 2012 American Chemical Society)
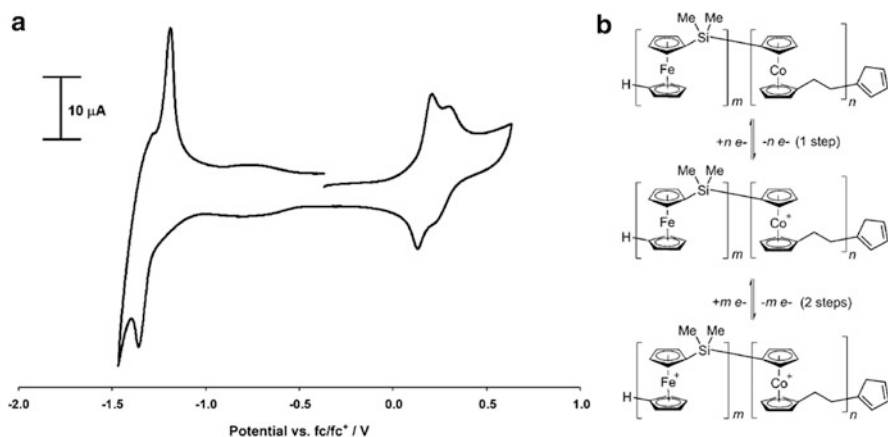
Fig. 10 Cyclic voltammogram of poly(ferrocenylsilane)-*b*-poly(cobalteceniumethylene) (**a**) and the corresponding structures of the diblock copolymer (**b**) (reprinted with permission from [181]. Copyright 2011 Wiley)
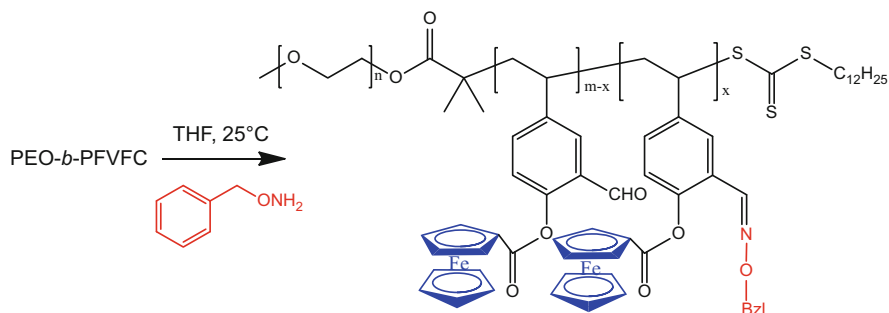
Fig. 11 Copolymer with ferrocene-based block (out of 2-formyl-4-vinylphenyl ferrocenecarboxylate, *FVFC*), which forms the core of the micelles but also allows conjugation with substrate, yielding conjugation sensors [186]

manipulation of the polymer interactions, which will be briefly described later (see section "Inclusion Complexation").

Further Metal–Ligand Complexes

Stable metal complexes can be achieved by use of chelating ligands such as phenanthroline, pyridine, bipyridine or terpyridine moieties. These concepts are especially appealing in supramolecular chemistry, generating advanced polymer structures by noncovalent binding [190–193]. Because mainly transition metal complexes are used, the resulting macromolecular structures are very often redox-sensitive. Therefore, there are many examples of such electrochemically active, metal-based polymers in the literature, although only a short overview can be given here. One difference between these metal-based polymers and metallocene-based polymers is the ease of metal exchange: the ligand-containing polymer can be prepared without metal, and the redox-sensitivity is invoked after addition of the metal [e.g., Fe(II), Zn(II) and Ru(II)] and its rather strong complexation to the chelating units. In principle, different cations can be used for complexation. This freedom, which is similar to the electrostatic complexation between different multivalent counterions and polyelectrolytes (see section "Electrostatic Attraction"), is barely possible for ferrocene-based polymers. Moreover, electrolysis of sacrificial metal electrodes in the presence of the chelating polymer is sufficient to produce the desired electroactive polymers [194].

In particular, ruthenium complexes have been utilized for the redox stimulation of polymers. Interestingly, the internal changing of the electrochemical potential by the self-oscillating Belousov–Zhabotinsky reaction led to a response of such electroactive systems (e.g., peristaltic motions of ruthenium-containing gels and oscillating micellization events) [195]. However, these examples are not electrochemically controlled by electrode processes [196], although the Ru(II)/Ru(III) couple is very active electrochemically. Therefore, polymers with complexing ligands (and complexes) in the side chain have been prepared [197–199]. The backbone can even be conjugated [107, 200–202]. In certain cases, the conjugated backbone can be produced photochemically, allowing the introduction of other redox-sensitive groups (e.g., viologen), which finally endow the soluble photopolymerized polymer with electrochemically induced solubility features [203].

Even advanced structures with a hemimetallocene or dicarbonylhydrazine structure have been formed [204, 205]. End-group modification is also known (e.g., see Fig. 12) [116, 206, 207]. For cobalt complexes, dendrimers with polypyridyl end groups were prepared, whose solubility can be manipulated directly by electrochemical means [208].

The proper choice of stoichiometry allowed the formation of block-like arrangements or even star-shaped polymers with electroactive metal centers [209]. An interesting example is given for metallo-supramolecular polymers, which can even reversibly form gels [210–214]. Thus, supramolecular polymers can be made by use of bifunctional linkers. Here, the redox active units are located in the main chain

Fig. 12 Polymeric, redox-active triarylamines (*pTARA*) with a redox-sensitive ruthenium end group prepared by nitroxide-mediated polymerization (reprinted with permission from [116]. Copyright 2013 American Chemical Society)
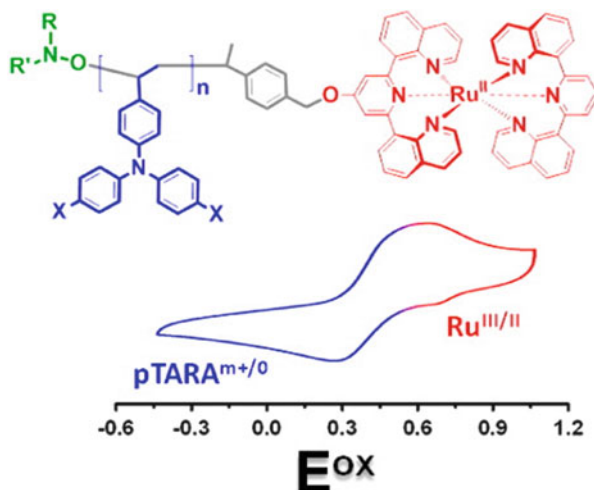
(Fig. 13) [215, 216]. This concept can be used even for dendritic species [217, 218], while the ruthenium complex can be part of the crosslinking units [219].

Porphyrin-based complexes pass their redox sensitivity on to the corresponding polymers. Advanced conjugated main-chain structures with attached dendrons have been introduced [220]. Grafting of porphyrin-zinc main-chain polymers onto carbon nanotubes was reported [221]. An interesting example dealing with a nonelectrochemically switched polymer was recently given. Here, polymers with porphyrin-iron end groups could be switched between linear and cyclic polymers by a dimerization procedure (Fig. 14) [222, 223].

Some special examples are also present in the literature [224, 225]. Helical polymers were obtained by interaction of redox-active copper centers with a rather rigid and bent polyphenanthroline [225]. Polymer decoration with cyanoferrates has also been achieved [226, 227], which leads us directly to next section.

2.1.2 Electrochemically Induced Complexation

Electrostatic Attraction

Transfer of electrons can naturally lead to changes in the charge (valency) of the redox-active species. Therefore, it is an obvious consequence to study the interaction of switchable counterions with "macroions" [228] or other multiple-charged objects like polyelectrolytes [229]. The group of Anson was one of the first to investigate the complexation of electrochemically switchable counterions with strong polyelectrolytes [230–232]. In some cases, the cationic polysiloxanes became insoluble through oxidation of complexed ferrocyanide. The polyelectrolyte–counterion complex then deposited onto the electrode as a thin
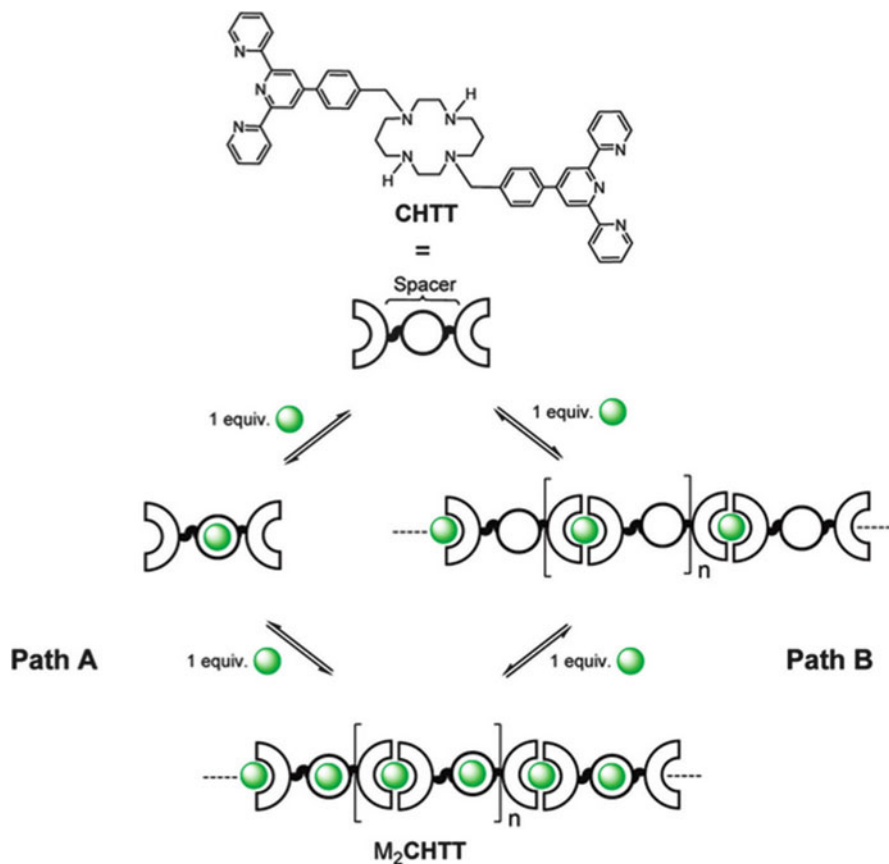
Fig. 13 Supramolecular, redox-active polymers formed by coordination bonding, yielding redox-active gels (utilizing multitopic cyclam bis-terpyridine ligands, *CHTT*) (reprinted with permission from [210]. Copyright 2009 American Chemical Society)

film, which could be redissolved after changing the potential for counterion reduction (Fig. 15).

Poly(diallyldimethylammonium chloride) (PDADMAC) and ferri-/ferrocyanide show a similar behavior [233]. In most cases, the ferri-/ferrocyanide (trivalent/tetravalent hexacyanoferrate[III]/[II]) couple exhibits an unexpected interaction pattern with strong cationic polyelectrolytes. Hereby, the trivalent ferricyanide favors complexation compared with the tetravalent ferrocyanide [234, 235]. Although the higher charged ferrocyanide is supposed to release a higher number of monovalent counterions, this entropic contribution is less dominant for the ferrocyanide. This conclusion was derived from entropy measurements [232], clearly emphasizing the enthalpic repulsion between the highly hydrated, weakly polarizable ferrocyanide and the somewhat hydrophobic polymeric backbone [236]. This leads to pronounced ion-specific effects. In contrast, some systems
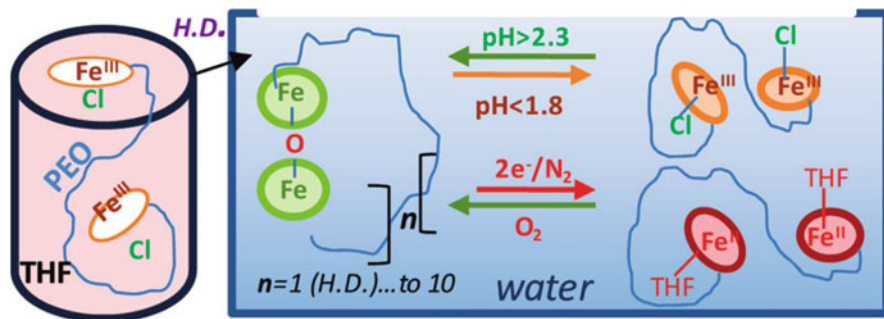
Fig. 14 Redox switching between cyclic polymers and linear polymers; *PEO* poly(ethylene oxide), *THF* tetrahydrofuran, *H.D.* high dilution (reprinted with permission from [223]. Copyright 2011 American Chemical Society)
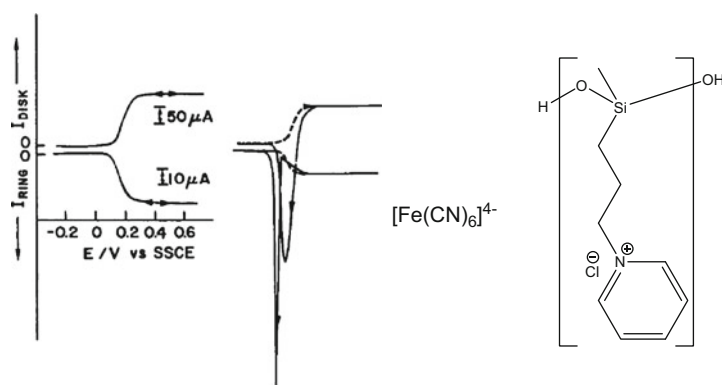
Fig. 15 Direct observation of reversible film formation on a rotating ring/disk electrode upon oxidation of hexacyanoferrate (IV) (initial disk potential scan from low to high potentials, from *left to right*), showing ferrocyanide oxidation in the absence (*left*) and presence (*right*) of cationic polyelectrolyte. Upon reversing the disk potential, a clear cathodic peak is discerned in the case of the polymer-containing system (*right*) due to dissolution of ferricyanide-containing film. Further film-escaping ferricyanides react at the ring electrode with constant potential, which results in a cathodic peak of the ring current (reprinted from Journal of Electroanalytical Chemistry, 258(2), Manshi Ohyanagi, Fred C. Anson, Electrodeposition of polyelectrolyte-metal complexes, 469–477, Copyright 1989, with permission from Elsevier [231])

containing nonquaternized, primary polyamines favor interaction with the tetravalent ferrocyanide [232, 237–239], as indicated by the swelling of thin films in the presence of ferricyanide. The increased hydrophilicity of these protonated polyamines might be explained by the lower number of carbon atoms per charge and by possible hydrogen bonding with the counterions.

Similar processes play a role for the interaction of multivalent counterions with anionic polyelectrolytes [240, 241]. Hereby, ferrous Fe^{2+} is oxidized in the presence of poly(acrylic acid). Importantly, the chelating abilities of citric acid allow a tuning of the ion–polymer interactions, allowing a higher mobility of the
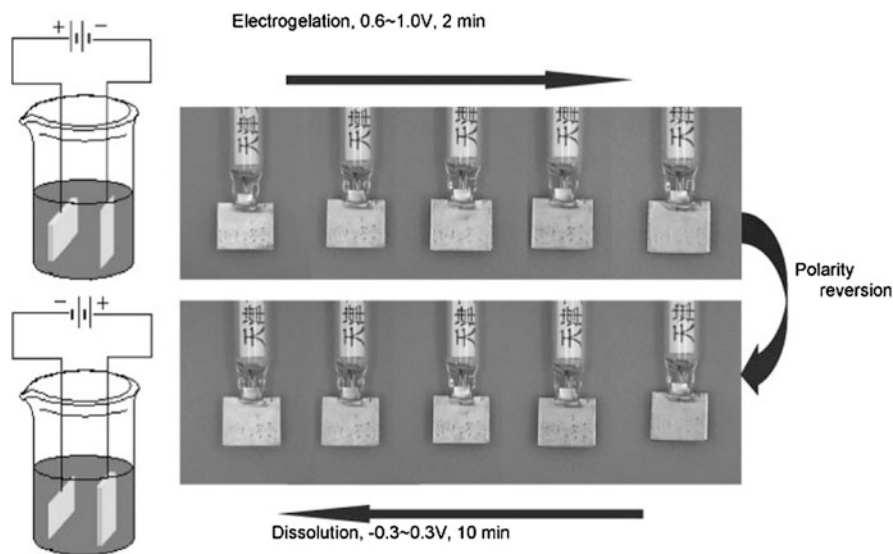
Fig. 16 Reversible electrochemical gelation of poly(acrylic acid) onto electrodes in the presence of ferrous ions (reprinted with permission from [241]. Copyright 2010 Wiley)

electroactive counterions. As a result, a hydrogel layer is formed on top of the electrode upon oxidation, but it is dissolved again upon reduction (Fig. 16). For another thallium-based system, the mobility of counterions was determined electrochemically and compared with self-diffusion NMR experiments [242]. Both methods provide consistent results.

As shown above, it has been known for some time that the solubility of polyelectrolytes in aqueous media can be influenced by the electrochemical switching of the counterions. However, this principle has only recently been applied to trigger electrochemically built-up micellar aggregates from unimolecular solutions by adjusting the solubility of one part of a binary block-like copolymer [235]. Hereby, the electrolysis of ferrocyanide to ferricyanide led to the formation of vesicles (polymersomes). In contrast to real film formation, the solubilizing part, poly (ethylene oxide) (PEO), prevented film deposition on the electrode. Instead, bilayer film formation in bulk solution was favored under vesicle build-up with an insoluble polyelectrolyte complex as the vesicle wall, sandwiched between a well-hydrated PEO brush.

Multivalent counterions have also been used as redox mediators for oxidation/reduction of redox-active sites that are covalently bound to the polyelectrolyte [177]. In this case, the oxidized redox-active sites are shielded by their interaction with the polyanion. This prevents reduction of the redox polymer, unless a mobile cationic mediator, $[Ru(NH_3)_6]^{2+}$, which interacts with the polyelectrolyte, is added. In this example, no real solubility changes were observed.

In a further study, the interaction between protonated poly(4-vinyl pyridine) and anionic $[Mo(CN)_8]^{4-}$/cationic osmium species was investigated [176]. The diffusion properties of both $[Mo(CN)_8]^{4-}$ and the polymer could be separated

Fig. 17 Coupling of the conformation of a weak polyelectrolyte brush with the pH modulated by electrolysis of water (reprinted with permission from [246]. Copyright 2013 American Chemical Society)
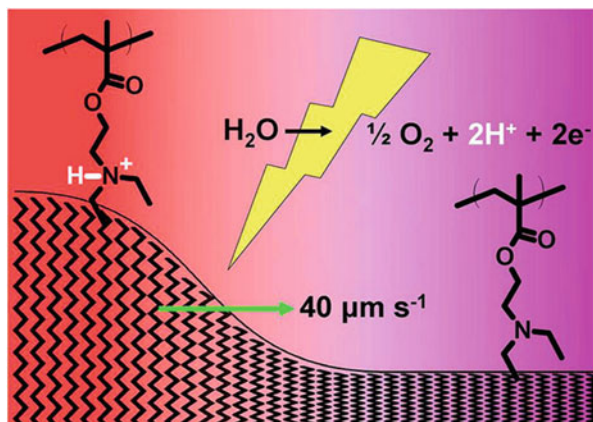
electrochemically (rotating ring electrode) by labeling the polyelectrolyte with ferrocene units. Adsorption of the complex on the electrode was found, although no electrochemical effect on the film formation was reported.

Electrochemically Induced Protonation and Deprotonation

The "(de-)complexation" of polymers/polyelectrolytes with protons can be regarded as a tool for electrochemical manipulation. Under certain conditions, electrode reactions can lead to a net generation of hydronium or hydroxide ions under electrolysis of water [243]. These ions can interact with pH-responsive entities, leading to changes in solubility and conformation (e.g. Fig. 17) [244–247].

Inclusion Complexation

Inclusion complexation is often based on hydrophobic interactions, leading to an uptake of a hydrophobic guest into a hydrophobic cavity (e.g., for cyclodextrins or calixarenes). Ionic interactions can also induce a threading of a guest into the cavity of a host. By switching the charge and hydrophilicity of either guest or host, the host–guest interaction can be manipulated electrochemically. At the same time, the solubility might be altered comparing with the original state of the polymer. Referring to Fig. 4, such a behavior can be achieved by incorporating complexation sites on the polymer, while the low molecular mass redox-active compounds bind to the polymer upon exerting a redox stimulus. Electrochemically induced complexation does not necessarily need to take place between polymeric species and low molecular mass, redox-active species. Regarding inclusion complexation, the switchable attraction between complexing entities can be employed while the redox-active groups are attached to the polymer (mixed concept; refer to Fig. 4). In addition, binary polymer–polymer interactions can be triggered. Then, inclusion

complexation can play a crucial role in changing the supramolecular conformation and solubility upon exerting redox stimuli [57, 58, 248–251]. For example, an advanced way of changing the bulk solubility of proteins by complexation has been described recently [248]. A combination of supramolecular chemistry (inclusion complexation) and covalent attachment of redox active groups leads to a complexation between cyclodextrins and ferrocene units, which is not based on electrostatic attraction, but on hydrophobic interactions. Therefore, precise attachment of ferrocene at a certain spot of the protein allowed the oriented adsorption at cyclodextrin-modified electrodes. Upon electrochemical oxidation, the complex between cyclodextrin and the ferrocene moiety is weakened and the protein is released into solution. Accordingly, protein release was also established by reduction of tethered flavin [252, 253]. Similar principles hold also true for ferrocene-labeled dendrimers [249, 250]. Here, scanning electrochemical microscopy allowed the imaging of and writing into cyclodextrin-modified patterned glass surfaces [250].

This principle is also well known for gel formation, which will be discussed in Sect. 2.3 [254]. Here, either the polymer-bound ferrocene units interact with cyclodextrin (mixed concept) [170, 171, 255] or a cyclodextrin-based polymer allows the inclusion of ferrocene, which then also endows electrochemical properties (electrochemically induced complexation; Fig. 18) [256, 257].

Taking this one step further, competitive inclusion complexation of cyclodextrin with either polymer-bound, associating alkyl side chains or ferrocene is dependent on the different oxidation states of ferrocene. This leads to a switching between the gel state and molecularly dissolved polymer [254]. This very special case can be categorized as electrochemically induced complexation, although, interestingly, the polymer has no direct interaction with the redox active sites (Fig. 19).

By use of bifunctional monomers based on cyclodextrins and ferrocenes, a switchable supramolecular polymerization is feasible [258, 259]. However, inclusion complexation is not only limited to cyclodextrins or ferrocene. Anionic calixarenes can also interact with cationic, redox-active viologens [57]. The reduced, uncharged viologen is repelled from the calixarene site. In the case of bifunctional calixarenes and viologens (two viologen or calixarene sites per molecule), a supramolecular polymerization takes place in water, which can be reversed upon reduction of the viologen units (Fig. 20). Even orthogonal stimuli can be applied, meaning that the supramolecular polymer is only present at low pH and high equilibrium potential [58]. After electrolysis, monomeric dicalixarenes and viologen-based molecules are present at low potential. A similar approach was applied for the generation/decomposition of block copolymers from telechelic homopolymers [105].

Charge-Transfer Complexation

Charge-transfer complexation is another example in line with the inclusion complexation concept. Although the redox-active groups are attached to the polymer, their interaction with other units of beneficial electronic structure can be regarded
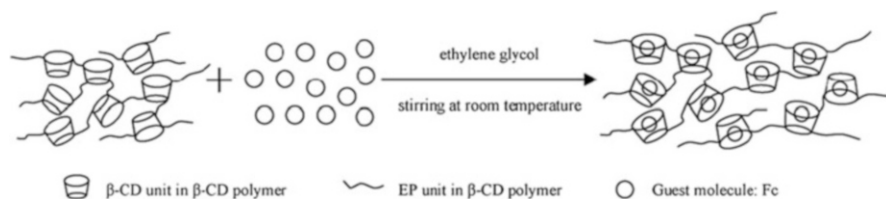
Fig. 18 Inclusion complexes of ferrocene into β-cyclodextrin (*β-CD*)-based polymers, leading to an electrochemically induced (de-)complexation (reprinted from Zhang et al. [256])
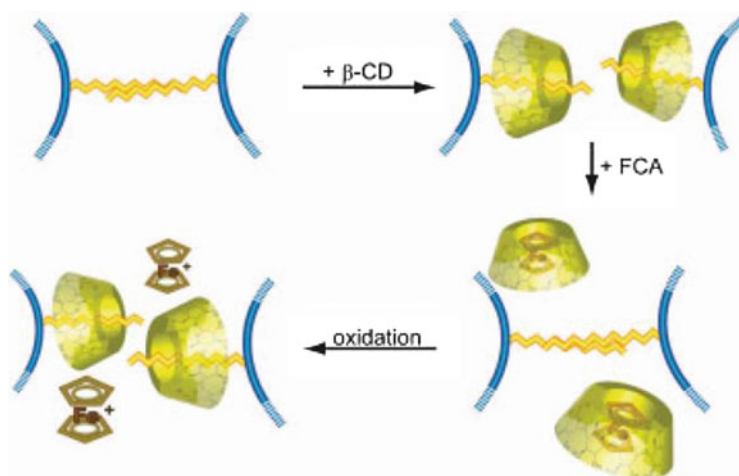

Fig. 19 Peculiar behavior of a ferrocene and β-cyclodextrin (*β-CD*)-containing system, allowing gel–sol transitions without any direct interaction of the ferrocene species with the polymer; *FCA* ferrocenecarboxylic acid (reprinted with permission from [254]. Copyright 2006 Wiley)
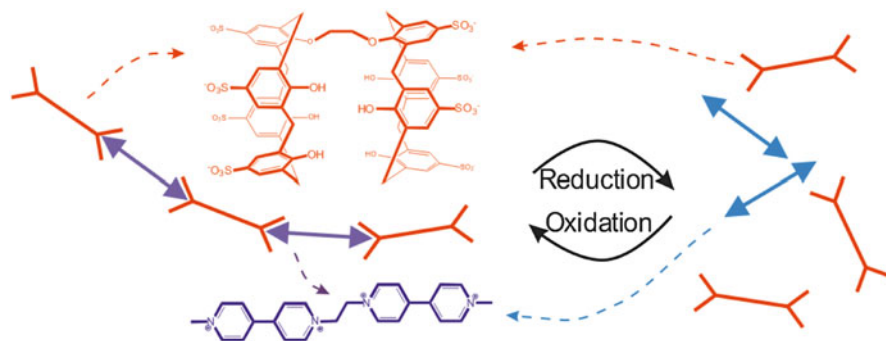

Fig. 20 Supramolecular redox-active (de-)polymerization (with kind permission from Springer Science + Business Media: Colloid and Polymer Science, Plamper [18], figure 1) [57]
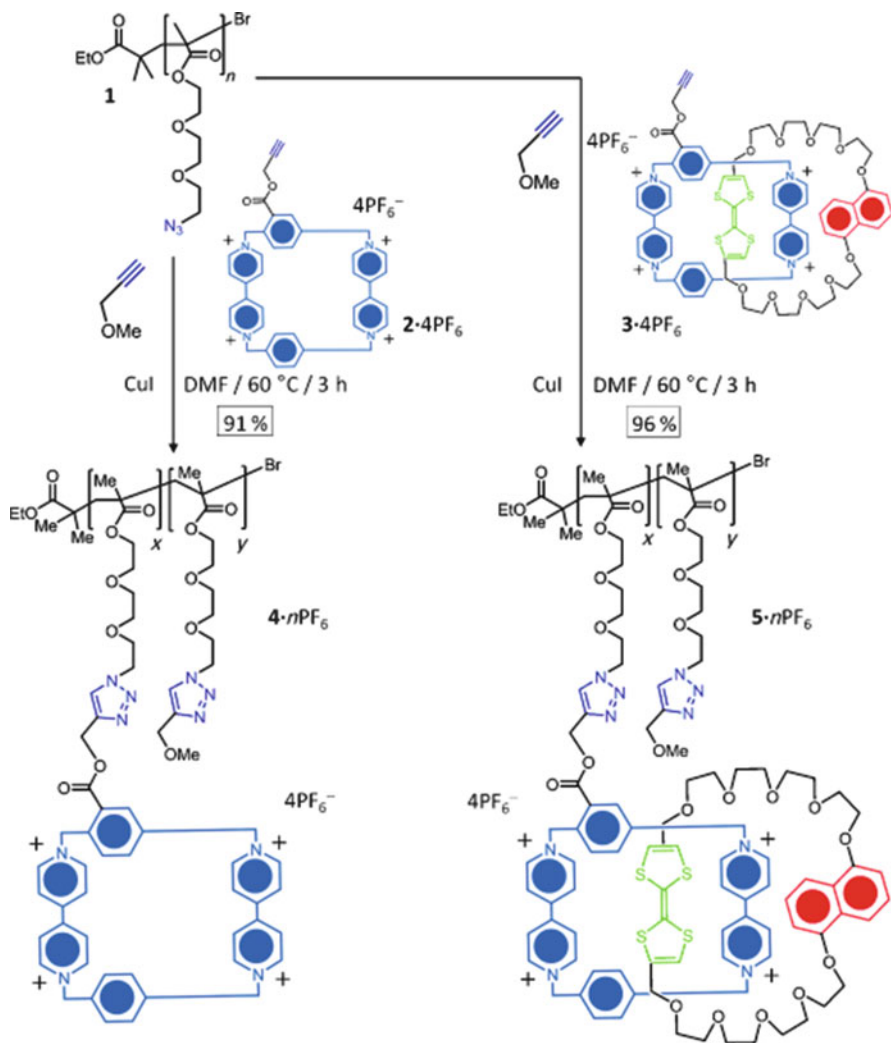
Fig. 21 Preparation of a switchable polycatenane, where – depending on the oxidation state – either the tetrathiafulvalene or the naphthyl moiety is hosted within the viologen-based ring (reprinted with permission from [251]. Copyright 2009 Wiley)

as a complexation. Tetrathiafulvalene (TTF) is an appealing unit because it has the ability to form charge-transfer complexes with electron acceptors such as tetracyanoquinodimethane (TCNQ) or even viologen derivatives [260, 261]. These complexes show a remarkable conductivity (supramolecular organic metals). In addition, TTF and viologen also give charge-transfer complexes [108]. As an intriguing example, electrochemical manipulation of supramolecular catenanic polymers can be obtained [251]. In DMF, a net rotation of the hooked, electroactive

TTF-based rings can be achieved, which are attached to a polymeric backbone by threading them onto side-group cyclobis (paraquat-*p*-phenylene)-based rings. Upon oxidation of TTF, the charge-transfer complex between the paraquat units (viologens) and TTF is replaced by like-charge repulsion, which leads to a rotation of the hooked rings (Fig. 21).

Similarly, intramolecular charge-transfer complexation was obtained by alternating copolymerization of tetracyanoquinodimethane (TCNQ) with ferrocene into one chain [91, 111]. Spectroscopic and electrochemical analyses of mixtures of the monomeric units showed clear intramolecular charge-transfer complexation. In a related study, poly(methylated ferrocenylsilanes) were shown to interact with tetracyanoethylene [262]. A similar concept is valid for viologen-based polymers [55].

Generally, it cannot be excluded that charge-transfer complexation gives an additional driving force for complexation in the examples listed above or below (e.g., [57] or [230]). For example, in addition to electrostatic effects, charge-transfer complexation was accounted for when discussing the special interactions of hexacyanoferrates with aromatic polyelectrolytes [230].

2.2 (Self-)assembled Structures in Suspension

The former section aimed to give an overview of the different chemistries of electrochemical switching of polymers. This section emphasizes the utilization of these principles for the switching of self-assembled structures such as micelles, capsules or vesicles. Astonishingly, although numerous reports on redox-sensitive polymers are known, hardly any efforts have been taken until recently to address the morphological changes of electroactive micellar aggregates. Only in the last ~5 years has there been an increased interest in the electrochemical micellization of polymers. Permeability changes of capsules or vesicles have been investigated sparsely [263–265], although they have been known for some time. In any case, most investigations were not conducted electrochemically. This means that further studies are needed on electrochemical switching of, e.g., micellar shapes, and numerous applications are expected. Rheological control [266, 267] and uptake and release applications are just two examples, which can be performed – in principle – by use of a simple electrical switch. As already mentioned in the "Introduction", this switching has the advantage that no chemicals need to be added.

2.2.1 Chemical Redox for Self-assembled Systems

Some recent examples dealing with chemical redox reactions will be addressed.

An organo-soluble polyferrocenylsilane within a bis-lipophilic diblock copolymer turns partly organo-insoluble upon chemical redox switching in organic solvent [268]. Then, the unimeric polymer aggregates into spherical micelles (Fig. 22).
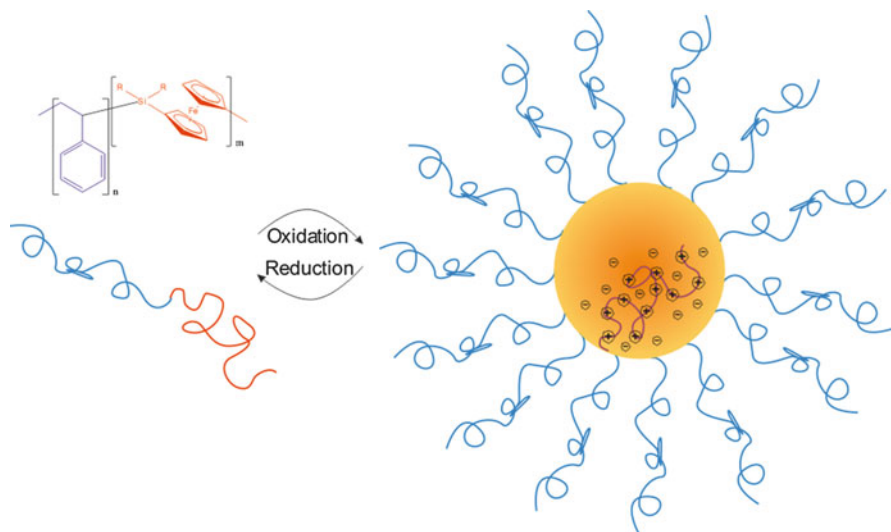
Fig. 22 Redox-induced micellization in organic media [268]

Similarly, amorphous polyferrocenylsilanes, e.g., poly(ferrocenylphenyl-methylsilane), gave spherical micelles whereas semicrystaline poly(ferrocenyldi-methylsilane) self-assembled into ribbon-like micelles upon chemical oxidation of the organometallic block [269]. A comb-like, amphiphilic copolymer of an amino-containing poly(ferrocenylsilane) backbone and alkyl side groups aggregates in solution. The use of chemical redox agents allowed control of guest release from these micellar-type aggregates [270]. By use of poly(vinylferrocene), an aqueous system related to that shown in Fig. 22 could be generated, which even exhibited thermosensitive properties [271].

Supramolecular polymers which iron-complexes along the anionic main chain were complexed with cationic block copolymers (Fig. 23) [272, 273]. However, the applied redox reaction hardly changed the micellar morphologies, although the payload could be released and entrapped upon a chemical redox stimulus. Similarly, nanoparticles were developed for the redox-triggered release of drugs (here by redox-induced scission of polymer-attached trimethyl-locked benzoquinone) [274].

Another interesting application was given for diselenide-based block copolymers, where both oxidants as well as reductants forced the systems to a demicellization [275]. This system was further developed to allow the disassembly of the micelles by application of oxidants, whereas micellization was favored in the presence of reductants [276]. In continuation, selenium-based peptides and dendrimers self-assembled into different morphologies, depending on the oxidation state [277, 278]. Also, small selenium-based amphiphiles form complexes with polyelectrolytes, but the amphiphilic character of the amphiphile and – in turn – the complex decreases after oxidation [279]. In general, the literature contains a
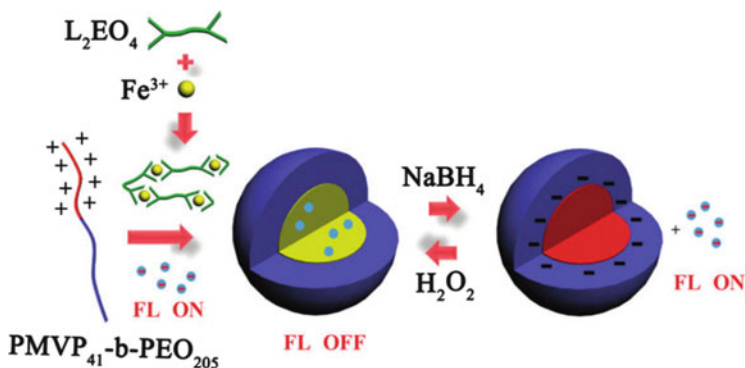
Fig. 23 Supramolecular, redox-active polyelectrolytes can be used for interpolyelectrolyte complexation with bis-hydrophilic block copolymers, yielding micelles with redox-sensitive release properties; *FL* fluorescence (reprinted with permission from [273]. Copyright 2012 American Chemical Society)

number of examples where decomposition of disulfide bridges changes the macro-molecular architecture and also the hydrophilic/hydrophobic balance (e.g. [280]). With biological and medical relevance, chemical redox on thiols or disulfide groups can change the morphology and uptake properties of micelles, vesicles, and dendrimers [281–286]. For instance, glutathione allowed the release of disulfide shell-crosslinked micelles [287]. Similar principles hold true for core-crosslinked micelles/nanoparticles/stars [288, 289]. But, as already mentioned, this chemistry is seldom applicable for electrochemical switching. This is also true for the full oxidation of thioethers to sulfoxides and sulfones, which could be used for destruction of vesicles by increasing the overall hydrophilicity of related block copolymers [33, 290].

The use of tetraaniline-based block copolymers allowed a change in micellar morphology upon chemical redox (Fig. 24) [291].

These examples deal mainly with covalently linked redox-active groups, but complexation between small redox-active counterions and polyelectrolytes has also been tested [292]. Here, peroxodisulfate acted as a bridging counterion, whose bridging abilities were stronger than those of sulfate ions (which were obtained upon addition of mild reductants).

2.2.2 Electrochemical Manipulation of Self-assembled Systems

After these examples related to chemical redox, we will now discuss electrochemically induced changes in micellar morphologies:

One of the first electrochemical examples of manipulation of the solubilizing abilities of amphiphilic polymers was investigated for viologen-based polysoaps [54]. Interestingly, hydrophobic dye molecules could be reversibly incorporated and released in (probably) unimolecular micelles of the redox-active polysoap
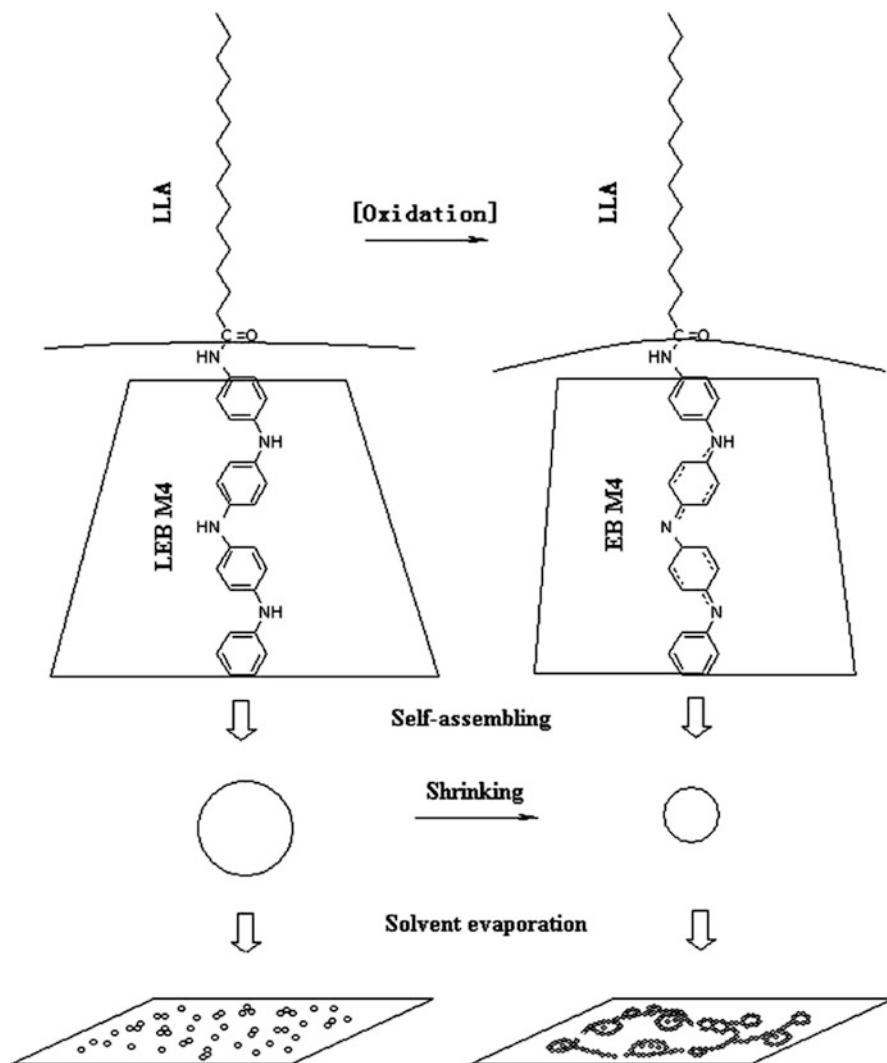
Fig. 24 Change in curvature upon oxidation of tetraaniline-*b*-poly(L-lactate) and the changes in the resulting self-assembled structures; *LLA* L-lactic acid (reprinted with permission from [291]. Copyright 2006 Wiley)

(here, only the chemical redox trigger was tested). However, morphological changes were not reported.

Redox-active vesicles were investigated for polysiloxane-based block copolymers with hydrophilic polyferrocenylsilanes as corona constituents. However, no change in morphology of the micellar aggregates upon oxidation was reported, although the number of cationic charges in the corona block increased considerably upon electrochemical switching [293].
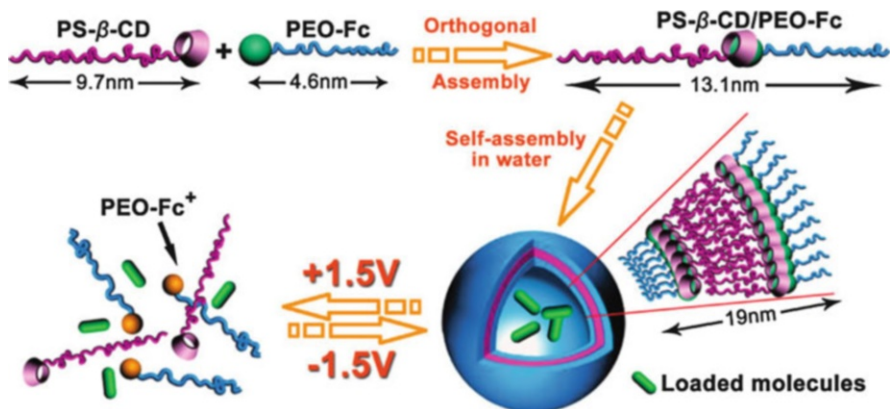
Fig. 25 Electrochemically induced decomposition of supramolecular vesicles; *PS-β-CD* cyclodextrin-terminated polystyrene, *PEO-Fc* ferrocene-terminated poly(ethylene oxide) (reprinted with permission from [295]. Copyright 2010 American Chemical Society)

An electrochemically induced change of spherical micelles to larger aggregates was observed for coumarin-containing block copolymers [294]. Electrochemical addressability was also found for ferrocene-based micelles of block copolymers, which can undergo conjugation with hydroxylamines in terms of an oxime function [186]. After conjugation micelles are formed, whose size can be manipulated by the oxidation state of the ferrocene units (here only reported by chemical redox).

A real electrochemical switching towards vesicles was obtained by a supramolecular, switchable linkage of ferrocene-terminated poly(ethylene oxide) (PEO) and cyclodextrin-terminated polystyrene (PS) in water (mixed concept) [295]. Upon oxidation, the ferrocene–cyclodextrin linkage is broken and the PEO dissolved unimolecularly, while reduction of the ferrocenium ions leads to reversible vesicle formation (Fig. 25). Interestingly, this system appears to have hardly any limitations due to the PS, which is reported to be below its glass transition temperature and should slow down the morphological changes. It can be assumed that the presence of DMF plasticizes the PS, which is supposed to be macroscopically insoluble. Similar switching mechanisms were applied for supramolecular block copolymer brushes [296, 297].

An oligomeric polyaniline-based diblock or triblock copolymer with PEO as water-soluble block allowed another electrochemical switching of vesicles [298–301]. Upon electrochemical oxidation, the vesicles disintegrated into puck-like micelles and the original vesicles could be re-formed upon reduction (Fig. 26) [298]. Similarly, aniline pentamers were incorporated into multiblock copolymers [302].

In contrast to low molecular mass surfactants [303–306], there are hardly any examples of polymeric systems going from unimers to micelles. Even more, it becomes obvious that electrochemical switching of micellar morphologies is generally rare. Side reactions such as polymer adsorption and film formation on the
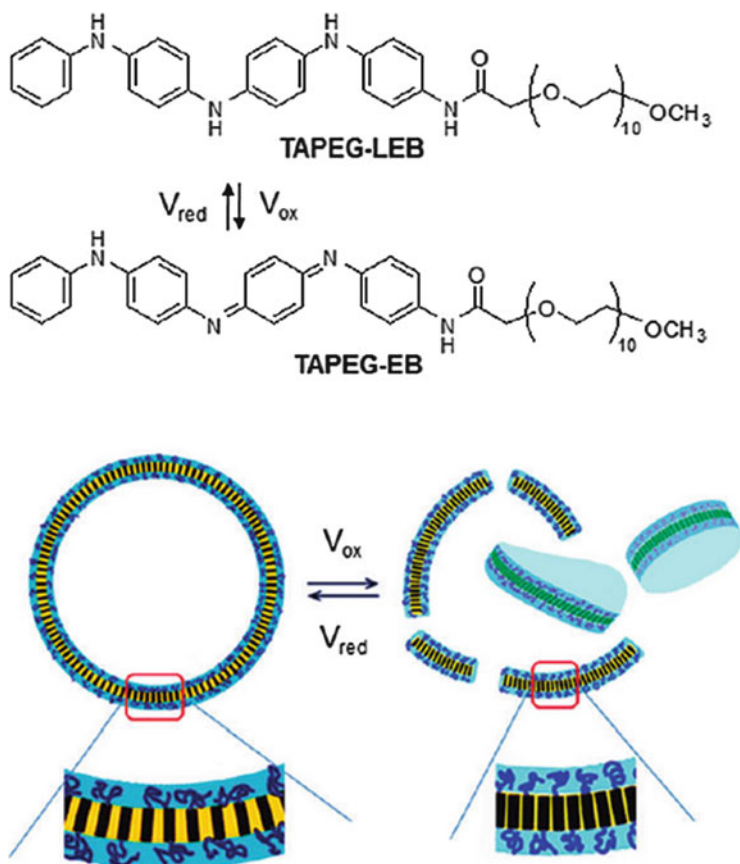
Fig. 26 Reversible electrochemical switching between vesicles and its puck-like fragments; *TAPEG-EB* tetraaniline-modified poly(ethylene glycol) with tetraaniline in the emeraldine base form, *TAPEG-LEB* with tetraanaline in the leucoemeraldine form (reprinted with permission from [298]. Copyright 2011 American Chemical Society)

electrode instead of bulk aggregation probably contribute to the scarcity of electrochemical approaches [166]. A rational solution to these problems might be the decoupling of the aggregation from the real electrochemical process by use of mobile, electroactive complexants. As highlighted above, the ability to complex with the polymer alters upon electrochemical switching. This allows a change of solubility of one part of the polymer and the subsequent induction of different micellar morphologies somewhat apart from the electrode interface. This principle might also explain the success of the supramolecular example given above (Fig. 25) [295], where soluble PEO with just one ferrocene unit can decouple from the micelle and react at the electrode, shifting the equilibrium towards demicellization. In accordance, long, soluble polymers probably prevent electrode adsorption for just one rather small terminal redox-active group (see also Fig. 28) [81, 104].
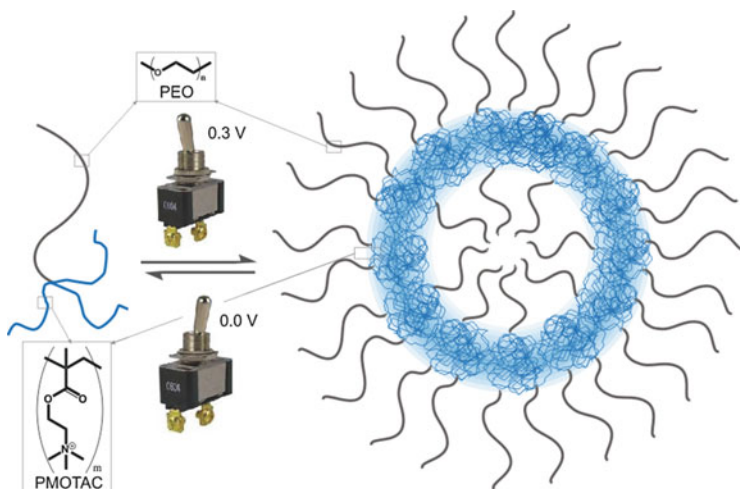
Fig. 27 Probably the first reversible electrochemical switching between the unimeric state and the self-assembled state, induced by complexation of a bis-hydrophilic polycation with hexacyanoferrates in aqueous media to form vesicles; *PEO* poly(ethylene oxide), *PMOTAC* poly(methacryloyloxyethyltrimethylammonium chloride) (reprinted with permission from [235]. Copyright 2009 American Chemical Society)

One of the first electrochemical examples of switching between unimers of a binary, bis-hydrophilic polymer and its micellar structures was given recently by the author [235]. Here, miktoarm stars of PEO and cationic poly(methacryloyloxyethyltrimethylammonium chloride) (PMOTAC) were complexed with anionic hexacyanoferrates, which induced vesicle formation at a certain ratio of ferro- and ferricyanide. Because the ratio of the two ions can be controlled electrochemically, vesicle formation was induced at high equilibrium potentials, whereas unimers were present at low equilibrium potential even after several electrolysis cycles (Fig. 27).

Another system that is reported to switch between unimers and micelles was given for TTF-terminated poly(*N*-isopropylacrylamide). It was also reported to be electrochemically active (Fig. 28); however, switching between micelles and unimers was achieved by chemical means [81].

Interestingly, complex formation between the terminal TTF group and a tetracationic cyclophane could be controlled by electrochemical means, as suggested by cyclovoltammetry results [104, 307]. Rather similarly, the supramolecular complexation of a viologen-based cyclophane with a dendron- and polyacrylamide-decorated TTF led to reverse vesicles, which were destroyed upon oxidation of the TTF [308]. Interestingly, the cyclophane needs to de-thread from a coiled/H-bonded oligomeric polyacrylamide backbone [309].

Preformed micelles could be either deposited and crosslinked electrochemically [310] or disassembled due to strong electrode–micelle interactions [311].
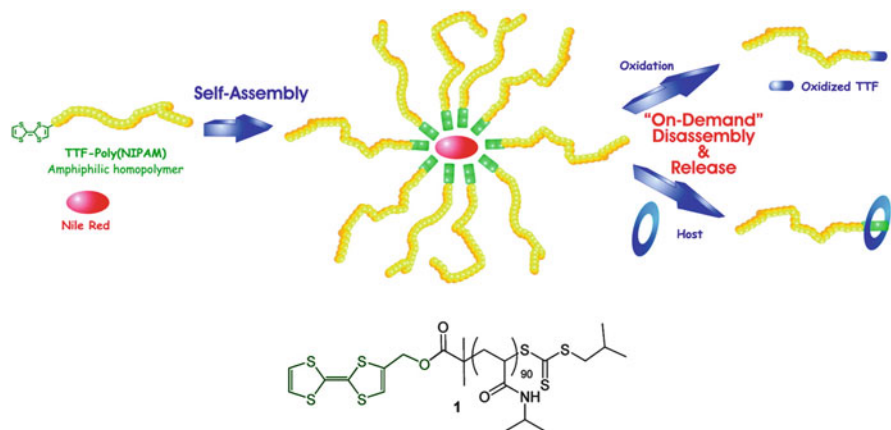
Fig. 28 A tetrathiafulvalene end group can be used to induce micellization, which can be reversed upon oxidation allowing a release of guest molecules; *TTF-Poly(NIPAM)* tetrathiafulvalene-terminated poly(*N*-isopropylacrylamide) (reprinted with permission from [81]. Copyright 2010 American Chemical Society)

2.2.3 Capsules and Other Colloids

This section addresses colloidal [312] and especially capsular systems, which are not generated by direct self-assembly as encountered for, e.g., vesicles [313]. Therefore, numerous preparation steps are often required, which leads to structures away from the thermodynamic equilibrium (e.g., layer-by-layer assemblies of interpolyelectrolyte capsules) [314]. Also for capsules, most examples deal with chemical redox-switching instead of electrochemical manipulation:

Disulfide bridges can be used to decompose layer-by-layer membranes and capsules [315]. Older investigations dealt with nylon capsules prepared by interfacial ("emulsion") polymerization. By use of a grafting procedure, redox-active chains (e.g., viologen- or ferrocene-based polymers) could be attached to the capsules (Fig. 29) [316, 317].

At the same time, the permeability could be altered by use of chemical redox, which leads to either a swollen corona or a hydrophobic corona. Permeability changes in planar membranes could be also induced electrochemically in multibilayer films where poly(styrene sulfonate) was complexed with ferrocene- or viologen-based surfactants [318, 319].

One prominent recent example was given for layer-by-layer assemblies of polyferrocenylsilane-based polycations with linear polyanions on template particles (Fig. 30) [320]. Upon oxidation, the charge balance is disturbed (more cationic charges) and changes in the permeability were found.

Ferrocene-containing elastomeric core–shell particles were prepared and tested for their redox- and mechano-chromic response [321]. Patchy hollow capsules were prepared from poly(vinylferrocene)-*block*-poly(methyl methacrylate) using an emulsion and partial organic solvent evaporation technique [322]. Upon oxidation,
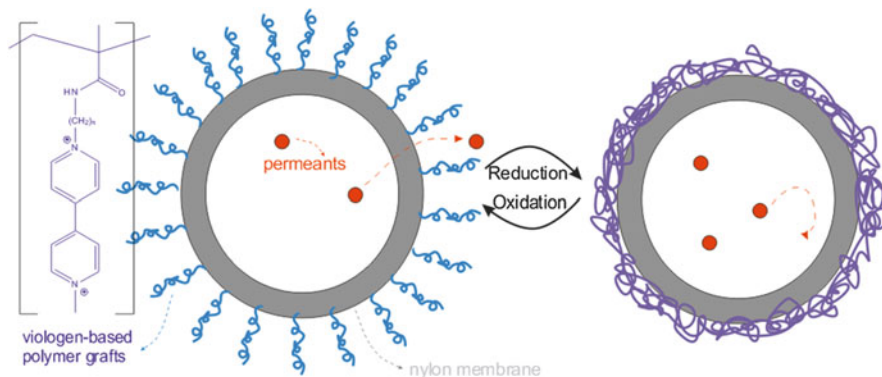
Fig. 29 Redox-induced change in capsule permeability [316]

the organometallic microphase-separated domains led again to an increase in capsule permeability (Fig. 31). This principle was also adapted for polyaniline-based capsules for the release of self-healing agents or for protection against corrosion [323, 324].

By templating and crosslinking, tubuli with an electroactive interior were generated [166, 325]. These tubuli are still electrochemically active in organic solvent, although the interior polyferrocenylsilane is shielded by a rather thin poly (dialkylsiloxane) shell (Fig. 32).

In connection to porous multilayers, the vesicles made of small pH-sensitive amphiphiles can release their cargo into their interpolyelectrolyte complex surroundings upon electrochemical change of pH [244, 326]. Another release application was reported for loaded polypyrrole nanoparticles. Depending on the applied potential, two guest molecules could be released selectively, which was explained by charge interactions between the polypyrrole in the different oxidation stages and the charge of the guest molecules [327].

2.3 Gels and Microgels

Polymeric gels are defined as crosslinked polymers that can be swollen by solvent. Gels in the nanometer to micrometer length scale are regarded as microgels and are sometimes called nanogels. Therefore, this section has a strong link to Sect. 2.1 and the principles mentioned there are valid for (micro-) gels as well. Because gels are typically macroscopic objects, their electrochemical responsiveness can even be exploited on larger length scales [328], implying their use in, e.g., actuator purposes [329, 330]. Solvation of the network in one state can be switched to a shrunken network in the other redox state. Because the electroactive gels are often in conjunction with electrodes, there is an overlap of this section with the next section
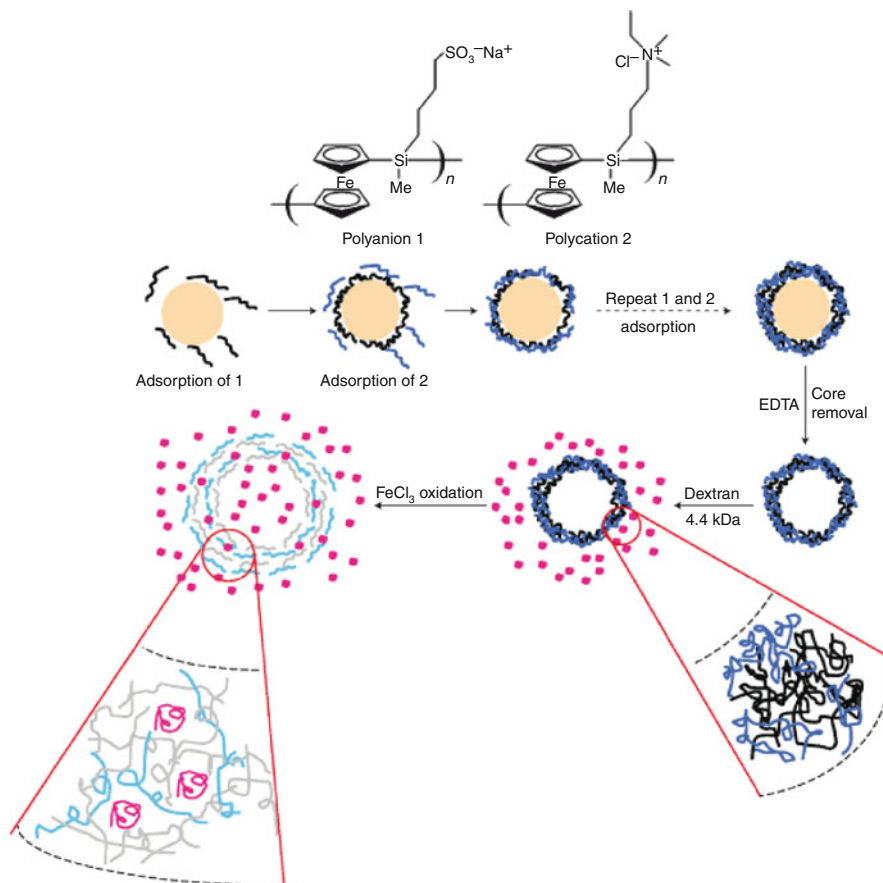
Fig. 30 Redox-active interpolyelectrolyte complexes can be assembled onto sacrificial templates, leading to hollow capsules after a layer-by-layer deposition. Upon oxidation, the capsules show a change in permeability, allowing an uptake of guest molecules (reprinted by permission from Macmillan Publishers Ltd: Nature Materials [320], copyright 2006)

(Sect. 2.4 on modified electrodes). Only topics of major interest are addressed because redox-active gels have been reviewed recently [11, 331].

The first part (Sect. 2.3.1 and Sect. 2.3.2) deals with macroscopic gels and still differentiates between electrochemical and chemical redox reactions. Generally, the velocity of a chemical redox reaction is limited by diffusion processes into the gel, which might become an issue for the electrochemical switching (concomitant diffusion of co-ions). Further, the electrochemical addressability of redox centers inside the gel needs to be clarified before good electrochemical switchability can be expected. Hence, the switching method of choice is dependent on the specific system under investigation. Therefore, systems in which the redox processes alter the properties of gels without electron transfer at an electrode interface (chemical redox) will be addressed briefly.
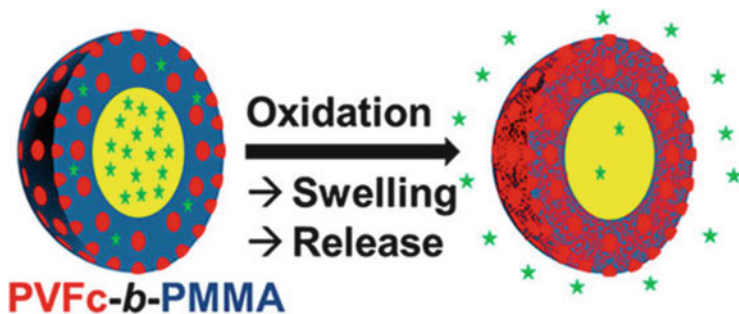
Fig. 31 Patchy capsule, which leads to changes in permeability upon oxidation of the ferrocene-based polymer; *PVFc-b-PMMA* poly(vinylferrocene)-*block*-poly(methyl methacrylate) (reprinted with permission from [322]. Copyright 2012 American Chemical Society)
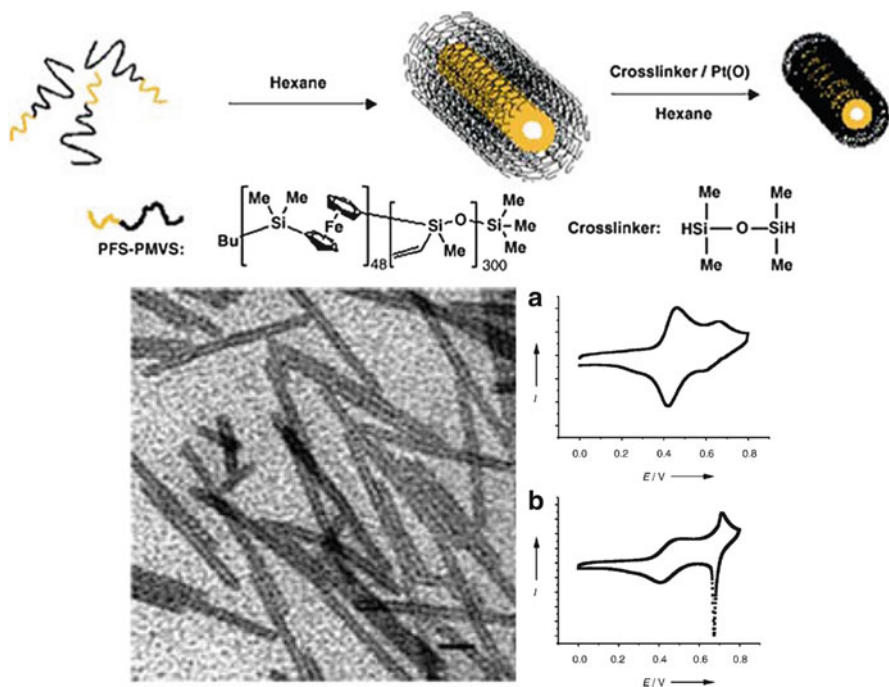
Fig. 32 Preparation pathway (*top*) for electroactive tubuli (TEM image *bottom left*), generated upon crosslinking of the shell. The polyferrocenylsilane is located along the inner wall, preventing electrode adsorption. Cyclic voltammograms are shown on the *bottom right*: *top CV* crosslinked tubuli; *bottom CV* diblock copolymer in common solvent, indicating adsorption processes (reprinted with permission from [166]. Copyright 2004 Wiley)

2.3.1 Manipulation of Gels by Chemical Redox

A number of gel systems with disulfide/thiol chemistry have been developed [332], which are reviewed in Sui et al. [11]. As mentioned, electrochemical addressability is barely feasible for such systems. However, disulfide-based gels and microgels could be obtained by mild aerobic oxidation by applying an enzymatic environment (horse-radish peroxidase) [333].

As another example, the response of electroactive systems to an internal change in the electrochemical potential by the self-oscillating Belousov–Zhabotinsky reaction leads to peristaltic motions of ruthenium-containing gels (Fig. 33) [196, 334–338]. However, these examples are not electrochemically controlled by electrode processes, although the gel swells and contracts autonomously without further addition of chemicals. This behavior is a result of the oscillating reaction that takes place inside the gel. This reaction imparts temporal and spacial variation in the chemical potential, which is translated to the redox-sensitive polymer. Typically, a polymer-bound ruthenium complex changes its charge upon continuation of this oscillating reaction, which leads to a cycling of the osmotic pressure: the gel reacts by uptake or release of solvent in the form of peristaltic motions. This behavior was used to construct self-walking gels [339].

Chemical oxidants also allowed switchable hydrogel formation by reversible competitive hosting of low molecular mass ferrocene units within cyclodextrins. Here, cyclodextrin complexes the otherwise-associating alkyl side chains, which reduces the viscosity of this well-formulated mixture. However, the alkyl groups start to associate under gel formation when reduced ferrocenecarboxylic acid is added. Then, ferrocene interacts preferentially with the cyclodextrin. This state can be reversed upon chemical oxidation due to the unfavorable inclusion complexation of ferrocenium units with cyclodextrin [254]. Based on similar mechanisms, a redox-dependent shape memory polymer has been generated [340] and also the adhesion of different gels can be switched [341].

Hydrophobically modified and branched poly(ethylene imine) was investigated by rheology [255]. The oxidation of the terminal ferrocene units leads to a decrease in viscosity due to the reduced hydrophobicity and the reduced associating tendency of these moieties. Similarly, the hydrophobicity of a ferrocene-based gel for release applications could be tuned by the reaction with oxidants [342].

An interesting example was given by the use of opals embedded into a ferrocene-derived redox-active polymer matrix [343]. By redox reaction, the distance between the embedded silica particles could be easily manipulated, leading to a shift in color, as shown by spectroscopic means.

Fig. 33 Peristaltic
transport of objects within a
redox-active gel tubuli,
induced by the self-
oscillating Belousov–
Zhabotinsky reaction
(reprinted with permission
from [338]. Copyright 2012
Wiley)
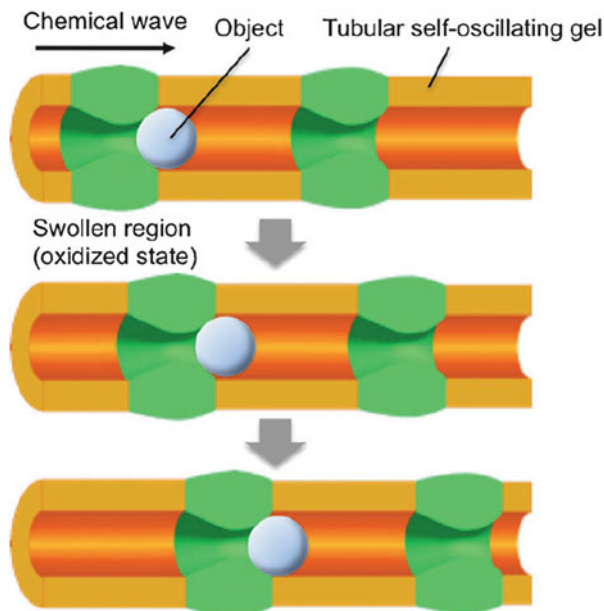
2.3.2 Electrochemical Manipulation of Gels

Electrochemically Induced Solvation of Gels

Metal-Coordinating Gels

The last approach described in the previous section, which used ferrocene-based
polymers [328], has been further developed (Fig. 34) [344] after assessing the
reversibility of the electrochemical reaction [345].

A polymer gel based on an (inverse) opal was applied in order to obtain shorter
switching times, which are also desirable for electrochemical color display pur-
poses [346]. Hence, an all-color display was developed that, dependent on the
applied potential, could reversibly switch between blue, green, red, and black.
Here, crosslinked polyferrocenylsilane gels were partly swollen with glutaronitrile
electrolyte. The degree of swelling was controlled electrochemically. Subse-
quently, the distance between the voids formed by the silica beads, which were
etched by hydrofluoric acid treatment, could be altered. It should be mentioned that
there are also other concepts for electrically switchable photonic crystals that are
not directly connected to electrochemically induced solvation [347–349].

A rather old example for switching deals again with ferrocene-modified polymer
networks. Thin films on an electrochemical quartz crystal microbalance were tested
for changes in their viscoelastic properties in response to an overpotential
[350, 351]. In this example, the electrochemical properties are dependent on
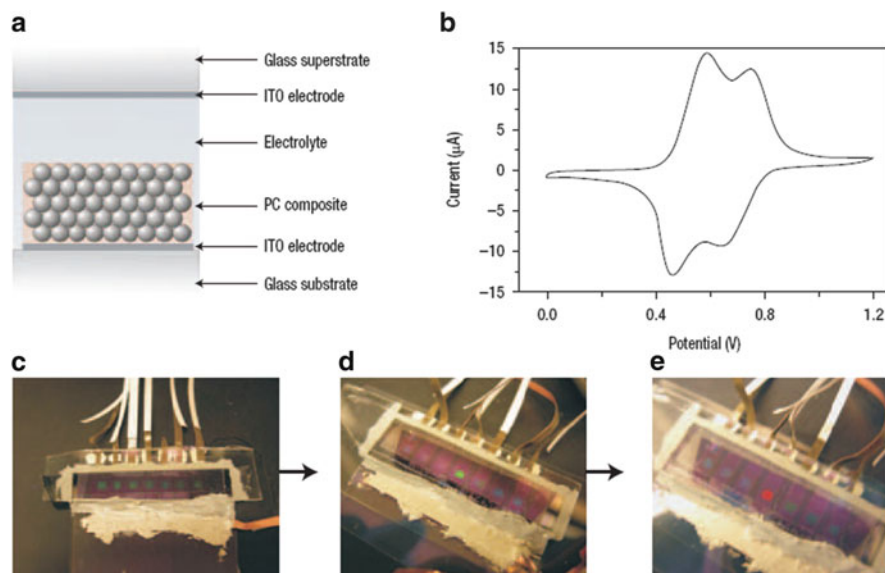
Fig. 34 Scheme of an electrochemical cell loaded with a photonic crystal, which is embedded in an electroactive gel matrix (**a**). the swelling of the composite photonic crystal can be controlled by electrochemical means (CV, **b**), leading to color displays (**c–e**; only one pixel is addressed, showing different colors at different electrode potentials) (reprinted by permission from Macmillan Publishers Ltd: Nature Photonics [344], copyright 2007)
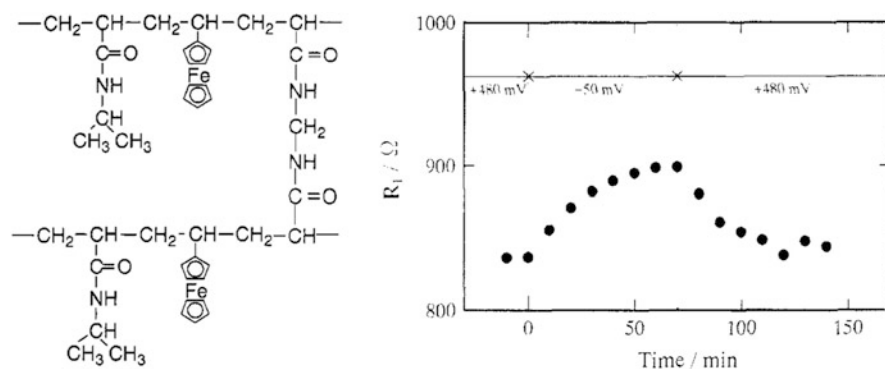
Fig. 35 Electromechanical impedance of ferrocene-modified poly(N-isopropyl acrylamide) gels in response to variations in electrode potential (reprinted with permission from [350]. Copyright 1994 American Chemical Society)

temperature and the temperature-responsive properties can be manipulated by electrochemistry (Fig. 35).

A supramolecular hydrogel was constructed on the basis of the complexation of ferrocene-terminated thermosensitive block copolymer with cyclodextrin-modified
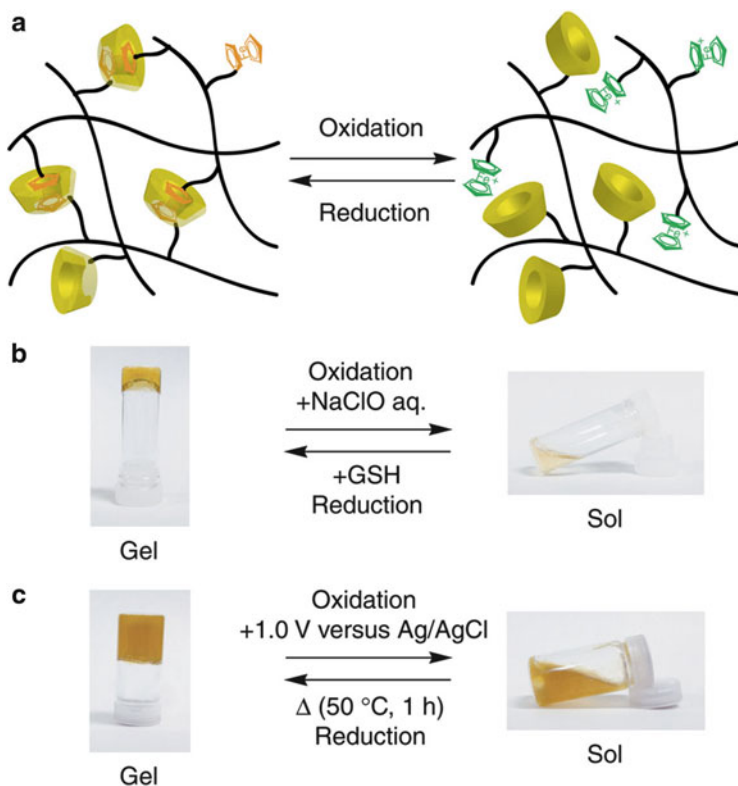
Fig. 36 Supramolecular gel based on inclusion complexation (**a**, *left*) can be switched to a sol state (**a**, *right*) either using chemical reagents (**b**) or electrochemical reactions (**c**) (reprinted by permission from Macmillan Publishers Ltd: Nat Commun [353], copyright 2011)

nanoparticles (mixed concept; refer also to section "Electrochemically Induced Complexation of Gels") [352]. Thus, a sol–gel switching was possible. Similarly, mixtures of poly(acrylic acid) with either cyclodextrin or ferrocene end groups gave redox-sensitive self-healing materials (Fig. 36) [353, 354]. The strength of the gel could also be modulated by redox reactions [355].

Cationic, anionic, and nonionic polyferrocenylsilane-based hydrogels were recently introduced [356–358]. In the case of anionic, permanently charged hydrogels, the electrochemical oxidation to ferrocenium imparts a polyampholytic behavior together with a color change. In addition, oxidation leads to shrinkage of the gel and to a loss of elasticity; upon reduction, the former properties could be reached reversibly.

Other Examples

Biorelated electroactive gels were reported for gelatin, grafted with aniline pentamers [359, 360]. Using chitin-based polyelectrolytes, gelation was dependent on the pH and the valency of counterions, which could both be manipulated electrochemically. This behavior was applied for stimulated drug release [361]. Electroactive poly(hydroquinone) forms hydrogen bonding to chitosan under formation of electroactive hydrogels [362]. Interestingly, the formation of these redox-sensitive hydrogels is easily achieved by mixing hydroquinone with chitosan in the presence of air. However, little is known on the morphological changes during electrochemical redox.

Another application of quinone-based hydrogels and its nanotube composites ranges into actuating purposes [363]. Analogously, conducting composite hydrogels made of carbon nanotubes and poly(N-isopropyl acrylamide) provide a way to heat the samples by current flow through the hydrogels. At the same time, the gels shrink due to their thermoresponsiveness, as electrochemical reactions are less dominant in this case [364]. Other conducting/electroactive hydrogels were achieved using polylactide and tetraaniline-containing block copolymers [365], employing possible stereocomplexation [366].

Electrochemically Induced Complexation of Gels

Size changes and actuating abilities are reported for poly(acrylic acid) (PAA) gels attached to electrodes [367, 368]. Movable copper ions are reduced, leading to a decomplexation with PAA and to a concomitant swelling. Macroscopically, a bending and stretching motion was observed. The same switching principle holds also for photoelectrochemical switching (not real electrochemical switching), where TiO_2 particles induce the reduction of the copper/silver ions upon illumination [369, 370].

For an improvement in switching time, the switchable copper counterions were replaced by an electrochemically induced change in pH. Freely moving hydroquinone can be oxidized at the electrode under release of protons. A concomitant protonation of PAA lead to its shrinkage [371]. Taking protons as complexants, the dissolution of a gel based on hydrogen bonding between poly(methacrylic acid) and poly(ethyloxazoline) is influenced by pH changes induced by electrolysis of water [372]. At the same time, insulin release from the gel can be controlled by an electric current.

In another example, polyanionic species can give a hydrogel in the presence of complexing iron species. However, the mechanical properties of the hydrogel are very dependent on the oxidation state of the iron ions, leading to reversible electrochemical switching of the gel's mechanical properties (Fig. 37) [373].

For more applications of polyelectrolyte gels, please refer to a recent review [374]. In the rest of this section, some special aspects are addressed that can lead to application of the hydrogels as actuators.
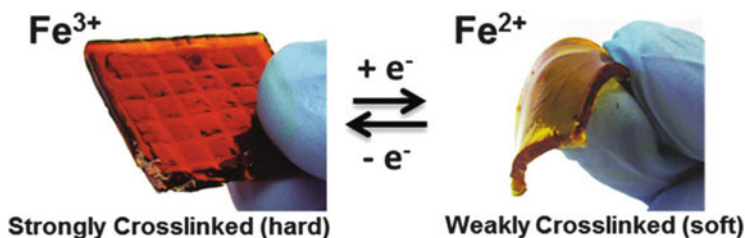
Fig. 37 Changes in the mechanical properties of a hydrogel film induced by electrochemical means (reprinted with permission from [373]. Copyright 2012 American Chemical Society)

As early as 1965, platinum nanoparticles were introduced into a PAA-based hydrogel, which becomes (at least partly) electronically conductive. The electrode protruded into the network. Upon electrolysis of water, either protons or hydroxide ions were formed under gas evolution, which led to a shrinkage or expansion of this hybrid hydrogel [243].

There has been some debate on the swelling/collapse of polyelectrolyte gels in electric fields in general [375–377]. One report was given for poly(acryl amide) gels in acetone–water mixtures [378]. The influence of the electric field on the polymeric charges and the forced collapse was accounted for; however, later it was realized that other effects also play a role [379]. In particular, the application of a potential leads to current flow and changes in local pH [245], as reported previously [243, 380]. However, pH changes cannot explain all the observed phenomena. This indicates that the underlying principles are still not fully understood [381], although these hydrogel actuators have been optimized (Fig. 38) [382, 383] and different models have been invented [384]. The electrical, active transport of a gel polyelectrolyte(/surfactant) complex (gel walker) was reported long before the discovery of the peristaltic movements of gels (refer also to Fig. 33) [385, 386].

An interesting example is given for metallo-supramolecular polymers, which gelate under certain conditions [387]. By electrode reactions, the gel and sol states can be switched reversibly (Fig. 39) [210]. Even silk fibroin solution can electrogelate when the local pH is altered electrochemically [388].

Please refer also to the examples of the mixed switching concept mentioned in the section "Metal-Coordinating Gels" (e.g., [352–355]).

2.3.3 Microgels

Redox-sensitive microgels are rare, especially when it comes to electrochemical switching. Thus, examples for "chemical" switching are given first. The crosslinking degree is often modulated by chemical redox [389]. As already mentioned, disulfide bridges can be used for reversible crosslinking [390–394]. This chemistry was even used for bond formation between different microgels [395]. Other cleavable crosslinkers that can be cut by oxidation (e.g.,
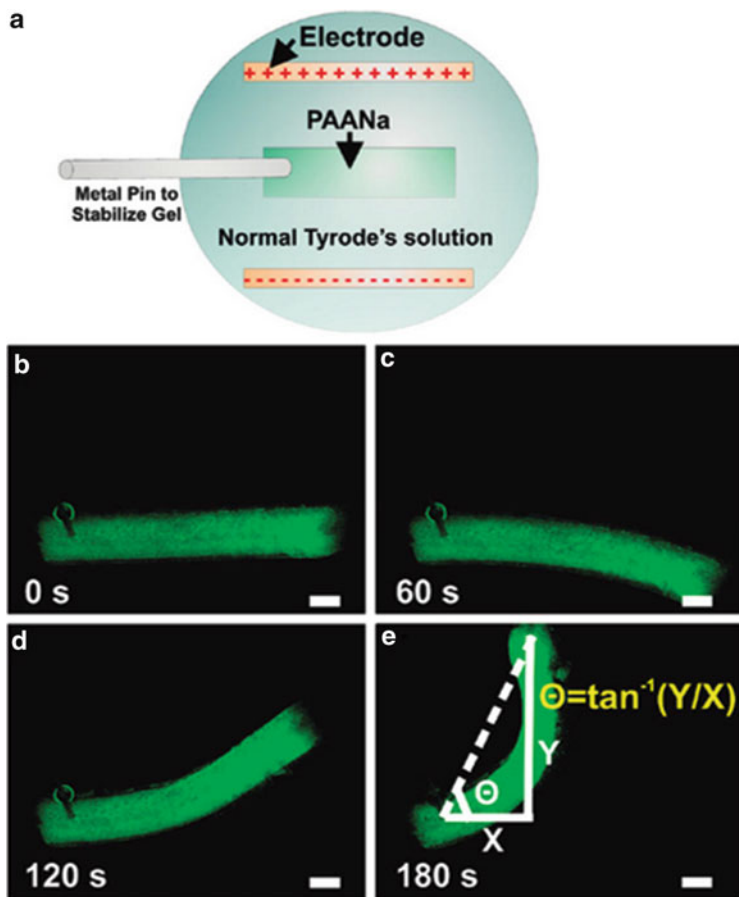
Fig. 38 (**a–e**) Bending of a porous poly(acrylic acid)-based hydrogel film (porosity was increased by removing sacrificial, embedded colloids) in an electric field (reprinted with permission from [382]. Copyright 2010 American Chemical Society)
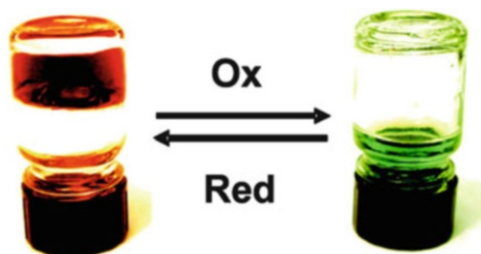

Fig. 39 Sol–gel transition for a metallo-supromolecular polymer using a bis-terpyridine linker (reprinted with permission from [210]. Copyright 2009 American Chemical Society)

N,*N*′-(1,2-dihydroxyethylene)bisacrylamide) are known. The periodate-mediated cleavage was used for the generation of hollow microgels and yolk/shell structures [34, 396]. After cleavage, the linear chains can penetrate the shell, leading to hollow particles.

As examples of microgels with a constant degree of crosslinking, poly (ferrocenylsilane)-based gel particles could be oxidized, which yielded an electrostatically driven attachment of silica nanoparticles [397, 398]. Larger micrometer-sized poly(ferrocenylsilane)-based microspheres were prepared using microfluidics [399].

Considering the Belousov–Zhabotinsky reaction, the same oscillating mechanism that was utilized for macroscopic gels was also applied to microgels [400, 401]. The viscosity of the system cycles periodically. The same authors synthesized microgel particles with sites of both complexed ruthenium salts and viologen units. Whereas the ruthenium complex can be photooxidized under viologen reduction, the viologen acts as an acceptor and redox mediator. It returns to the dicationic state after providing electrons at a platinum surface for hydrogen evolution [402].

Reports on an electrochemical addressing of microgels are very rare. Poly(vinyl pyridine)-based microgels show a pronounced swelling at low pH, which can be adjusted by electrochemical means [403]. Electrochemical injection of charge into a redox-active microgel is dependent on different parameters (size of microgel, location of redox-active site, etc.). Still, electroactivity was proven for two types of microgels with redox-active moieties along the network [404, 405]. For example, the polyferrocenylsilane backbone was decorated with vinylimidazolium residues, promoting a poly(ionic liquid) behavior (Fig. 40). Hence, ion exchange led to remarkable changes in solubility [404]. However, only a little is known on the changes in morphology upon electrochemical switching. Electrochemical address-ability of microgels containing ruthenium complexes has also been reported; leading to an electrogenerated chemiluminescence [405].

After addressing free-standing gels and gels in dispersion (microgels), there is a strong overlap with the next section, where thin films of, e.g., gels on electrodes, are discussed (typically in the size range of tens to hundreds of nanometer).

2.4 Thin Films: Modified Electrodes and Membranes

The topic of thin films, active coatings, sensor electrodes, and electrode modification for energy storage has been a very active branch of electrochemical research in the past [406–409]. Abundant examples are reported on this subject in the current literature [73], including immobilized redox-active proteins [410]. Therefore, this section cannot give a deep review on this topic, but will mainly emphasize the issues that are related to those addressed so far (Sect. 2.1). This section provides a possible starting point for entering this area of research more deeply. A discussion on thin films made of electrochemical polymerization of active monomers (e.g., aniline) will be only briefly covered here. Most products of these electrochemical
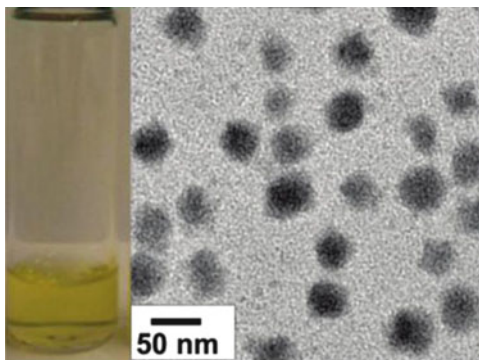
polymerizations are sparingly soluble [411] but electron-conducting in doped states (e.g., polyaniline, polypyrrole, and polythiophene) [412–418]. Then, such or other electrode systems provide switchable wetting and surface energy ("electrowetting"), which can be traced back in some cases to reorientation of amphiphiles on the surface [419]. There will be an encounter with this switchable surface energy in some of the cases discussed below, but this review cannot give an overview on these applied voltage-dependent surface and wetting effects (e.g., refer to [420, 421]).

Regarding preformed polymers, Sect. 2.1 mentions different examples where soluble polymers are prone to form thin films on electrodes upon electrochemical switching. These examples are not listed here again, but the reader is referred to Sect. 2.1. Here, the main interest is in permanent films or gel layers, where electrode processes change their interior structure. This might be accompanied by an exchange of solvent and solutes. Importantly, the electrochemistry of thin films can take place at rather short switching times by directly setting the local concentration of the redox partners with help of the electrode potential. In contrast, time-consuming bulk electrolysis is needed for an efficient manipulation of reasonable sample sizes for the other examples mentioned before.

2.4.1 Electrochemically Induced Complexation

After having assessed the permeation of small solutes through different polymer layers [422], the electrochemically induced complexation will be discussed again. Polymer- and polyelectrolyte-modified electrodes and supramolecular polymers on top of electrodes have been reviewed recently [423, 424].

Here, we will consider changes in the accessibility of electrodes to electroactive substances by switchable polymer films, which are not directly redox-sensitive. A gating of hexacyanoferrates could be modulated by the presence of cholesterol, which complexes the collapsed poly(vinyl pyridine) matrix (hydrophobic at the pH used) [425]. The preparation of this membrane leads to pores that are filled upon complexation with cholesterol. At the same time, the accessibility of the electrode
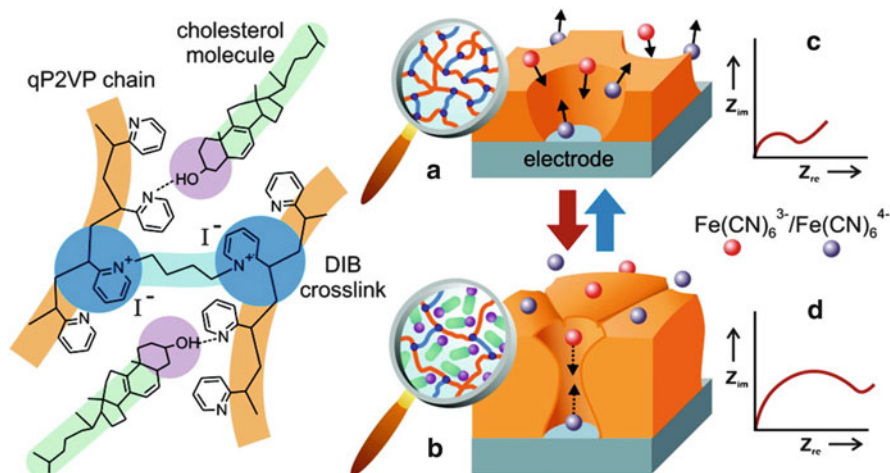
Fig. 41 Swelling of a crosslinked poly(2-vinylpyridine) film (*qP2VP*), which is partially quaternized with diiodobutane(*DIB*) crosslinks, on top of an electrode in the absence (*A*) and presence (*B*) of cholesterol. Graphs *C* and *D* show the related changes in impedance as a result of changes in the pore size (reprinted with permission from [425]. Copyright 2007 American Chemical Society)

towards the probe is reduced (Fig. 41). Hence, the addressability of redox probes in solution is connected with the porosity of thin insulating films [426].

Porous structures were modified with polymers and the ion transport of differently charged probes was investigated, leading to possible ion-exclusion for polyzwitterionic brushes [427].

Introduction of the thermosensitive component poly(*N*-isopropyl acrylamide) (PNIPAM) allowed a switching of electrode accessibility with hexacyanoferrates with temperature (film formation by interpolyelectrolyte complexation of oppositely charged PNIPAMs within a layer-by-layer approach; see also below) [428]. Similarly, electrode reactions could be modulated by the assemblies of PNIPAM with clay platelets [429]. The close packing of poly(vinyl pyridine) chains, which act as chelating agents for other metal ions, prevented the efficient electron transfer of hexacyanoferrates [430]. Such polymer films on top of electrodes can be prepared by electrochemically triggered polymerizations [18, 431–434].

The direct complexation of polycation films with metal salts and the self-exchange within thin poly(vinylpyridine)/metallate complexes was investigated using the rotating disk electrode technique [435, 436]. Both for iridates and ferrates, the electron conduction within the polymer–complex film is rapid, providing an experimental window to the electron transfer at the film/–electrolyte interface. There was some debate on the electron transport mechanism (electron hopping versus ion mobility) and charging mechanism of these films, which require charge neutrality during electrochemical switching (either by expulsion/uptake of electroactive species or by penetration/release of small counterions from the electrolyte) [437–441]. An ejection of hexacyanoferrates upon switching was detected

using a scanning electrochemical microscope [442]. The actual mechanism seems to be dependent on the degree of loading with electroactive ions [440]. Interestingly, there are redox couples where the species with lower charge number interacts strongly with the cationic polyelectrolyte species (e.g., $[IrCl_6]^{2-}$, which is bound more efficiently than $[IrCl_6]^{3-}$; this unexpected course is also known for $[Fe(CN)_6]^{3-}$ with respect to $[Fe(CN)_6]^{4-}$; see the discussion in the section "Electrostatic Attraction" in Sect. 2.1.2). This selectivity leads to ion rectification [443], as seen for e.g. rotating disk electrode experiments [438, 444–447].

Other investigations on such complex films are known [448, 449]. The electroactivity in nonpolar solvent is then very dependent on the water content of the organic solvent, which allows the construction of a water sensor [233]. Polyelectrolyte brushes [450, 451] attracted oppositely charged counterions such as ruthenium complexes or hexacyanoferrate to electrode interfaces [452–456], while the surface energy could be altered electrochemically (Fig. 42) [234].

Poly(ionic liquid) brushes with terminated ferrocene units acted similarly, while the interfacial resistance was probed by hexacyanoferrate [457]. Chemical and electrochemical switching of local pH at an electrode-grafted poly(vinyl pyridine) brush again allowed modulation of hexacyanoferrate chemistry (Fig. 43) [458]. Octacyanomolybdate was used as catalyst for the oxidation of ascorbic acid [459]. Even heteropolyanions (Keggin ions) could be entrapped in polymer films electrochemically [460]. Further, thermoresponsive or pH-responsive cationic copolymer films modulated the hexacyanoferrate or ferrocenedicarboxylic acid electrochemistry by temperature or variation of pH and perchlorate concentration, respectively [461–463]. Besides these complexes with cationic polyelectrolyte films, electroactive cationic counterions (e.g., the europium couple) interacted with anionic networks [464]. Similarly, copper ions within a PAA matrix [367] allowed the construction of actuators [465]. Besides these binary systems (polyelectrolyte/electroactive counterions), multiresponsive electrode modification with an interpenetrating gel network of poly(acrylic) acid and poly(diethyl acrylamide) allowed the modulation of hexacyanoferrate electrochemistry [368].

Ternary systems with interpolyelectrolyte complexes (IPECs) assembled in multilayers (layer-by-layer assemblies) were intensively investigated in the presence of electroactive counterions. Obviously, the multivalent counterions provide a small, mobile filler for uncompensated charges, especially in the presence of higher amounts of monovalent charge [466]. Hence, not all charges of one chain find their counterpart in another chain, probably due to steric reasons. Thus, hexacyanoferrates were entrapped into layer-by-layer assemblies on top of electrodes, acting as a redox mediator for the addressability of ferrocene derivatives in organic solvent [467]. These polar films are probably rigid due to the contact with organic media, although diffusional processes within the film were not current-limiting.

To increase the mobility, most of the work is related to hydrated IPEC multilayers in contact with aqueous solutions [468]. For weak polyelectrolytes, electrolysis of water at rather extreme electrode potentials can induce dissolution of the layer-by-layer assemblies [469]. In the presence of electroactive counterions, an odd–even modulation of the charge-transfer resistance of the hexacyanoferrate
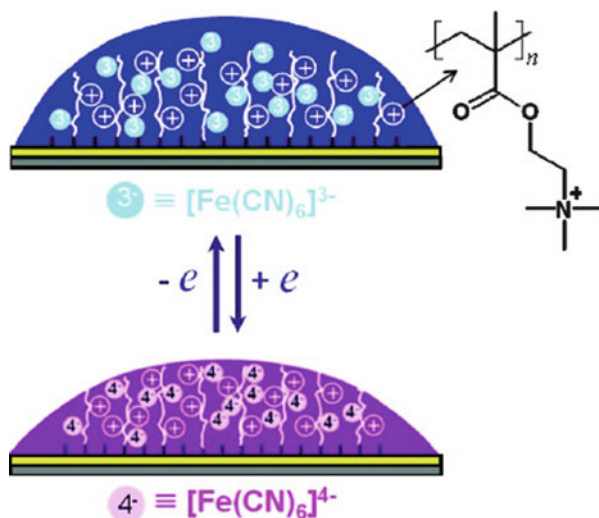
Fig. 42 The contact angle of water on an electrode can be modulated electrochemically by using a complex of hexacyanoferrate with a polycation brush, which is grafted from the electrode (reprinted with permission from [234]. Copyright 2008 American Chemical Society)
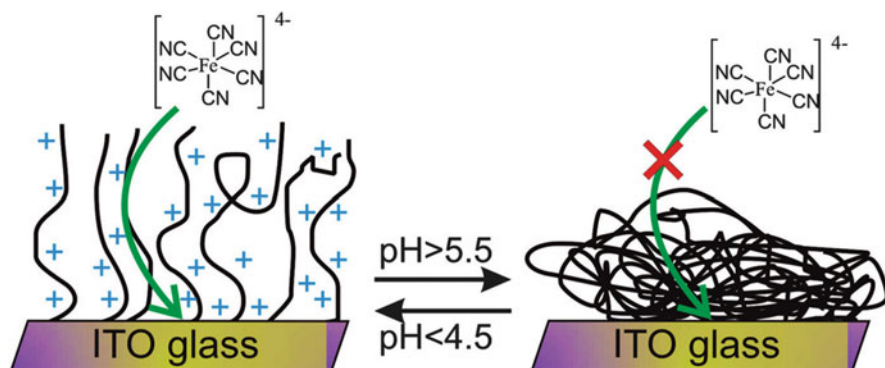

Fig. 43 Accessibility of an electrode can be modulated by pH (also by pH changes induced by water electrolysis) when using pH-responsive poly(vinyl pyridine) as grafts (reprinted with permission from [458]. Copyright 2010 American Chemical Society)

couple was detected with layer number using electrochemical impedance spectroscopy [470]. A repulsion/attraction between the surface charge and the hexacyanoferate charge was discussed. Interestingly, ferricyanide was enriched within the multilayers, but diffused faster within the layers than the ferrocyanide (Fig. 44) [466, 471–473]. On some occasions, cationic species such as $[Os(bipy)_3]^{3+}$ or $[Ru(NH_3)_6]^{2+}$ can be expelled from the film, indicating an excess of positive charges within the films [474, 475]. Using impedance spectroscopy, information on the capillary structure within the layers could be obtained [476].
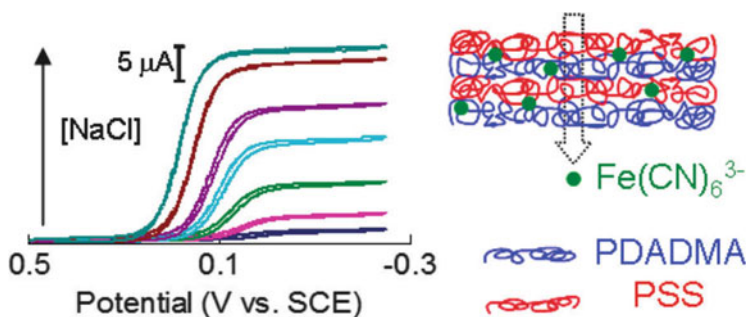
Fig. 44 NaCl increases the permeability of polyelectrolyte multilayers for the redox-active ferricyanide, as seen by rotating disk electrode measurements (reprinted with permission from [471]. Copyright 2011 American Chemical Society)
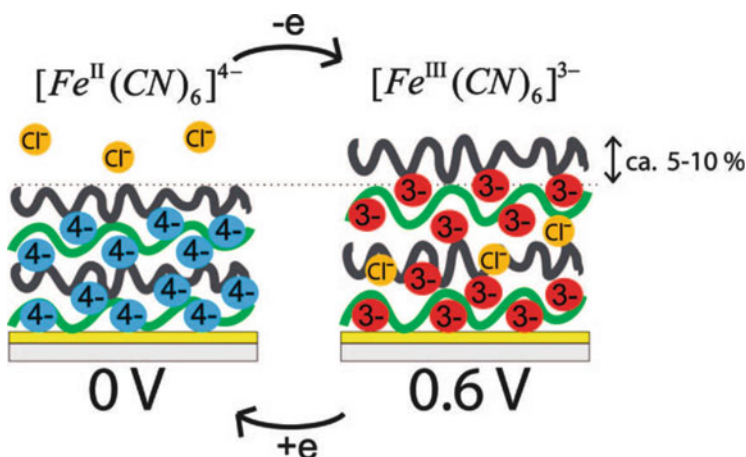
Fig. 45 Electrochemically induced swelling of interpolyelectrolyte multilayers doped with hexacyanoferrates for actuating purposes (reprinted with permission from [237]. Copyright 2008 American Chemical Society)

The enrichment of anionic counterions inside the film was also found for systems in which the switching between the ferri-/ferrocyanide couple allowed the formation of an actuating device (Fig. 45) [237–239, 477, 478].

Hexacyanoferrates are the precursors for nanoparticles of compounds such as Prussian blue [479]. Hence, Prussian blue can be prepared inside the multilayers [480]. In another approach, the particles were prepared and co-assembled with a polyelectrolyte. The color and surface charge of these particles can be switched and, therefore, disassembly of the nanoparticle–polyelectrolyte multilayers is also feasible [481–483].

This multilayer approach was further developed for the release from vesicles for cell engineering [244, 326]. Also related, permeability changes in planar membranes could be also induced electrochemically, where poly(styrene sulfonate) was

complexed with ferrocene- or viologen-based surfactants [318, 319]. Interestingly, these principles could even be used in applications where platinum grids acted as a conducting support for the membrane. Hence, electrochemical manipulation of membrane permeability was successfully tested for hydrophilic fluorescent dyes.

Multilayers of boronic acid-modified polyacrylamide with a polycation gave a platform for interaction of redox-sensitive Alizarin Red S molecules, which gave covalent attachment in the form of a boronic acid ester, in equilibrium with the free dye [484].

Other electroactive coatings can be obtained by a slightly different approach, leading to biosensors. Redox-active enzymes were embedded, e.g., in layer-by-layer assemblies together with polyelectrolytes [485, 486]. This time, the interaction of the enzyme with the polymer was hardly altered, but the presence of substrates generated an electrochemical signal. Similarly, enzymes were deposited on electrodes together with polyelectrolyte-based micelles to yield another generation of biosensors [487]. Biosensor-related research in general is a very active branch of science (see also the section "Coordinating Metal Centers" in Sect. 2.4.2) [488–490].

2.4.2   Electrochemically Induced Solvation

Covalently Bound Redox Moieties

Viologen is again a prominent motif for inducing electrosensitivity to films [49, 491]. One of the first reports on polyviologen dealt with its complex formation with tetracyanoquinodimethane (TCNQ), leading to electron-conducting films due to the formation of charge-transfer complexes. Charge-transfer complexation of poly(dithiafulvene)s and poly(viologen)s led to a reduced electroactivity perpendicular to the thin films [108]. The photochromic properties of viologen-based films were reported [42, 492–495]. Thus, electrochromic devices were realized on the basis of poly(viologen)-based multilayers [496] or conjugated structures (Fig. 46) [497–499].

The catalytic properties were also investigated for these interpolyelectrolyte complexes [500–502], which could be used for the catalytic reduction of oxygen [503]. Viologen can also act as a mediator for the electrochemical conversion of other species [500]. Besides this electrochromism and electrocatalysis, the ion transport was investigated using radiolabeled calcium ions within multilayers of poly(styrene sulfonate) and polyviologens (Fig. 47) [504, 505]. A conjugated version of these polyelectrolyte-based layer-by-layer assemblies was accomplished, which led also to caffeine sensing [506].

The mechanical properties of such interpolyelectrolyte multilayers could be switched electrochemically [507], allowing their dissolution in the case of TEMPO-modified layer-by-layer assemblies [508]. Surface modification of, e.g., polyethylene with viologenic units is reported [509, 510], while viologen-containing membranes were created in order to influence the permeability using redox reactions [511, 512]. Such a gating membrane could be even constructed on
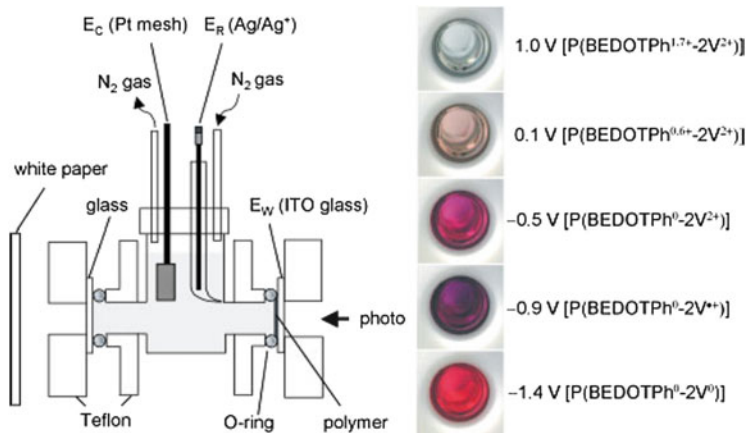
Fig. 46 Electrochromic device based on a transparent, polymer-coated electrode (with a thiophene- and viologen-based polymer) (reprinted with permission from [497]. Copyright 2005 Wiley)
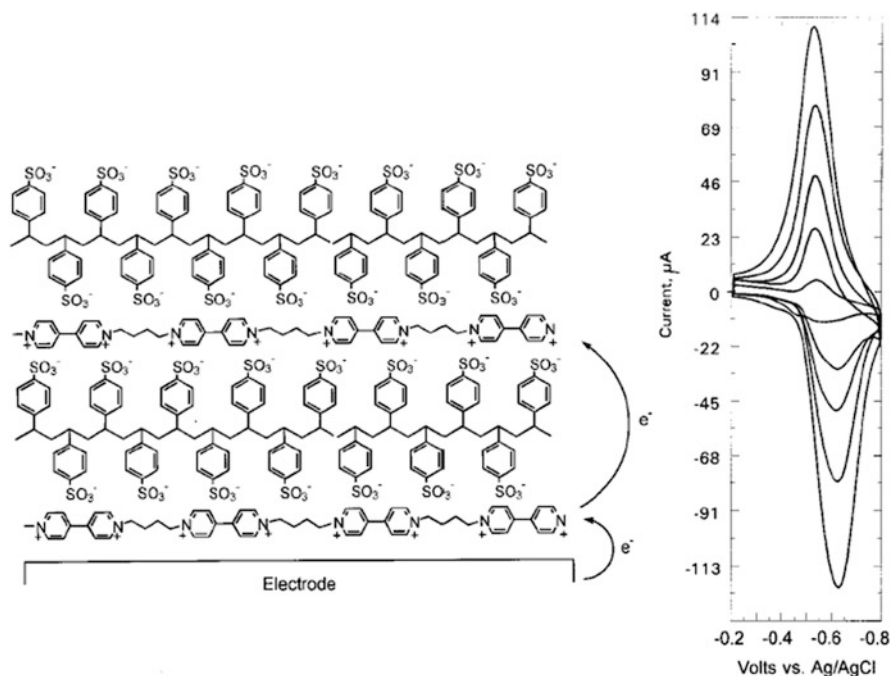

Fig. 47 Electroactive interpolyelectrolyte multilayers obtained from a poly(viologen) (**a**). Electron transport between the layers is facile, as indicated by the cyclic voltammograms (**b**), which were recorded for increasing layer numbers (reprinted with permission from [504]. Copyright 1998 Wiley)

the basis of viologen-containing stacked bilayers made of amphiphiles and poly-electrolytes [318, 513, 514]. The permeation reduction was caused by changes in fluidity imposed by the electrochemical reduction [318]. Polymers of viologen were embedded into nanopores and the electrochemical switching allowed a release of electrostatically bound guest entities [515]. A humidity sensor was realized by detecting swelling-dependent impedance changes in viologen films [516]. Films of quaternized 2,2′-bipyridine derivatives of viologen were also prepared electro-chemically [517] and copolyviologen films produced by electrochemical polymer-ization [518, 519].

An oligoaniline-based polymer was used for electroactive suprahydrophobic surfaces [520]. Vitamin C could be detected on oligoaniline-modified polyurea [521] and a related phenothiazine-based brush could be used for data storage [522].

Tetracyanoquinodimethane-modified electrodes are described in literature. The protonation equilibria/counterion distributions upon reduction were addressed [523–529]. Their composite structures with silver are also reported [530].

Silicon surfaces could be grafted with TTF-containing conjugated polymers [531]. These electrodes benefited from attachment of the redox-active groups to a conducting polymer backbone.

Hydroquinone was introduced onto a grafted polymer, which was attached to a carbon black electrode [532]. Nitroxide-based polymers and their modified elec-trodes have been discussed as efficient components for battery applications (e.g., [10, 124, 533–537]). These polymers can even be used as active surfaces for electrochemical writing on the nanoscale using a current-sensing atomic force microscope [538].

The preparation of electrochromic, solvent-processable, thiophene-based poly-mers allowed electrode modification (e.g., upon spray casting) [539–541]. At the same time, the color of the film could be switched electrochemically. In addition, special derivatives of polyaniline [542] showed a multielectrochromic behavior (Fig. 48) [543, 544].

The "intramolecular" complexation of ruthenium complexes with a thiophene-based backbone could be modulated electrochemically [545]. On similar thiophene-based polymer electrodes, the ion flux and ion exchange into the polymer could be resolved by scanning ion conductance microscopy [546].

Composites of polypyrrole and polyols allowed the preparation of an electrode array that bent upon water sorption and generated a voltage output on piezoelectric contact [547]. However, this assembly was not directly based on electrochemical processes, but relied more on the dynamics of the composite generated by water vapor gradients, which was coupled to a piezoelectric output.

Besides rather conventional monomers [548–550], exotic monomers can also be electropolymerized [551]; e.g., electro-oxidation of magnesium porphine leads to polymer film formation [552]. Porphyrin derivatives can act as counterions in thiophene-derived electrode layers, which allowed oxygen evolution in sea water upon irradiation [553]. The preparation of films of pyrrole with anthraquinone side groups was successful [554]. Layer-by-layer assemblies could be fixed by electro-chemical coupling of carbazoles [555]. The interaction of such organic electrode surfaces with biological molecules was investigated by force measurements using
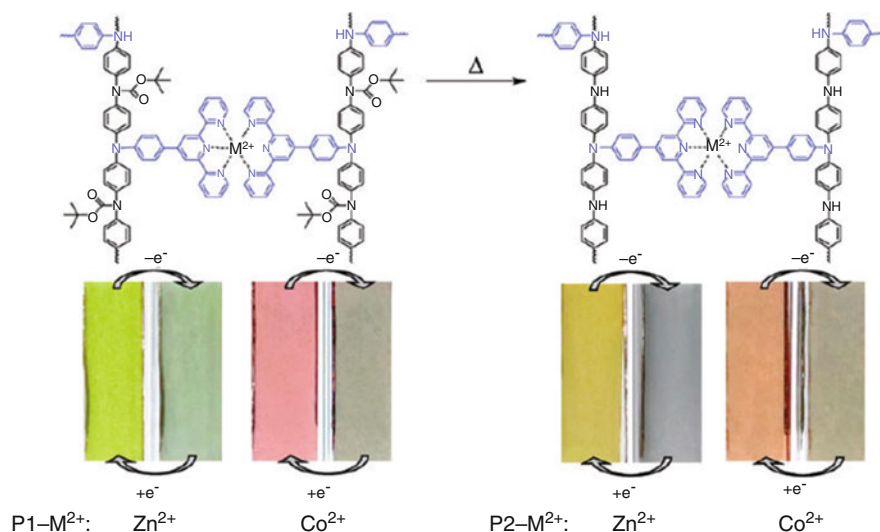
Fig. 48 Electrochromic films based on metal-complexed polyaniline derivatives (reprinted with permission from [544]. Copyright 2012 American Chemical Society)

atomic force microscopy (AFM) [556]. Sophisticated polymer structures could also be prepared by use of an electrochemical AFM setup. Here, thiophene derivatives (EDOT) could be polymerized into nanowires by electrochemical Dip-Pen Nanolithography [557]. A related investigation of hybrid electrode surfaces covered with polymer-grafted gold particles could be achieved using electrochemical AFM [558].

The electropolymerization of dopamine leads to conjugated polydopamine films, which can serve on electrodes as neural interfaces [559]. In some cases, the molecular design allowed the preparation of water sensors [549]. Also, β-cyclodextrin can be electropolymerized with the formation of thin films [560]. Electropolymerized pyrrole served for actuating purposes [561–563] and films of electropolymerized monomers could be modified with polymer grafts (Fig. 49) [564, 565].

A functional pyrrole and thiophene-containing monomer was equipped with an initiator for atom transfer radical polymerization (ATRP). The underlying conducting polymer layer allowed conformational changes in polyzwitterionic or polyampholytic brushes, leading to changes in hydrophilicity of the surface (Fig. 50) [566, 567].

Electrodes covered with conducting polymers could be site-selectively modified using a polymer-analogous click reaction [568, 569]. Gradient structures were also obtained on bipolar electrodes, which were covered with electrochemically reducing/oxidizing polyfluorenes [570]. Modified electrodes with deposited nanotube/graphene oxide [571, 572] conducting films and hydrogels were used, e.g., for drug release applications, which are reviewed elsewhere [37, 573–575].
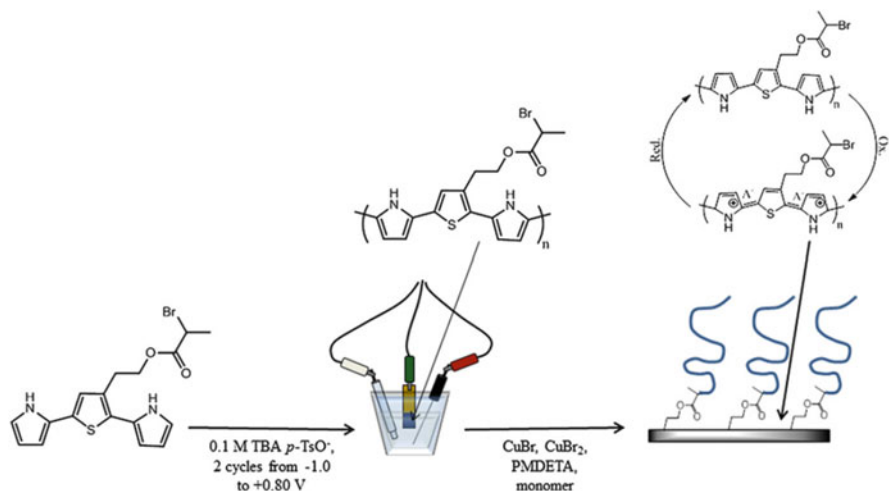
Fig. 49 Electropolymerization of an initatior for atom transfer radical polymerization; the resulting macroinitiator is employed for preparation of polymer-grafted electrodes with an electroactive polythiophene anchor (reprinted from Strover LT, Malmstrom J, Laita O, Reynisson J, Aydemir N, Nieuwoudt MK, Williams DE, Dunbar PR, Brimble MA, Travas-Sejdic J (2013) A new precursor for conducting polymer- based brush interfaces with electroactivity in aqueous solution. Polymer 54:1305–1317. Copyright 2013, with permission from Elsevier [564])
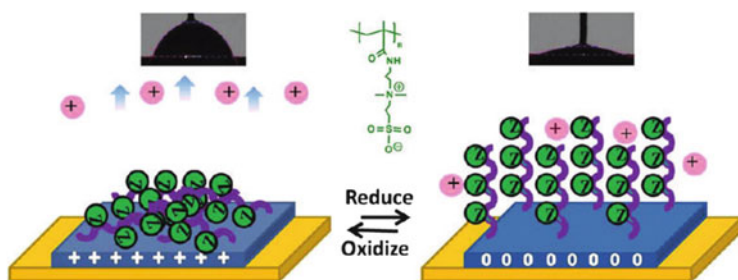
Fig. 50 Polyzwitterionic brushes change conformation in response to a change in the redox state of an underlying polpyrrole film; the water contact angle changes with applied potential (reprinted with permission from [566]. Copyright 2012 American Chemical Society)

Coordinating Metal Centers

Plasma-polymerized vinylferrocene was one of the first electrode coatings developed [576, 577]. Using a radiotracer method, the uptake/release of counterions into similar electrode coatings upon oxidation/reduction could be investigated [527]. Recently, two charge transport mechanisms were found in thin ferrocene-containing composite films (electron hopping and bounded diffusion) [578].
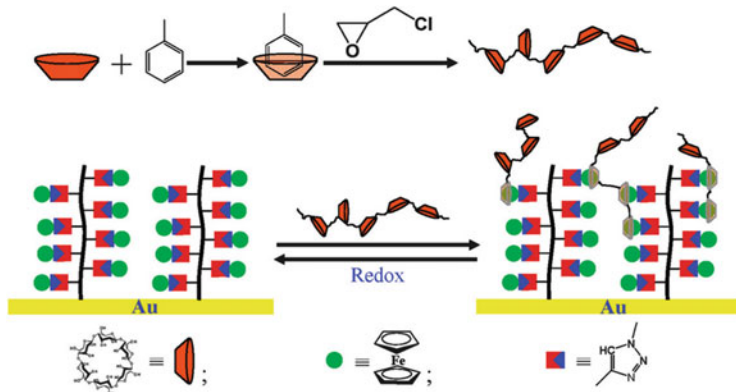
Fig. 51 Reversible attachment of a cyclodextrin polymer onto a ferrocene-modified electrode (reprinted with permission from [583]. Copyright 2010 American Chemical Society)

Ferrocene units were tethered to electrodes by telechelic poly(ethylene oxide) [579] and showed preferential adsorption of pyrene end groups to highly oriented pyrolytic graphite [580]. Ferrocene-based polymer brushes were grafted from conducting surfaces, which imparted special electrochemical behavior [581–584]; e.g., the interaction of these surfaces with cyclodextrin could be modulated by electrochemical means (Fig. 51) [583, 585].

Layer-by-layer assemblies of ferrocene-based polymers allowed the release of co-embedded guest molecules by electrochemical disassembly and the control of cell adhesion [586–591]. Covalently bound multilayers were used for sensing [592]. In accordance, complex multilayer sandwich-type electrode coatings were prepared by the Langmuir–Blodgett technique from ferrocene-containing and ruthenium-containing air–water interfaces [593, 594]. Besides a rectification behavior [595], the electrochemistry of the outer iron-containing layers was determined by the surface pressure during the deposition of ruthenium-containing inner layers. Charge could be stored in the outer layers, and discharge was possible by photoinduced electron transfer [596]. Other advanced electrode modifications with ferrocene are known, e.g., liquid-crystalline ferrocene-based thin electrode films [597]. Also, electron transport via ferrocene coatings on the interior of defined pores is very dependent on the spacer between the ferrocene unit and pore wall. Pores were established in block-copolymer thin films on gold electrodes [598]. The accessibility of pores could be modulated by the oxidation state of the ferrocene-containing polymers [599].

Thin hydrogel films made of ferrocene-modified poly(ethylene imine) with embedded enzymes can act as biosensors for glucose [600, 601]. Similarly, other glucose-dependent biosensors have been constructed [602–604]; e.g., a poly (vinylferrocene)–enzyme composite deposited on an electrode acted as a mediator for glucose oxidation [605–610]. Immunosensors were realized on glassy carbon electrodes by ferrocene-dendrimer-modified antibodies, which quench electrochemiluminescence [611].

The friction and the adhesion forces of ferrocene-containing polymer films was investigated as a function of the oxidation state using electrochemical atomic force microscopy [612].

Thin films of polymeric ruthenium complexes were constructed that could – depending on the ligand chemistry – show reversible or irreversible electrochromism [613, 614] or electrogenerated chemiluminescence [615].

Bound ruthenium complexes within multilayers allowed the examination of charge hopping, showing modulated electrochemistry that depended on the outermost layer [616]. Ruthenium complexes were also used as mediators for the electrochemical reaction of hexacyanoferrates. By use of the hydrodynamically modulated rotating disk electrode technique, the electrochemical redox of the metallates could be resolved from the redox processes occurring in the films [617–619]. Other complexes were also oxidized by a mediated electrode process [620, 621]. A glucose sensor was developed using an osmium bipyridine-containing polymer coating [622, 623]. Not only poly(vinyl pyridine)-based polymers were used; poly(allylamine) complexes containing osmium are known for allowing a redox-driven swelling in multilayers with enzymes or other polyanions [624–630]. Poly(vinyl imidazole) acted as an efficient anchor for the ruthenium complexes [631].

Metal complexes with, e.g., phenantroline derivatives, could be (electro-) polymerized to form electroactive films [203, 632–637]. Polymeric complexes of nickel allowed a switching of the mechanical properties of the film according to the redox state and the presence of barium ions [638]. Dissolution of sacrificial metal electrodes into electrolytes containing chelating polymer provided the desired electroactive films [639, 640]. Even mixed metal polymers (containing, e.g., Pd and Cu) have been constructed, which are very useful for catalytic purposes [194].

3 General Conclusion

In conclusion, it can be anticipated that new effects and interesting applications can be found for the huge number of uninvestigated patterns of electrochemical manipulation of polymers. In particular, the exploration of the numerous polyelectrolyte–counterion combinations that have not been addressed so far by electrochemical means, might open up new possibilities. Charge-transfer complexation might also gain importance. Catalysis by electrode films and control of micellar morphologies are just two further aspects that merit future attention. A challenge for researchers is the improvement of the time scale for bulk conversions, while electrochemical transformation of thin films allows rapid switching. As a possible future aim, feedback-controlled rheology manipulation as part of damping devices might be possible using electrochemical means, if the switching times approach the millisecond range. The addressability of all redox active sites needs to be verified, especially for larger gel samples or polymer self-assemblies. Otherwise, a part might be hidden in the interior of the structure. In these cases, the use of redox mediators might help to overcome the problem. In some cases, the use of chemical

Table 2 Typical organometallic, redox-active units used for electroactive polymers
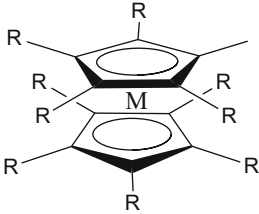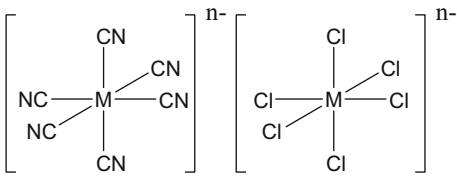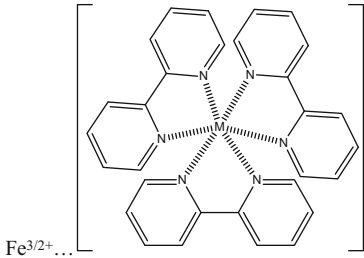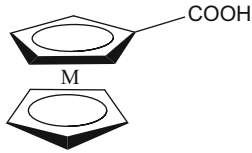
Name	Structure
Metallocenes	and related structures
Complexes with terpyridines, phenanthrolins, etc.	And related structures with nitrogen–metal interactions

R indicates a proper location for binding to a polymer

Table 3 Typical small electro-active species in interaction with polymers and polyelectrolytes

Name	Structure
Metallates	
Metal cations	and related structures
Metallocenes for complexation	and related structures
Protons	H^+

redox might then be the method of choice, allowing redox manipulation without considering the distance and the effective electron transfer between electrode and electroactive sites. The chemical stability of, e.g., ferrocene-containing polymers after oxidation, is also an issue that needs to be addressed in order to establish long-lasting, reversible systems with numerous switching events. However, there is no common optimum approach to all problems in the field. In general, a number of different redox-active groups have been shown to be suitable entities (see Tables 1,

2, and 3) but the choice of switching principles needs to be clarified for each specific demand. In some cases, it can be beneficial to uncouple electron transfer and polymer by use of smaller electroactive, complexing entities (especially when the direct addressability is reduced). However, the overall concentration and the ratio between polymer and electroactive species needs to be adjusted to optimize the complexation equilibrium and, hence, the switching abilities. Furthermore, such binary systems are more difficult to recycle because the smaller ions are more volatile and the ratio of the two components might change in some application (e.g., during dialysis). If these points are detrimental, then direct attachment of redox-active sites might be preferred. As a final perspective, redox-sensitive hydrogen bonding might become important [641–645]. This review will hopefully stimulate further research in this interesting area.

References

1. Stuart MAC, Huck WTS, Genzer J, Müller M, Ober C, Stamm M, Sukhorukov GB, Szleifer I, Tsukruk VV, Urban M, Winnik F, Zauscher S, Luzinov I, Minko S (2010) Emerging applications of stimuli-responsive polymer materials. Nat Mater 9:101–113
2. Chen T, Ferris R, Zhang J, Ducker R, Zauscher S (2010) Stimulus-responsive polymer brushes on surfaces: transduction mechanisms and applications. Progr Polym Sci 35:94–112
3. Mittal V (2010) Synthesis of environmentally responsive polymers by atom transfer radical polymerization: generation of reversible hydrophilic and hydrophobic surfaces. Polymers 2:40–56
4. Liu X, Abbott NL (2009) Spatial and temporal control of surfactant systems. J Colloid Interface Sci 339:1–18
5. Brown P, Butts CP, Eastoe J (2013) Stimuli-responsive surfactants. Soft Matter 9:2365–2374
6. Plamper FA, McKee JR, Laukkanen A, Nykänen A, Walther A, Ruokolainen J, Aseyev V, Tenhu H (2009) Miktoarm stars of poly(ethylene oxide) and poly(dimethylaminoethyl methacrylate): manipulation of micellization by temperature and light. Soft Matter 5:1812–1821
7. Nguyen T-T-T, Turp D, Wagner M, Müllen K (2013) Photoswitchable conductivity in a rigidly dendronized salt. Angew Chem Int Ed Engl 52:669–673
8. Aseyev V, Tenhu H, Winnik FM (2011) Non-ionic thermoresponsive polymers in water. Adv Polym Sci 242:29–89
9. Lallana E, Tirelli N (2013) Oxidation-responsive polymers: which groups to use, how to make them, what to expect from them (biomedical applications). Macromol Chem Phys 214:143–158
10. Gracia R, Mecerreyes D (2013) Polymers with redox properties: materials for batteries, biosensors and more. Polym Chem 4:2206–2214
11. Sui X, Feng X, Hempenius MA, Vancso GJ (2013) Redox active gels: synthesis, structures and applications. J Mater Chem B 1:1658–1672
12. Qi S, Iida H, Liu L, Irle S, Hu W, Yashima E (2013) Electrical switching behavior of a [60] fullerene-based molecular wire encapsulated in a syndiotactic poly(methyl methacrylate) helical cavity. Angew Chem Int Ed Engl 52:1049–1053

13. Perera UGE, Ample F, Kersell H, Zhang Y, Vives G, Echeverria J, Grisolia M, Rapenne G, Joachim C, Hla SW (2013) Controlled clockwise and anticlockwise rotational switching of a molecular motor. Nat Nanotechnol 8:46–51

14. Iordache A, Oltean M, Milet A, Thomas F, Baptiste B, Saint-Aman E, Bucher C (2012) Redox control of rotary motions in ferrocene-based elemental ball bearings. J Am Chem Soc 134:2653–2671

15. Matyjaszewski K, Xia J (2001) Atom transfer radical polymerization. Chem Rev 101:2921–2990

16. Braunecker WA, Matyjaszewski K (2007) Controlled/living radical polymerization: features, developments, and perspectives. Progr Polym Sci 32:93–146

17. Chong YK, Le TPT, Moad G, Rizzardo E, Thang SH (1999) A more versatile route to block copolymers and other polymers of complex architecture by living radical polymerization: the RAFT process. Macromolecules 32:2071–2074

18. Plamper FA (2014) Polymerizations under electrochemical control. Colloid Polym Sci 292:777–783

19. Bahrenburg J, Renth F, Temps F, Plamper F, Richtering W (2014) Femtosecond spectroscopy reveals huge differences in the photoisomerisation dynamics between azobenzenes linked to polymers and azobenzenes in solution. Phys Chem Chem Phys 16:11549–11554

20. Plamper FA, Walther A, Müller AHE, Ballauff M (2007) Nanoblossoms: light-induced conformational changes of cationic polyelectrolyte stars in the presence of multivalent counterions. Nano Lett 7:167–171

21. Plamper FA, Schmalz A, Ballauff M, Müller AHE (2007) Tuning the thermoresponsiveness of weak polyelectrolytes by pH and light: lower and upper critical-solution temperature of poly(N, N-dimethylaminoethyl methacrylate). J Am Chem Soc 129:14538–14539

22. Murray RW (1984) Polymer modification of electrodes. Annu Rev Mater Sci 14:145–169

23. Imisides MD, John R, Riley PJ, Wallace GG (1991) The use of electropolymerization to produce new sensing surfaces: a review emphasizing electrodeposition of heteroaromatic compounds. Electroanalysis 3:879–889

24. Kuwabata S, Yoneyama H (2007) Organic polymer modified electrodes. Encycl Electrochem 11:413–426

25. Podlovchenko BI, Andreev VN (2002) Electrocatalysis on polymer-modified electrodes. Russ Chem Rev 71:837–851

26. Bredas J-L, Beljonne D, Coropceanu V, Cornil J (2004) Charge-transfer and energy-transfer processes in π-conjugated oligomers and polymers: a molecular picture. Chem Rev 104:4971–5003

27. Venkataraman D, Russell TP (2012) Polymer electronics: power from polymers. J Polym Sci Part B Polym Phys 50:1013

28. Kola S, Sinha J, Katz HE (2012) Organic transistors in the new decade: toward n-channel, printed, and stabilized devices. J Polym Sci Part B Polym Phys 50:1090–1120

29. Liu F, Gu Y, Jung JW, Jo WH, Russell TP (2012) On the morphology of polymer-based photovoltaics. J Polym Sci Part B Polym Phys 50:1018–1044

30. Mike JF, Lutkenhaus JL (2013) Electrochemically active polymers for electrochemical energy storage: opportunities and challenges. ACS Macro Lett 2:839–844

31. Tseng RJ, Huang J, Ouyang J, Kaner RB, Yang Y (2005) Polyaniline nanofiber/gold nanoparticle nonvolatile memory. Nano Lett 5:1077–1080

32. Senthilkumar ST, Selvan RK, Melo JS (2013) Redox additive/active electrolytes: a novel approach to enhance the performance of supercapacitors. J Mater Chem A 1:12386–12394

33. Napoli A, Valentini M, Tirelli N, Müller M, Hubbell JA (2004) Oxidation-responsive polymeric vesicles. Nat Mater 3:183–189

34. Nayak S, Gan D, Serpe MJ, Lyon LA (2005) Hollow thermoresponsive microgels. Small 1:416–421

35. Meng F, Hennink WE, Zhong Z (2009) Reduction-sensitive polymers and bioconjugates for biomedical applications. Biomaterials 30:2180–2198

36. Bang E-K, Lista M, Sforazzini G, Sakai N, Matile S (2012) Poly(disulfide)s. Chem Sci 3:1752–1763
37. Huo M, Yuan J, Tao L, Wei Y (2014) Redox-responsive polymers for drug delivery: from molecular design to applications. Polym Chem 5:1519–1528
38. Chailapakul O, Fujishima A, Tipthara P, Siriwongchai H (2001) Electroanalysis of glutathione and cephalexin using the boron-doped diamond thin-film electrode applied to flow injection analysis. Anal Sci 17(ICAS2001):i419–i422
39. Xu H, Sun W, Zhu H, Du F, Liu F, Xu Y, He Y (2013) Design of electrochemical detection of thiols based on the cleavage of the disulfide bond coupled with thionine modified gold nanoparticle-assisted amplification. Chem Commun 49:9603–9605
40. Szajewski RP, Whitesides GM (1980) Rate constants and equilibrium constants for thiol-disulfide interchange reactions involving oxidized glutathione. J Am Chem Soc 102:2011–2026
41. Factor A, Heinsohn GE (1971) Polyviologens - a novel class of cationic polyelectrolyte redox polymers. J Polym Sci Part B 9:289–295
42. Simon MS, Moore PT (1975) Novel polyviologens. Photochromic redox polymers with film-forming properties. J Polym Sci Polym Chem Ed 13:1–16
43. Lin F, Cheng SZD, Harris FW (2002) Aromatic poly(pyridinium salt)s. Part 3. Photoreduction in amide solvents. Polymer 43:3421–3430
44. Kamogawa H, Mizuno H, Todo Y, Nanasawa M (1979) Syntheses of polymerizable viologens bearing a terminal vinyl group. J Polym Sci Polym Chem Ed 17:3149–3157
45. Gao L-P, Ding G-J, Li C-L, Wang Y-C (2011) Photochromic and electrochromic performances of new types of donor/acceptor systems based on crosslinked polyviologen film and electron donors. Appl Surf Sci 257:3039–3046
46. Avram E, Lacatus C, Mocanu G (2001) Polymers with pendent functional groups VII. Polysaccharide derivatives containing viologen groups. Eur Polym J 37:1901–1906
47. Wadhwa K, Nuryyeva S, Fahrenbach AC, Elhabiri M, Platas-Iglesias C, Trabolsi A (2013) Intramolecular redox-induced dimerization in a viologen dendrimer. J Mater Chem C 1:2302–2307
48. Zhou C, Tian J, Wang J-L, Zhang D-W, Zhao X, Liu Y, Li Z-T (2013) A three-dimensional cross-linking supramolecular polymer stabilized by the cooperative dimerization of the viologen radical cation. Polym Chem 5:341–345
49. Dalton EF, Murray RW (1991) Viologen(2+/1+) and viologen(1+/0) electron-self-exchange reactions in a redox polymer. J Phys Chem 95:6383–6389
50. Raymo FM, Alvarado RJ (2004) Electron transport in bipyridinium films. Chem Rec 4:204–218
51. Nagarale RK, Bhattacharya B, Jadhav NA, Singh PK (2011) Synthesis and electrochemical study of a functional ionic polymer. Macromol Chem Phys 212:1751–1757
52. Laschewsky A (1995) Molecular concepts, self-organization and properties of polysoaps. Adv Polym Sci 124:1–86
53. Anton P, Heinze J, Laschewsky A (1993) Redox-active monomeric and polymeric surfactants. Langmuir 9:77–85
54. Anton P, Laschewsky A, Ward MD (1995) Solubilization control by redox-switching of polysoaps. Polym Bull 34:331–335
55. Yamaguchi I, Mizoguchi N, Sato M (2009) Self-doped polyphenylenes containing electron-accepting viologen side group. Macromolecules 42:4416–4425
56. Ko HC, Park S-A, Paik W-K, Lee H (2002) Electrochemistry and electrochromism of the polythiophene derivative with viologen pendant. Synth Met 132:15–20
57. Guo D-S, Chen S, Qian H, Zhang H-Q, Liu Y (2010) Electrochemical stimulus-responsive supramolecular polymer based on sulfonatocalixarene and viologen dimers. Chem Commun 46:2620–2622

58. Ma X, Sun R, Li W, Tian H (2011) Novel electrochemical and pH stimulus-responsive supramolecular polymer with disparate pseudorotaxanes as relevant unimers. Polym Chem 2:1068–1070
59. Moon K, Grindstaff J, Sobransingh D, Kaifer AE (2004) Cucurbit[8]uril-mediated redox-controlled self-assembly of viologen-containing dendrimers. Angew Chem Int Ed 43:5496–5499
60. Wang P, Martin BD, Parida S, Rethwisch DG, Dordick JS (1995) Multienzymic synthesis of poly(hydroquinone) for use as a redox polymer. J Am Chem Soc 117:12885–12886
61. Yamamoto T, Kimura T, Shiraishi K (1999) Preparation of pi-conjugated polymers composed of hydroquinone, p-benzoquinone, and p-diacetoxyphenylene units. Optical and redox properties of the polymers. Macromolecules 32:8886–8896
62. Yamamoto T, Kimura T (1998) Preparation of pi-conjugated poly(hydroquinone-2,5-diyl) and poly(p-benzoquinone-2,5-diyl) and their electrochemical behavior. Macromolecules 31:2683–2685
63. Schroeter M, Behl M, Kaiser C, Lendlein A (2013) Synthesis and properties of poly (p-phenylene ethynylene)s with oxidation- and reduction-sensitive moieties. Macromol Chem Phys 214:1215–1224
64. Takada K, Gopalan P, Ober CK, Abruna HD (2001) Synthesis, characterization, and redox reactivity of novel quinone-containing polymer. Chem Mater 13:2928–2932
65. Moulay S, Mehdaoui R (2004) Hydroquinone/catechol-bearing polyacrylic acid: redox polymer. React Funct Polym 61:265–275
66. Gupta SK, Weber WP (2000) Synthesis and electrochemistry of copoly(dimethylanthraquinonylene/3,3,5,5-tetramethyl-4-oxa-3,5-disila-1,7-heptanylenes). Macromolecules 33:108–114
67. Allen NS, Hurley JP, Rahman A, Follows GW, Weddell I (1993) Synthesis, properties and photocuring behavior of poly(2-acrylamido-anthraquinone). Eur Polym J 29:1155–1160
68. Yamamoto T, Shiraishi K (1998) Preparation of new main-chain-type polyquinones and their electrochemical response. Chem Lett 27(9):895–896
69. Hall HK Jr, Padias AB, Williams PA, Gosau J-M, Boone HW, Park D-K (1995) Novel polyaromatic quinone imines. Macromolecules 28:1–8
70. Yamamoto T, Etori H (1995) Poly(anthraquinone)s having a π-conjugation system along the main chain. Synthesis by organometallic polycondensation, redox behavior, and optical properties. Macromolecules 28:3371–3379
71. Kenny T, Aly SM, Brisard G, Fortin D, Harvey PD (2013) The Pt-organometallic version of perigraniline: going blue. Macromol Rapid Commun 34:511–515
72. Oyaizu K, Hatemata A, Choi W, Nishide H (2010) Redox-active polyimide/carbon nanocomposite electrodes for reversible charge storage at negative potentials: expanding the functional horizon of polyimides. J Mater Chem 20:5404–5410
73. Milczarek G, Inganäs O (2012) Renewable cathode materials from biopolymer/conjugated polymer interpenetrating networks. Science 335:1468–1471
74. Algharaibeh Z, Pickup PG (2013) Charge trapping in poly(1-amino-anthraquinone) films. Electrochim Acta 93:87–92
75. Choi W, Endo S, Oyaizu K, Nishide H, Geckeler KE (2013) Robust and efficient charge storage by uniform grafting of TEMPO radical polymer around multi-walled carbon nanotubes. J Mater Chem A 1:2999–3003
76. Anton P, Koeberle P, Laschewsky A (1992) Structure and properties of zwitterionic polysoaps: functionalization by redox-switchable moieties. Progr Colloid Polym Sci 89:56–59
77. Nielsen MB, Lomholt C, Becher J (2000) Tetrathiafulvalenes as building blocks in supramolecular chemistry II. Chem Soc Rev 29:153–164
78. Martin N (2013) Tetrathiafulvalene: the advent of organic metals. Chem Commun 49:7025–7027

79. Inagi S, Naka K, Chujo Y (2007) Functional polymers based on electron-donating TTF and derivatives. J Mater Chem 17:4122–4135
80. Wang C, Chen Q, Sun F, Zhang D, Zhang G, Huang Y, Zhao R, Zhu D (2010) Multistimuli responsive organogels based on a new gelator featuring tetrathiafulvalene and azobenzene groups: reversible tuning of the gel–sol transition by redox reactions and light irradiation. J Am Chem Soc 132:3092–3096
81. Bigot J, Charleux B, Cooke G, Delattre F, Fournier D, Lyskawa J, Sambe L, Stoffelbach F, Woisel P (2010) Tetrathiafulvalene end-functionalized poly(N-isopropylacrylamide): a new class of amphiphilic polymer for the creation of multistimuli responsive micelles. J Am Chem Soc 132:10796–10801
82. Coffen DL, Chambers JQ, Williams DR, Garrett PE, Canfield ND (1971) Tetrathioethylenes. J Am Chem Soc 93:2258–2268
83. Le Van H, Schukat G, Fanghaenel E, Libera L (1979) Tetrathiafulvalenes. VIII. Ethylene-bridged polymeric tetrathiafulvalenes. J Prakt Chem 321:475–487
84. Pittman CU Jr, Liang Y-F, Ueda M (1979) Synthesis of polyesters containing tetrathia-fulvalene groups in the backbone. Macromolecules 12:355–359
85. Trinh VQ, Van Hinh L, Schukat G, Fanghaenel E (1989) Tetrathiafulvalenes. XXV. Conjugatively connected polymeric tetrathiafulvalenes (TTF). J Prakt Chem 331:826–834
86. Le Van H, Schukat G, Fanghaenel E (1979) Tetrathiafulvalenes. VII. Arylene-bridged polymeric tetrathiafulvalenes. J Prakt Chem 321:299–307
87. Roth HK, Krinichnyi VI (1993) ESR studies on polymers with particular electronic and magnetic properties. Macromol Chem Macromol Symp 72:143–159
88. Gruber H, Patzsch J, Schrodner M, Roth HK, Fanghaenel E (1991) Electrical properties of poly(tetrathiafulvalenes). Synth Met 42:2331–2334
89. Gruber H, Bartl A, Doege HG, Bauriegel L, Schubert G, Patzsch J (1991) Redox properties of poly(tetrathiafulvalenes). Synth Met 43:3025–3028
90. Frenzel S, Arndt S, Gregorious RM, Müllen K (1995) Synthesis of tetrathiafulvalene poly-mers. J Mater Chem 5:1529–1537
91. Hertler WR (1976) Charge-transfer polymers containing 7,7,8,8-tetracyanoquinodimethan and tetrathiafulvalene. J Org Chem 41:1412–1416
92. Hou Y, Wan X, Yang M, Ma Y, Huang Y, Chen Y (2008) A novel poly(aryleneethynylene) with tetrathiafulvalene (TTF) side chains: synthesis, self-assembly, and electroactive prop-erty. Macromol Rapid Commun 29:719–723
93. Inagi S, Naka K, Iida D, Chujo Y (2006) Synthesis of electron-donating polymer having vinylogous TTF in the main chain. Polym J 38:1146–1151
94. Pittman CU Jr, Narita M, Liang YF (1976) Synthesis of tetrathiafulvalene-containing poly-amides. Macromolecules 9:360–361
95. Zhang X-C, Zhang Y, Wang C-Y, Lai G-Q, Zhang L, Shen Y-J (2009) Fluorene oligomer with tetrathiafulvalenes as pendant groups: synthesis, electrochemical and spectroscopic properties. Polym Bull 63:815–827
96. Liu Y, Wang C, Li M, Lai G, Shen Y (2008) Synthesis and spectroscopic and electrochemical properties of TTF-derivatized polycarbazole. Macromolecules 41:2045–2048
97. Kanibolotsky AL, Forgie JC, Gordeyev S, Vilela F, Skabara PJ, Lohr JE, Petersen BM, Jeppesen JO (2008) The introduction of pyrrolotetrathiafulvalene into conjugated architec-tures: synthesis and electronic properties. Macromol Rapid Commun 29:1226–1230
98. Skabara PJ, Berridge R, McInnes EJL, West DP, Coles SJ, Hursthouse MB, Müllen K (2004) The electroactivity of tetrathiafulvalene vs. polythiophene: synthesis and characterization of a fused thieno-TTF polymer. J Mater Chem 14:1964–1969
99. Huchet L, Akoudad S, Levillain E, Roncali J, Emge A, Baeuerle P (1998) Spectroelectro-chemistry of electrogenerated tetrathiafulvalene-derivatized poly(thiophenes): toward a rational design of organic conductors with mixed conduction. J Phys Chem B 102:7776–7781

100. Bryce MR, Chissel AD, Gopal J, Kathirgamanathan P, Parker D (1991) Towards highly oriented polythiophenes incorporating mesogenic or tetrathiafulvalene substituents. Synth Met 39:397–400
101. Yamamoto T, Shimizu T (1997) New π-conjugated polymers containing tetrathiafulvalene as the monomeric unit. J Mater Chem 7:1967–1968
102. Shimizu T, Yamamoto T (1999) Preparation of a new poly(arylacetylene) with a tetrathiafulvalene (TTF) unit in the side chain. Chem Commun 1999(6):515–516
103. Divisia-Blohorn B, Genoud F, Salhi F, Mueller H (2002) Poly(dibenzylidenetetrathiapentalene): a redox-active, linearly extended TTF polymer. J Phys Chem B 106:6646–6651
104. Bigot J, Charleux B, Cooke G, Delattre F, Fournier D, Lyskawa J, Stoffelbach F, Woisel P (2010) Synthesis and properties of tetrathiafulvalene end-functionalized polymers prepared via RAFT polymerization. Macromolecules 43:82–90
105. Sambe L, Belal K, Stoffelbach F, Lyskawa J, Delattre F, Bria M, Sauvage FX, Sliwa M, Humblot V, Charleux B, Cooke G, Woisel P (2014) Multi-stimuli responsive supramolecular diblock copolymers. Polym Chem 5:1031–1036
106. Naka K, Inagi S, Chujo Y (2005) Synthesis of soluble electron-donating polymers containing vinylogous TTF by oxidative dimerization of 1,4-bisdithiafulvenyl-2,5-dialkoxybenzene. J Polym Sci Part A Polym Chem 43:4600–4608
107. Naka K, Uemura T, Chujo Y (2001) Alternating pi-conjugated copolymer of dithiafulvene with 2,2′-bipyridyl units. J Polym Sci Part A Polym Chem 39:4083–4090
108. Wang X, Naka K, Itoh H, Uemura T, Chujo Y (2003) Preparation of oriented ultrathin films via self-assembly based on charge transfer interaction between pi-conjugated poly (dithiafulvene) and acceptor polymer. Macromolecules 36:533–535
109. Lupinski JH, Kopple KD (1964) Electroconductive polymers. Science 146:1038–1039
110. Francis CV, Joo P, Chambers JQ (1987) Electrochemistry of polyurethanes containing tetracyanoquinodimethane units in the polymer backbone. J Phys Chem 91:6315–6321
111. Huang W, Han CD (2012) Synthesis and intramolecular charge-transfer interactions of a donor-acceptor type polymer containing ferrocene and TCNAQ moieties. Macromolecules 45:4425–4428
112. Itoh T, Mitsuda Y, Nakasaka K, Uno T, Kubo M, Yamamoto O (2006) Solid polymer electrolytes based on comblike polymers. J Power Sources 163:252–257
113. Gervaldo M, Liddell PA, Kodis G, Brennan BJ, Johnson CR, Bridgewater JW, Moore AL, Moore TA, Gust D (2010) A photo- and electrochemically-active porphyrin-fullerene dyad electropolymer. Photochem Photobiol Sci 9:890–900
114. Huang H-Y, Lee Y-T, Yeh L-C, Jian J-W, Huang T-C, Liang H-T, Yeh J-M, Chou Y-C (2013) Photoactively electroactive polyamide with azo group in the main chain via oxidative coupling polymerization. Polym Chem 4:343–350
115. Yurchenko O, Freytag D, Zur Borg L, Zentel R, Heinze J, Ludwigs S (2012) Electrochemically induced reversible and irreversible coupling of triarylamines. J Phys Chem B 116:30–39
116. Schroot R, Friebe C, Altuntas E, Crotty S, Jäger M, Schubert US (2013) Nitroxide-mediated polymerization of styrenic triarylamines and chain-end functionalization with a ruthenium complex: toward tailored photoredox-active architectures. Macromolecules 46:2039–2048
117. Mangione MI, Spanevello RA, Rumbero A, Heredia D, Marzari G, Fernandez L, Otero L, Fungo F (2013) Electrogenerated conductive polymers from triphenylamine end-capped dendrimers. Macromolecules 46:4754–4763
118. Kim K, Fang Y-K, Kwon W, Pyo S, Chen W-C, Ree M (2013) Tunable electrical memory characteristics of brush copolymers bearing electron donor and acceptor moieties. J Mater Chem C 1:4858–4868
119. Richter TV, Buehler C, Ludwigs S (2012) Water- and ionic-liquid-soluble branched polythiophenes bearing anionic and cationic moieties. J Am Chem Soc 134:43–46

120. Yang R, Chao D, Liu H, Berda EB, Wang S, Jia X, Wang C (2013) Synthesis, electrochemical properties and inhibition performance of water-soluble self-doped oligoaniline derivative. Electrochim Acta 93:107–113

121. Chen R, Benicewicz BC (2003) Preparation and properties of poly(methacrylamide)s containing oligoaniline side chains. Macromolecules 36:6333–6339

122. Wang S, Berda EB, Lu X, Li X, Wang C, Chao D (2013) Tuning the fluorescent response of a novel electroactive polymer with multiple stimuli. Macromol Rapid Commun 34:1648–1653

123. Henson ZB, Zhang Y, Nguyen T-Q, Seo JH, Bazan GC (2013) Synthesis and properties of two cationic narrow band Gap conjugated polyelectrolytes. J Am Chem Soc 135:4163–4166

124. Janoschka T, Hager MD, Schubert US (2012) Powering up the future: radical polymers for battery applications. Adv Mater 24:6397–6409

125. Hauffman G, Maguin Q, Bourgeois J-P, Vlad A, Gohy J-F (2013) Micellar cathodes from self-assembled nitroxide-containing block copolymers in battery electrolytes. Macromol Rapid Commun 51:101–108

126. Rostro L, Baradwaj AG, Boudouris BW (2013) Controlled radical polymerization and quantification of solid state electrical conductivities of macromolecules bearing pendant stable radical groups. ACS Appl Mater Interfaces 5:9896–9901

127. Lu J-J, Ma J-Q, Yi J-M, Shen Z-L, Zhong Y-J, Ma C-A, Li M-C (2014) Electrochemical polymerization of pyrrole containing TEMPO side chain on Pt electrode and its electrochemical activity. Electrochim Acta 130:412–417

128. Son S, Namgung R, Kim J, Singha K, Kim WJ (2012) Bioreducible polymers for gene silencing and delivery. Acc Chem Res 45:1100–1112

129. Fluharty AL (1974) Biochemistry of the thiol group. Thiol Group 2:589–668

130. Grzelczak M, Vermant J, Furst EM, Liz-Marzan LM (2010) Directed self-assembly of nanoparticles. ACS Nano 4:3591–3605

131. Kleijn SEF, Lai SCS, Koper MTM, Unwin PR (2014) Electrochemistry of nanoparticles. Angew Chem Int Ed 53:3558–3586

132. Whittell GR, Manners I (2007) Metallopolymers: new multifunctional materials. Adv Mater 19:3439–3468

133. Wang X, McHale R (2010) Metal-containing polymers: building blocks for functional (nano) materials. Macromol Rapid Commun 31:331–350

134. Lehn JM (1988) Supramolecular chemistry - molecules, supermolecules, and molecular functional units (Nobel lecture). Angew Chem 100:91–116

135. Lehn J-M (2002) Supramolecular polymer chemistry-scope and perspectives. Polym Int 51:825–839

136. Hudson RDA (2001) Ferrocene polymers: current architectures, syntheses and utility. J Organomet Chem 637–639:47–69

137. Herfurth C, Voll D, Buller J, Weiss J, Barner-Kowollik C, Laschewsky A (2012) Radical addition fragmentation chain transfer (RAFT) polymerization of ferrocenyl (Meth)acrylates. J Polym Sci Part A Polym Chem 50:108–118

138. Tonhauser C, Mazurowski M, Rehahn M, Gallei M, Frey H (2012) Water-soluble poly (vinylferrocene)-b-poly(ethylene oxide) diblock and miktoarm star polymers. Macromolecules 45:3409–3418

139. Whittell GR, Hager MD, Schubert US, Manners I (2011) Functional soft materials from metallopolymers and metallosupramolecular polymers. Nat Mater 10:176–188

140. Hardy CG, Ren L, Zhang J, Tang C (2012) Side-chain metallocene-containing polymers by living and controlled polymerizations. Isr J Chem 52:230–245

141. Abd-El-Aziz AS, Agatemor C, Etkin N (2014) Sandwich complex-containing macromolecules: property tunability through versatile synthesis. Macromol Rapid Commun 35:513–559

142. Gallei M (2014) The renaissance of side-chain ferrocene-containing polymers: scope and limitations of vinylferrocene and ferrocenyl methacrylates. Macromol Chem Phys 215:699–704

143. Gul A, Akhter Z, Siddiq M, Sarfraz S, Mirza B (2013) Ferrocene-based aliphatic and aromatic poly(azomethine)esters: synthesis, physicochemical studies, and biological evaluation. Macromolecules 46:2800–2807

144. Manners I (1999) Poly(ferrocenylsilanes): novel organometallic plastics. Chem Commun 1999(10):857–865

145. Nguyen MT, Diaz AF, Dement'ev VV, Pannell KH (1993) High molecular weight poly(ferrocenediyl-silanes): synthesis and electrochemistry of [−(C5H4)Fe(C5H4)SiR2-]n, R = Me, Et, n-Bu, n-Hex. Chem Mater 5:1389–1394

146. Rulkens R, Lough AJ, Manners I, Lovelace SR, Grant C, Geiger WE (1996) Linear oligo (ferrocenyldimethylsilanes) with between two and nine ferrocene units: electrochemical and structural models for poly(ferrocenylsilane) high polymers. J Am Chem Soc 118:12683–12695

147. Nelson JM, Nguyen P, Petersen R, Rengel H, Macdonald PM, Lough AJ, Manners I, Raju NP, Greedan JE, Barlow S, O'Hare D (1997) Thermal ring-opening polymerization of hydrocarbon-bridged [2]ferrocenophanes: synthesis and properties of poly(ferrocenylethylene)s and their charge-transfer polymer salts with tetracyanoethylene. Chem Eur J 3:573–584

148. Zou S, Hempenius MA, Schönherr H, Vancso GJ (2006) Force spectroscopy of individual stimulus-responsive poly(ferrocenyldimethylsilane) chains: towards a redox-driven macromolecular motor. Macromol Rapid Commun 27:103–108

149. Zou S, Korczagin I, Hempenius MA, Schönherr H, Vancso GJ (2006) Single molecule force spectroscopy of smart poly(ferrocenylsilane) macromolecules: towards highly controlled redox-driven single chain motors. Polymer 47:2483–2492

150. Wang X, Guerin G, Wang H, Wang Y, Manners I, Winnik MA (2007) Cylindrical block copolymer micelles and co-micelles of controlled length and architecture. Science 317:644–647

151. Gaedt T, Ieong NS, Cambridge G, Winnik MA, Manners I (2009) Complex and hierarchical micelle architectures from diblock copolymers using living, crystallization-driven polymerizations. Nat Mater 8:144–150

152. Gilroy JB, Gaedt T, Whittell GR, Chabanne L, Mitchels JM, Richardson RM, Winnik MA, Manners I (2010) Monodisperse cylindrical micelles by crystallization-driven living self-assembly. Nat Chem 2:566–570

153. Flanagan JB, Margel S, Bard AJ, Anson FC (1978) Electron transfer to and from molecules containing multiple, noninteracting redox centers. Electrochemical oxidation of poly (vinylferrocene). J Am Chem Soc 100:4248–4253

154. Smith TW, Kuder JE, Wychick D (1976) Voltammetric behavior of poly(vinylferrocene). J Polym Sci Polym Chem Ed 14:2433–2448

155. Qi H, Chang J, Abdelwahed SH, Thakur K, Rathore R, Bard AJ (2012) Electrochemistry and electrogenerated chemiluminescence of π-stacked poly(fluorenemethylene) oligomers. Multiple, interacting electron transfers. J Am Chem Soc 134:16265–16274

156. Saji T, Pasch NF, Webber SE, Bard AJ (1978) Electrochemical behavior of polymers in aprotic media. 1. Polyvinylnaphthalene and polyvinylanthracene. J Phys Chem 82:1101–1105

157. Pendin AA, Leont'evskaya PK, Suverneva OL, Rozenkova IV, Nikol'skii BP (1987) Oxidative decomposition of ferrocenes (ferricenium cations) under the action of molecular oxygen. Dokl Akad Nauk SSSR 293:1411–1415

158. Zotti G, Schiavon G, Zecchin S, Favretto D (1998) Dioxygen-decomposition of ferrocenium molecules in acetonitrile: the nature of the electrode-fouling films during ferrocene electrochemistry. J Electroanal Chem 456:217–221

159. Tonhauser C, Alkan A, Schömer M, Dingels C, Ritz S, Mailänder V, Frey H, Wurm FR (2013) Ferrocenyl glycidyl ether: a versatile ferrocene monomer for copolymerization with ethylene oxide to water-soluble, thermoresponsive copolymers. Macromolecules 46:647–655

160. Bruna S, Gonzalez-Vadillo AM, Nieto D, Pastor CJ, Cuadrado I (2012) Redox-active macrocyclic and linear oligo-carbosiloxanes prepared via hydrosilylation from 1,3-divinyl-1,3-dimethyl-1,3-diferrocenyldisiloxane. Macromolecules 45:781–793

161. Mazurowski M, Gallei M, Li J, Didzoleit H, Stühn B, Rehahn M (2012) Redox-responsive polymer brushes grafted from polystyrene nanoparticles by means of surface initiated atom transfer radical polymerization. Macromolecules 45:8970–8981

162. Hardy CG, Ren L, Tamboue TC, Tang C (2011) Side-chain ferrocene-containing (meth) acrylate polymers: synthesis and properties. J Polym Sci Part A Polym Chem 49:1409–1420

163. Droulia M, Anastasaki A, Rokotas A, Pitsikalis M, Paraskevopoulou P (2011) Statistical copolymers of methyl methacrylate and 2-methacryloyloxyethyl ferrocenecarboxylate: monomer reactivity ratios, thermal and electrochemical properties. J Polym Sci Part A Polym Chem 49:3080–3089

164. Parab K, Jakle F (2009) Synthesis, characterization, and anion binding of redox-active triarylborane polymers. Macromolecules 42:4002–4007

165. Zamora M, Bruna S, Alonso B, Cuadrado I (2011) Polysiloxanes bearing pendant redox-active dendritic wedges containing ferrocenyl and (η6-aryl)tricarbonylchromium moieties. Macromolecules 44:7994–8007

166. Wang X-S, Winnik MA, Manners I (2004) Swellable, redox-active shell-crosslinked organometallic nanotubes. Angew Chem Int Ed 43:3703–3707

167. Garcia Armada MP, Losada J, Lopez-Villanueva FJ, Frey H, Alonso B, Casado CM (2008) Electrochemical and bioelectrocatalytical properties of novel block-copolymers containing interacting ferrocenyl units. J Organomet Chem 693:2803–2811

168. Chen T, Wang L, Jiang G, Wang J, Dong X, Wang X, Zhou J, Wang C, Wang W (2005) Electrochemical behavior of poly(ferrocenyldimethylsilane-b-dimethylsiloxane) films. J Phys Chem B 109:4624–4630

169. Mao X, Rutledge GC, Hatton TA (2013) Polyvinylferrocene for noncovalent dispersion and redox-controlled precipitation of carbon nanotubes in nonaqueous media. Langmuir 29:9626–9634

170. Ritter H, Mondrzik BE, Rehahn M, Gallei M (2010) Free radical homopolymerization of a vinylferrocene/cyclodextrin complex in water. Beilstein J Org Chem 6:60

171. Zuo F, Luo C, Ding X, Zheng Z, Cheng X, Peng Y (2008) Redox-responsive inclusion complexation between β-cyclodextrin and ferrocene-functionalized poly(N-isopropylacrylamide) and its effect on the solution properties of this polymer. Supramol Chem 20:559–564

172. Salmon A, Jutzi P (2001) Water soluble ferrocenyl and polyferrocenyl compounds: synthesis and electrochemistry. J Organomet Chem 637–639:595–608

173. Xiao A, Li Z, Zhou S, Zheng Q, Shen Y, Chen Z, Zheng W, Hao A (2012) Synthesis, electrochemical behaviors and anion recognition of a novel star-[polystyrene-b-poly (ferrocenyloxy ethyl acrylate)]6 with hexafunctional cyclotriphosphazene core. Polym Plast Technol Eng 51:521–525

174. Martos-Maldonado MC, Casas-Solvas JM, Quesada-Soriano I, Garcia-Fuentes L, Vargas-Berenguel A (2013) Poly(amido amine)-based mannose-glycodendrimers as multielectron redox probes for improving lectin sensing. Langmuir 29:1318–1326

175. Elbert J, Mersini J, Vilbrandt N, Lederle C, Kraska M, Gallei M, Stuehn B, Plenio H, Rehahn M (2013) Reversible activity modulation of surface-attached grubbs second generation type catalysts using redox-responsive polymers. Macromolecules 46:4255–4267

176. Kobayashi N, Anson FC (1997) Effects of adsorption and association with multiply charged counterions on the electrochemical responses of an electroactive polyelectrolyte. J Electroanal Chem 421:99–104

177. Hatozaki O, Anson FC (1997) Intramolecular electron transfer within a water-soluble, ferrocene-labeled polyacrylate. J Electroanal Chem 420:195–199

178. Zhou N, Zhang Z, Zhu J, Cheng Z, Zhu X (2009) RAFT polymerization of styrene mediated by ferrocenyl-containing RAFT agent and properties of the polymer derived from ferrocene. Macromolecules 42:3898–3905

179. Ren L, Zhang J, Hardy CG, Doxie D, Fleming B, Tang C (2012) Preparation of cobaltocenium-labeled polymers by atom transfer radical polymerization. Macromolecules 45:2267–2275

180. Ren L, Hardy CG, Tang S, Doxie DB, Hamidi N, Tang C (2010) Preparation of side-chain 18-e cobaltocenium-containing acrylate monomers and polymers. Macromolecules 43:9304–9310

181. Gilroy JB, Patra SK, Mitchels JM, Winnik MA, Manners I (2011) Main-chain heterobimetallic block copolymers: synthesis and self-assembly of polyferrocenylsilane-b-poly (cobaltoceniumethylene). Angew Chem Int Ed 50:5851–5855

182. Zhang J, Ren L, Hardy CG, Tang C (2012) Cobaltocenium-containing methacrylate homopolymers, block copolymers, and heterobimetallic polymers via RAFT polymerization. Macromolecules 45:6857–6863

183. Mayer UFJ, Gilroy JB, O'Hare D, Manners I (2009) Ring-opening polymerization of 19-electron [2]cobaltocenophanes: a route to high-molecular-weight, water-soluble polycobaltocenium polyelectrolytes. J Am Chem Soc 131:10382–10383

184. Feng C, Shen Z, Yang D, Li Y, Hu J, Lu G, Huang X (2009) Synthesis of well-defined amphiphilic graft copolymer bearing poly(2-acryloyloxyethyl ferrocenecarboxylate) side chains via successive SET-LRP and ATRP. J Polym Sci Part A Polym Chem 47:4346–4357

185. Zhai S, Shang J, Yang D, Wang S, Hu J, Lu G, Huang X (2012) Successive SET-LRP and ATRP synthesis of ferrocene-based PPEGMEA-g-PAEFC well-defined amphiphilic graft copolymer. J Polym Sci Part A Polym Chem 50:811–820

186. Xiao Z-P, Cai Z-H, Liang H, Lu J (2010) Amphiphilic block copolymers with aldehyde and ferrocene-functionalized hydrophobic block and their redox-responsive micelles. J Mater Chem 20:8375–8381

187. Kutnyánszky E, Hempenius MA, Vancso JG (2014) Polymer bottlebrushes with a redox responsive backbone feel the heat: synthesis and characterization of dual responsive poly (ferrocenylsilane)s with PNIPAM side chains. Polym Chem 5:771–783

188. de Denus CR, Baker P, Toner J, McKevitt S, Todd EK, Abd-El-Aziz AS (2003) Electrochemical investigations of oligomers and polymers containing ruthenium- and iron-arene complexes. Macromol Symp 196:113–123

189. Abd-El-Aziz AS (2002) Monomers, oligomers and polymers containing arenes with pendent transition metal moieties. Coord Chem Rev 233–234:177–191

190. Hoogenboom R, Schubert US (2006) The use of (metallo)supramolecular initiators for living/controlled polymerization techniques. Chem Soc Rev 35:622–629

191. Schubert US, Eschbaumer C (2002) Macromolecules containing bipyridine and terpyridine metal complexes: towards metallosupramolecular polymers. Angew Chem Int Ed 41:2892–2926

192. Lehn J-M (2010) Dynamers: dynamic molecular and supramolecular polymers. Aust J Chem 63:611–623

193. Happ B, Winter A, Hager MD, Schubert US (2012) Photogenerated avenues in macromolecules containing Re(I), Ru(II), Os(II), and Ir(III) metal complexes of pyridine-based ligands. Chem Soc Rev 41:2222–2255

194. Magdesieva TV, Nikitin OM, Yakimansky AV, Goikhman MY, Podeshvo IV (2011) New heterobimetallic Cu(I)-Pd(II)-containing polymer complexes: electrochemical synthesis and application in catalysis. Electrochim Acta 56:3666–3672

195. Ueki T, Shibayama M, Yoshida R (2013) Self-oscillating micelles. Chem Commun 49:6947–6949

196. Yoshida R, Takahashi T, Yamaguchi T, Ichijo H (1996) Self-oscillating gel. J Am Chem Soc 118:5134–5135

197. Breul AM, Schäfer J, Friebe C, Schlütter F, Paulus RM, Festag G, Hager MD, Winter A, Dietzek B, Popp J, Schubert US (2012) Synthesis and characterization of poly(methyl methacrylate) backbone polymers containing side-chain pendant ruthenium(II) bis-terpyridine complexes with an elongated conjugated system. Macromol Chem Phys 213:808–819

198. Brennan JL, Keyes TE, Forster RJ (2011) Electrochemical properties of ruthenium metallopolymer: monolayer-protected gold cluster nanocomposites. J Electroanal Chem 662:30–35

199. Leech D, Forster RJ, Smyth MR, Vos JG (1991) Effect of composition of polymer backbone on spectroscopic and electrochemical properties of ruthenium(II) bis(2,2′-bipyridyl)-containing 4-vinylpyridine/styrene copolymers. J Mater Chem 1:629–635

200. Wang L, Puodziukynaite E, Vary RP, Grumstrup EM, Walczak RM, Zolotarskaya OY, Schanze KS, Reynolds JR, Papanikolas JM (2012) Competition between ultrafast energy flow and electron transfer in a Ru(II)-loaded polyfluorene light-harvesting polymer. J Phys Chem Lett 3:2453–2457

201. Trouillet L, De Nicola A, Guillerez S (2000) Synthesis and characterization of a new soluble, structurally well-defined conjugated polymer alternating regioregularly alkylated thiophene oligomer and 2,2′-bipyridine units: metal-free form and Ru(II) complex. Chem Mater 12:1611–1621

202. Manca P, Scanu R, Zucca A, Sanna G, Spano N, Pilo MI (2013) Electropolymerization of a Ru(II)-terpyridine complex ethynyl-terthiophene functionalized originating different metallopolymers. Polymer 54:3504–3509

203. Martre A, Laguitton-Pasquier H, Deronzier A, Harriman A (2003) Preparation and properties of a soluble polypyrrole-polypyridyl-ruthenium(II)-viologen dyad. J Phys Chem B 107:2684–2692

204. Qin Y, Cui C, Jäkle F (2008) Tris(1-pyrazolyl)borate (scorpionate) functionalized polymers as scaffolds for metallopolymers. Macromolecules 41:2972–2974

205. Lin W, Zheng Y, Zhang J, Wan X (2011) Fabrication of core-shell nanostructures from near-infrared electrochromic amphiphilic diblock copolymers containing pendant dinuclear ruthenium group through assembly and their optical, electrochemical, and electrooptical properties. Macromolecules 44:5146–5154

206. Zhou G, He J, Harruna II, Geckeler KE (2008) Fullerene and ruthenium dual end-functionalized thermosensitive polymers: synthesis, characterization, electrochemical properties, and self-assembly. J Mater Chem 18:5492–5501

207. Marin V, Holder E, Hoogenboom R, Schubert US (2004) Mixed iridium(III) and ruthenium(II) polypyridyl complexes containing poly(ε-caprolactone)-bipyridine macroligands. J Polym Sci Part A Polym Chem 42:4153–4160

208. Takada K, Storrier GD, Goldsmith JI, Abruna HD (2001) Electrochemical and adsorption properties of PAMAM dendrimers surface-functionalized with polypyridyl cobalt complexes. J Phys Chem B 105:2404–2411

209. Farah AA, Pietro WJ (2004) Telechelic poly(ε-caprolactones) with tethered mixed ligand ruthenium(II) chromophores. Can J Chem 82:595–607

210. Gasnier A, Royal G, Terech P (2009) Metallo-supramolecular gels based on a multitopic cyclam bis-terpyridine platform. Langmuir 25:8751–8762

211. Gasnier A, Barbe J-M, Bucher C, Duboc C, Moutet J-C, Saint-Aman E, Terech P, Royal G (2010) Soluble heterometallic coordination polymers based on a bis-terpyridine-functionalized dioxocyclam ligand. Inorg Chem 49:2592–2599

212. Gasnier A, Barbe J-M, Bucher C, Denat F, Moutet J-C, Saint-Aman E, Terech P, Royal G (2008) Acid–base-driven interconversion between a mononuclear complex and supramolecular coordination polymers in a terpyridine-functionalized dioxocyclam ligand. Inorg Chem 47:1862–1864

213. Gasnier A, Bucher C, Moutet J-C, Royal G, Saint-Aman E, Terech P (2011) Redox-responsive metallo-supramolecular polymers and gels containing bis-terpyridine appended cyclam ligand. Macromol Symp 304:87–92

214. Sato T, Higuchi M (2013) An alternately introduced heterometallo-supramolecular polymer: synthesis and solid-state emission switching by electrochemical redox. Chem Commun 49:5256–5258
215. Barron JA, Glazier S, Bernhard S, Takada K, Houston PL, Abruna HD (2003) Photophysics and redox behavior of chiral transition metal polymers. Inorg Chem 42:1448–1455
216. Hjelm J, Constable EC, Figgemeier E, Hagfeldt A, Handel R, Housecroft CE, Mukhtar E, Schofield E (2002) A rod-like polymer containing {Ru(terpy)2} units prepared by electrochemical coupling of pendant thienyl moieties. Chem Commun 2002(3):284–285
217. Newkome GR, He E, Godinez LA, Baker GR (2000) Electroactive metallomacromolecules via tetrabis(2,2′:6′,2″-terpyridine)ruthenium(II) complexes: dendritic nanonetworks toward constitutional isomers and neutral species without external counterions. J Am Chem Soc 122:9993–10006
218. Storrier GD, Takada K, Abruna HD (1999) Synthesis, characterization, electrochemistry, and EQCM studies of polyamidoamine dendrimers surface-functionalized with polypyridyl metal complexes. Langmuir 15:872–884
219. Farah AA, Pietro WJ (1999) Synthesis and characterization of partially crosslinked poly (N-vinylcarbazole-vinyl alcohol) copolymers with polypyridyl Ru(II) luminophores. Potential materials for electroluminescence. Polym Bull 43:135–142
220. Li B, Fu Y, Han Y, Bo Z (2006) Synthesis and optical properties of dendronized porphyrin polymers. Macromol Rapid Commun 27:1355–1361
221. Hijazi I, Jousselme B, Jegou P, Filoramo A, Campidelli S (2012) Formation of linear and hyperbranched porphyrin polymers on carbon nanotubes via a CuAAC "grafting from" approach. J Mater Chem 22:20936–20942
222. Schappacher M, Deffieux A (2011) Reversible switching between linear and ring polystyrenes bearing porphyrin end groups. J Am Chem Soc 133:1630–1633
223. Schappacher M, Deffieux A (2011) Reversible switching between linear and ring poly(EO)s bearing iron tetraphenylporphyrin ends triggered by solvent, pH, or redox stimuli. Macromolecules 44:4503–4510
224. Kaya I, Aydin A (2009) Synthesis and characterization of chelate polymers containing etheric diphenyl ring in the backbone: thermal, optical, electrochemical, and morphological properties. Polym Adv Technol 22:951–961
225. de Hatten X, Asil D, Friend RH, Nitschke JR (2012) Aqueous self-assembly of an electroluminescent double-helical metallopolymer. J Am Chem Soc 134:19170–19178
226. Liang G, Wu Q, Qin W, Bao S, Zhu F, Wu Q (2013) Poly(benzyl-l-glutamate) decorated with cyanoferrate complex: synthesis, characterization and electrochemical properties. Polym Chem 4:3821–3828
227. Bao S, Ni H, Wu Q, Gao H, Liang G, Zhu F, Wu Q (2014) Waterborne redox-active helix-coil-helix triblock metallopolymers: synthesis, disassembly and electrochemical behaviors. Polymer 55:2205–2212
228. Kulesza PJ, Dickinson EV, Williams ME, Hendrickson SM, Malik MA, Miecznikowski K, Murray RW (2001) Electron self-exchange dynamics of hexacyanoferrate in redox polyether hybrid molten salts containing polyether-tailed counterions. J Phys Chem B 105:5833–5838
229. Schanze KS, Shelton AH (2009) Functional polyelectrolytes. Langmuir 25:13698–13702
230. Ohyanagi M, Anson FC (1989) Electrochemical behavior of electroactive counterions in solutions of polyelectrolytes. J Phys Chem 93:8377–8382
231. Ohyanagi M, Anson FC (1989) Electrodeposition of polyelectrolyte-metal complexes. J Electroanal Chem Interfacial Electrochem 258:469–477
232. Kobayashi J, Anson FC (1991) Association of electroactive counterions with polyelectrolytes. 2. Comparison of electrostatic and coordinative bonding to a mixed polycation-polypyridine. J Phys Chem 95:2595–2601
233. Liang J, Elliot MC, Cammarata V (2009) Polyallylammonium ferrocyanide films for trace water detection in halogenated solvents. Electroanalysis 21:2542–2548

234. Spruijt E, Choi E-Y, Huck WTS (2008) Reversible electrochemical switching of polyelectrolyte brush surface energy using electroactive counterions. Langmuir 24:11253–11260
235. Plamper FA, Murtomäki L, Walther A, Kontturi K, Tenhu H (2009) e-Micellization: electrochemical, reversible switching of polymer aggregation. Macromolecules 42:7254–7257
236. Noftle RE, Pletcher D (1990) An interpretation of the formal potential for the ferricyanide/ferrocyanide couple as a function of solvent composition. J Electroanal Chem Interfacial Electrochem 293:273–277
237. Grieshaber D, Vörös J, Zambelli T, Ball V, Schaaf P, Voegel J-C, Boulmedais F (2008) Swelling and contraction of ferrocyanide-containing polyelectrolyte multilayers upon application of an electric potential. Langmuir 24:13668–13676
238. Ball V, Hübsch E, Schweiss R, Voegel J-C, Schaaf P, Knoll W (2005) Interactions between multivalent ions and exponentially growing multilayers: dissolution and exchange processes. Langmuir 21:8526–8531
239. Hübsch E, Fleith G, Fatisson J, Labbe P, Voegel JC, Schaaf P, Ball V (2005) Multivalent ion/polyelectrolyte exchange processes in exponentially growing multilayers. Langmuir 21:3664–3669
240. Peng F, Li G, Liu X, Wu S, Tong Z (2008) Redox-responsive gel–sol/sol–gel transition in poly(acrylic acid) aqueous solution containing Fe(III) ions switched by light. J Am Chem Soc 130:16166–16167
241. He S, Ren B, Liu X, Tong Z (2010) Reversible electrogelation in poly(acrylic acid) aqueous solutions triggered by redox reactions of counterions. Macromol Chem Phys 211:2497–2502
242. Ciszkowska M, Zeng L, Stejskal EO, Osteryoung JG (1995) Transport of thallium (I) counterion in polyelectrolyte solution determined by voltammetry with microelectrodes and by pulsed-field-gradient, spin-echo NMR. J Phys Chem 99:11764–11769
243. Hamlen RP, Kent CE, Sharer SN (1965) Electrolytically activated contractile polymer. Nature 206:1149–1150
244. Graf N, Albertini F, Petit T, Reimhult E, Vörös J, Zambelli T (2011) Electrochemically stimulated release from liposomes embedded in a polyelectrolyte multilayer. Adv Funct Mater 21:1666–1672
245. Doi M, Matsumoto M, Hirose Y (1992) Deformation of ionic polymer gels by electric fields. Macromolecules 25:5504–5511
246. Dunderdale GJ, Fairclough JPA (2013) Coupling pH-responsive polymer brushes to electricity: switching thickness and creating waves of swelling or collapse. Langmuir 29:3628–3635
247. Cho C, Jeon J-W, Lutkenhaus J, Zacharia NS (2013) Electric field induced morphological transitions in polyelectrolyte multilayers. ACS Appl Mater Interfaces 5:4930–4936
248. Yang L, Gomez-Casado A, Young JF, Nguyen HD, Cabanas-Danes J, Huskens J, Brunsveld L, Jonkheijm P (2012) Reversible and oriented immobilization of ferrocene-modified proteins. J Am Chem Soc 134:19199–19206
249. Nijhuis CA, Huskens J, Reinhoudt DN (2004) Binding control and stoichiometry of ferrocenyl dendrimers at a molecular printboard. J Am Chem Soc 126:12266–12267
250. Nijhuis CA, Sinha JK, Wittstock G, Huskens J, Ravoo BJ, Reinhoudt DN (2006) Controlling the supramolecular assembly of redox-active dendrimers at molecular printboards by scanning electrochemical microscopy. Langmuir 22:9770–9775
251. Olson MA, Braunschweig AB, Fang L, Ikeda T, Klajn R, Trabolsi A, Wesson PJ, Benitez D, Mirkin CA, Grzybowski BA, Stoddart JF (2009) A bistable poly[2]catenane forms nanosuperstructures. Angew Chem Int Ed 48:1792–1797
252. Yu Y, Heidel B, Parapugna TL, Wenderhold-Reeb S, Song B, Schoenherr H, Grininger M, Noell G (2013) The flavoprotein dodecin as a redox probe for electron transfer through DNA. Angew Chem Int Ed 52:4950–4953
253. Grininger M, Nöll G, Trawöger S, Sinner E-K, Oesterhelt D (2008) Electrochemical switching of the flavoprotein dodecin at gold surfaces modified by flavin-DNA hybrid linkers. Biointerphases 3:51–58

254. Tomatsu I, Hashidzume A, Harada A (2006) Redox-responsive hydrogel system using the molecular recognition of b-cyclodextrin. Macromol Rapid Commun 27:238–241
255. Zhu L, Shangguan Y, Sun Y, Ji J, Zheng Q (2010) Rheological properties of redox-responsive, associative ferrocene-modified branched poly(ethylene imine) and its modulation by beta-cyclodextrin and hydrogen peroxide. Soft Matter 6:5541–5546
256. Zhang W, Chen M, Diao G (2011) Preparation and electrochemical behavior of water-soluble inclusion complex of ferrocene with beta-cyclodextrin polymer. Electrochim Acta 56:5129–5136
257. Knudsen B, Kergl BE, Paulsen H, Durnev V, Ritter H (2013) Noncovalent linkage of telechelic oligo(dimethylsiloxanes) via end group attachment of host-cyclodextrins and guest-adamantanes or guest-ferrocenes. J Polym Sci Part A Polym Chem 51:2472–2482
258. Yan Q, Feng A, Zhang H, Yin Y, Yuan J (2013) Redox-switchable supramolecular polymers for responsive self-healing nanofibers in water. Polym Chem 4:1216–1220
259. Dong R, Su Y, Yu S, Zhou Y, Lu Y, Zhu X (2013) A redox-responsive cationic supramolecular polymer constructed from small molecules as a promising gene vector. Chem Commun 49:9845–9847
260. Jorgensen T, Hansen TK, Becher J (1994) Tetrathiafulvalenes as building-blocks in supramolecular chemistry. Chem Soc Rev 23:41–51
261. Bryce MR (1985) Tetrathiafulvalenes (TTF) and their selenium and tellurium analogs (TSF and TTeF). Electron donors for organic metals. Aldrichimica Acta 18:73–77
262. Pudelski JK, Foucher DA, Honeyman CH, Macdonald PM, Manners I, Barlow S, O'Hare D (1996) Synthesis, characterization, and properties of high molecular weight poly(methylated ferrocenylsilanes) and their charge transfer polymer salts with tetracyanoethylene. Macromolecules 29:1894–1903
263. Meng F, Zhong Z, Feijen J (2009) Stimuli-responsive polymersomes for programmed drug delivery. Biomacromolecules 10:197–209
264. Wang L, Chierico L, Little D, Patikarnmonthon N, Yang Z, Azzouz M, Madsen J, Armes SP, Battaglia G (2012) Encapsulation of biomacromolecules within polymersomes by electroporation. Angew Chem Int Ed 51:11122–11125
265. Lin C, Zhu W, Yang H, An Q, Tao C-A, Li W, Cui J, Li Z, Li G (2011) Facile fabrication of stimuli-responsive polymer capsules with gated pores and tunable shell thickness and composite. Angew Chem Int Ed 50:4947–4951
266. Schwarz G, Maisch S, Ullrich S, Wagenhofer J, Kurth DG (2013) Electrorheological fluids based on metallo-supramolecular polyelectrolyte-silicate composites. ACS Appl Mater Interfaces 5:4031–4034
267. Zhang WL, Choi HJ, Seo Y (2013) Facile fabrication of chemically grafted graphene oxide-poly(glycidyl methacrylate) composite microspheres and their electrorheology. Macromol Chem Phys 214:1415–1422
268. Rider DA, Winnik MA, Manners I (2007) Redox-controlled micellization of organometallic block copolymers. Chem Commun 2007(43):4483–4485
269. Eloi J-C, Rider DA, Cambridge G, Whittell GR, Winnik MA, Manners I (2011) Stimulus-responsive self-assembly: reversible, redox-controlled micellization of polyferrocenylsilane diblock copolymers. J Am Chem Soc 133:8903–8913
270. Janczewski D, Song J, Csanyi E, Kiss L, Blazso P, Katona RL, Deli MA, Gros G, Xu J, Vancso GJ (2012) Organometallic polymeric carriers for redox triggered release of molecular payloads. J Mater Chem 22:6429–6435
271. Schmidt BVKJ, Elbert J, Barner-Kowollik C, Gallei M (2014) Individually addressable thermo- and redox-responsive block copolymers by combining anionic polymerization and RAFT protocols. Macromol Rapid Commun 35:708–714
272. Yan Y, Lan Y-R, de Keizer A, Drechsler M, Van As H, Cohen Stuart MA, Besseling NAM (2010) Redox responsive molecular assemblies based on metallic coordination polymers. Soft Matter 6:3244–3248

273. Zhao L, Yan Y, Huang J (2012) Redox-gated potential micellar carriers based on electrostatic assembly of soft coordination suprapolymers. Langmuir 28:5548–5554

274. Cho H, Bae J, Garripelli Vivek K, Anderson Joel M, Jun H-W, Jo S (2012) Redox-sensitive polymeric nanoparticles for drug delivery. Chem Commun 48:6043–6045

275. Ma N, Li Y, Xu H, Wang Z, Zhang X (2010) Dual redox responsive assemblies formed from diselenide block copolymers. J Am Chem Soc 132:442–443

276. Ren H, Wu Y, Ma N, Xu H, Zhang X (2012) Side-chain selenium-containing amphiphilic block copolymers: redox-controlled self-assembly and disassembly. Soft Matter 8:1460–1466

277. Miao X, Cao W, Zheng W, Wang J, Zhang X, Gao J, Yang C, Kong D, Xu H, Wang L, Yang Z (2013) Switchable catalytic activity: selenium-containing peptides with redox-controllable self-assembly properties. Angew Chem Int Ed Engl 52:7781–7785

278. Liu J, Pang Y, Zhu Z, Wang D, Li C, Huang W, Zhu X, Yan D (2013) Therapeutic nanocarriers with hydrogen peroxide-triggered drug release for cancer treatment. Biomacromolecules 14:1627–1636

279. Han P, Ma N, Ren H, Xu H, Li Z, Wang Z, Zhang X (2010) Oxidation-responsive micelles based on a selenium-containing polymeric superamphiphile. Langmuir 26:14414–14418

280. Ryu J-H, Roy R, Ventura J, Thayumanavan S (2010) Redox-sensitive disassembly of amphiphilic copolymer based micelles. Langmuir 26:7086–7092

281. Yuan W, Zou H, Guo W, Shen T, Ren J (2013) Supramolecular micelles with dual temperature and redox responses for multi-controlled drug release. Polym Chem 4:2658–2661

282. Wang Y, Wang H, Liu G, Liu X, Jin Q, Ji J (2013) Self-assembly of near-monodisperse redox-sensitive micelles from cholesterol-conjugated biomimetic copolymers. Macromol Biosci 13:1084–1091

283. Ping Y, Wu D, Kumar JN, Cheng W, Lay CL, Liu Y (2013) Redox-responsive hyperbranched poly(amido amine)s with tertiary amino cores for gene delivery. Biomacromolecules 14:2083–2094

284. Cerritelli S, Velluto D, Hubbell JA (2007) PEG-SS-PPS: reduction-sensitive disulfide block copolymer vesicles for intracellular drug delivery. Biomacromolecules 8:1966–1972

285. Klaikherd A, Nagamani C, Thayumanavan S (2009) Multi-stimuli sensitive amphiphilic block copolymer assemblies. J Am Chem Soc 131:4830–4838

286. Dong W-F, Kishimura A, Anraku Y, Chuanoi S, Kataoka K (2009) Monodispersed polymeric nanocapsules: spontaneous evolution and morphology transition from reducible hetero-PEG PICmicelles by controlled degradation. J Am Chem Soc 131:3804–3805

287. Wang K, Luo G-F, Liu Y, Li C, Cheng S-X, Zhuo R-X, Zhang X-Z (2012) Redox-sensitive shell cross-linked PEG-polypeptide hybrid micelles for controlled drug release. Polym Chem 3:1084–1090

288. Jiang G, Wang Y, Zhang R, Wang R, Wang X, Zhang M, Sun X, Bao S, Wang T, Wang S (2012) Preparation of redox-sensitive shell cross-linked nanoparticles for controlled release of bioactive agents. ACS Macro Lett 1:489–493

289. Bapat AP, Ray JG, Savin DA, Sumerlin BS (2013) Redox-responsive dynamic-covalent assemblies: stars and miktoarm stars. Macromolecules 46:2188–2198

290. Napoli A, Boerakker MJ, Tirelli N, Nolte RJM, Sommerdijk NAJM, Hubbell JA (2004) Glucose oxidase-based self-destructing polymeric vesicles. Langmuir 20:3487–3491

291. Wang H, Guo P, Han Y (2006) Synthesis and surface morphology of tetraaniline-block-poly (L-lactate) diblock oligomers. Macromol Rapid Commun 27:63–68

292. Jia X, Chen D, Jiang M (2006) Preparation of PEO-b-P2VPH+−S2O82- micelles in water and their reversible UCST and redox-responsive behavior. Chem Commun 2006(16):1736–1738

293. Power-Billard KN, Spontak RJ, Manners I (2004) Redox-active organometallic vesicles: aqueous self-assembly of a diblock copolymer with a hydrophilic polyferrocenylsilane polyelectrolyte block. Angew Chem Int Ed 43:1260–1264

294. Dahmane S, Lasia A, Zhao Y (2008) Electrochemically active block copolymer micelles containing coumarin moieties. Macromol Chem Phys 209:1065–1072
295. Yan Q, Yuan J, Cai Z, Xin Y, Kang Y, Yin Y (2010) Voltage-responsive vesicles based on orthogonal assembly of two homopolymers. J Am Chem Soc 132:9268–9270
296. Feng A, Yan Q, Zhang H, Peng L, Yuan J (2014) Electrochemical redox responsive polymeric micelles formed from amphiphilic supramolecular brushes. Chem Commun 50:4740–4742
297. Szillat F, Schmidt BVKJ, Hubert A, Barner-Kowollik C, Ritter H (2014) Redox-switchable supramolecular graft polymer formation via ferrocene–cyclodextrin assembly. Macromol Rapid Commun 35(14):1293–1300
298. Kim H, Jeong S-M, Park J-W (2011) Electrical switching between vesicles and micelles via redox-responsive self-assembly of amphiphilic rod-coils. J Am Chem Soc 133:5206–5209
299. Yang Z, Wang X, Yang Y, Liao Y, Wei Y, Xie X (2010) Synthesis of electroactive tetraaniline-PEO-tetraaniline triblock copolymer and its self-assembled vesicle with acidity response. Langmuir 26:9386–9392
300. Hu J, Zhuang X, Huang L, Lang L, Chen X, Wei Y, Jing X (2008) pH/potential-responsive large aggregates from the spontaneous self-assembly of a triblock copolymer in water. Langmuir 24:13376–13382
301. Huang L, Hu J, Lang L, Chen X, Wei Y, Jing X (2007) Synthesis of a novel electroactive ABA triblock copolymer and its spontaneous self-assembly in water. Macromol Rapid Commun 28:1559–1566
302. Song L, Du B, Chen L, Deng M, Sun H, Pang X, Zhang P, Chen X (2013) Synthesis of electroactive and biodegradable multiblock copolymers based on poly(ester amide) and aniline pentamer. J Polym Sci Part A Polym Chem 51:4722–4731
303. Takeoka Y, Aoki T, Sanui K, Ogata N, Yokoyama M, Okano T, Sakurai Y, Watanabe M (1995) Electrochemical control of drug release from redox-active micelles. J Control Release 33:79–87
304. Saji T, Hoshino K, Aoyagui S (1985) Reversible formation and disruption of micelles by control of the redox state of the head group. J Am Chem Soc 107:6865–6868
305. Wang K, Guo D-S, Wang X, Liu Y (2011) Multistimuli responsive supramolecular vesicles based on the recognition of p-sulfonatocalixarene and its controllable release of doxorubicin. ACS Nano 5:2880–2894
306. Xing L-B, Yu S, Wang X-J, Wang G-X, Chen B, Zhang L-P, Tung C-H, Wu L-Z (2012) Reversible multistimuli-responsive vesicles formed by an amphiphilic cationic platinum (II) terpyridyl complex with a ferrocene unit in water. Chem Commun 48:10886–10888
307. Sambe L, Stoffelbach F, Lyskawa J, Delattre F, Fournier D, Bouteiller L, Charleux B, Cooke G, Woisel P (2011) Host-guest modulation of the micellization of a tetrathiafulvalene-functionalized poly(N-isopropylacrylamide). Macromolecules 44:6532–6538
308. Zhang K-D, Zhou T-Y, Zhao X, Jiang X-K, Li Z-T (2012) Redox-responsive reverse vesicles self-assembled by pseudo[2]rotaxanes for tunable dye release. Langmuir 28:14839–14844
309. Zhang K-D, Zhao X, Wang G-T, Liu Y, Zhang Y, Lu H-J, Jiang X-K, Li Z-T (2011) Foldamer-tuned switching kinetics and metastability of [2]rotaxanes. Angew Chem Int Ed 50:9866–9870, S9866/9861-S9866/9816
310. Ouhib F, Desbief S, Lazzaroni R, Melinte S, Dutu CA, Jerome C, Detrembleur C (2013) Electrografting onto ITO substrates of poly(thiophene)-based micelles decorated by acrylate groups. Polym Chem F 4:4151–4161
311. Dutta K, Kundu PP (2013) Reversible assembly and disassembly of amphiphilic assemblies by electropolymerized polyaniline films: effects rendered by varying the electropolymerization potential. J Phys Chem B 117:7797–7805
312. Liu YD, Park BJ, Kim YH, Choi HJ (2011) Smart monodisperse polystyrene/polyaniline core-shell structured hybrid microspheres fabricated by a controlled releasing technique and their electro-responsive characteristics. J Mater Chem 21:17396–17402

313. Plamper FA, Gelissen AP, Timper J, Wolf A, Zezin AB, Richtering W, Tenhu H, Simon U, Mayer J, Borisov OV, Pergushov DV (2013) Spontaneous assembly of miktoarm stars into vesicular interpolyelectrolyte complexes. Macromol Rapid Commun 34:855–860

314. Xu W, Choi I, Plamper FA, Synatschke CV, Müller AHE, Tsukruk VV (2013) Nondestructive light-initiated tuning of layer-by-layer microcapsule permeability. ACS Nano 7:598–613

315. Zelikin AN, Quinn JF, Caruso F (2006) Disulfide cross-linked polymer capsules: en route to biodeconstructible systems. Biomacromolecules 7:27–30

316. Okahata Y, Ariga K, Seki T (1986) Redox-sensitive permeation from a capsule membrane grafted with viologen-containing polymers. J Chem Soc Chem Commun 1986(1):73–75

317. Okahata Y, Ariga K (1987) Functional capsule membranes. Part 28. A capsule membrane grafted with viologen-containing polymers as a reactor of electron-transfer catalysis in heterophases. J Chem Soc Perkin Trans 2:1003–1008

318. Okahata Y, Enna G (1988) Permeability-controllable membranes. 7. Electrochemical responsive gate membranes of a multibilayer film containing a viologen group as redox sites. J Phys Chem 92:4546–4551

319. Okahata Y, Enna G, Takenouchi K (1989) Permeability-controllable membranes. Part 8. Electrical redox sensitive permeation through a multibilayer-immobilized film containing a ferrocenyl group as a redox site. J Chem Soc Perkin Trans 2:835–843

320. Ma Y, Dong W-F, Hempenius MA, Möhwald H, Vancso GJ (2006) Redox-controlled molecular permeability of composite-wall microcapsules. Nat Mater 5:724–729

321. Scheid D, Lederle C, Vowinkel S, Schafer CG, Stuhn B, Gallei M (2014) Redox- and mechano-chromic response of metallopolymer-based elastomeric colloidal crystal films. J Mater Chem C 2:2583–2590

322. Staff RH, Gallei M, Mazurowski M, Rehahn M, Berger R, Landfester K, Crespy D (2012) Patchy nanocapsules of poly(vinylferrocene)-based block copolymers for redox-responsive release. ACS Nano 6:9042–9049

323. Lv L-P, Zhao Y, Vilbrandt N, Gallei M, Vimalanandan A, Rohwerder M, Landfester K, Crespy D (2013) Redox responsive release of hydrophobic self-healing agents from polyaniline capsules. J Am Chem Soc 135:14198–14205

324. Vimalanandan A, Lv L-P, Tran TH, Landfester K, Crespy D, Rohwerder M (2013) Redox-responsive self-healing for corrosion protection. Adv Mater 25:6980–6984

325. Wang H, Wang X, Winnik MA, Manners I (2008) Redox-mediated synthesis and encapsulation of inorganic nanoparticles in shell-cross-linked cylindrical polyferrocenylsilane block copolymer micelles. J Am Chem Soc 130:12921–12930

326. Graf N, Tanno A, Dochter A, Rothfuchs N, Vörös J, Zambelli T (2012) Electrochemically driven delivery to cells from vesicles embedded in polyelectrolyte multilayers. Soft Matter 8:3641–3648

327. Ge J, Neofytou E, Cahill TJ III, Beygui RE, Zare RN (2012) Drug release from electric-field-responsive nanoparticles. ACS Nano 6:227–233

328. Hempenius MA, Cirmi C, Lo Savio F, Song J, Vancso GJ (2010) Poly(ferrocenylsilane) gels and hydrogels with redox-controlled actuation. Macromol Rapid Commun 31:772–783

329. De Luca V, Digiamberardino P, Di Pasquale G, Graziani S, Pollicino A, Umana E, Xibilia MG (2013) Ionic electroactive polymer metal composites: fabricating, modeling, and applications of postsilicon smart devices. J Polym Sci Part B Polym Phys 51:699–734

330. McDowell JJ, Zacharia NS, Puzzo D, Manners I, Ozin GA (2010) Electroactuation of alkoxysilane-functionalized polyferrocenylsilane microfibers. J Am Chem Soc 132:3236–3237

331. Piepenbrock M-OM, Lloyd GO, Clarke N, Steed JW (2010) Metal- and anion-binding supramolecular gels. Chem Rev 110:1960–2004

332. Gyarmati B, Vajna B, Nemethy A, Laszlo K, Szilagyi A (2013) Redox- and pH-responsive cysteamine-modified poly(aspartic acid) showing a reversible sol–gel transition. Macromol Biosci 13:633–640

333. Singh S, Topuz F, Hahn K, Albrecht K, Groll J (2013) Embedding of active proteins and living cells in redox-sensitive hydrogels and nanogels through enzymatic cross-linking. Angew Chem Int Ed Engl 52:3000–3003
334. Tabata O, Hirasawa H, Aoki S, Yoshida R, Kokufuta E (2002) Ciliary motion actuator using self-oscillating gel. Sens Actuators, A 95:234–238
335. Maeda S, Hara Y, Yoshida R, Hashimoto S (2008) Peristaltic motion of polymer gels. Angew Chem Int Ed Engl 47:6690–6693
336. Murase Y, Hidaka M, Yoshida R (2010) Self-driven gel conveyer: autonomous transportation by peristaltic motion of self-oscillating gel. Sens Actuators B 149:272–283
337. Yoshida R (2010) Self-oscillating gels driven by the belousov-zhabotinsky reaction as novel smart materials. Adv Mater 22:3463–3483
338. Shiraki Y, Yoshida R (2012) Autonomous intestine-like motion of tubular self-oscillating gel. Angew Chem Int Ed Engl 51:6112–6116
339. Maeda S, Hara Y, Sakai T, Yoshida R, Hashimoto S (2007) Self-walking gel. Adv Mater 19:3480–3484
340. Dong Z-Q, Cao Y, Yuan Q-J, Wang Y-F, Li J-H, Li B-J, Zhang S (2013) Redox- and glucose-induced shape-memory polymers. Macromol Rapid Commun 34:867–872
341. Nakahata M, Takashima Y, Harada A (2014) Redox-responsive macroscopic gel assembly based on discrete dual interactions. Angew Chem Int Ed Engl 53:3617–3621
342. Akhoury A, Bromberg L, Hatton TA (2011) Redox-responsive gels with tunable hydrophobicity for controlled solubilization and release of organics. ACS Appl Mater Interfaces 3:1167–1174
343. Arsenault AC, Miguez H, Kitaev V, Ozin GA, Manners I (2003) A polychromic, fast response metallopolymer gel photonic crystal with solvent and redox tunability: a step towards photonic ink (P-ink). Adv Mater 15:503–507
344. Arsenault AC, Puzzo DP, Manners I, Ozin GA (2007) Photonic-crystal full-color displays. Nat Photonics 1:468–472
345. Kulbaba K, MacLachlan MJ, Evans CEB, Manners L (2001) Organometallic gels: characterization and electrochemical studies of swellable, thermally crosslinked poly (ferrocenylsilane)s. Macromol Chem Phys 202:1768–1775
346. Puzzo DP, Arsenault AC, Manners I, Ozin GA (2009) Electroactive inverse opal: a single material for all colors. Angew Chem Int Ed 48:943–947
347. Liu J, Mao Y, Ge J (2013) Electric field tuning of magnetically assembled photonic crystals. J Mater Chem C 1:6129–6135
348. Lu Y, Meng C, Xia H, Zhang G, Wu C (2013) Fast electrically driven photonic crystal based on charged block copolymer. J Mater Chem C 1:6107–6111
349. Galisteo-López JF, Ibisate M, Sapienza R, Froufe-Pérez LS, Blanco Á, López C (2011) Self-assembled photonic structures. Adv Mater 23:30–69
350. Tatsuma T, Takada K, Matsui H, Oyama N (1994) A redox gel. Electrochemically controllable phase transition and thermally controllable electrochemistry. Macromolecules 27:6687–6689
351. Oyama N, Tatsuma T, Takahashi K (1993) Electrochemical characterization of a thermoresponsive N-isopropylacrylamide-vinylferrocene copolymer film by the use of quartz crystal oscillators. J Phys Chem 97:10504–10508
352. Du P, Liu J, Chen G, Jiang M (2011) Dual responsive supramolecular hydrogel with electrochemical activity. Langmuir 27:9602–9608
353. Nakahata M, Takashima Y, Yamaguchi H, Harada A (2011) Redox-responsive self-healing materials formed from host-guest polymers. Nat Commun 2:1521–1526
354. Chuo T-W, Wei T-C, Liu Y-L (2013) Electrically driven self-healing polymers based on reversible guest-host complexation of β-cyclodextrin and ferrocene. J Polym Sci Part A Polym Chem 51:3395–3403

355. Nakahata M, Takashima Y, Hashidzume A, Harada A (2013) Redox-generated mechanical motion of a supramolecular polymeric actuator based on host-guest interactions. Angew Chem Int Ed Engl 52:5731–5735
356. Hempenius MA, Cirmi C, Song J, Vancso GJ (2009) Synthesis of poly(ferrocenylsilane) polyelectrolyte hydrogels with redox controlled swelling. Macromolecules 42:2324–2326
357. Sui X, van Ingen L, Hempenius MA, Vancso GJ (2010) Preparation of a rapidly forming poly(ferrocenylsilane)-poly(ethylene glycol)-based hydrogel by a thiol-michael addition click reaction. Macromol Rapid Commun 31:2059–2063
358. Sui X, Feng X, Di Luca A, van Blitterswijk CA, Moroni L, Hempenius MA, Vancso GJ (2013) Poly(N-isopropylacrylamide)-poly(ferrocenylsilane) dual-responsive hydrogels: synthesis, characterization and antimicrobial applications. Polym Chem 4:337–342
359. Liu Y, Hu J, Zhuang X, Zhang P, Wei Y, Wang X, Chen X (2012) Synthesis and characterization of novel biodegradable and electroactive hydrogel based on aniline oligomer and gelatin. Macromol Biosci 12:241–250
360. Li L, Ge J, Guo B, Ma PX (2014) In situ forming biodegradable electroactive hydrogels. Polym Chem 5:2880–2890
361. Ding F, Shi X, Jiang Z, Liu L, Cai J, Li Z, Chen S, Du Y (2013) Electrochemically stimulated drug release from dual stimuli responsive chitin hydrogel. J Mater Chem B 1:1729–1737
362. He J, Zhang A, Zhang Y, Guan Y (2011) Novel redox hydrogel by in situ gelation of chitosan as a result of template oxidative polymerization of hydroquinone. Macromolecules 44:2245–2252
363. Goswami SK, McAdam CJ, Lee AMM, Hanton LR, Moratti SC (2013) Linear electrochemical actuators with very large strains using carbon nanotube-redox gel composites. J Mater Chem A 1:3415–3420
364. Wu J, Ren Y, Sun J, Feng L (2013) Carbon nanotube-coated macroporous poly(N-isopropylacrylamide) hydrogel and its electrosensitivity. ACS Appl Mater Interfaces 5:3519–3523
365. Cui H, Cui L, Zhang P, Huang Y, Wei Y, Chen X (2014) In situ electroactive and antioxidant supramolecular hydrogel based on cyclodextrin/copolymer inclusion for tissue engineering repair. Macromol Biosci 14:440–450
366. Cui H, Shao J, Wang Y, Zhang P, Chen X, Wei Y (2013) PLA-PEG-PLA and its electroactive tetraaniline copolymer as multi-interactive injectable hydrogels for tissue engineering. Biomacromolecules 14:1904–1912
367. Takada K, Tanaka N, Tatsuma T (2005) A redox actuator based on reversible formation of bond between poly(acrylic acid) gel and Cu^{2+} ion. J Electroanal Chem 585:120–127
368. Palleau E, Morales D, Dickey MD, Velev OD (2013) Reversible patterning and actuation of hydrogels by electrically assisted ionoprinting. Nat Commun 4:2257
369. Takada K, Miyazaki T, Tanaka N, Tatsuma T (2006) Three-dimensional motion and transformation of a photoelectrochemical actuator. Chem Commun 2006(19):2024–2026
370. Tatsuma T, Takada K, Miyazaki T (2007) UV-light-induced swelling and visible-light-induced shrinking of a TiO2-containing redox gel. Adv Mater 19:1249–1251
371. Takada K, Iida T, Kawanishi Y, Yasui T, Yuchi A (2011) An electrochemical actuator based on reversible changes in volume of poly(acrylic acid) gel induced by quinone redox. Sens Actuators B 160:1586–1592
372. Kwon IC, Bae YH, Kim SW (1991) Electrically erodible polymer gel for controlled release of drugs. Nature 354:291–293
373. Calvo-Marzal P, Delaney MP, Auletta JT, Pan T, Perri NM, Weiland LM, Waldeck DH, Clark WW, Meyer TY (2012) Manipulating mechanical properties with electricity: electroplastic elastomer hydrogels. ACS Macro Lett 1:204–208
374. Chiarelli P, De Rossi D (2012) Polyelectrolyte intelligent gels: Design and applications. In: Ciferri A, Perico A (eds) Ionic interactions in natural and synthetic macromolecules. Wiley, Hoboken. doi: 10.1002/9781118165850.ch15

375. Shiga T (1997) Deformation and viscoelastic behavior of polymer gels in electric fields. Adv Polym Sci 134:131–163

376. Grodzinsky AJ, Shoenfeld NA (1977) Tensile forces induced in collagen by means of electromechanochemical transductive coupling. Polymer 18:435–443

377. Jin S, Gu J, Shi Y, Shao K, Yu X, Yue G (2013) Preparation and electrical sensitive behavior of poly (N-vinylpyrrolidone-co-acrylic acid) hydrogel with flexible chain nature. Eur Polym J 49:1871–1880

378. Tanaka T, Nishio I, Sun ST, Ueno-Nishio S (1982) Collapse of gels in an electric field. Science 218:467–469

379. Grimshaw PE, Nussbaum JH, Grodzinsky AJ, Yarmush ML (1990) Kinetics of electrically and chemically induced swelling in polyelectrolyte gels. J Chem Phys 93:4462–4472

380. Fragala A, Enos J, LaConti A, Boyack J (1972) Electrochemical activation of a synthetic artificial muscle membrane. Electrochim Acta 17:1507–1522

381. Glazer PJ, van Erp M, Embrechts A, Lemay SG, Mendes E (2012) Role of pH gradients in the actuation of electro-responsive polyelectrolyte gels. Soft Matter 8:4421–4426

382. O'Grady ML, Kuo P-L, Parker KK (2010) Optimization of electroactive hydrogel actuators. ACS Appl Mater Interfaces 2:343–346

383. Jackson N, Cordero N, Stam F (2013) 3-D interdigitated electrodes for uniform stimulation of electro-responsive hydrogels for biomedical applications. J Polym Sci Part B Polym Phys 51:1523–1528

384. Li H, Luo R, Lam KY (2009) Multiphysics modeling of electrochemomechanically smart microgels responsive to coupled pH/electric stimuli. Macromol Biosci 9:287–297

385. Osada Y, Okuzaki H, Hori H (1992) A polymer gel with electrically driven motility. Nature 355:242–244

386. Morales D, Palleau E, Dickey MD, Velev OD (2014) Electro-actuated hydrogel walkers with dual responsive legs. Soft Matter 10:1337–1348

387. Miller AK, Li Z, Streletzky KA, Jamieson AM, Rowan SJ (2012) Redox-induced polymerisation/depolymerisation of metallo-supramolecular polymers. Polym Chem 3:3132–3138

388. Kojic N, Panzer MJ, Leisk GG, Raja WK, Kojic M, Kaplan DL (2012) Ion electrodiffusion governs silk electrogelation. Soft Matter 8:6897–6905

389. Nayak S, Lyon LA (2004) Ligand-functionalized core/shell microgels with permselective shells. Angew Chem Int Ed 43:6706–6709

390. Oh JK, Bencherif SA, Matyjaszewski K (2009) Atom transfer radical polymerization in inverse miniemulsion: a versatile route toward preparation and functionalization of microgels/nanogels for targeted drug delivery applications. Polymer 50:4407–4423

391. Bajomo M, Steinke JHG, Bismarck A (2007) Inducing pH responsiveness via ultralow thiol content in polyacrylamide (micro)gels with labile crosslinks. J Phys Chem B 111:8655–8662

392. Syrett JA, Haddleton DM, Whittaker MR, Davis TP, Boyer C (2011) Functional, star polymeric molecular carriers, built from biodegradable microgel/nanogel cores. Chem Commun 47:1449–1451

393. Zhang J, Li C, Wang Y, Zhuo R-X, Zhang X-Z (2011) Controllable exploding microcapsules as drug carriers. Chem Commun 47:4457–4459

394. Wang Z-K, Wang L-H, Sun J-T, Han L-F, Hong C-Y (2013) In situ generation of bioreducible and acid labile nanogels/microgels simply via adding water into the polymerization system. Polym Chem 4:1694–1699

395. Gaulding JC, Smith MH, Hyatt JS, Fernandez-Nieves A, Lyon LA (2012) Reversible inter- and intra-microgel cross-linking using disulfides. Macromolecules 45:39–45

396. Hu X, Tong Z, Lyon LA (2010) Multicompartment core/shell microgels. J Am Chem Soc 132:11470–11472

397. Kulbaba K, Resendes R, Cheng A, Bartole A, Safa-Sefat A, Coombs N, Stover HDH, Greedan JE, Ozin GA, Manners I (2001) Polyferrocenylsilane and magnetic ceramic microspheres. Adv Mater 13:732–736

398. Kulbaba K, Cheng A, Bartole A, Greenberg S, Resendes R, Coombs N, Safa-Sefat A, Greedan JE, Stöver HDH, Ozin GA, Manners I (2002) Polyferrocenylsilane microspheres: synthesis, mechanism of formation, size and charge tunability, electrostatic self-assembly, and pyrolysis to spherical magnetic ceramic particles. J Am Chem Soc 124:12522–12534

399. Sui X, Shui L, Cui J, Xie Y, Song J, van den Berg A, Hempenius Mark A, Julius Vancso G (2014) Redox-responsive organometallic microgel particles prepared from poly (ferrocenylsilane)s generated using microfluidics. Chem Commun 50:3058–3060

400. Suzuki D, Yoshida R (2008) Temporal control of self-oscillation for microgels by cross-linking network structure. Macromolecules 41:5830–5838

401. Suzuki D, Taniguchi H, Yoshida R (2009) Autonomously oscillating viscosity in microgel dispersions. J Am Chem Soc 131:12058–12059

402. Okeyoshi K, Yoshida R (2009) Hydrogen generating gel systems induced by visible light. Soft Matter 5:4118–4123

403. Cook JP, Riley DJ (2012) Electrical switching of microgel swelling and collapse for display applications. J Polym Sci Part B Polym Phys 50:516–522

404. Sui X, Hempenius MA, Vancso GJ (2012) Redox-active cross-linkable poly(ionic liquid)s. J Am Chem Soc 134:4023–4025

405. Pinaud F, Russo L, Pinet S, Gosse I, Ravaine V, Sojic N (2013) Enhanced electrogenerated chemiluminescence in thermoresponsive microgels. J Am Chem Soc 135:5517–5520

406. Albery WJ, Hillman AR (1982) Modified electrodes. Annu Rep Prog Chem Sect C 78:377–437

407. Faulkner LR (1984) Chemical microstructures on electrodes. Chem Eng News 62:28–38, 43–25

408. Chidsey CED, Murray RW (1986) Electroactive polymers and macromolecular electronics. Science 231:25–31

409. Hillman AR (1987) Polymer modified electrodes: preparation and characterization. Electrochem Sci Technol Polym 1:103–239

410. Nöll T, Nöll G (2011) Strategies for "wiring" redox-active proteins to electrodes and applications in biosensors, biofuel cells, and nanotechnology. Chem Soc Rev 40:3564–3576

411. Bardini L, Ceccato M, Hinge M, Pedersen SU, Daasbjerg K, Marcaccio M, Paolucci F (2013) Electrochemical polymerization of allylamine copolymers. Langmuir 29:3791–3796

412. McCullough RD (1998) The chemistry of conducting polythiophenes. Adv Mater 10:93–116

413. Roncali J (1992) Conjugated poly(thiophenes): synthesis, functionalization, and applications. Chem Rev 92:711–738

414. Waltman RJ, Bargon J (1986) Electrically conducting polymers: a review of the electropolymerization reaction, of the effects of chemical structure on polymer film properties, and of applications towards technology. Can J Chem 64:76–95

415. Shirakawa H, MacDiarmid A, Heeger A (2003) Focus article: twenty-five years of conducting polymers. Chem Commun 2003(1):1–4

416. Wessling B (2010) New insight into organic metal polyaniline morphology and structure. Polymers 2:786–798

417. Patton DL, Taranekar P, Fulghum T, Advincula R (2008) Electrochemically active dendritic-linear block copolymers via raft polymerization: synthesis, characterization, and electrodeposition properties. Macromolecules 41:6703–6713

418. Li M, Zhang J, Nie H-J, Liao M, Sang L, Qiao W, Wang ZY, Ma Y, Zhong Y-W, Ariga K (2013) In situ switching layer-by-layer assembly: one-pot rapid layer assembly via alternation of reductive and oxidative electropolymerization. Chem Commun 49:6879–6881

419. Isaksson J, Tengstedt C, Fahlman M, Robinson N, Berggren M (2004) A solid-state organic electronic wettability switch. Adv Mater 16:316–320

420. Mugele F, Baret J-C (2005) Electrowetting: from basics to applications. J Phys Condens Matter 17:R705–R774

421. Verplanck N, Coffinier Y, Thomy V, Boukherroub R (2007) Wettability switching techniques on superhydrophobic surfaces. Nanoscale Res Lett 2:577–596

422. Ikeda T, Schmehl R, Denisevich P, Willman K, Murray RW (1982) Permeation of electroactive solutes through ultrathin polymeric films on electrode surfaces. J Am Chem Soc 104:2683–2691
423. Tagliazucchi M, Calvo EJ (2009) Electrochemically active polyelectrolyte-modified electrodes. Adv Electrochem Sci Eng 11:57–115
424. Maeda H, Sakamoto R, Nishihara H (2013) Metal complex oligomer and polymer wires on electrodes: tactical constructions and versatile functionalities. Polymer 54:4383–4403
425. Tokarev I, Orlov M, Katz E, Minko S (2007) An electrochemical gate based on a stimuli-responsive membrane associated with an electrode surface. J Phys Chem B 111:12141–12145
426. Claro PCDS, Coustet ME, Diaz C, Maza E, Cortizo MS, Requejo FG, Pietrasanta LI, Ceolin M, Azzaroni O (2013) Self-assembly of PBzMA-b-PDMAEMA diblock copolymer films at the air-water interface and deposition on solid substrates via Langmuir-Blodgett transfer. Soft Matter 9:10899–10912
427. Calvo A, Yameen B, Williams FJ, Soler-Illia GJAA, Azzaroni O (2009) Mesoporous films and polymer brushes helping each other to modulate ionic transport in nanoconfined environments. An interesting example of synergism in functional hybrid assemblies. J Am Chem Soc 131:10866–10868
428. Jaber JA, Schlenoff JB (2005) Polyelectrolyte multilayers with reversible thermal responsivity. Macromolecules 38:1300–1306
429. Dou Y, Han J, Wang T, Wei M, Evans DG, Duan X (2012) Temperature-controlled electrochemical switch based on layered double hydroxide/poly(N-Isopropylacrylamide) ultrathin films fabricated via layer-by-layer assembly. Langmuir 28:9535–9542
430. Liu A, Chen M, Qian D-J (2010) Electrochemical behaviors of nanoporous coordination polymer multilayers in hexacyanoferrate solution. Colloids Surf A 366:183–190
431. Lee CS, Bell JP (1995) Kinetic study of the aqueous electropolymerization of acrylamide, acrylonitrile and N, N'-methylene-bisacrylamide on an aluminum alloy cathode. J Mater Sci 30:3827–3833
432. Reuber J, Reinhardt H, Johannsmann D (2006) Formation of surface-attached responsive gel layers via electrochemically induced free-radical polymerization. Langmuir 22:3362–3367
433. Bünsow J, Johannsmann D (2008) Electrochemically produced responsive hydrogel films: influence of added salt on thickness and morphology. J Colloid Interface Sci 326:61–65
434. Bünsow J, Mänz M, Vana P, Johannsmann D (2010) Electrochemically induced RAFT polymerization of thermoresponsive hydrogel films: impact on film thickness and surface morphology. Macromol Chem Phys 211:761–767
435. Oyama N, Anson FC (1979) Polymeric ligands as anchoring groups for the attachment of metal complexes to graphite electrode surfaces. J Am Chem Soc 101:3450–3456
436. Shigehara K, Oyama N, Anson FC (1981) Evaluation of rate constants for redox self-exchange reactions from electrochemical measurements with rotating-disk electrodes coated with polyelectrolytes. Inorg Chem 20:518–522
437. Braun H, Storck W, Doblhofer K (1983) Thermodynamic aspects of redox reactions on electrodes coated with thin, ion exchanging polymer films. J Electrochem Soc 130:807–811
438. Niwa K, Doblhofer K (1986) The interrelation between the electrochemical behavior of a polymer-coated electrode and the ion exchange properties of the coating. Electrochim Acta 31:549–553
439. Doblhofer K, Armstrong RD (1988) Membrane-type coatings on electrodes. Electrochim Acta 33:453–460
440. Oh SM, Faulkner LR (1989) Electron transport dynamics in partially quaternized poly (4-vinylpyridine) thin films containing ferri/ferrocyanide. J Electroanal Chem Interfacial Electrochem 269:77–97
441. Lindholm B (1988) Chronocoulometric and rotating disk electrode determination of the charge propagation current through poly-4-vinylpyridine films containing hexachloroiridate anions. J Electroanal Chem Interfacial Electrochem 250:341–354

442. Kwak J, Anson FC (1992) Monitoring the ejection and incorporation of ferricyanide [Fe(CN) 63-] and ferrocyanide [Fe(CN)64-] counterions at protonated poly(4-vinylpyridine) coatings on electrodes with the scanning electrochemical microscope. Anal Chem 64:250–256

443. Han J-H, Kim KB, Bae JH, Kim BJ, Kang CM, Kim HC, Chung TD (2011) Ion flow crossing over a polyelectrolyte diode on a microfluidic chip. Small 7:2629–2639

444. Doblhofer K, Lange R (1987) Hexachloroiridate(III/IV) on polymer-coated electrodes. Investigation of the membrane permeability and the charge-transport mechanism. J Electroanal Chem Interfacial Electrochem 229:239–247

445. Ybarra G, Moina C, Florit MI, Posadas D (2008) Current rectification by mediating electroactive polymers. Electrochim Acta 53:3955–3959

446. Salloum DS, Schlenoff JB (2004) Rectified ion currents through ultrathin polyelectrolyte complex: toward chemical transistors. Electrochem Solid State Lett 7:E45–E47

447. Braun H, Decker F, Doblhofer K, Sotobayashi H (1984) The redox-reaction hexacyanoferrate (III)/hexacyanoferrate(II) ([Fe(CN)6]3-/4-) on electrodes coated with fixed charge polymer films - observation of membrane permeability modulation by the electrode potential. Ber Bunsen Ges Phys Chem 88:345–350

448. Conklin SD, Heineman WR, Seliskar CJ (2005) Spectroelectrochemical sensing based on multimode selectivity simultaneously achievable in a single device. 18. Preparation and characterization of cross-linked quaternized poly(4-vinylpyridinium) films. Electroanalysis 17:1433–1440

449. Conklin SD, Heineman WR, Seliskar CJ (2007) Spectroelectrochemical sensing based on multimode selectivity simultaneously achievable in a single device. 19. Preparation and characterization of films of quaternized poly(4-vinylpyridine)-silica. Electroanalysis 19:523–529

450. Pincus TYAPA (2011) Collapse of polyelectrolyte brushes in electric fields. EPL 95:48003

451. Wang K, Zangmeister RA, Levicky R (2008) Equilibrium electrostatics of responsive polyelectrolyte monolayers. J Am Chem Soc 131:318–326

452. Farina R, Laugel N, Pincus P, Tirrell M (2013) Brushes of strong polyelectrolytes in mixed mono- and tri-valent ionic media at fixed total ionic strengths. Soft Matter 9:10458–10472

453. Choi E-Y, Azzaroni O, Cheng N, Zhou F, Kelby T, Huck WTS (2007) Electrochemical characteristics of polyelectrolyte brushes with electroactive counterions. Langmuir 23:10389–10394

454. Combellas C, Kanoufi F, Sanjuan S, Slim C, Tran Y (2009) Electrochemical and spectroscopic investigation of counterions exchange in polyelectrolyte brushes. Langmuir 25:5360–5370

455. Yu B, Zhou F, Bo Y, Hou X, Liu W (2007) Electrochemical impedance spectroscopy of poly (1-ethyl 3-(2-methacryloyloxy ethyl) imidazolium chloride) brushes with locally generated Pd. Electrochem Commun 9:1749–1754

456. Shen G, Tercero N, Gaspar MA, Varughese B, Shepard K, Levicky R (2006) Charging behavior of single-stranded DNA polyelectrolyte brushes. J Am Chem Soc 128:8427–8433

457. Yu B, Hu H, Wang D, Huck WTS, Zhou F, Liu W (2009) Electrolyte-modulated electrochemistry and electrocatalysis on ferrocene-terminated polyelectrolyte brushes. J Mater Chem 19:8129–8134

458. Tam TK, Pita M, Trotsenko O, Motornov M, Tokarev I, Halamek J, Minko S, Katz E (2010) Reversible "closing" of an electrode interface functionalized with a polymer brush by an electrochemical signal. Langmuir 26:4506–4513

459. Thangamuthu R, Senthilkumar SM, Pillai KC (2006) Octacyanomolybdate-doped-poly (4-vinylpyridine) ionomer film electrode for the electrocatalytic oxidation of L-ascorbic acid. J Solid State Electrochem 11:126–133

460. To Thi Kim L, Debiemme-Chouvy C, Gabrielli C, Perrot H (2012) Redox switching of heteropolyanions entrapped in polypyrrole films investigated by ac electrogravimetry. Langmuir 28:13746–13757

461. Fandrich A, Buller J, Wischerhoff E, Laschewsky A, Lisdat F (2012) Electrochemical detection of the thermally induced phase transition of a thin stimuli-responsive polymer film. ChemPhysChem 13:2020–2023

462. Song S, Hu N (2010) Dual-switchable bioelectrocatalysis synergistically controlled by pH and perchlorate concentration based on poly(4-vinylpyridine) films. J Phys Chem B 114:11689–11695

463. Garcia TA, Gervasi CA, Rodriguez Presa MJ, Otamendi JI, Moya SE, Azzaroni O (2012) Molecular transport in thin thermoresponsive poly(N-isopropylacrylamide) brushes with varying grafting density. J Phys Chem C 116:13944–13953

464. Lange R, Doblhofer K, Storck W (1988) Europium(II/III) on poly(styrenesulfonate) coated electrodes of stable electrochemical performance. Electrochim Acta 33:385–388

465. Baughman RH (1996) Conducting polymer artificial muscles. Synth Met 78:339–353

466. Farhat TR, Schlenoff JB (2001) Ion transport and equilibria in polyelectrolyte multilayers. Langmuir 17:1184–1192

467. Cheng Y, Murtomäki L, Corn RM (2000) Electrochemical characterization of the ultrathin polypeptide film/1,2-dichloroethane liquid|liquid interface. J Electroanal Chem 483:88–94

468. Park M-K, Deng S, Advincula RC (2004) pH-sensitive bipolar ion-permselective ultrathin films. J Am Chem Soc 126:13723–13731

469. Boulmedais F, Tang CS, Keller B, Vörös J (2006) Controlled electrodissolution of polyelectrolyte multilayers: a platform technology towards the surface-initiated delivery of drugs. Adv Funct Mater 16:63–70

470. Pardo-Yissar V, Katz E, Lioubashevski O, Willner I (2001) Layered polyelectrolyte films on Au electrodes: characterization of electron-transfer features at the charged polymer interface and application for selective redox reactions. Langmuir 17:1110–1118

471. Ghostine RA, Schlenoff JB (2011) Ion diffusion coefficients through polyelectrolyte multilayers: temperature and charge dependence. Langmuir 27:8241–8247

472. Ghostine RA, Markarian MZ, Schlenoff JB (2013) Asymmetric growth in polyelectrolyte multilayers. J Am Chem Soc 135:7636–7646

473. Farhat TR, Schlenoff JB (2003) Doping-controlled ion diffusion in polyelectrolyte multilayers: mass transport in reluctant exchangers. J Am Chem Soc 125:4627–4636

474. Han S, Lindholm-Sethson B (1999) Electrochemistry at ultrathin polyelectrolyte films self-assembled at planar gold electrodes. Electrochim Acta 45:845–853

475. El Haitami AE, Martel D, Ball V, Nguyen HC, Gonthier E, Labbe P, Voegel J-C, Schaaf P, Senger B, Boulmedais F (2009) Effect of the supporting electrolyte anion on the thickness of PSS/PAH multilayer films and on their permeability to an electroactive probe. Langmuir 25:2282–2289

476. Silva TH, Garcia-Morales V, Moura C, Manzanares JA, Silva F (2005) Electrochemical impedance spectroscopy of polyelectrolyte multilayer modified gold electrodes: influence of supporting electrolyte and temperature. Langmuir 21:7461–7467

477. Zahn R, Boulmedais F, Vörös J, Schaaf P, Zambelli T (2010) Ion and solvent exchange processes in PGA/PAH polyelectrolyte multilayers containing ferrocyanide. J Phys Chem B 114:3759–3768

478. Zahn R, Coullerez G, Vörös J, Zambelli T (2012) Effect of polyelectrolyte interdiffusion on electron transport in redox-active polyelectrolyte multilayers. J Mater Chem 22:11073–11078

479. Roy X, Hui JKH, Rabnawaz M, Liu G, MacLachlan MJ (2011) Prussian blue nanocontainers: selectively permeable hollow metal-organic capsules from block ionomer emulsion-induced assembly. J Am Chem Soc 133:8420–8423

480. Laugel N, Boulmedais F, El Haitami AE, Rabu P, Rogez G, Voegel J-C, Schaaf P, Ball V (2009) Tunable synthesis of Prussian blue in exponentially growing polyelectrolyte multilayer films. Langmuir 25:14030–14036

481. Wood K, Zacharia NS, Schimidt DJ, Wrightman SN, Andaya BJ, Hammond PT (2008) Electroactive controlled release thin films. Proc Natl Acad Sci USA 105:2280–2285

482. DeLongchamp DM, Hammond PT (2004) High-contrast electrochromism and controllable dissolution of assembled Prussian blue/polymer nanocomposites. Adv Funct Mater 14:224–232

483. Schmidt DJ, Cebeci FC, Kalcioglu ZI, Wyman SG, Ortiz C, Van Vliet KJ, Hammond PT (2009) Electrochemically controlled swelling and mechanical properties of a polymer nanocomposite. ACS Nano 3:2207–2216

484. Shariki S, Cox OTL, Tickell DA, Pereira Morais MP, van den Elsen JMH, James TD, Dale SEC, Bending S, Marken F (2012) Coil-by-coil assembly of poly[acrylamide-co-3-(methacryl-amido)-phenylboronic acid] with polydiallyldimethyl-ammonium to give alizarin red S responsive films. J Mater Chem 22:18999–19006

485. Gromova MS, Sigolaeva LV, Fastovets MA, Evtushenko EG, Babin IA, Pergushov DV, Amitonov SV, Eremenko AV, Kurochkin IN (2011) Improved adsorption of choline oxidase on a polyelectrolyte LBL film in the presence of iodide anions. Soft Matter 7:7404–7409

486. Chen J, Tran TO, Ray MT, Brunski DB, Keay JC, Hickey D, Johnson MB, Glatzhofer DT, Schmidtke DW (2013) Effect of surfactant type and redox polymer type on single-walled carbon nanotube modified electrodes. Langmuir 29:10586–10595

487. Sigolaeva LV, Pergushov DV, Synatschke CV, Wolf A, Dewald I, Kurochkin IN, Fery A, Müller AHE (2013) Co-assemblies of micelle-forming diblock copolymers and enzymes on graphite substrate for an improved design of biosensor systems. Soft Matter 9:2858–2868

488. Araque E, Villalonga R, Gamella M, Martinez-Ruiz P, Reviejo J, Pingarron JM (2013) Crumpled reduced graphene oxide-polyamidoamine dendrimer hybrid nanoparticles for the preparation of an electrochemical biosensor. J Mater Chem B 1:2289–2296

489. Fang Y, Wang E (2013) Electrochemical biosensors on platforms of graphene. Chem Commun 49:9526–9539

490. Cosnier S, Holzinger M (2011) Electrosynthesized polymers for biosensing. Chem Soc Rev 40:2146–2156

491. Tokue H, Oyaizu K, Sukegawa T, Nishide H (2014) TEMPO/viologen electrochemical heterojunction for diffusion-controlled redox mediation: a highly rectifying bilayer-sandwiched device based on cross-reaction at the interface between dissimilar redox polymers. ACS Appl Mater Interfaces 6:4043–4049

492. Kamogawa H, Katsuta S, Masato N (1982) Organic solid photochromism by photoreduction mechanism: thionine-reductant system. J Appl Polym Sci 27:1621–1628

493. Kamogawa H, Masui T, Amemiya S (1984) Organic solid photochromism by photoreduction mechanism: viologen embedded in solid polar aprotic polymer matrix. J Polym Sci Polym Chem Ed 22:383–390

494. Kamogawa H, Amemiya S (1985) Organic solid photochromism by photoreduction mechanism: polar aprotic viologen copolymers. J Polym Sci Polym Chem Ed 23:2413–2423

495. Kamogawa H, Sato S (1988) Organic solid photochromism by photoreduction mechanism: aryl viologens embedded in poly(N-vinyl-2-pyrrolidone). J Polym Sci Part A Polym Chem 26:653–656

496. Jain V, Yochum H, Wang H, Montazami R, Hurtado MAV, Mendoza-Galvan A, Gibson HW, Heflin JR (2008) Solid-state electrochromic devices via ionic self-assembled multilayers (ISAM) of a polyviologen. Macromol Chem Phys 209:150–157

497. Ko HC, Kim S, Lee H, Moon B (2005) Multicolored electrochromism of a poly{1,4-bis[2-(3,4-ethylenedioxy)thienyl]benzene} derivative bearing viologen functional groups. Adv Funct Mater 15:905–909

498. Krompiec M, Grudzka I, Filapek M, Skorka L, Krompiec S, Lapkowski M, Kania M, Danikiewicz W (2011) An electrochromic diquat-quaterthiophene alternating copolymer: a polythiophene with a viologen-like moiety in the main chain. Electrochim Acta 56:8108–8114

499. Goto H (2013) Crystal-liquid crystal ordered double layer electroactive polymer prepared with phase transition sequential polymerization, showing metallic electrochromism-bronze, silver, and gold. J Polym Sci Part A Polym Chem 51:3097–3102

500. Akahoshi H, Toshima S, Itaya K (1981) Electrochemical and spectroelectrochemical properties of polyviologen complex modified electrodes. J Phys Chem 85:818–822
501. Laurent D, Schlenoff JB (1997) Multilayer assemblies of redox polyelectrolytes. Langmuir 13:1552–1557
502. Stepp J, Schlenoff JB (1997) Electrochromism and electrocatalysis in viologen polyelectrolyte multilayers. J Electrochem Soc 144:L155–L157
503. Oyama N, Oki N, Ohno H, Ohnuki Y, Matsuda H, Tsuchida E (1983) Electrocatalytic reduction of oxygen by poly(viologen)-poly(sulfonate) complex coated on graphite electrodes. J Phys Chem 87:3642–3647
504. Schlenoff JB, Laurent D, Ly H, Stepp J (1998) Redox-active polyelectrolyte multilayers. Adv Mater 10:347–349
505. Schlenoff JB, Laurent D, Ly H, Stepp J (1998) Redox-active polyelectrolyte multilayers. Chem Eng Technol 21:757–759
506. Rochat S, Swager TM (2013) Water-soluble cationic conjugated polymers: response to electron-rich bioanalytes. J Am Chem Soc 135:17703–17706
507. Reisch A, Moussallem MD, Schlenoff JB (2011) Electrochemically addressed cross-links in polyelectrolyte multilayers: cyclic duravoltammetry. Langmuir 27:9418–9424
508. Takahashi S, Aikawa Y, Kudo T, Ono T, Kashiwagi Y, Anzai J-I (2014) Electrochemical decomposition of layer-by-layer thin films composed of TEMPO-modified poly(acrylic acid) and poly(ethyleneimine). Colloid Polym Sci 292:771–776
509. Mori M, Ishihara M, Okumura J, Yamaguchi K, Nakamae K (2003) Immobilization of viologen moieties on poly(acrylic acid)-grafted polyethylene surface. Sen'i Gakkaishi 59:260–265
510. Ng SW, Neoh KG, Wong YT, Sampanthar JT, Kang ET, Tan KL (2001) Surface graft copolymerization of viologens on polymeric substrates. Langmuir 17:1766–1772
511. Liu X, Neoh KG, Kang ET (2004) Synthesis and characterization of viologen-containing polyvinylidene fluoride redox-sensitive membranes. Surf Interface Anal 36:1037–1040
512. Liu X, Neoh KG, Kang ET (2003) Redox-sensitive microporous membranes prepared from poly(vinylidene fluoride) grafted with viologen-containing polymer side chains. Macromolecules 36:8361–8367
513. Shimomura M, Utsugi K, Horikoshi J, Okuyama K, Hatozaki O, Oyama N (1991) Two-dimensional ordering of viologen polymers fixed on charged surface of bilayer membranes: a peculiar odd-even effect on redox potential and absorption spectrum. Langmuir 7:760–765
514. Shimomura M, Utsugi K, Okuyama K (1986) Odd-even effect on absorption spectra of reduced viologen ionene polymers complexed with anionic bilayer membranes. J Chem Soc Chem Commun 1986(24):1805–1807
515. Sato K, Nakahodo T, Fujihara H (2011) Redox-active π-conjugated polymer nanotubes with viologen for encapsulation and release of fluorescent dye in the nanospace. Chem Commun 47:10067–10069
516. Pfeifer KB, Hughes RC, Jenkins MW, Schneider TW (1999) Viologen polymer-coated impedance sensors for midrange humidity levels and other volatile organic compounds. J Electrochem Soc 146:794–799
517. Willman KW, Murray RW (1982) Viologen homopolymer, polymer mixture and polymer bilayer films on electrodes. Electropolymerization, electrolysis, spectroelectrochemistry, trace analysis and photoreduction. J Electroanal Chem Interfacial Electrochem 133:211–231
518. Wang N, Damlin P, Esteban BM, Aaritalo T, Kankare J, Kvarnstrom C (2013) Electrochemical synthesis and characterization of copolyviologen films. Electrochim Acta 90:171–178
519. Kelaidopoulou A, Kokkinidis G, Coutouli-Argyropoulou E (1998) Electrochemical behavior of N-methyl-N-(3-indol-1-yl-propyl)-4,4′-bipyridinium. Anodic polymerization and redox properties of the viologen unit of monomer and polymer film. Electrochim Acta 43:987–997
520. Chang K-C, Lu H-I, Peng C-W, Lai M-C, Hsu S-C, Hsu M-H, Tsai Y-K, Chang C-H, Hung W-I, Wei Y, Yeh J-M (2013) Nanocasting technique to prepare lotus-leaf-like

superhydrophobic electroactive polyimide as advanced anticorrosive coatings. ACS Appl Mater Interfaces 5:1460–1467

521. Yeh L-C, Huang T-C, Huang Y-P, Huang H-Y, Chen H-H, Yang T-I, Yeh J-M (2013) Synthesis electroactive polyurea with aniline-pentamer-based in the main chain and its application in electrochemical sensor. Electrochim Acta 94:300–306

522. Golriz AA, Kaule T, Untch MB, Kolman K, Berger R, Gutmann JS (2013) Redox active polymer brushes with phenothiazine moieties. ACS Appl Mater Interfaces 5:2485–2494

523. Inzelt G, Day RW, Kinstle JF, Chambers JQ (1983) Electrochemistry and electron spin resonance of tetracyanoquinodimethane modified electrodes. Evidence for mixed-valence radical anions in the reduction process. J Phys Chem 87:4592–4598

524. Inzelt G, Chambers JQ, Kinstle JF, Day RW (1984) Protonation equilibria and charge transport in electroactive tetracyanoquinodimethane polymer films. J Am Chem Soc 106:3396–3401

525. Inzelt G, Bacskai J, Chambers JQ, Day RW (1986) The effect of the counter ion concentration on the electrochemistry of tetracyanoquinodimethane polymer film electrodes. J Electroanal Chem Interfacial Electrochem 201:301–314

526. Inzelt G, Szabo L, Chambers JQ, Day RW (1988) Cyclic voltammetric and potentiometric behavior of tetracyanoquinodimethane polymer film electrodes. Effect of the nature and the concentration of the supporting electrolyte. J Electroanal Chem Interfacial Electrochem 242:265–275

527. Inzelt G, Horanyi G, Chambers JQ (1987) Radiotracer study of the sorption of counter- and co-ions in tetracyanoquinodimethane and poly(vinylferrocene) modified electrodes. Electrochim Acta 32:757–763

528. Joo P, Chambers JQ (1985) Solvent effects on the electrochemistry of tetracyanoquino-dimethane polymer modified electrodes. J Electrochem Soc 132:1345–1350

529. Karimi H, Chambers JQ (1987) Electrochemistry of tetracyanoquinodimethane polymer-modified electrodes. Effect of polymer film composition on site-site interactions. J Electroanal Chem Interfacial Electrochem 217:313–329

530. Shelton RD, Chambers JQ, Schneider W (1991) Preconcentration and voltammetric deter-mination of silver at TCNQ polymer film electrodes. J Electroanal Chem Interfacial Electrochem 305:217–228

531. Yzambart G, Fabre B, Camerel F, Roisnel T, Lorcy D (2012) Controlled grafting of tetrathiafulvalene (TTF) containing diacetylenic units on hydrogen-terminated silicon sur-faces: from redox-active TTF monolayer to polymer films. J Phys Chem C 116:12093–12102

532. Tamaki T, Ito T, Yamaguchi T (2007) Immobilization of hydroquinone through a spacer to polymer grafted on carbon black for a high-surface-area biofuel cell electrode. J Phys Chem B 111:10312–10319

533. Novak P, Müller K, Santhanam KSV, Haas O (1997) Electrochemically active polymers for rechargeable batteries. Chem Rev 97:207–281

534. Nishide H, Iwasa S, Pu Y-J, Suga T, Nakahara K, Satoh M (2004) Organic radical battery: nitroxide polymers as a cathode-active material. Electrochim Acta 50:827–831

535. Hung M-K, Wang Y-H, Lin C-H, Lin H-C, Lee J-T (2012) Synthesis and electrochemical behaviour of nitroxide polymer brush thin-film electrodes for organic radical batteries. J Mater Chem 22:1570–1577

536. Chae IS, Koyano M, Sukegawa T, Oyaizu K, Nishide H (2013) Redox equilibrium of a zwitterionic radical polymer in a non-aqueous electrolyte as a novel Li + host material in a Li-ion battery. J Mater Chem A 1:9608–9611

537. Cao L, Sadaf S, Beladi-Mousavi SM, Walder L (2013) PolyTEMPO and polyviologen on carbon nanotubes: syntheses, structures and organic battery applications. Eur Polym J 49:1923–1934

538. Hyakutake T, Park JY, Yonekuta Y, Oyaizu K, Nishide H, Advincula R (2010) Nanolithographic patterning via electrochemical oxidation of stable poly(nitroxide radical)s to poly(oxoammonium salt)s. J Mater Chem 20:9616–9618

539. Shi P, Amb CM, Dyer AL, Reynolds JR (2012) Fast switching water processable electrochromic polymers. ACS Appl Mater Interfaces 4:6512–6521

540. Welterlich I, Charov O, Tieke B (2012) Deeply colored polymers containing 1,3,4,6-tetraarylpyrrolo[3,2-b]pyrrole-2,5-dione (IsoDPP) units in the main chain. Macromolecules 45:4511–4519

541. Akpinar HZ, Udum YA, Toppare L (2013) Spray-processable thiazolothiazole-based copolymers with altered donor groups and their electrochromic properties. J Polym Sci Part A Polym Chem 51:3901–3906

542. Guo B, Finne-Wistrand A, Albertsson A-C (2012) Electroactive hydrophilic polylactide surface by covalent modification with tetraaniline. Macromolecules 45:652–659

543. Huang L-T, Yen H-J, Liou G-S (2011) Substituent effect on electrochemical and electrochromic behaviors of ambipolar aromatic polyimides based on aniline derivatives. Macromolecules 44:9595–9610

544. Maier A, Tieke B (2012) Coordinative layer-by-layer assembly of electrochromic thin films based on metal ion complexes of terpyridine-substituted polyaniline derivatives. J Phys Chem B 116:925–934

545. Weinberger DA, Higgins TB, Mirkin CA, Liable-Sands LM, Rheingold AL (1999) Terthienyl-based redox-switchable hemilabile ligands: transition metal polymeric complexes with electrochemically tunable or switchable coordination environments? Angew Chem Int Ed 38:2565–2568

546. Laslau C, Williams DE, Wright BE, Travas-Sejdic J (2011) Measuring the ionic flux of an electrochemically actuated conducting polymer using modified scanning ion conductance microscopy. J Am Chem Soc 133:5748–5751

547. Ma M, Guo L, Anderson DG, Langer R (2013) Bio-inspired polymer composite actuator and generator driven by water gradients. Science 339:186–189

548. Li J, Aoki K (1998) Electrochemical gelation of poly(3-hexylthiophene) film. J Electroanal Chem 453:107–112

549. Tatsuma T, Hioki Y, Oyama N (1995) Dependence of swelling behavior and electrochemical activity of water-soluble polythiophene films on the nature of the electrolyte. J Electroanal Chem 396:371–376

550. Homma T, Kondo M, Kuwahara T, Shimomura M (2012) Electrochemical polymerization of aniline in the presence of poly(acrylic acid) and characterization of the resulting films. Polymer 53:223–228

551. Zhang K, Tieke B, Forgie JC, Vilela F, Skabara PJ (2012) Donor-acceptor conjugated polymers based on p- and o-benzodifuranone and thiophene derivatives: electrochemical preparation and optical and electronic properties. Macromolecules 45:743–750

552. Vorotyntsev MA, Konev DV, Devillers CH, Bezverkhyy I, Heintz O (2010) Magnesium (II) polyporphine: the first electron-conducting polymer with directly linked unsubstituted porphyrin units obtained by electrooxidation at a very low potential. Electrochim Acta 55:6703–6714

553. Chen J, Wagner P, Tong L, Wallace GG, Officer DL, Swiegers GF (2012) A porphyrin-doped polymer catalyzes selective, light-assisted water oxidation in seawater. Angew Chem Int Ed 51:1907–1910

554. Moteki S, Sykes AG (1998) Synthetic and electrochemical studies of anthraquinone-substituted poly(pyrrole) films. J Electroanal Chem 447:91–95

555. Li M, Ishihara S, Akada M, Liao M, Sang L, Hill JP, Krishnan V, Ma Y, Ariga K (2011) Electrochemical-coupling layer-by-layer (ECC-LbL) assembly. J Am Chem Soc 133:7348–7351

556. Gelmi A, Higgins MJ, Wallace GG (2013) Resolving sub-molecular binding and electrical switching mechanisms of single proteins at electroactive conducting polymers. Small 9:393–401

557. Maynor BW, Filocamo SF, Grinstaff MW, Liu J (2002) Direct-writing of polymer nanostructures: poly(thiophene) nanowires on semiconducting and insulating surfaces. J Am Chem Soc 124:522–523

558. Huang K, Anne A, Bahri MA, Demaille C (2013) Probing individual redox PEGylated gold nanoparticles by electrochemical-atomic force microscopy. ACS Nano 7:4151–4163

559. Kang K, Lee S, Kim R, Choi IS, Nam Y (2012) Electrochemically driven, electrode-addressable formation of functionalized polydopamine films for neural interfaces. Angew Chem Int Ed 51:13101–13104

560. Corona-Avendano S, Ramirez-Silva MT, Romero-Romo M, Rojas-Hernandez A, Palomar-Pardave M (2013) Influence of the HClO4 concentration on the β-CD electropolimerization over a carbon paste electrode and on dopamine's electrochemical response. Electrochim Acta 89:854–860

561. Kaneto K, Sonoda Y, Takashima W (2000) Direct measurement and mechanism of electro-chemomechanical expansion and contraction in polypyrrole films. Jpn J Appl Phys Part 1 (39):5918–5922

562. Sonoda Y, Takashima W, Kaneto K (2001) Characteristics of soft actuators based on polypyrrole films. Synth Met 119:267–268

563. Smela E, Gadegaard N (1999) Surprising volume change in PPy/DBS. An atomic force microscopy study. Adv Mater 11:953–957

564. Strover LT, Malmstrom J, Laita O, Reynisson J, Aydemir N, Nieuwoudt MK, Williams DE, Dunbar PR, Brimble MA, Travas-Sejdic J (2013) A new precursor for conducting polymer-based brush interfaces with electroactivity in aqueous solution. Polymer 54:1305–1317

565. Malmstrom J, Nieuwoudt MK, Strover LT, Hackett A, Laita O, Brimble MA, Williams DE, Travas-Sejdic J (2013) Grafting from poly(3,4-ethylenedioxythiophene): a simple route to versatile electrically addressable surfaces. Macromolecules 46:4955–4965

566. Pei Y, Travas-Sejdic J, Williams DE (2012) Reversible electrochemical switching of polymer brushes grafted onto conducting polymer films. Langmuir 28:8072–8083

567. Pei Y, Travas-Sedjic J, Williams DE (2012) Electrochemical switching of conformation of random polyampholyte brushes grafted onto polypyrrole. Langmuir 28:13241–13248

568. Hansen TS, Daugaard AE, Hvilsted S, Larsen NB (2009) Spatially selective functionalization of conducting polymers by "electroclick" chemistry. Adv Mater 21:4483–4486

569. Hansen TS, Lind JU, Daugaard AE, Hvilsted S, Andresen TL, Larsen NB (2010) Complex surface concentration gradients by stenciled "electro click chemistry". Langmuir 26:16171–16177

570. Inagi S, Nagai H, Tomita I, Fuchigami T (2013) Parallel polymer reactions of a polyfluorene derivative by electrochemical oxidation and reduction. Angew Chem Int Ed 52:6616–6619

571. Abidian MR, Kim D-H, Martin DC (2006) Conducting-polymer nanotubes for controlled drug release. Adv Mater 18:405–409

572. Weaver CL, LaRosa JM, Luo X, Cui XT (2014) Electrically controlled drug delivery from graphene oxide nanocomposite films. ACS Nano 8:1834–1843

573. Svirskis D, Travas-Sejdic J, Rodgers A, Garg S (2010) Electrochemically controlled drug delivery based on intrinsically conducting polymers. J Control Release 146:6–15

574. Guiseppi-Elie A (2010) Electroconductive hydrogels: synthesis, characterization and bio-medical applications. Biomaterials 31:2701–2716

575. Green RA, Baek S, Poole-Warren LA, Martens PJ (2010) Conducting polymer-hydrogels for medical electrode applications. Sci Technol Adv Mater 11:014107

576. Daum P, Murray RW (1979) Chemically modified electrodes. Part XXII. Solvent effects on the electrochemistry of thin films of plasma polymerized vinylferrocene. J Electroanal Chem Interfacial Electrochem 103:289–294

577. Daum P, Murray RW (1981) Charge-transfer diffusion rates and activity relationships during oxidation and reduction of plasma-polymerized vinylferrocene films. J Phys Chem 85:389–396

578. Akhoury A, Bromberg L, Hatton TA (2013) Interplay of electron hopping and bounded diffusion during charge transport in redox polymer electrodes. J Phys Chem B 117:333–342
579. Anne AS, Demaille C, Moiroux J (2002) Terminal attachment of polyethylene glycol (PEG) chains to a gold electrode surface. Cyclic voltammetry applied to the quantitative characterization of the flexibility of the attached PEG chains and of their penetration by mobile PEG chains. Macromolecules 35:5578–5586
580. Anne A, Bahri MA, Chovin A, Demaille C, Taofifenua C (2014) Probing the conformation and 2D-distribution of pyrene-terminated redox-labeled poly(ethylene glycol) chains end-adsorbed on HOPG using cyclic voltammetry and atomic force electrochemical microscopy. Phys Chem Chem Phys 16:4642–4652
581. Kim B-Y, Ratcliff EL, Armstrong NR, Kowalewski T, Pyun J (2010) Ferrocene functional polymer brushes on indium tin oxide via surface-initiated atom transfer radical polymerization. Langmuir 26:2083–2092
582. Sakakiyama T, Ohkita H, Ohoka M, Ito S, Tsujii Y, Fukuda T (2005) Fabrication and electrochemical properties of high-density graft films with ferrocene moieties on ITO substrates. Chem Lett 34:1366–1367
583. Xu LQ, Wan D, Gong HF, Neoh K-G, Kang E-T, Fu GD (2010) One-pot preparation of ferrocene-functionalized polymer brushes on gold substrates by combined surface-initiated atom transfer radical polymerization and "click chemistry". Langmuir 26:15376–15382
584. Peter M, Hempenius MA, Kooij ES, Jenkins TA, Roser SJ, Knoll W, Vancso GJ (2004) Electrochemically induced morphology and volume changes in surface-grafted poly (ferrocenyldimethylsilane) monolayers. Langmuir 20:891–897
585. Kutner W, Doblhofer K (1992) Simultaneous cyclic voltammetry and electrochemical quartz-crystal microbalance study at polymer film-modified electrodes of molecular inclusion of ferrocene by β-cyclodextrin polymer and carboxymethylated β-cyclodextrin polymer as well as ferrocenecarboxylic acid by β-cyclodextrin polymer. J Electroanal Chem 326:139–160
586. Hempenius MA, Peter M, Robins NS, Kooij ES, Vancso GJ (2002) Water-soluble poly (ferrocenylsilanes) for supramolecular assemblies by layer-by-layer deposition. Langmuir 18:7629–7634
587. Song J, Janczewski D, Ma Y, van Ingen L, Ee Sim C, Goh Q, Xu J, Vancso GJ (2013) Electrochemically controlled release of molecular guests from redox responsive polymeric multilayers and devices. Eur Polym J 49:2477–2484
588. Song J, Janczewski D, Ma Y, Hempenius M, Xu J, Vancso GJ (2013) Redox-controlled release of molecular payloads from multilayered organometallic polyelectrolyte films. J Mater Chem B 1:828–834
589. Sun Y-X, Ren K-F, Wang J-L, Chang G-X, Ji J (2013) Electrochemically controlled stiffness of multilayers for manipulation of cell adhesion. ACS Appl Mater Interfaces 5:4597–4602
590. Sun Y-X, Ren K-F, Zhao Y-X, Liu X-S, Chang G-X, Ji J (2013) Construction of redox-active multilayer film for electrochemically controlled release. Langmuir 29:11163–11168
591. Song J, Janczewski D, Ma Y, Hempenius M, Xu J, Vancso GJ (2013) Disassembly of redox responsive poly(ferrocenylsilane) multilayers: the effect of blocking layers, supporting electrolyte and polyion molar mass. J Colloid Interface Sci 405:256–261
592. Feng X, Cumurcu A, Sui X, Song J, Hempenius MA, Vancso GJ (2013) Covalent layer-by-layer assembly of redox-active polymer multilayers. Langmuir 29:7257–7265
593. Aoki A, Miyashita T (1999) A structural effect on electrochemical behavior of hetero-deposited redox polymer Langmuir-Blodgett films containing ferrocene and tris(bipyridine) ruthenium derivatives. J Electroanal Chem 473:125–131
594. Aoki A, Miyashita T (1996) Electrochemical behavior of hetero-deposited redox polymer Langmuir-Blodgett films with ferrocene and tris(bipyridine)ruthenium derivatives. Chem Lett 25(7):563–564

595. Denisevich P, Willman KW, Murray RW (1981) Unidirectional current flow and charge state trapping at redox polymer interfaces on bilayer electrodes: principles, experimental demonstration, and theory. J Am Chem Soc 103:4727–4737
596. Matsui J, Shimada T, Miyashita T (2011) Electrochemical charging and photochemical discharging in heterodeposited polymer nanosheet assembly. J Mater Chem 21:17498–17504
597. Cheng Z, Ren B, Zhao D, Liu X, Tong Z (2009) Novel thermotropic liquid crystalline and redox-active complexes of ionically self-assembled poly(ferrocenylsilane) and dendritic amphiphiles. Macromolecules 42:2762–2766
598. Li F, Pandey B, Ito T (2012) Linker-based control of electron propagation through ferrocene moieties covalently anchored onto insulator-based nanopores derived from a polystyrene-poly(methylmethacrylate) diblock copolymer. Langmuir 28:16496–16500
599. Elbert J, Krohm F, Rüttiger C, Kienle S, Didzoleit H, Balzer BN, Hugel T, Stühn B, Gallei M, Brunsen A (2014) Thin films: polymer-modified mesoporous silica thin films for redox-mediated selective membrane gating. Adv Funct Mater 24:1493
600. Meredith MT, Hickey DP, Redemann JP, Schmidtke DW, Glatzhofer DT (2013) Effects of ferrocene methylation on ferrocene-modified linear poly(ethylenimine) bioanodes. Electrochim Acta 92:226–235
601. Meredith MT, Kao D-Y, Hickey D, Schmidtke DW, Glatzhofer DT (2011) High current density ferrocene-modified linear poly(ethylenimine) bioanodes and their use in biofuel cells. J Electrochem Soc 158:B166–B174
602. Bunte C, Rühe J (2009) Photochemical generation of ferrocene-based redox-polymer networks. Macromol Rapid Commun 30:1817–1822
603. Zhang S, Yang W, Niu Y, Sun C (2004) Multilayered construction of glucose oxidase and poly(allylamine)ferrocene on gold electrodes by means of layer-by-layer covalent attachment. Sens Actuators B 101:387–393
604. Cass AEG, Davis G, Francis GD, Hill HAO, Aston WJ, Higgins IJ, Plotkin EV, Scott LDL, Turner APF (1984) Ferrocene-mediated enzyme electrode for amperometric determination of glucose. Anal Chem 56:667–671
605. Patel H, Li X, Karan HI (2003) Amperometric glucose sensors based on ferrocene containing polymeric electron transfer systems-a preliminary report. Biosens Bioelectron 18:1073–1076
606. Gülce A, Gülce H (2005) Polyvinylferrocenium modified Pt electrode for anaerobic glucose monitoring. J Biochem Biophys Methods 62:81–92
607. Zhang ZB, Yuan SJ, Zhu XL, Neoh KG, Kang ET (2010) Enzyme-mediated amperometric biosensors prepared via successive surface-initiated atom-transfer radical polymerization. Biosens Bioelectron 25:1102–1108
608. Nagel B, Warsinke A, Katterle M (2007) Enzyme activity control by responsive redoxpolymers. Langmuir 23:6807–6811
609. Saito T, Watanabe M (1998) Characterization of poly(vinylferrocene-co-2-hydroxyethyl methacrylate) for use as electron mediator in enzymic glucose sensor. React Funct Polym 37:263–269
610. Saito T, Watanabe M (1999) Electron transfer reaction from glucose oxidase to an electrode via redox copolymers. Polym J 31:1149–1154
611. Deng S, Lei J, Liu Y, Huang Y, Ju H (2013) A ferrocenyl-terminated dendrimer as an efficient quencher via electron and energy transfer for cathodic electrochemiluminescent bioanalysis. Chem Commun 49:2106–2108
612. Song J, Vancso GJ (2011) Responsive organometallic polymer grafts: electrochemical switching of surface properties and current mediation behavior. Langmuir 27:6822–6829
613. Zeng Q, McNally A, Keyes TE, Forster RJ (2008) Redox induced switching dynamics of a three colour electrochromic metallopolymer film. Electrochim Acta 53:7033–7038
614. Lu Y (2010) Preparation of novel polypyridyl ruthenium complex polymers with high sensitivity for electrogenerated chemiluminescence via copolymerization. Photochem Photobiol Sci 9:392–397

615. Abruna HD, Bard AJ (1982) Electrogenerated chemiluminescence. 40. A chemiluminescent polymer based on the tris(4-vinyl-4′-methyl-2,2′-bipyridyl)ruthenium(II) system. J Am Chem Soc 104:2641–2642

616. Tagliazucchi M, Calvo EJ (2010) Charge transport in redox polyelectrolyte multilayer films: the dramatic effects of outmost layer and solution ionic strength. ChemPhysChem 11:2957–2968

617. Cassidy JF, Vos JG (1987) Polymer-modified electrodes. Part V. The use of hydrodynamically modulated rotating-disk electrodes in the study of the mediated oxidation of hexacyanoferrate(4-) at ruthenium-containing polymer-modified electrodes. J Electroanal Chem Interfacial Electrochem 218:341–345

618. Cassidy JF, Vos JG (1988) Polymer modified electrodes. VI. Nonstationary processes at polymer-coated rotating disk electrodes. A study of [Ru(bpy)2Cl(PVP)5]Cl films as three-dimensional mediators. J Electrochem Soc 135:863–868

619. Cassidy JF, Ross AG, Vos JG (1986) An electrochemical study of the oxidation of ferrocyanide mediated by electrodes modified with ruthenium-containing polymers. Anal Chem Symp Ser 25:269–276

620. Ikeda T, Leidner CR, Murray RW (1982) Kinetics of electron transfer reactions of metal complexes at impermeable redox active polymeric films on electrode surfaces and charge transport within the polymer film. J Electroanal Chem Interfacial Electrochem 138:343–365

621. Leidner CR, Murray RW (1984) Electron-transfer reactions of iron, ruthenium, and osmium bipyridine and phenanthroline complexes at polymer/solution interfaces. J Am Chem Soc 106:1606–1614

622. Kang H, Liu R, Sun H, Zhen J, Li Q, Huang Y (2012) Osmium bipyridine-containing redox polymers based on cellulose and their reversible redox activity. J Phys Chem B 116:55–62

623. Xue C, Luo F-T, Chen J, Liu H (2006) Synthesis and biosensing application of highly water-soluble and cross-linkable poly(p-phenyleneethynylene) containing osmium(II) complex and aldehyde groups. Anal Chim Acta 569:27–34

624. Forzani ES, Perez MA, Teijelo ML, Calvo EJ (2002) Redox driven swelling of layer-by-layer enzyme-polyelectrolyte multilayers. Langmuir 18:9867–9873

625. Tagliazucchi M, Grumelli D, Calvo EJ (2006) Nanostructured modified electrodes: role of ions and solvent flux in redox active polyelectrolyte multilayer films. Phys Chem Chem Phys 8:5086–5095

626. Calvo EJ, Forzani E, Otero M (2002) Gravimetric and viscoelastic changes during the oxidation-reduction of layer-by-layer self assembled enzyme multilayers wired by an Os-containing poly(allylamine) polymer. J Electroanal Chem 538–539:231–241

627. Grumelli DE, Garay F, Barbero CA, Calvo EJ (2006) Dynamics of ion exchange between self-assembled redox polyelectrolyte multilayer modified electrode and liquid electrolyte. J Phys Chem B 110:15345–15352

628. Tagliazucchi M, Calvo EJ, Szleifer I (2008) Molecular theory of chemically modified electrodes by redox polyelectrolytes under equilibrium conditions: comparison with experiment. J Phys Chem C 112:458–471

629. Tagliazucchi M, Williams FJ, Calvo EJ (2007) Effect of acid–base equilibria on the Donnan potential of layer-by-layer redox polyelectrolyte multilayers. J Phys Chem B 111:8105–8113

630. Tagliazucchi M, Calvo EJ, Szleifer I (2008) Redox and acid–base coupling in ultrathin polyelectrolyte films. Langmuir 24:2869–2877

631. Geraty S, Vos JG (1984) Polymer modified electrodes. Part III. Characterization, electrochemical and photochemical properties of ruthenium containing poly(N-vinylimidazole) coatings. J Electroanal Chem Interfacial Electrochem 176:389–393

632. Brown KL, Hou X, Banks O, Krueger KA, Hinson J, Peaslee GF, DeYoung PA, Alger SM, Benzer J, Neils TL (2011) Characterization of tris (5-amino-1,10-phenanthroline) ruthenium (II/III) polymer films using cyclic voltammetry and Rutherford backscattering spectrometry. Int J Chem 3:12–19

633. Paulson SC, Sapp SA, Elliott CM (2001) Electrochemical and spectroelectrochemical investigations into the nature of charge-trapping in electrochemically-generated homopolymer films of tris(4-vinyl-4′-methyl-2,2′-bipyridine)ruthenium(II). J Phys Chem B 105:8718–8724

634. Chiericato G, Silva APS (2008) Spectroelectrochemistry and investigation of charge transport mechanisms of iron poly(pyridyl) redox polymers. Polyhedron 27:1860–1866

635. Chardon-Noblat S, Cripps GH, Deronzier A, Field JS, Gouws S, Haines RJ, Southway F (2001) Synthesis, structure, and physicochemical characterizations of a new cationic ruthenium(I)-ruthenium(I) tetracarbonyl bipyridine dimer precursor for the electrochemical synthesis of an organometallic ruthenium(0) polymer. Organometallics 20:1668–1675

636. Saito M, Endo A, Shimizu K, Sato GP (2000) Electrochemical polymerization of tetraphenylporphyrinatoruthenium(II) complexes with diaza compounds as axial ligands. Electrochim Acta 45:3021–3028

637. Venkatanarayanan A, Spehar-Deleze A-M, Dennany L, Pellegrin Y, Keyes TE, Forster RJ (2008) Ruthenium aminophenanthroline metallopolymer films electropolymerized from an ionic liquid: deposition and electrochemical and photonic properties. Langmuir 24:11233–11238

638. Tedim J, Freire C, Hillman AR (2009) Modulation of electroactive polymer film dynamics by metal ion complexation and redox switching. Soft Matter 5:2603–2613

639. Magdesieva TV, Dolganov AV, Yakimansky AV, Goikhman MY, Podeshvo IV, Kudryavtsev VV (2008) New Cu(I) complexes with biquinolyl-containing polymer ligands as electrocatalysts for O2 activation in the oxidation of alcohols. Electrochim Acta 53:3960–3972

640. Magdesieva TV, Dolganov AV, Yakimansky AV, Goikhman MY, Podeshvo IV (2009) New Cu(I) complexes with 2,2′-biquinolyl and 2,2′-quinolyl-pyridine containing polymer ligands as electrocatalysts for O2 activation in the oxidation of aliphatic amines. Electrochim Acta 54:1444–1451

641. Ge Y, Lilienthal RR, Smith DK (1996) Electrochemically-controlled hydrogen bonding. Selective recognition of urea and amide derivatives by simple redox-dependent receptors. J Am Chem Soc 118:3976–3977

642. Ge Y, Miller L, Ouimet T, Smith DK (2000) Electrochemically controlled hydrogen bonding. o-Quinones as simple redox-dependent receptors for arylureas. J Org Chem 65:8831–8838

643. Bu J, Lilienthal ND, Woods JE, Nohrden CE, Hoang KT, Truong D, Smith DK (2005) Electrochemically controlled hydrogen bonding. Nitrobenzenes as simple redox-dependent receptors for arylureas. J Am Chem Soc 127:6423–6429

644. Chan-Leonor C, Martin SL, Smith DK (2005) Electrochemically controlled hydrogen bonding. Redox-dependent formation of a 2:1 diarylurea/dinitrobenzene2- complex. J Org Chem 70:10817–10822

645. Woods JE, Ge Y, Smith DK (2008) Electrochemically controlled hydrogen bonding. Electrolyte effects in an oxidation-based arylurea-amide system. J Am Chem Soc 130:10070–10071

Index